Durham E-Theses

A geophysical investigation of the nova scotian continental shelf

Goodacre, Alan Kenneth

A GEOPHYSICAL INVESTIGATION OF THE

NOVA SCOTIAN CONTINENTAL SHELF

by

Alan Kenneth Goodacre

A thesis submitted for the degree of

Doctor of Philosophy in the University of Durham

Graduate Society   March, 1976

ABSTRACT

A major east-west structural discontinuity, termed the Minas
Basin - Chedabucto Bay - Orpheus fault zone, transects Nova Scotia
and the adjacent Nova Scotian continental shelf. To the north of this
discontinuity, the geophysical evidence indicates structural continuity
between the late Precambrian basement rocks of southeastern Newfoundland
and eastern Cape Breton Island. The generally dense basement rocks
of the northern Scotian Shelf are pierced by intrusions of magnetic
granite and traversed by linear belts of volcanic rocks. The basement
is depressed into a regional east-west trough which is filled by
Palaeozoic and younger sedimentary rocks. To the south of the major
east-west discontinuity, the southern Scotian Shelf consists of a
southeasterly dipping early Palaeozoic basement complex intruded by
granite and overlain by a wedge of late Palaeozoic and younger
sedimentary rocks which reach their maximum thickness east of Sable
Island. The most notable feature on the Nova Scotian continental
shelf is the Orpheus Graben which lies along the Minas Basin -
Chedabucto Bay - Orpheus fault zone and which is filled with Mesozoic
sedimentary rocks. Many of the basement structural features on the
Nova Scotian continental shelf appear to be products of continental
collisions during the early Palaeozoic Era while other features are
probably due to continental separation in the late Palaeozoic and
Mesozoic Eras. In particular, the Minas Basin - Chedabucto Bay -
Orpheus fault zone was probably initiated in Siluro-Devonian times
as the result of the thrusting of the northwestern portion of Africa
into the late Precambrian rocks of the Avalon (Acado-Baltic) Platform

of southeastern New Brunswick, eastern Cape Breton Island and south-eastern Newfoundland. Later on, the Orpheus Graben was formed along the existing zone of weakness probably in Triassic or Jurassic time as a result of continental break-up and the formation of the present-day Atlantic Ocean.

ACKNOWLEDGEMENTS

was done through the Computer Science Centre of the Department of Energy, Mines and Resources.

Last, but not least, I thank my wife, Lise, who, while busy raising our young family, was always a source of encouragement and understanding during our interesting and rewarding stay at the University of Durham.

TABLE OF CONTENTS

i

CHAPTER 1

INTRODUCTION

1.1 DESCRIPTION OF AREA OF INVESTIGATION

The continental shelf area under investigation in this thesis
is about 200 km wide and 700 km long and runs northeast from Cape
Sable, on the southern tip of Nova Scotia to Burin Peninsula, New-
foundland (Figure 1.1). The northwest-southeast trending Laurentian
Channel is the major bathymetric feature on the Nova Scotian
continental shelf and it separates St. Pierre Bank on the northeast
from a series of banks and basins to the southwest. Except for the
Laurentian Channel, the bathymetric trends, where they can be defined,
are primarily northeast-southwest as in Hermitage Channel or
approximately east-west as in the severely dissected area north of
Banquereau.

1.2 IMPORTANCE OF THE NOVA SCOTIAN CONTINENTAL SHELF

Since the advent in the late 1960's of the concept of moving
"plates" of lithosphere (McKenzie and Parker, 1967; Morgan, 1968), a
major revolution has taken place in concepts of the earth's geological
structure and history and an orderly network of hitherto poorly
related observations and theories is currently being woven together.
There are, nevertheless, many unsolved problems and some of these
involve continental shelves and margins. For example, little is yet
known about the transition from continental to oceanic crust at con-
tinental margins nor are the causes of the considerable warping,
fracturing and vertical movement of continental shelves completely

Figure 1.1:   Location map showing the main bathymetric

features of the continental shelf off

Nova Scotia and southern Newfoundland.

Maximum depth of the Laurentian Channel

is 535 meters in the area between Cape Breton

Island and Newfoundland. Maximum depth on the

Scotian Shelf is 291 meters in Emerald Basin.

3

ELEVATION
(meters)

100
-100
-200
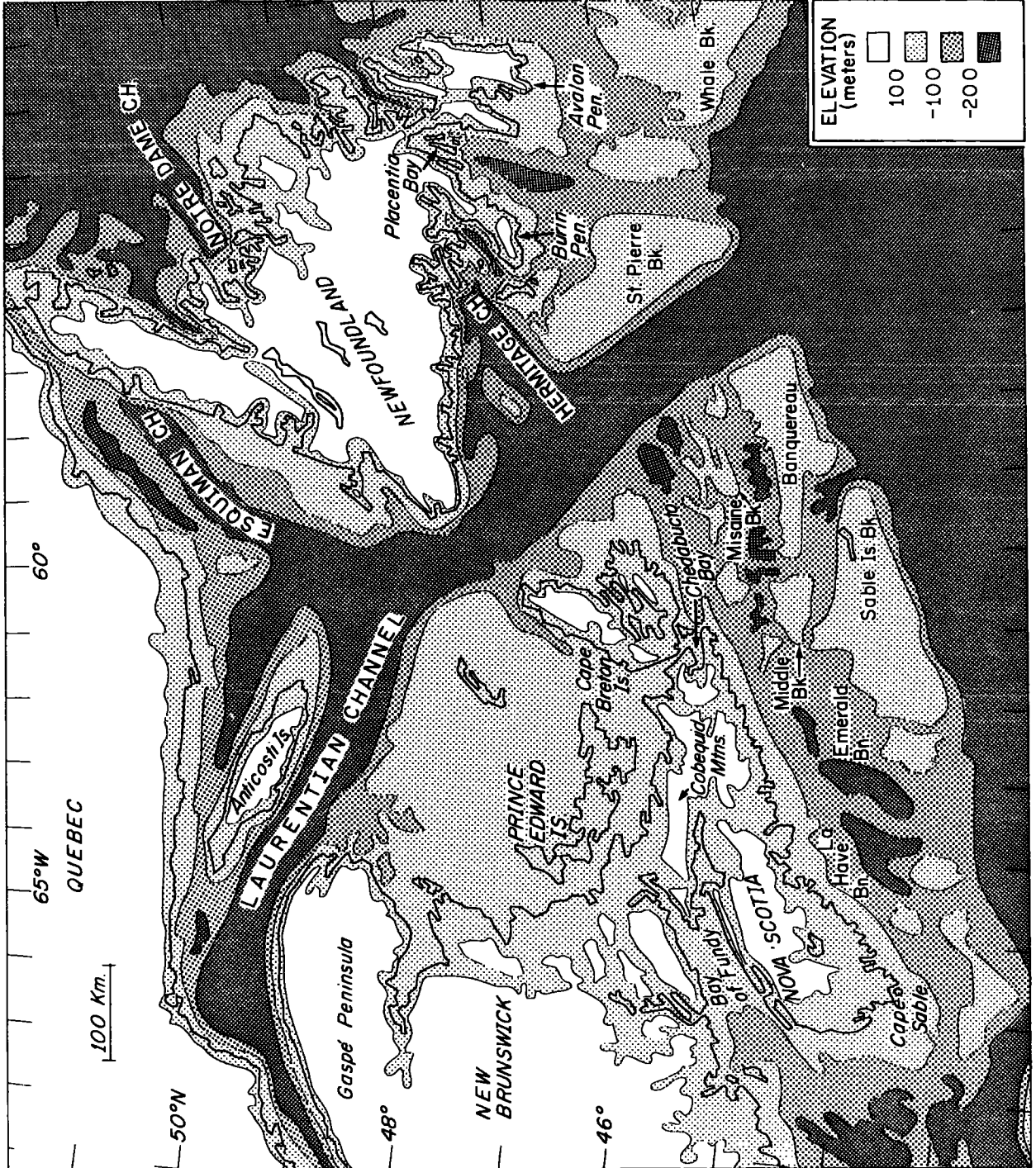
understood although considerable progress has been made in the last
decade or so, towards solving these problems (e.g. Drake et al.,
1959; Worzel, 1968; Bott and Dean, 1972).

The continental shelf off Nova Scotia, Canada is of interest
from the point of view of plate tectonics because most of the geological
structures are probably relics of collisions of continental land masses
during the Palaeozoic Era (e.g. McKerrow and Ziegler, 1972) while some
of the structures may be due to the separation of Africa and North
America during the Mesozoic Era (e.g. Stephens and Cooper, 1973). There
were at least two Palaeozoic collisions which affected the Scotian Shelf.
The first collision, which brought the Baltic and Canadian shields to-
gether, locally brought the 600 m.y. old rocks of the Avalon Platform
(Poole, 1967), now preserved in southeastern Newfoundland and parts of
Cape Breton Island, central Nova Scotia and southeastern New Brunswick
(Zone H in Figure 1.2), into proximity with the 1000 m.y. old basement
rocks of the St. Lawrence Platform, which is exposed in northwestern
Newfoundland (Zone A of Figure 1.2) and lies beneath the Gulf of
St. Lawrence in the area north of the Laurentian Channel (Figure 1.1).
The first approach of two land masses and their subsequent collision is
manifested by the Taconic (Ordovician) and Acadian (Devonian) Orogenies.
The second collision occurred when Gondwanaland and Laurasia came to-
gether in late Palaeozoic time and produced the Hercynian Orogeny in
Europe and the Appalachian Orogeny in North America (e.g. Burrett,
1972). Some of the Devonian tectonic activity that affected the Avalon

Platform may reflect early stages of the second collision (McKerrow and Ziegler, 1972). A major geological problem is to determine the relationship of southern Nova Scotia (Zone I in Figure 1.2) and the adjacent continental shelf to the rest of the Canadian Maritime Appalachians. Schenk (1971) suggests that this area may have once been part of northwest Africa. One of the puzzling aspects of the second continental collision is why it affected a wide band in Europe and Africa running from southern England to Morocco but apparently only two narrow zones in the Canadian maritimes. One zone runs northeast through the Bay of Fundy, eastern Prince Edward Island and the central part of western Newfoundland, the other zone extends east from the Bay of Fundy, runs south of the Cobequid Highlands and passes out to sea through Chedabucto Bay (Figure 1.1).

It is also interesting to note that there was very little tectonic activity associated with the opening of the Atlantic when North America moved away (in a relative sense) from Africa (e.g. Pitman and Talwani, 1972). Apart from a few scattered Triassic and younger dikes, Mesozoic tectonic activity was restricted mainly to the Bay of Fundy – Chedabucto Bay zone. Because the Scotian Shelf is adjacent to a passive margin it has probably been subjected to downwarping and fracturing, tectonic processes that are common to passive margins (Bott, 1971); the Scotian Shelf should therefore, provide scientists with an opportunity to outline the evolution of a passive-margin-type continental shelf.

Figure 1.2:   Map showing main Tectonic zones bordering

the Nova Scotian Continental shelf (after

Williams et al., 1972)

Zone A: Cambro-Ordovician carbonate rocks

unconformably overlying Grenville basement

rocks. Transported rocks are ophiolite

complexes.

Zone B: Cambro-Ordovician carbonate rocks uncon-

formably overlying polyphase deformed schists.

Zone C: Thick clastic sedimentary and volcanic rocks

overlying gneissic basement rocks.

Zone D: Mainly lower and middle Ordovician mafic

volcanic rocks.

Zone E: Chiefly lower and middle Ordovician

sedimentary and volcanic rocks.

Zone F: Generally Ordovician slates and other

sedimentary rocks with minor mafic and

ultramafic intrusions.

Zone G: Pre-middle Ordovician metasedimentary rocks,

gneisses and migmatites. Some intrusive

Devonian granite.

Zone H: Thick succession of late Precambrian volcanic

and sedimentary rocks overlain in places by

Cambrian and Ordovician shales and sandstones.

Zone I: Thick succession of Cambro-Ordovician shales

and greywackes intruded by Devonian granite.

Some Ordovician/Silurian mafic volcanic rocks.
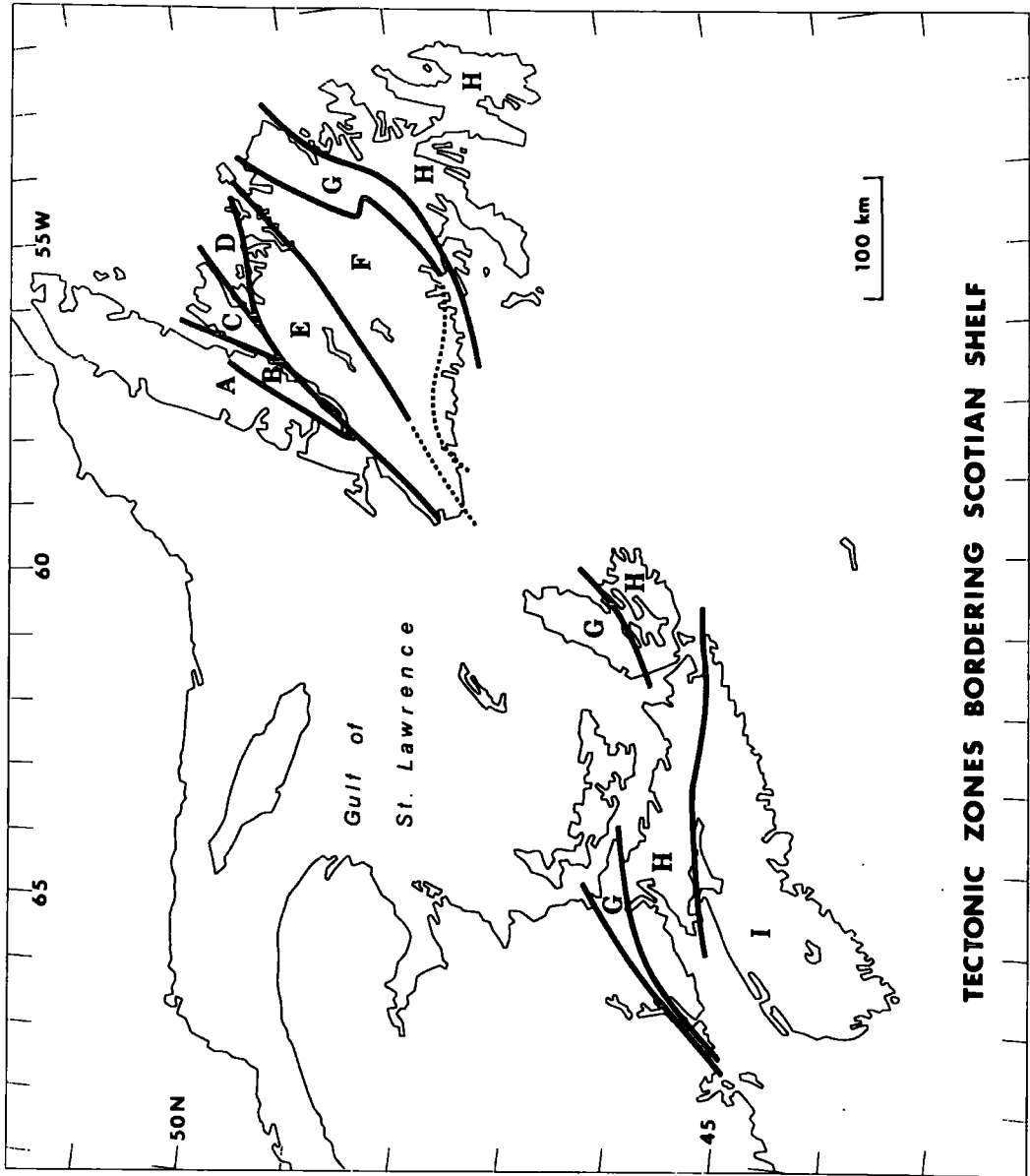
TECTONIC ZONES BORDERING SCOTIAN SHELF

The Scotian Shelf is currently of great economic interest
since the discovery of oil at Sable Island (Figure 1.1).

1.3 SCOPE OF THE THESIS.

The main emphasis in this thesis is on a structural interpre-
tation of underwater gravity data obtained on the Scotian Shelf by
the Gravity Division of the Earth Physics Branch of the Department
of Energy, Mines and Resources, Ottawa during the summers of 1970 and
1971 (Stephens et al., 1971; Stephens and Cooper, 1973) but, where
they are available, published magnetic anomalies and seismic data are
incorporated into the analysis. Because the underwater gravity obser-
vations are spaced about 13 km apart, only structures whose lateral
dimensions are of the order of tens of kilometers or greater can be
effectively considered so the thesis is oriented more towards problems
of scientific interest rather than those of purely commercial interest.
In addition, the problems studied relate primarily to the continental
shelf and adjacent land areas as there is insufficient geophysical
information to study the continental margin proper.

Because there are not enough non-classified seismic data to
accurately delineate the Mezozoic and younger sedimentary rocks and to
enable a proper study of the fracturing and downwarping of the contin-
ental shelf and other interesting problems related to the separation
of Africa and North America, I have concentrated on studying the
deeper-seated structures associated with plate convergence during the
Palaeozoic Era. Correlations between geophysical data are developed

where possible on adjacent land areas and applied to the Scotian

Shelf; the success of these extrapolations depends upon the degree

of correlation which is obtained on land. In some areas, convincing

extrapolations are unattainable but the geophysical data still set

limits on:

    (i)   the variation of the magnitude of physical parameters

           such as density, magnetization, and seismic velocity

    (ii) The shapes and sizes of geological structures.

The analysis is mainly a "static" one in that it gives an

indication of the present-day geological structure but it does not

give direct information about the geological history of the area.

An exception to this, however, is combined analysis of gravity and

magnetic data which, under favourable conditions, puts limits on

the direction of the remanent magnetization in the subjacent rocks

and hence distinguishes between regions of differing paleomagnetic

history. Because such analysis has broad application to studies

of areas of difficult geological access, I devote a significant

part of the thesis to combined analysis of gravity and magnetic

data. Other aspects of the thesis are concerned with the use of

non-linear optimization in modelling gravity, magnetic and seismic

data.

Because there is increasing evidence that the Scotian Shelf and

the adjacent province of Nova Scotia are transected by a major east-

west trending fault zone which passes through Chedabucto Bay, I have,

for convenience, split the Scotian Shelf up into three sections for

study: a northern and southern section on either side of the fault

Figure 1.3:   The northern, central and southern

               sections of the Nova Scotian

               continental shelf
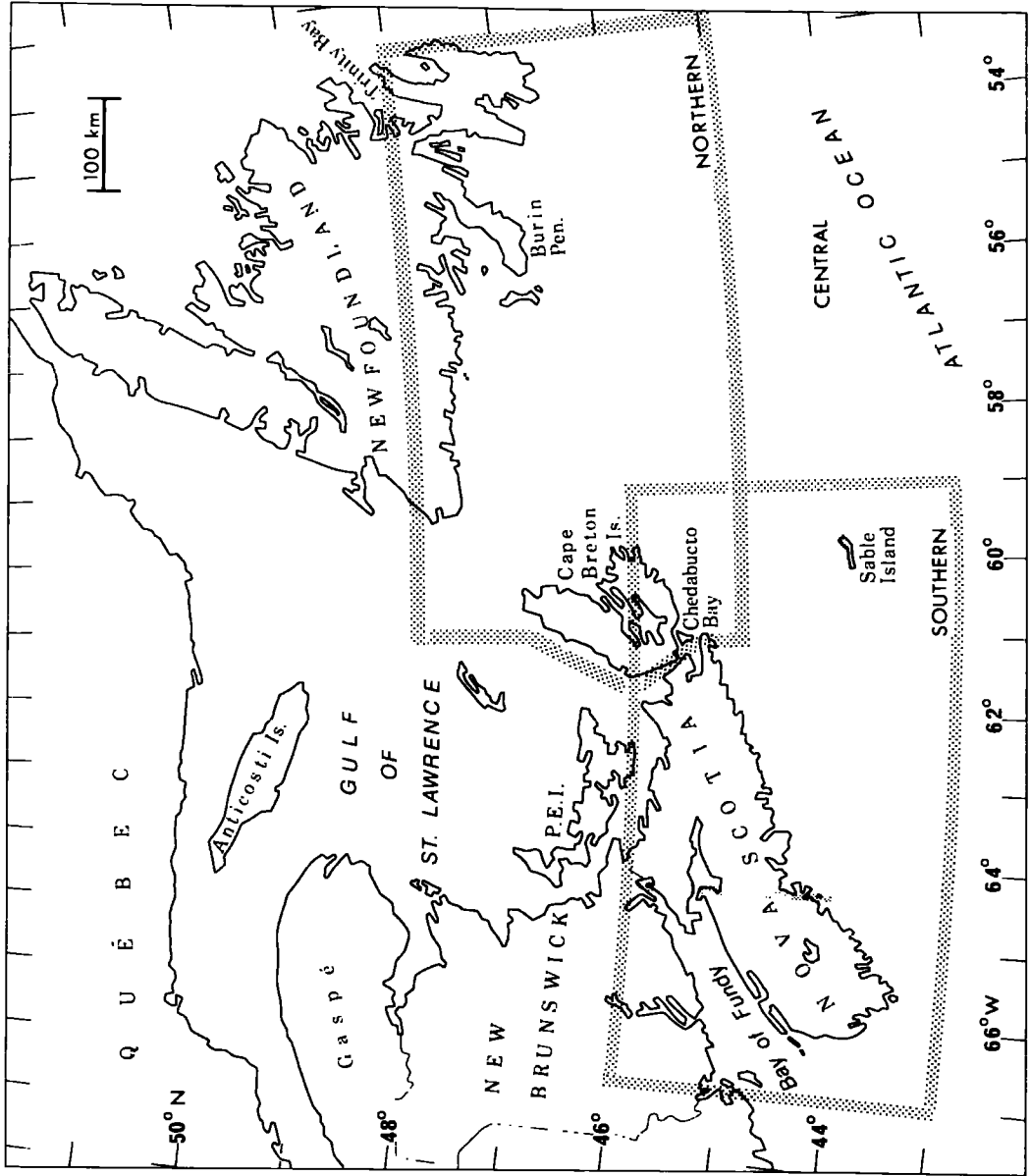
zone and a central section which encompasses it (Figure 1.3). A chapter is devoted to each section and each chapter summarizes the available land geology and provides a structural interpretation of the major geophysical features in the water-covered areas. The final chapter discusses the overall structure and paleohistory of the Scotian Shelf.

CHAPTER 2

OBSERVATION AND REDUCTION OF THE GRAVITY DATA AND ESTIMATION

OF THE ERRORS IN THE BOUGUER ANOMALIES

2.1 THE SURVEY EQUIPMENT

2.1.1 Underwater gravity meter, cable and winch.

The underwater gravity meter used to survey the Scotian Shelf

is manufactured by LaCoste and Romberg of Austin, Texas, U.S.A.

The instrument is essentially a land-gravity meter suspended in

gimbal rings and housed in a water-tight case (Figure 2.1). After

the instrument is lowered to the sea floor, the gravimeter is

levelled automatically and operated by means of a remote control

unit on board the ship. A reliable electrical connection between

the gravity meter and the control unit is important and this is

provided by an armoured 13-wire cable which also supports the

instrument as it is lowered to and raised from the sea floor. A

hydraulic winch (Figure 2.2) provides smooth, positive control

and facilitates safe handling of the gravity meter.

Previous experience with the gravity meter (Goodacre, 1964)

indicates that it provides an observed gravity value accurate to

about ± 0.2 mgal.

2.1.2 Navigation

Horizontal positioning of the ship was accomplished by Decca

navigation supplemented by radar fixes when the ship was sufficiently

close to shore. The Decca receiver measures phase differences be-

Figure 2.1:   The LaCoste and Romberg underwater gravity
               meter ready for lowering to the sea floor.
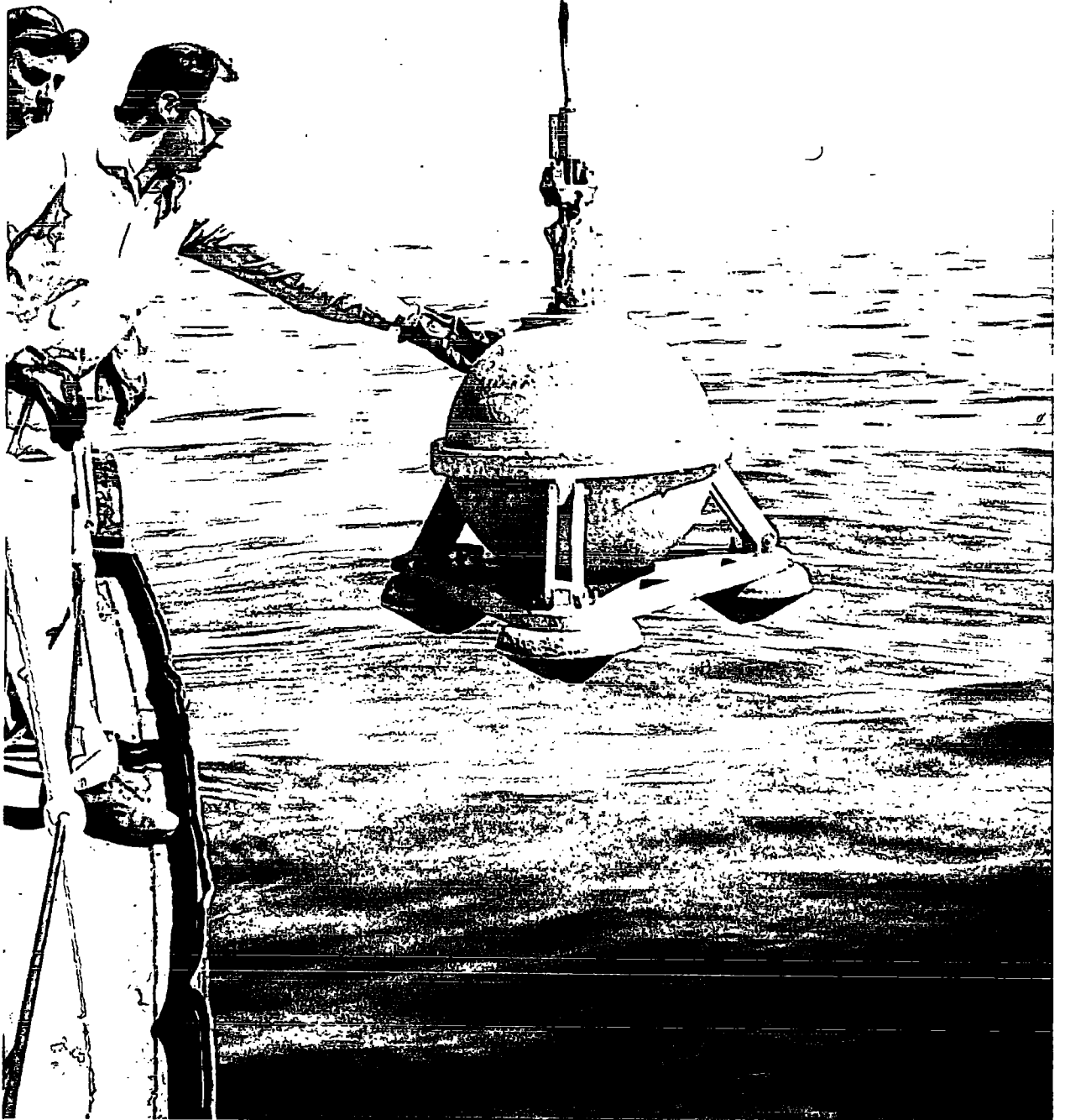
Figure 2.2:   The hydraulic winch wound with armoured

multi-wire cable.
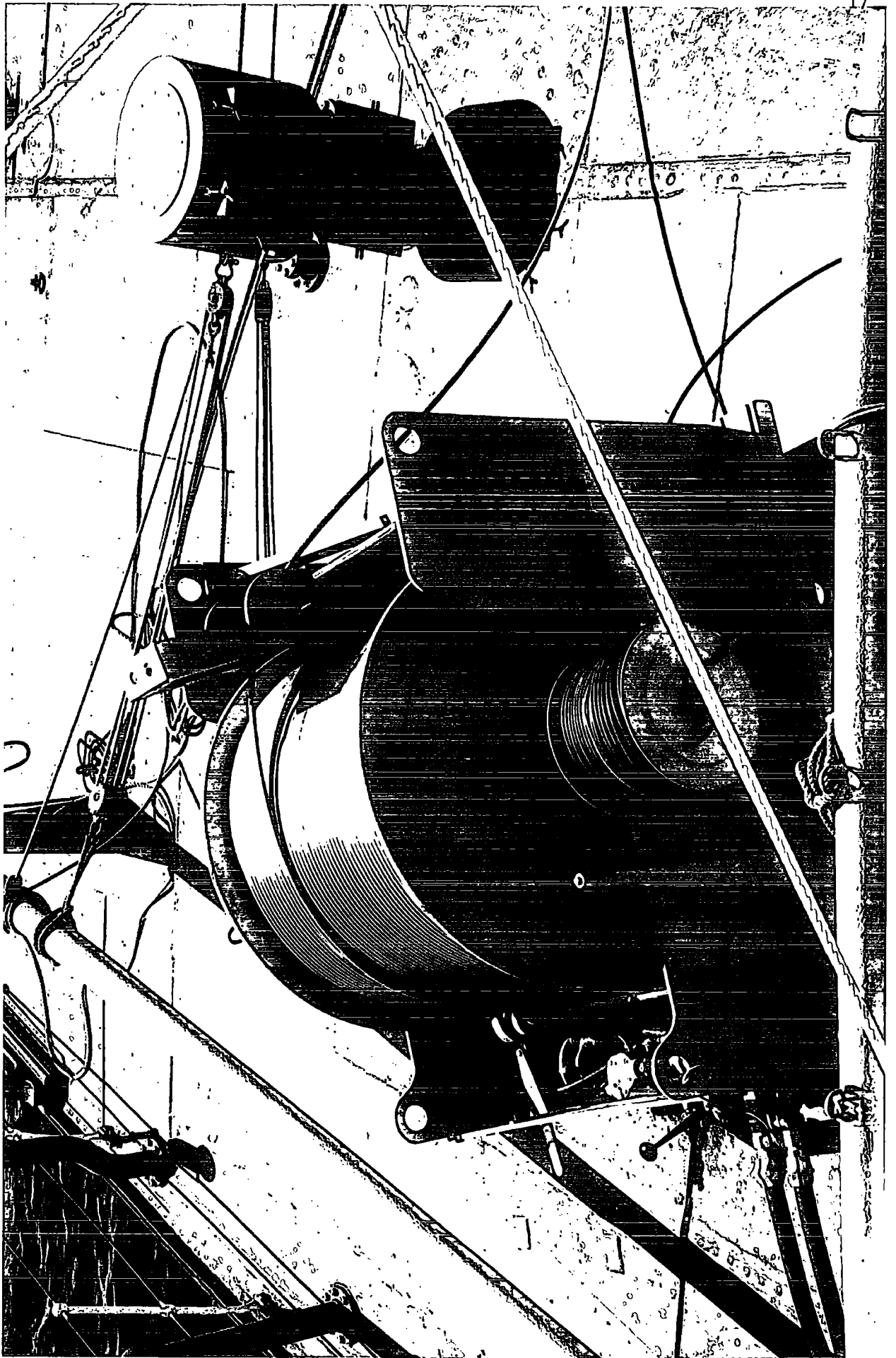
tween signals received from shore-based transmitting stations.
The intersection of lines of constant phase differences defines a
position which is converted to geographical coordinates by means of
charts, or when greater accuracy is required, by digital electronic
computers.

The error in a Decca position depends upon the time of day
when the reading is taken and on the distance between the ship and
the transmitter. Errors are generally greater at night time and in
those areas which are far away from the transmitters. A comparison
of 27 sets of Decca and satellite navigation fixes indicates average
random error in the Decca fixes is about 0.8 km (Goodacre et al.,
1973).

2.1.3. Echo Sounder and Pressure Gauge

The C.N.A.V. Sackville is fitted with a Kelvin-Hughes echo
sounder and a Westrex precision recorder for water depth determin-
ations. The echo sounder is calibrated for a standard speed of
sound in water of 1463 m/s. However the speed of sound in water
varies both in space and time so the harmonic mean speed of sound
was computed from representative velocity-depth data supplied by
the Canadian Oceanographic Data Centre, Department of Energy, Mines
and Resources, Ottawa, and correctons applied to the echo sounder
results. Independent depth measurements were obtained during the
gravity surveys from a Bourns pressure transducer mounted inside
the underwater gravity meter and corrections to the depth readings
were applied using pressure-depth data supplied by the Oceano-

graphic Data Centre.

The two sets of data were compared using the method of least squares and it was found that the echo sounder depth measurements are systematically about 1% shallower than the pressure gauge results and that the standard deviation of a single depth measurement is about ± 5 m (Stephens et al., 1971). No explanation is offered for the systematic discrepancy between the two sets of data but it must be pointed out that it is exceedingly difficult to reduce systematic errors in depth measurement to less than 1% and random errors to less than 2 m.

2.2 THE GRAVITY OBSERVATIONS

Table 2.1 summarizes the cruises made on the C.N.A.V. Sackville. I was in charge of the first cruise in 1970 and took part in planning the remaining two cruises in 1970. R. Cooper and L. Stephens planned and were in charge of the May and September cruises, respectively, in 1971. The three of us participated in preliminary interpretations of the gravity data (Stephens et al., 1971; Goodacre et al., 1973). A more detailed interpretation, including modelling of the geophysical anomalies is presented here.

The regional underwater gravity stations were spaced about 13 km apart on a rectangular grid to provide uniform coverage. When there was sufficient time, detailed traverses were made across interesting gravitational features. During normal operations about 10 to 15 minutes were required to position the ship and obtain a gravity reading and about 40 to 45 minutes were taken to steam between

TABLE 2.1

Summary of the 1970 Underwater Gravity Surveys on the

CNAV Sackville

	Cruise 1	Cruise 2	Cruise 3
Cruise dates	June 8 to June 28	Aug. 5 to Aug. 13	Sept.10 to Sept.30
No. of days at sea	16	8	18
Observers	A.K.Goodacre R.V.Cooper E.S.Wainwright D.M.Ablett	R.V.Cooper L.E.Stephens D.M.Ablett	R.V.Cooper L.E.Stephens J.M.McCance
No. of observations	335	150	207
No. stations per day	21	19	12
Decca chains used	6 and 7	6 and 7	2, 6 and 7

Summary of the 1971 Underwater Gravity Surveys on the

CNAV Sackville

	Cruise 1	Cruise 2
Cruise dates	May 3 to May 28	Sept. 8 to Sept. 28
No. of days at sea	21½	5
Party Chief	R.V.Cooper	L.E.Stephens
Observers	J.Over J. McCance J.Powell	J.Over J.McCance B.Hearty
No. of observations	339	110
No. of stations per day	16	22
Decca chains used	6 and 7	2, 6 and 7

stations; in good weather about 20 to 24 stations were occupied each day. Whenever possible, the gravity meter was read at a land gravity base station or a sea-floor station was occupied in order to determine the instrument's drift rate.

2.3 METHOD OF DATA REDUCTION

The gravity data over the Scotian Shelf are presented in the form of simple Bouguer anomalies (see map in pocket) to make them compatible with the gravity data over the adjacent land areas (Garland, 1953; Weaver, 1967) and the Gulf of St. Lawrence (Goodacre et al., 1969).

To reduce the underwater gravity values to a common datum, the observed gravity readings are extrapolated to the sea surface taking into account the standard free air vertical gradient of gravity and the attraction of the layer of water above the instrument according to the following formula:

$$g_s = g_o \ (1-2 \ d/R) + 4\pi\gamma\rho d$$

$$= (g_o - 0.223d) \ \text{mgal}$$

where g_s is the gravity at the surface   (mgal)

g_o is the observed gravity   (mgal)

d is the water depth   (m)

R is the radius of the earth   (m)

ρ is the density of sea water (gm/cm^3)

and γ is the gravitational constant

Bouguer anomalies are then calculated by adding to the surface gravity value a correction of .069d mgal for the mass deficiency of water with respect to rock of standard density of 2.67 gm/cm^3 and subtracting a theoretical gravity value g_{th} at the station computed from the International Gravity Formula of 1930. The simple Bouguer anomaly is given by

$$\Delta g_{Bouguer} = (g_o - 0.154d - g_{th}) \text{ mgal}$$

and is a function of observed sea bottom gravity, theoretical sea level gravity and a linear correction for water depth.

2.4 SOURCES OF ERROR IN THE BOUGUER ANOMALIES

In areas of rugged underwater topography the approximation of the topographic variations by a plane surface is not adequate and a terrain correction is applied to the "simple" Bouguer anomaly to form a "complete" Bouguer anomaly. I have not made a detailed study of terrain corrections for the Scotian Shelf but previous experience (Goodacre et al., 1969) indicates it is unlikely to exceed about 1 mgal except in the rugged area north of Banquereau.

Marine tides (e.g. Bott, 1961) were not taken into account as they are relatively small (± 1 metre) over the Scotian Shelf and the magnitude of the correction is only about ± 0.2 mgal.

The vertical gradient of gravity may not be constant but experience on the Shipborne Gravimeter Testing Range near Halifax, N.S. (Goodacre, 1964) indicates that the errors in the adopted

vertical gradient due to anomalous mass distributions is probably less than 0.5 mgal if the water depth is less than 300 m, a value greater than any depth observed on the Scotian Shelf.

2.5 ESTIMATES OF SYSTEMATIC AND RANDOM ERRORS IN THE ANOMALIES

Estimates of the magnitude of systematic and random errors in the Bouguer anomalies are summarized in Table 2.2. Systematic errors of up to 1 or 2 mgal may occur in the data particularly where the water is deep and where the stations are far away from the Decca transmitter.

Random errors are estimated to be of the order of 1.3 mgal. Although these errors are caused by an accumulation of errors in: (1) the observed gravity reading, (2) the horizontal position of the gravity meter and (3) the observed water depth, the single most important source of random error in the Bouguer anomaly is in the vertical positioning of the gravity meter, therefore improved resolution and accuracy of depth measurements will pay good dividends.

TABLE 2.2

SUMMARY OF SYSTEMATIC AND RANDOM ERRORS

IN THE BOUGUER ANOMALIES

	Random errors mgal	Systematic errors mgal
Observed gravity	0.2	0.1
Water depth correction	0.7	0.3
Navigation	0.6	1 to 2
Vertical gradient	0.4	
Lack of terrain correction		up to 1
Lack of marine tide correction	0.2	

CHAPTER 3

INTERPRETATION METHODS

3.1 INTRODUCTION

This chapter describes two interpretation methods which have
been used extensively in the study of the geophysical anomalies
on the Scotian Shelf. The first method is combined analysis of
gravity and magnetic data; the second method is the application of
non-linear optimization techniques to modelling gravity, magnetic,
and seismic data. .

3.2 GENERAL REMARKS ABOUT COMBINED ANALYSIS

Combined analysis of geophysical data can give much important
information. For example, if good correlation can be established
between two sets of data in one area, one set of data can then be
used to extrapolate results to an adjacent area where the other
set is not available. Combined analysis of geophysical data also
determines the ratios of physical parameters; these ratios help
to set limits on the possible range of composition of the rocks
that create the geophysical anomalies and significant variations
of these ratios from one area to another indicate that the different
areas show, in one manner or another, significant geological
differences.

An example of the usefulness of combined analysis of geophy-
sical data is that, in the case of gravity and seismic data, the
determination of the ratio of density contrast to velocity contrast
indicates whether the density and velocity variations are due solely
to phase or compositional changes in the subjacent rocks or due to a

combination of these with partial melting (e.g. Goodacre, 1972).
In the case of gravity and magnetic data, determination of the ratio
of the contrast of magnetic moment per unit volume to density
contrast may allow us to set an upper limit to the magnetization
contrast. This is normally difficult to do from magnetic data alone
because magnetization can vary by several orders of magnitude.
Density, on the other hand, varies by less than, say, 25%, in the
crust. Therefore, an estimate of the maximum allowable density
contrast, provides a reasonable upper limit to the magnetization
contrast. This in turn gives us some idea of the magnetite content
of the rock.

However, as mentioned in the introductory chapter, perhaps the
most important aspect of combined analysis of gravity and magnetic
data is that it provides an estimate of the direction of the total
magnetization vector. This plus a knowledge of, or a reasonable
estimate of, the ratio of remanent to induced magnetization (the
Koenigsberger ratio) allows us to estimate the direction of the
remanent magnetization vector and this latter direction, when
considered in conjunction with palaeomagnetic data, provides
information about the geological history of the region studied. An
interesting application of the combined analysis of gravity and
magnetic data is the work of Lundbak (1956) who, as Deutsch (1969)
points out, presented at a meeting in 1952 an "early Palaeozoic"
pole position one or two years before any comparable pole positions
obtained by conventional techniques were published.

There are some problems which combined analysis cannot solve. For example, combined analysis of gravity and magnetic data gives no further information about the magnitude and distribution of anomalous mass or magnetic moment than does an interpretation of either the gravity of the magnetic field alone.

Combined analysis of gravity and magnetic data can be accomplished by Fourier analysis (Cordell and Taylor, 1971) or by solving sets of linear equations; the latter approach is used here. Important aims of the linear analysis presented in this thesis are:

(1) to determine the degree of linear correlation that exists between gravity and magnetic data.

(2) to obtain confidence limits of the various quantities that characterize the relationship and,

(3) to detect situations where the system of equations to be solved is poorly conditioned.

These aims are met by the FORTRAN subroutine MULREG (Appendix 1) which provides the coefficient of multiple correlation between the dependent parameter and the independent paramters and t-values of the regression coefficients. The t-values are closely related to the eigenvalues of the matrix of coefficients of the normal equations (Appendix 2) and the presence of one or more very small t-values in relation to the other t-values indicates an ill-conditioned system of equations. Bott and Hutton (1971) give examples of ill-conditioned systems that arise in studies of magnetic anomalies. Bott (personal communication) finds that problems of ill conditioning are less severe in the analysis of

Figure 3.1 (A) The potential field anomaly due
                 to an anomalous source body.

           (B) An equivalent layer representation
                of the source body showing the
                relationship of the jth prism to the
                i^{th} observation point (solid circle).
                The extra prism to the right of the
                equivalent layer shows how a prism is
                defined by the coordinates U1, U2, V1,
                V2, W1 and W2 (see expression 3.2).

(A)

(B)
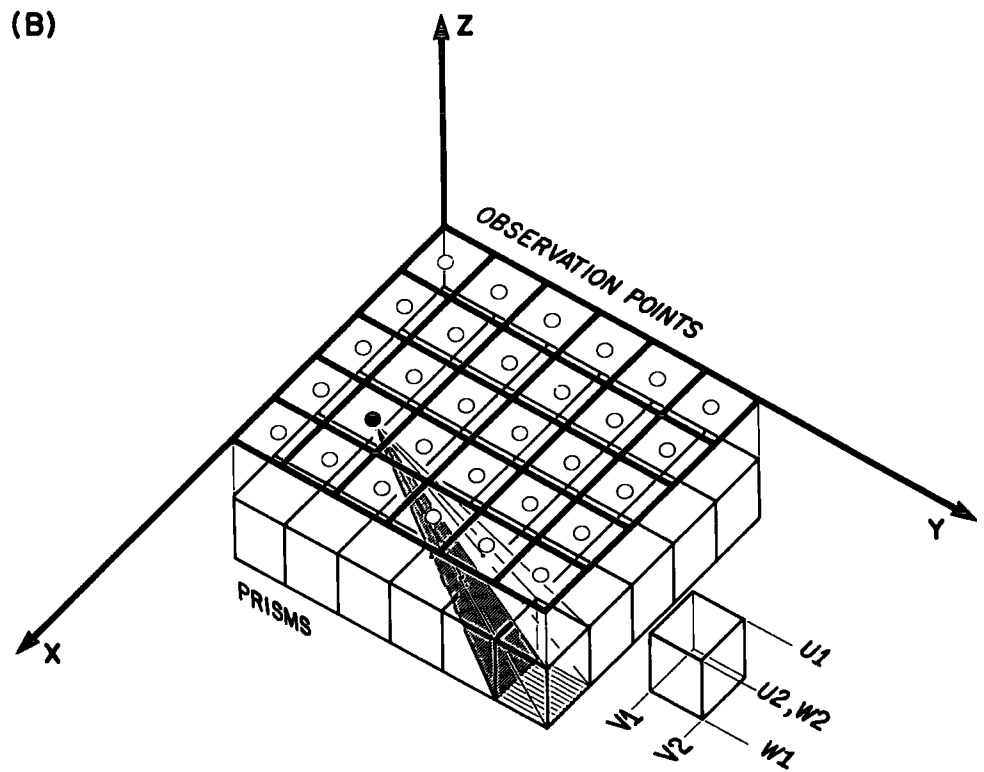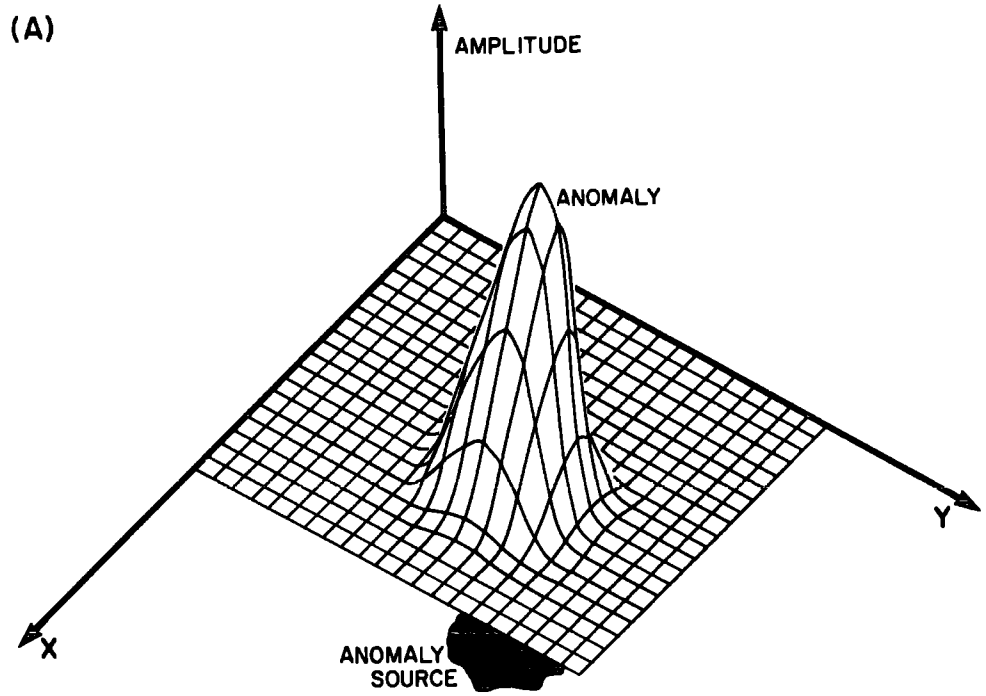
gravity fields than in the study of magnetic fields.

3.3 RELATION OF GRAVITY AND MAGNETIC FIELDS.

If the ratio of magnetic moment per unit volume, m (u,v,w),
to the mass per unit volume, d (u,v,w), has a constant value R,
everywhere throughout a given heterogeneous body (u,v and w are
the bodypoint coordinates) and if the direction of the total
magnetization vector (the vector sum of the permanent and induced
magnetizations) is everywhere the same, the magnetic potential,
V, of a body can be expressed as a linear combination of the three
components G_x, G_y, and G_z of its gravitational attraction:

$$\frac{\gamma}{R} V (x, y, z) = a\, G_x(x, y, z) + b\, G_y(x, y, z) + c\, G_z(x, y, z) + h$$

(3.1)

where a, b and c are the direction cosines defining the

orientation of the total magnetization vector.

h is an additive constant which takes into account

the regional level of the gravity field.

R is the ratio of magnetization contrast to density

contrast.

γ is the gravitational constant.

x, y and z are the field point coordinates.

The component of magnetic attraction in some arbitrary direction,
s, is obtained by taking the directional derivative of V, i.e.
$\frac{\delta V}{\delta s}$; the resulting expression involves nine partial derivatives of
the gravity field, five of which are independent quantities. This

relation was first published by Eotvos (1906) based on a memoir by
Poisson (1826) and the above conditions are referred to as the
"Poisson conditions" (e.g. Bott and Ingles, 1973). Although some
authors (Baranov, 1957 and Bott et al., 1966) recognise that
Poisson's relation holds for heterogeneous bodies, others (Garland,
1951 and Cordell and Taylor, 1971) restrict its application to
homogeneous bodies. The fact that the relation holds for hetero-
geneous bodies renders it more useful in practice than if it applied
solely to homogeneous ones but the important question is whether the
Poisson conditions hold throughout the geological structure under
investigation.

Equation 3.1 indicates that if we know the gravity and magnetic
fields at a sufficient number of points we can determine the ratio
R, the direction cosines a, b and c and the additive constant h.
Conversely, if we know (or assume) the values of R, a, b, c and h
we can calculate the magnetic field from the derivatives of the
three components of the gravity field and vice versa. The main
problems in performing these calculations are to obtain the
required components of the gravity field from the observed data and
to compute the required derivatives. A method and its theoretical
justification was published by Baranov (1953) and used by Lundbak
(1956). Two methods which circumvent some of the computational
difficulties in Baranov's method involve either Fourier analysis
of the gravity and magnetic fields (Cordell and Taylor, 1971) or
the representation of the gravity and magnetic fields by means of
an equivalent layer of rectangular blocks which have appropriate

values of density and magnetization (Bott and Ingles, 1973).

The theoretical basis for the transformations described above is that if it is possible to suitably reproduce one component of a gravity (or magnetic) field by sets of functions that satisfy Laplace's equation such as those of the form of

$$\sin [\, jx \,] \, . \, \sin [\, ky \,] \, . \, e^{-(j^2 + k^2)^{\frac{1}{2}} z}$$

$$\text{or} \quad \ln [\, x + (x^2 + y^2 + z^2)^{\frac{1}{2}} \,] + \ln [\, y + (x^2 + y^2 + z^2)^{\frac{1}{2}} \,]$$

$$+ \arctan \left[\frac{xy}{z \, (x^2 + y^2 + z^2)^{\frac{1}{2}}} \right], \text{ etc.}$$

then, by suitable integration and differentiation of these functions, we can specify analytically

(i) the gravity (or magnetic) potential

(ii) other components of the gravity (or magnetic) field

(iii) derivatives of these components

Once these are obtained, we can calculate the pseudo-magnetic (or pseudo-gravity) anomaly. Mathematically, it is probably easier to understand the process via Fourier analysis (Cordell and Taylor, 1971) but physically, it seems easier to visualize the transformation using the equivalent layer method (Bott and Ingles, 1973). Bott and Ingles (1973) apply the equivalent layer method to gravity and magnetic profiles; I make the straightforward extension to areally distributed data.

3.4 DESCRIPTION OF THE METHOD

The ratio of magnetic moment to mass and the direction of the
total magnetization vector can be computed either by

(1) transforming the observed gravity anomaly into three
separate magnetic anomalies in the measured direction for three
orthogonal directions of magnetization then determining the
proportions of each of the three computed magnetic anomalies required
to reproduce the observed magnetic field; or by the reverse
procedure of

(2) transforming the observed magnetic anomaly into separate
gravity anomalies corresponding to each of three orthogonal
directions of the total magnetization vector and determining the
proportions of each of the three computed gravity anomalies
required to reproduce the observed gravity anomaly.

In the first case the direction and magnitude of the total
magnetization vector can be found because the observed magnetic
field can be regarded as a linear combination of three partial
magnetic anomalies due, respectively, to three orthogonal components
of the total magnetization vector and the required combination is
obtained by a least-square fit of the three calculated anomalies to
the observed anomaly. In the second case, each set of blocks
magnetized in each of the three orthogonal directions of magnetiz-
ation reproduces the magnetic anomaly, therefore any linear combina-
tion of the three sets of magnetized blocks will also reproduce
the magnetic anomaly. The proportion required of each set is
determined by the linear combination of the three corresponding sets

of gravitating blocks needed to produce a set of blocks which will closely reproduce the observed gravity anomaly. However, rather than work with the derived quantity of density, I prefer to work directly with the gravity anomaly.

To perform the calculation in the first case we:

(i) approximate the source that produces the observed gravity anomaly by an equivalent layer of rectangular prisms (Figure 3.1). The number of blocks, M, must be at least one less than the number of gravity observations, N.

(ii) calculate the gravitational attractions, a_{ij}, of each prism at each gravity observation point; a_{ij} is the attraction of the jth block at the ith observation point and this value is calculated using the following expression for a homogeneous rectangular prism (e.g. Goodacre, 1973):

$$a_{ij} = -d_j\gamma \; \left|\left|\left| \begin{array}{l} u \ln (v + r) + v \ln (u + r) \\[2mm] -w \arctan \dfrac{uv}{wr} \end{array} \right|_{x-u_1}^{x-u_2} \right|_{y-v_1}^{y-v_2} \right|_{z-w_1}^{z-w_2} \qquad (3.2)$$

where x, y, z are the coordinates of the ith observation point

(u_1, v_1, w_1), (u_2, v_1, w_1), (u_1, v_2, w_1) etc. define the corners of the jth prism

$r = (u^2 + v^2 + w^2)^{\frac{1}{2}}$

d_j is the density of the prism

γ is the gravitational constant

z is positive upwards

(iii) compute the prism density contrast values d_1, d_2 ...., d_M

that render the quantity $\|A\underline{d} - \underline{g}\|$ at least-squares minimum

where A is the N by M + 1 matrix composed of the elements

a_{ij} and a column vector whose elements are unity.

$\underline{d}$ is the vector of density values

$\underline{g}$ is the vector of observed gravity values

and the double bars indicate the norm or length of

the error vector.

The least squares minimization is achieved in the usual way by

solving the following matrix equation (Draper and Smith, 1966)

$$\underline{d} = (A^TA)^{-1} A^T \underline{g}$$

to find $\underline{d}$. A column vector whose elements are unity is added to the

matrix A to take into account any arbitrary constant regional level

present in the observed gravity data. In practice, the matrix

product A^TA is not inverted directly and some computational method

designed to minimize effects of ill-conditioning is used (e.g.

Anderssen,1969) to solve the equations. The procedure used here

is the Modified Doolittle Method of Gaussian elimination (Goulden,

1952) which takes advantage of the fact that the matrix A^TA is

symmetric. The IBM subroutine LLSQ, based on the Householder Method

(Golub, 1965) may also be used but provision must be made to solve

for an additive constant (e.g. h in expression 3.1). This is readily

done by adding a column of 1's to the matrix of observation equations

and solving for the additional unknown which is a constant multiplier.

In practice the Modified Doolittle Method and the modified version

of LLSQ give results which are the same to several significant figures.

(iv) Calculate, at each magnetic observation point, three sets of magnetic anomalies of the set of prisms for three orthogonal directions of the total magnetization vector where the magnetization contrast of each prism is numerically equal to its calculated density contrast; $\underline{b1}$ is the vector of values of length N corresponding to the first orthogonal direction, etc. The value of N may, in general, be different from that given in Section (iii).

An individual value of magnetic anomaly, $b1_{ij}$, of the jth prism at the ith observation point is given by:

$$
\begin{aligned}
b1_{ij} = \frac{-m_j}{d_j \gamma} \Bigg[& m_3 \left(f_1 \frac{\delta^G z}{\delta x} + f_2 \frac{\delta^G z}{\delta y} + f_3 \frac{\delta^G z}{\delta z} \right) \\
+ & m_1 \left(f_2 \frac{\delta^G x}{\delta y} + f_3 \frac{\delta^G x}{\delta z} + f_1 \frac{\delta^G x}{\delta x} \right) \\
+ & m_2 \left(f_3 \frac{\delta^G y}{\delta z} + f_1 \frac{\delta^G y}{\delta x} + f_2 \frac{\delta^G y}{\delta y} \right) \Bigg]
\end{aligned}
\tag{3.3}
$$

where m_j is the intensity of magnetization of the prism

d_j is the density of the prism

γ is the gravitational constant

m_1, m_2, m_3, are the direction cosines of the first, second or third orthogonal component of magnetization

f_1, f_2, f_3 are the direction cosines of the component of magnetic field being observed. (Throughout the

thesis these are specified by the direction of the earth's field since total magnetic field anomalies are considered).

The derivatives are given by the following expressions:

$$\frac{\delta G_z}{\delta x} = - d_j \gamma \left|\left|\left| \ln (v + r) \right.\right.\right. \begin{vmatrix} x -u_2 \\ x -u_1 \end{vmatrix} \begin{vmatrix} y -v_2 \\ y -v_1 \end{vmatrix} \begin{vmatrix} z -w_2 \\ z -w_1 \end{vmatrix}$$

$$\frac{\delta G_z}{\delta y} = - d_j \gamma \left|\left|\left| \ln (v + r) \right.\right.\right. \begin{vmatrix} x -u_2 \\ x -u_1 \end{vmatrix} \begin{vmatrix} y -v_2 \\ y -v_1 \end{vmatrix} \begin{vmatrix} z -w_2 \\ z -w_1 \end{vmatrix}$$

$$\frac{\delta G_z}{\delta z} = - d_j \gamma \left|\left|\left| \arctan \frac{uv}{wr} \right.\right.\right. \begin{vmatrix} x -u_2 \\ x -u_1 \end{vmatrix} \begin{vmatrix} y -v_2 \\ y -v_1 \end{vmatrix} \begin{vmatrix} z -w_2 \\ z -w_1 \end{vmatrix}$$

Expressions for the other derivatives are obtained by cyclic permutation of the field and body coordinate parameters.

As is the case for expression (3.2):

x, y, z, are the coordinates of the ith observation point

$r = (u^2 + v^2 + w^2)^{\frac{1}{2}}$

and (u_1, v_1, w_1), (u_2, v_1, w_1), (u_1, v_2, w_1) etc.

define the corners of the jth prism.

(v) Compute the vector $\underline{c}$ of coefficients which renders the quantity $\left|\left| B\underline{c} - \underline{m} \right|\right|$ a least-squares minimum

where B is the N by 4 matrix composed of the column vectors $\underline{b1}$, $\underline{b2}$ and $\underline{b3}$ and a column vector whose elements are unity. This latter vector allows

for a constant regional level of the

magnetic field.

$\underline{c}$ is the vector of coefficients c1, c2, c3.

$\underline{m}$ is the vector of observed magnetic anomalies.

The ratio of magnetization contrast to density contrast, R, is

given by the length of the vector $\underline{c}$, i.e.:

$$R = (c1^2 + c2^2 + c3^2)^{\frac{1}{2}}$$

and the x, y, and z-direction cosines of the total magnetization

vector are given by c1/R, c2/R, c3/R respectively. From these

the inclination, INC1, and the azimuth, AZI1, of the total

magnetization vector are given by:

$$INC1 = \arcsin (c3/R)$$

$$AZI1 = \arctan (c2/c1)$$

To perform the calculation in the second case we:

(i) Approximate the source of the magnetic anomalies by an

equivalent layer of blocks whose number, M, is at least one less

than the number of magnetic observations, N.

(ii) Compute the magnetic attractions of each block at each

magnetic observation point for the first of the three orthogonal

directions of total magnetization; p_{ij} is the attraction of

the jth block at the ith observation point calculated for the

first orthogonal direction of the total magnetization, etc.

(iii) Determine the vector of magnetization contrast values

that renders the quantity

$$\| P \underline{m1} - \underline{h} \| \quad \text{a least-squares minimum}$$

where P is the N by (M + 1) matrix of coefficients p_{ij} and a

column vector whose elements are unity. As before, this latter

vector takes into account a constant regional background:

ml is the vector of magnetization contrast

corresponding to the first orthogonal direction

of the total magnetization vector.

h is the vector of observed magnetic anomaly values.

(iv) Repeat (ii) and (iii) for the other two orthogonal directions

of magnetization to obtain m2 and m3.

(v) Calculate at each gravity observation point, three sets of

gravitational attractions produced by the equivalent layer of

prisms whose density values are numerically equal to the

corresponding three sets of magnetization contrasts ml, m2 and

m3; sl is the vector of gravity values corresponding to the first

orthogonal direction etc.

(vi) Determine the vector t of coefficients which renders the

quantity.

$$\| St - g \|$$ a least-squares minimum.

where S is the N by 4 matrix composed of column

vectors sl, s2 and s3 and a column vector whose

elements are unity.

As before this latter vector allows for a constant regional gravity

anomaly. The ratio of density contrast to magnetization contrast

Q is given by:

$$Q = (t1^2 + t2^2 + t3^2)^{\frac{1}{2}}$$

and the x, y and z-direction cosines of the total magnetization

vector are t1/Q, t2/Q and t3/Q respectively. The inclination,

INC2, and the azimuth, AZI2, are given by:

$$INC2 = \arcsin\ (t3/Q)$$

$$AZI2 = \arctan\ (t2/t1)$$

The subroutine MULREG provides the standard errors of the

quantities c1, c2, c3 and t1, t2, and t3. These are used to

calculate the standard errors in R, INC1, AZI1 and Q, INC2

AZI2 respectively.

Appendix 1 documents a FORTRAN main program MGTRAN and

companion subroutines COEFF, CG3D, MULREG and POLE which perform

the required calculations and provide numerical values and

standard errors of the inclination and azimuth of the total

magnetization vector and the ratio of magnetic moment to mass.

The program also gives the virtual magnetic north pole which

is consistent with the direction of the total magnetization vector

under the somewhat unrealistic but simple assumption that there is

no induced magnetization in the anomaly source.

3.5 DISCUSSION OF THE PROGRAM MGTRAN

3.5.1 Possible uncertainties in the representation of gravity and magnetic fields

In the second case discussed in section 3.4, the transform-

ation of a magnetic field to a gravity field depends upon the

assumption that an equivalent layer, magnetized in a uniform

direction, can reproduce an observed magnetic field no matter what

direction of magnetization is assumed. I know of no theoretical

justification for this but in practice this assumption is almost

always justified. Of course, in the special case where the

number of field point observations is equal to the number of

unknown magnetizations (plus the additive constant), an exact

fit can always be obtained as long as no singularity is present.

Occasionally, when there are more equations than unknowns, a good

fit can not be obtained for certain directions of magnetization.

As yet, no consistent pattern has emerged to indicate why. It

is probably related to the observation point – equivalent source

layer geometry and the angle of magnetization.

It is interesting to note that the assumption implies a

certain non-uniqueness in the source causing a magnetic field. For

example, the magnetic field due to a homogeneous body magnetized

in a uniform direction can be duplicated by an equivalent surface

layer of material magnetized in the same direction but in which

the intensity of magnetization varies in some suitable manner.

If another equivalent layer magnetized in a second, different,

direction can also reproduce the magnetic anomaly then there must

be a second, probably inhomogeneous, body magnetized in this

second direction which generates the same anomaly as the original

homogeneous, uniformly magnetized body. In general, if this

assumption is correct, there must be an infinite number of source

bodies, each magnetized in a different direction, that can

produce the same magnetic anomaly. One result of this is that the

direction of magnetization in a body can not be determined from the magnetic anomaly unless some restriction such as homogeneity is applied.

The non-uniqueness concerning the magnetic field transfers to the gravity field because a gravity anomaly can be associated with the source producing the magnetic anomaly through the application of expression 3.1. There should, therefore,be an infinite class of heterogeneous mass distributions each of which produces the same gravity anomaly as the original homogeneous body.

It is also worthwhile to point out that in the transformation of a gravity field to a magnetic field the generation of a good, or possibly an exact, approximation of a field at only a finite number of points is no guarantee of a good approximation of the derivatives of the field. To illustrate by means of a simple example, the gravity fields due to the infinite horizontal cylinder and prism shown in Figure 3.2 are coincident at the four locations $x = \pm 1.5$ km and $x = \pm 5.9$ km (see downward pointing arrows in Figure 3.2). Although in this case the vertical derivatives of the gravity field, $\dfrac{\delta^G z}{\delta z}$ are the same at these points, the horizontal derivatives, $\dfrac{\delta^G z}{\delta z}$ differ by 30%. This means that we might exactly represent, at four points, the gravity field due to the cylinder by the rectangular prism but we can not generate the correct magnetic anomaly because the horizontal derivatives are incorrect. The effect of this error is to give incorrect values of the direction of the total magnetization vector and of the ratio of magnetic moment to mass. Nevertheless, in practice, gravity

Figure 3.2: The gravitational attractions, and the

vertical and horizontal derivatives of these

attractions, of an infinite horizontal cylinder

and an infinite prism chosen to produce

approximately the same observed anomaly.
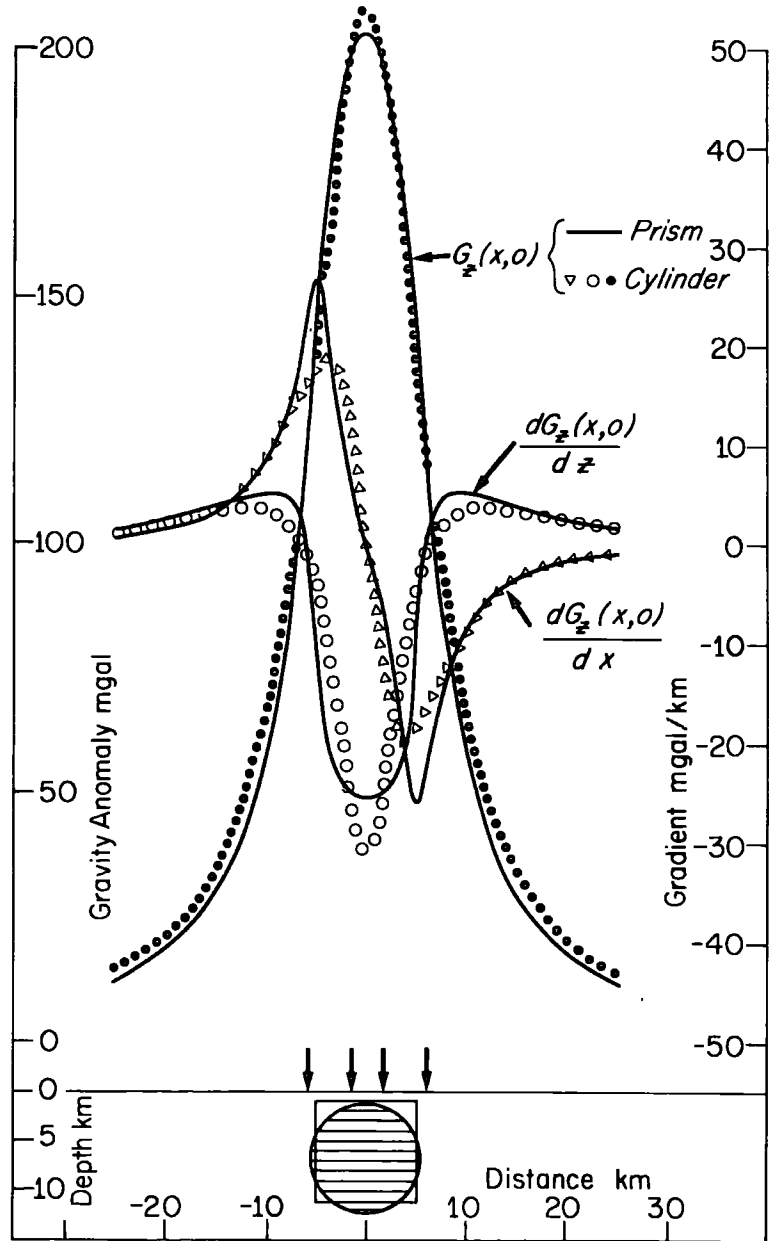
and magnetic fields are usually sufficiently well behaved and an
adequate number of blocks can be used to form the equivalent layer
of magnetic, gravitating matter that we can generate sufficiently
good approximations to the gravity and magnetic fields and their
derivatives. In this connection the equivalent layer of blocks
should not be too shallow or too deep. A depth equal to one or
two times the mean horizontal station spacing is usually
satisfactory (Bott, personal communication).

As in any interpretation method it is, of course, mandatory
that the anomaly observation points are sufficient in number and
properly placed to adequately delineate the gravity and magnetic
fields and it is also necessary to ensure that each system of
linear equations to be solved is linearly independent and
reasonably well conditioned through the proper placement of the
blocks forming the equivalent layer relative to the data points.

3.5.2 Background levels

As mentioned in Section 3.4, a constant regional anomaly
is allowed for when using an equivalent layer to represent a
gravity or magnetic field. It is important to do this otherwise
difficulties with "end-effects" will arise. For example, if
the regional level of the gravity field is +50 mgal and this
value is not removed from the data, it is impossible, with a
finite number of source bodies to generate an abrupt step from
0 to +50 mgal in the calculated gravity field at the boundaries
of the observed data. This problem and its effect is analogous

to Gibb's phenomenon in the Fourier series representation of a discontinuity in a function.

A small constant error in the background level of the gravity field is not serious in the transformation of a gravity field to a magnetic field because the error does not contribute to the horizontal derivatives of the gravity field. An unrecognised sloping regional gravity field will introduce some systematic error, however.

An incorrect background level of the magnetic field may also create a systematic error in the results because, if the background level is incorrect, an additional, unwanted distribution of magnetization is required when magnetic fields are generated for the three orthogonal directions of the total magnetization vector. The result of this is that each of the three vector components may be either greater or less in magnitude than it should be so that the resultant vector lies in the wrong direction, and its length, which determines the ratio of magnetic moment to mass, is too long or too short.

3.5.3   The effect of basement magnetization

As Bott (personal communication) has pointed out, the direction of total magnetization obtained from the combined analysis of gravity and magnetic anomalies is the vector difference between the direction of total magnetization in the anomalous source and the direction of total magnetization in the surrounding medium. It is readily seen that, if the total magnetization vectors in the source and in the surrounding medium have approximately the same magnitude but differ

slightly in direction, the resultant vector difference will exhibit

a small magnitude and be oriented in a direction that is significantly

different from the direction of total magnetization in the source.

On the other hand, if the magnitude of the total magnetization vector

in the surrounding medium is, say, a factor of ten smaller than the

total magnetization vector in the anomalous source, the resultant

difference vector will be similar in direction and magnitude to the

total magnetization vector in the source. As will be discussed later,

some situations are found over the Scotian Shelf where the calculated

direction of total magnetization is nearly at right angles to the

earth's field and this might be due to the effect of basement magne-

tization but in most of these cases the inferred geological situation

suggests that the magnetization of the source is significantly higher

than the magnetization of the adjacent rocks. It is implicit,

therefore, in the application of the program MGTRAN that the effect

of basement magnetization can be neglected.

3.5.4   Features of the program

        The program MGTRAN has the important features that it can be

applied to irregularly spaced gravity and magnetic observations and

that the gravity and magnetic observations need not be coincident.

Some computing time can be saved, however, if the observations

are coincident.   In the special case where the observational data

are regularly spaced and coincident,   the various inverse mat-

rices required in the transformation of the fields,   etc.

need to be computed only once and can then be applied repeatedly to different sets of input data. I have not considered this special case but the step from the program given here is straightforward.

3.6 TESTS OF THE PROGRAM MGTRAN ON MODELS

The program MGTRAN has been tested on gravity and magnetic fields produced by simple models (see Table 3.1 for their description); most models obey Poisson's conditions but two do not. Models 1 to 5 obey Poisson's conditions and are homogeneous cubes whose sides are 1 km in length and whose centres lie either 1 or 2 km below the observation plane. Models 6, 7 and 8 are physically the same and consist of four prisms of different sizes. Model 6 satisfies Poisson's conditions but 7 and 8 do not. In model 7 all prisms are homogeneous and magnetized in the same direction but the ratio of magnetization contrast to density contrast ranges from 0.01 to 0.1 emu/gm. In model 8 all prisms are homogeneous and have the same ratio of magnetization contrast to density contrast (0.01 emu/gm) but the direction of magnetization varies from one prism to another.

For trials 3 to 26, the observation points were spaced 1 km apart on a square grid. For some trials the equivalent layer prisms were centered beneath the observation points whereas for the other trials they lay in between. The equivalent layer parameters are given in Table 3.2.

Those trials (3, 21, 6, 12, 9 and 23) that exhibit a high degree of correlation ($r^2 = 0.9$) between observed and computed

TABLE 3.1
Model Parameters

Model	Coordinates of centre of cube x-km	y-km	z-km	Magnetization direction azimuth°	inclination°	Magnetization contrast emu/cm^3	Density contrast gm/cm^3
1	3.5	3.5	1.0	180.0	-30.0	.001	.1
2	4.0	4.0	1.0	180.0	-30.0	.001	.1
3	3.5	3.5	2.0	180.0	-30.0	.001	.1
4	3.5	3.5	2.0	-5.0	54.0	.001	.1
5	4.0	4.0	1.0	65.0	0.0	.001	.1
6a	4.0	4.0	1.0	-60.0	45.0	.001	-.1
6b	4.0	5.0	2.0	-60.0	45.0	.003	.3
6c	2.0	4.0	2.6	-60.0	45.0	.0001	.01
6d	6.5	5.5	0.6	-60.0	45.0	-.0005	-.05
7a	as for model 6			as for model 6		-.001	-.1
7b						.003	.3
7c						.0001	.01
7d						-.005	-.05
8a	as for model 6			45.0	-60.0	as for model 6	
8b				-10.0	0.0		
8c				80.0	-30.0		
8d				45.0	30.0		

Note: each cube is 1 km long, 1 km wide and 1 km deep and azimuth
and inclination of applied field are -25° and 75° respectively

TABLE 3.2

EQUIVALENT LAYER PARAMETERS

Trial	Length km	Width km	Thickness km	Depth of upper surface km	Reln. of equiv. source prisms to obs. pts.
3	1.	1.	.1	1.	IB
6	1.	1.	.1	1.	IB
9	1.	1.	.1	1.	IB
12	1.	1.	.1	1.	CB
13	.1	.1	.1	1.	CB
15	.1	.1	.1	1.	IB
19	1.	1.	.1	.1	CB
20	1.	1.	.1	.1	CB
21	1.	1.	.1	.1	CB
25	1.	1.	.1	.1	CB
26	1.	1.	.1	.1	CB

Dimensions refer to individual prisms; 36 prisms used in each trial except Trial 21 where 9 prisms were used.

IB – in between   CB – centered beneath

TABLE 3.3

TESTS OF PROGRAM MCTRAN

Trial	Model	Model Values Direction of Magnetization Vector AZ°	IN°	M/ρ emu/gm	NO	NP	Magnetic to Gravity trans. Direction of Magnetization Vector AZ°	IN°	ρ/M gm/emu	r²	Gravity to Magnetic trans. Direction of Magnetization Vector AZ°	IN°	M/ρ emu/gm	r²	Loca. of equiv. source prisms to obs. pts.
3	1	180.	-30.	.0100	49	36	180. (2.7)	-34.6 (5.0)	87.7 (6.5)	.926	180. (0.7)	-27.6 (1.1)	.0109 (.0002)	.995	IB
21	2	180.	-30.	.0100	49	9	-180. (2.4)	-67.8 (4.0)	117. (9.1)	.903	179. (204.)	-24.4 (1.4)	.0136 (.0005)	.982	CB
6	3	180.	-30.	.0100	49	36	177. (2.1)	-38.4 (2.7)	95.2 (4.5)	.974	180. (0.8)	-30.9 (1.1)	.0097 (.0002)	.994	IB
12	3	180.	-30.	.0100	49	36	-167. (7.1)	-63.1 (5.8)	116. (14.4)	.709	180. (0.9)	-29.2 (1.2)	.0102 (.0002)	.993	CB
9	4	-5.	54.	.00258	49	36	-5.4 (2.9)	64.8 (1.5)	355. (13.8)	.978	-5.1 (1.3)	55.3 (0.6)	.00265 (.00005)	.995	IB
15	6	-60.	45.	.0100	49	36	-104. (118.)	77.5 (9.5)	55.3 (11.0)	.543	-71.6 (84.7)	67.9 (10.1)	.00748 (.00184)	.504	IB
13	6	-60.	45.	.0100	49	36	-83.8 (103.)	75.8 (9.9)	68.0 (12.2)	.473	-67.0 (29.7)	24.4 (10.6)	.0136 (.0030)	.552	CB
19	6	-60.	45.	.0100	49	36	-78.2 (78.4)	79.5 (15.3)	61.3 (16.5)	.249	-76.8 (56.8)	12.8 (15.8)	.0210 (.0053)	.407	CB
20	6	-60.	45.	.0100	49	36	-31.1 (4.1)*	48.5 (12.6)*	106 (24.8)	.506	-47.2 (21.5)*	11.9 (12.7)*	.0210 (.0053)	.407	CB
23	5	65.	0.	.0100	49	36	90.9 (29.6)	4.4 (186.)	58.4 (15.8)	.703	65.5 (3.9)	-6.5 (458)	.0140. (.0005)	.975	CB
25	7	60.	45.	--	49	36	99.4 (145.)	79.9 (17.1)	6.4 (1.9)	.276	58.9 (31.6)	20.3 (16.)	.1040 (.0414)	.311	CB
26	8	--	--	.0100	49	36	89.8 (1680.)	78.4. (31.9)	27.3 (15.4)	.070	33.1 (47.5)	35.9 (18.1)	.0079 (.0060)	.157	CB

AZ - azimuth   IN - inclination   M - magnetization contrast   ρ - density contrast

NO - number of gravity or magnetic observations   NP - number of equivalent source prisms

r² - multiple correlation coefficient squared

( ) - standard deviation of quantity

* - value refers to direction obtained in rotated co-ordinate system

IB - in between   CB - centered beneath

Note: Azimuth and inclination of applied field are -25° and 75° respectively

gravity or magnetic fields (Table 3.1) generally give good results

which exhibit small scatter (as indicated by the standard deviations

of the angles and ratios given in brackets in Table 3.3) and are

close to the model values. For example the gravity to magnetic

transformation specifies the direction of magnetization to within

about 5 degrees and the ratio of magnetization contrast to density

constrast to within 40 per cent and often to within 10 per cent.*

Those trials which exhibit a low degree of correlation (15, 13, 19

and 20) give poor results.** Trials 3, 21, 6 and 12 indicate that

in the case of the gravity to magnetic transformation there is not

much difference between the results where the equivalent source

bodies are situated below and in between the data observation

points (trials 3 and 6) or directly beneath the data points

(trials 12 and 21) but in the case of the magnetic to gravity

transformation there are significant systematic errors in the

inclination values of trials 12 and 21. The gravity to magnetic

transformation therefore appears to be less sensitive to

observation point-equivalent source prism geometry than does the

reverse transformation.

The results of a potential field transformation should be

independent of the orientation of the system of the three

orthogonal components of magnetization used to describe the total

magnetization vector. Trials 19 and 20 and others not given in

Table 3.3 suggest that the gravity to magnetic field trans-

formation satisfies this criterion better than the magnetic to

gravity field transformation does.

* Better results, obtained with deeper equivalent layers, are given in
  Table 3.4.

** These are discussed further on page 54.

As might be expected, the program MGTRAN does not give meaningful results when the models do not satisfy the Poisson conditions. Trial 26 (using model 8 where each prism is magnetized in a different direction) gives very poor correlation between observed and computed fields. The result of trial 25 (using model 7 where each prism has a different intensity of magnetization) is dominated by the prism which has the highest ratio of magnetization to density contrast (0.1 emu/gm) since the calculated ratio of magnetization contrast to density contrast is 0.104 emu/gm and the direction of magnetization is reasonably close to that used for the model. Although more tests are required to demonstrate it, trials 25 and 26 suggest the procedure deteriorates more rapidly if the direction of magnetization in the same source body is not constant than if the ratio of magnetization contrast to density contrast is not uniform.

One aspect of Table 3.3 which remains unexplained is the set of poor results for trials 13, 15, 19 and 20. The reason for the poor correlation between observed and computed potential fields in these trials might be due to some unfavourable aspect of the direction of magnetization used for model 6 as this parameter differs from the directions used in models 1 through 5. Bott and Ingles (1973) point out that difficulties can arise in the transformation of two-dimensional anomalies for certain angles of magnetization and special cases of observation point-equivalent source prism geometry. Similar problems may arise in the transformation of areally distributed data but I have found no

theoretical examples. Alternatively, the poor correlation may be due to some difficulty in the observation point-equivalent source prism geometry. In order to try to find out the reason for the poor results of trials 13 to 20, further tests of the program MGTRAN were carried out using, as a source, a single prism 10 km long, 10 km wide and 5 km thick to generate gravity and magnetic anomalies over a square array of 100 observation points spaced 5 km apart. A square array of 49 equivalent source prisms spaced 5 km apart was used to approximate the gravity and magnetic fields. The depth and thickness of the equivalent source prisms and their horizontal positions with respect to the observation points were varied for the set of trials 61 to 77 in which the azimuth and inclination of the total magnetization vector were held at -60° and 45° respectively (the same as in trials 13 to 20). Trials 78 to 84 were done using various directions of magnetization.

Only the gravity to magnetic field transformation was considered during these further tests because of the undesirable sensitivity of the magnetic to gravity field transformation to a rotation of the system or orthogonal magnetization vectors and the generally poorer performance of the magnetic to gravity field transformation. The main conclusions from trials 61 to 77 (Table 3.4) are that the tops of the equivalent layer must lie at a depth equal to 1 to 2 times the station spacing and that the thickness of the equivalent layer is not critical. If the equivalent layer is too close to the surface (e.g. trials 61 to 66), large systematic errors occur and the results are sensitive to

TABLE 3.4

FURTHER TESTS OF MGTRAN (GRAVITY TO MAGNETIC FIELD TRANSFORMATION)

TRIAL	MODEL PARAMETERS			CALCULATED VALUES				EQUIV. SOURCE PRISMS		
	AZ deg	IN deg	M/ρ emu/gm	AZ deg	IN deg	M/ρ emu/gm	r^2	depth km	thick. km	locn.
61	-60.0	45.0	.0100	-67.9 (1.7)	64.5 (2.3)	.0077 (.0001)	.98	0.1	10.0	IB
62	-60.0	45.0	.0100	-58.1 (0.3)	36.2 (0.2)	.0120 (.0000)	.97	0.1	10.0	CB
65	-60.0	45.0	.0100	-57.4 (1.8)	29.1 (0.8)	.0139 (.0003)	.96	1.0	1.0	CB
66	-60.0	45.0	.0100	-58.3 (1.5)	37.3 (0.9)	.0111 (.0002)	.98	2.0	1.0	CB
67	-60.0	45.0	.0100	-59.4 (1.2)	42.6 (0.9)	.0103 (.0001)	.98	4.0	1.0	CB
68	-60.0	45.0	.0100	-60.3 (1.3)	43.4 (0.9)	.0102 (.0001)	.98	8.0	1.0	CB
69	-60.0	45.0	.0100	-59.2 (1.4)	43.1 (1.0)	.0101 (.0002)	.98	16.0	1.0	CB
70	-60.0	45.0	.0100	-58.8 (1.4)	39.9 (0.9)	.0109 (.0002)	.98	1.0	10.0	CB

cont'd

71	-60.0	45.0	.0100	-59.5 (1.5)	42.0 (1.0)	.0105 (.0002)	.98	2.0	10.0	CB
72	-60.0	45.0	.0100	-60.3 (1.6)	43.1 (1.1)	.0102 (.0002)	.98	4.0	10.0	CB
73	-60.0	45.0	.0100	-60.2 (1.1)	43.4 (0.8)	.0102 (.0001)	.98	8.0	10.0	CB
74	-60.0	45.0	.0100	-59.2 (1.8)	42.5 (1.3)	.0100 (.0002)	.96	16.0	10.0	CB
76	-60.0	45.0	.0100	-59.7 (0.9)	43.8 (0.6)	.0102 (.0001)	.99	8.0	10.0	IB
77	-60.0	45.0	.0100	-60.4 (1.2)	43.4 (0.9)	.0102 (.0001)	.98	8.0	50.0	CB
78	150.0	0.0	.0100	150.1 (0.7)	-0.6 (0.5)	.0103 (.0001)	.98	8.0	10.0	CB
79	150.0	0.0	.0100	150.2 (0.7)	-0.3 (0.5)	.0103 (.0001)	.99	8.0	10.0	IB
80	180.0	-30.0	.0100	179.7 (0.7)	-29.4 (0.5)	.0103 (.0001)	.99	8.0	10.0	CB
81	-5.0	54.0	.0100	-5.8 (1.2)	52.8 (0.9)	.0101 (.0001)	.99	8.0	10.0	CB
82	65.0	0.0	.0100	65.0 (0.7)	0.6 (0.5)	.0103 (.0001)	.99	8.0	10.0	CB

CONT'D

83	-25.0	75.0	.0100	-27.0 73.8 .0099 (3.0) (2.2) (.0002)	.99	8.0	10.0	CB
84	-25.0	-15.0	.0100	-24.7 -13.8 .0102 (0.8) (0.6) (.0001)	.98	8.0	10.0	CB

r^2 multiple correlation coefficient squared

( )   standard deviation of quantity

IB   in between

CB   centered beneath

AZ   azimuth

IN   inclination

M   magnetization contrast

ρ density contrast

Azimuth and inclination of applied field are -25° and 75° respectively

All trials done with 100 observation points and 49 equivalent source prisms - see text for details

the horizontal position relationship between the observation points and the equivalent layer prisms, i.e., whether the prisms are centered beneath or in between the observation points (CB or IB in Table 3.4). When the equivalent layer is deep enough, there is little effect on the results when the equivalent layer prisms are shifted horizontally by one-half the observation point spacing (e.g. trials 73 and 76 and trials 78 and 79). Trials 68, 73 and 77 show that the thickness of the equivalent layer is not critical when the top of the equivalent layer is deep enough. There is a suggestion from trials 66 and 71 that a thick equivalent layer gives somewhat better results than a thin one when the top of the layer is not quite deep enough. Referring back to the discussion in section 3.5.1, an equivalent layer whose upper surface is situated at a depth equal to one to two times the station spacing not only provides a suitable representation of the gravity field but also its derivatives.

The results in the lower portion of Table 3.4 show that there is no difficulty with the angle of magnetization used for trials 13 to 20 (Table 3.3). Trials 73 and 78 to 84 indicate that for a wide variety of directions of magnetization, the orientation can be produced to within about 2° and the ratio of magnetization contrast to density to within about 0.3% if there are sufficient observation points to define the anomaly fields and if the equivalent layer is suitably defined and located. At first glance it seems odd that the method works well when the equivalent layer is deeper than the source of the anomalies but the important point

is that the conditioning of the problem is determined solely by the observation point-equivalent layer source geometry and not by the observed anomalies.

Returning to the poor results of trials 13 to 20 in Table 3.3, it is clear that they are due, at least in part, to the equivalent layer's being too close to the surface so the problem was re-run using an equivalent layer situated 2 km beneath the observation points (spaced 1 km apart) rather than a 0.1 km as previously used. The results of this new run were noticeably better: AZ = -64.2^{o} (8.6), IN = 34.4^{o} (5.9), M/ρ = .0012 emu/gm (.0001) (standard deviations are given in brackets) indicating that the deeper equivalent layer produced better results. However, the calculated inclination still differed by some 9° from the model value of 45°. A possible reason for this remaining discrepancy is that one of the four anomaly source prisms (6d) lies at a shallow depth (see Table 3.1) and is very close to the edge of the array of observation points and, as a result, its gravity and magnetic anomalies are not sufficiently well defined.

To sum up the tests on the models, if an anomalous source body satisfies the Poisson conditions and if good representations of the potential fields are obtained, the equivalent layer method gives good results when the layer is suitably positioned. A measure of the quality of the results is the degree of correlation between observed and computed potential fields. The gravity to magnetic field transformation generally provides better correlation between observed and computed fields and is less prone to systematic errors than the magnetic to gravity field transformation. The

latter transformation is useful, however, because a comparison of the two sets of results gives some idea of the overall reliability of the analysis.

3.7 TESTS OF THE PROGRAM MGTRAN ON SURVEY DATA

3.7.1 Gilliss Seamount

The program MGTRAN has been applied to field data from the Gilliss Seamount in the Northwest Atlantic as the feature has been treated by Cordell and Taylor (1971) using Fourier analysis. The gravity and magnetic data were digitized at 5 km intervals* from the diagrams published by Cordell and Taylor (1971). A total of 45 data points was used. The equivalent layer consisted of 30 prisms 5 km wide and 5 km long and 3 km thick with their tops situated at a depth of 2 km for trials 51 to 54 and at a depth of 10 km for trial 55 when only the gravity to magnetic field transformation was done. Results are presented in Table 3.5. Table 3.5 indicates that trials 51 and 52, where the equivalent source bodies lie in between the data points, allow a better representation of the magnetic field than do trials 53 and 54. On the other hand, trials 53 and 54 provide better correlation between observed and computed potential fields. Although no single result agrees exactly with that of Cordell and Taylor (AZ = 21.8°, IN = 43.3°, M/ρ = .00329 emu/gm), trial 55 produces a direction of magnetization which is only about 3° away from Cordell and Taylor's value (Table 3.5). This is in accordance with the tests on models which indicate that the gravity to magnetic transformation is likely

* A smaller interval would probably give better results as the anomalies would be better defined.

TABLE 3-5

APPLICATION OF MGTRAN TO GILLISS SEAMOUNT

AZ = -21.8°   IN = 43.3°   M/ρ = .00329 emu/gm

Trial	Correlation between observed field and that produced by the equivalent layer representation Magnetic r² Z-comp	Magnetic r² X-comp	Magnetic r² Y-comp	Gravity r²	Magnetic to Gravity trans. Direction of Magnetization Vector AZ°	IN°	ρ/M gm/emu	r²	Gravity to Magnetic trans. Direction of Magnetization Vector AZ°	IN°	M/ρ emu/gm	r²	Relation of equiv. source prisms to observation points	Virtual Pole Q = ∞ M to G Lat.°	M to G Long.°	G to M Lat.°	G to M Long.°
51	.896	.927	.000	.980	19.6 (3.0)	43.4 (7.3)	308 (46.1)	.772	-12.0 (22.9)	64.5 (12.7)	.00153 (.0005)	.384	IB	79.4	-111.8	76.1	-95.2
52	.866	.355	.294	.980	-8.6 (33.0)*	70.0 (5.1)*	314 (33.4)	.782	-1.2 (12.5)†	75.9 (10.7)†	.00153 (.0005)	.384	IB	71.5	-63.3	62.4	-59.7
53	.514	.157	.000	.977	-18.2 (7.0)	54.0 (6.7)	285 (39.7)	.833	-25.5 (9.3)	33.8 (7.9)	.00282 (.0006)	.649	CB	75.1	-147.7	61.6	-178.1
54	.700	.037	.000	.977	-25.7 (10.4)*	51.8 (38.2)*	345 (37.9)	.848	-25.8 (11.9)*	33.8 (6.4)*	.00282 (.0006)	.649	CB	68.5	-149.8	61.5	-178.7
55	---- not calculated ----				--- not done ---				-24.1 (10.0)	40.8 (7.6)	.0023 (.0003)	.599	CB	--- not done ---		65.8	-172.5

r² - multiple correlation coefficient squared

AZ - azimuth   IN - inclination   ρ - density contrast   M - magnetization contrast

( ) - standard deviation of quantity

* - value refers to quantities obtained in rotated system of orthogonal components of magnetization

IB - in between   CB - centered beneath

Note: Azimuth and inclination of earth's field are -20° and 65° respectively

to provide a good answer if the degree of correlation between observed and calculated fields is reasonably high and if the equivalent layer is sufficiently deep.

The analysis shows that the north pole of the magnetic field which induced the remanent magnetism in the Gilliss Seamount probably lay somewhere in the vicinity of the Bering Strait or somewhat to the south at a distance depending on the Koenigsberger ratio (the straight line in Figure 3.3 gives an idea of the amount) and in a direction away from the present magnetic pole.

In general, the standard deviation of a virtual pole position is less than twice the largest angular error contained in the azimuth or inclination of the magnetization vector (Cox and Doell, 1960). The largest angular error in the direction of the total magnetization vector in trials 53 to 55 (gravity to magnetic field transformation) is about 10° so the standard deviations of pole positions 53G, 54G and 55G do not exceed about 20°. Errors of this magnitude, although rather large, are comparable to errors quoted for some of the poorer palaeomagnetic data given in catalogues (e.g. Hicken et al., 1972). The main difficulty in the palaeomagnetic application of the gravity to magnetic field transform is that, in general, one does not know the Koenigsberger ratio. This will be discussed more fully in Chapter 7.

Calculated ratios of magnetic moment to mass range from .00135 emu/gm to .00350 emu/gm. Assuming that the seamount is basaltic and offers a density contrast of about 1.8 gm/cm^{3} with respect to the surrounding sea water, these ratios correspond to

Figure 3.3: Virtual geomagnetic pole positions obtained

from Gilliss Seamount assuming an infinite

Koenigsberger ratio. Solid square is the pole

obtained by Cordell and Taylor (1971) using

Fourier analysis. Dots show poles obtained

by the program MGTRAN using various equivalent

layer representations. Tests on artificial

data indicate poles 53G, 54G and 55G (not shown

for the sake of clarity) should be the most

reliable.
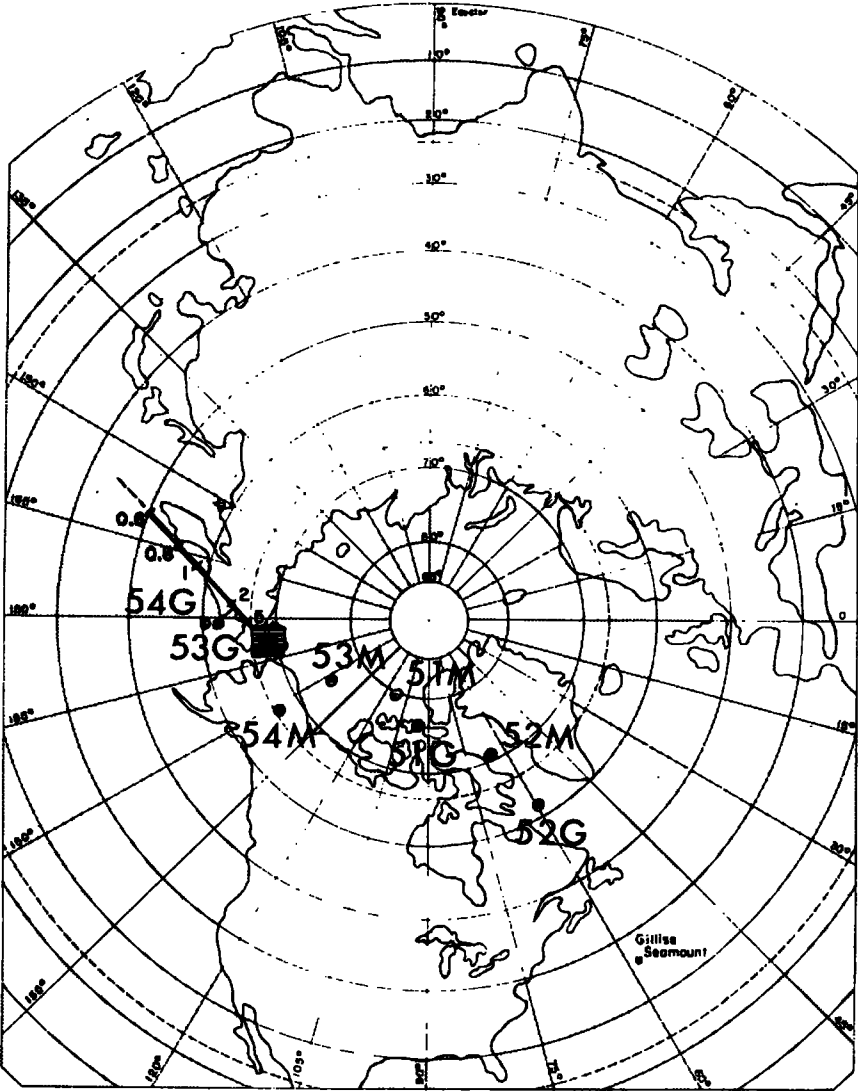
magnetic moments per unit volume of .0028 to .0063 emu/cm^3.

Measured values of induced and remanent magnetization of these

basaltic samples dredged from the seamount range from .0026 to

.0037 emu/cm^3. The calculated values of total magnetic moment

per unit volume agree quite well with the median observed values.

3.7.2 Sept Iles feature

Although the results from the Gilliss Seamount seem

reasonable, there is no direct information about the orientation

of the magnetization in the source rocks. Rock magnetism data

 recently became available (W. Fahrig, personal communication)

for a large undated Precambrian gabbroic anorthosite near Sept

Iles, Quebec and, because this geological feature produced large,

coincident gravity and magnetic anomalies (see Figures 7.1 and 7.2

in Chapter 7) and is in a continental rather than an oceanic

environment, it seemed worthwhile to apply the gravity to magnetic

field transformation to this feature and compare the calculated

quantities with those measured directly.

The gravity and magnetic anomalies are nearly circular and

have diameters of about 60 km and amplitudes of about 80 mgal and

1400 gamma respectively. The anomalies indicate that the major

portion of the intrusion lies under the waters of the St. Lawrence

River. Only the northern margin is exposed on land. Although it

is not apparent in Figure 7.2, there are intense magnetic anomalies

in a narrow annular zone at the margin of the main anomaly. These

suggest the possibility of an enhanced magnetization at the margin

of this Precambrian gabbroic anorthosite.

The rock magnetism data are summarized in Table 3.6. The samples are necessarily restricted to the northern margin of the intrusion. The mean susceptibility of the samples is .0051 emu/cm^3 and the mean Koenigsberger ratio is about 0.25. The directions of the natural remanent magnetization (NRM) vectors in individual samples exhibit a lot of scatter but the azimuths tend to fall into two groups, one at 320° and the other at 30°. The azimuth of the earth's field is 335° so the mean azimuth of one group lies slightly to the west; the second distinctly to the east. The inclinations of the NRM vectors cluster around 70° to 80° in either group. The double grouping of the NRM vectors indicates two directions of magnetization are present in the samples.

When the samples were cleaned using alternating field demagnetizing techniques, only two samples (7701 and 8001) exhibited stable directions of remanent magnetization (see bottom of Table 3.6). Interestingly enough the two directions are quite different from each other. The second stable direction (from sample 8001) could explain the NRM directions in the second group as being vector combinations of the stable remanent magnetization and a component in the direction of the earth's field but the azimuth of the first stable direction (from sample 7701) is not oriented sufficiently far enough to the west to create a vector combination which would have an azimuth of 320°. The NRM data suggest, therefore, that a third direction of magnetization may be present in the samples.

The preceeding discussion points out two possible difficulties

TABLE 3.6

Sept Iles Feature

No. of sites   10   No. of samples   72

Mean susceptibility   .0051 emu/cm^3 Mean Koenigsberger Ratio 0.25

Directions of remanent magnetization - uncleaned samples

SITE	AZIMUTH DEG	INCLINATION DEG	NO. OF SAMPLES	FISHER'S k-VALUES
75	320.7	38.7	7	14.8
76	29.9	78.0	8	45.2
77	329.1	48.0	8	6.7
78	320.0	66.4	6	11.6
79	321.8	76.5	7	13.2
80	14.3	70.0	7	11.9
81	306.0	80.3	7	18.5
82	68.7	81.4	7	11.2
83	22.8	76.7	7	33.5
84	37.6	63.2	8	9.3

Directions of magnetization - alternating field
cleaned samples

SAMPLE	AZIMUTH	INCLINATION
7701	-28.8	-21.4
8001	131.6	49.0

Note: azimuth and inclination of earth's field are -25°

and 75° respectively

in the application of the gravity to magnetic field transformation
to the Sept Iles feature. Firstly, the narrow,intense magnetic
anomalies at the margins indicate that the ratio of magnetization
contrast to density contrast may be higher at the margin of the
intrusion than throughout the main body and secondly, the rock
magnetism data indicate that more than one direction of magneti-
zation is present at the margin and possibly throughout the main
body. In doing the gravity to magnetic field transformation it
was discovered that better results could be obtained by modelling
the intrusion by a number of prisms of different sizes arranged
to approximate the shape of the intrusion in plan view rather
than by using a uniform array of rectangular prisms as was done
for the Gilliss Seamount. It was also necessary to delete some
of the observation points which were situated over the narrow,
intense magnetic anomalies at the margin. Table 3.7 gives the
results of three trials which produce a good agreement between
the calculated and observed magnetic anomalies everywhere except
at a few isolated places near the northern margin of the
intrusion. These trials were carried out using 68 observation
points and 33 source prisms.

As can be seen from Table 3.7, the results of the gravity
to magnetic field transformation depend to some extent on the
depth at which the source prisms are placed but, in general, the
results group together fairly well. The ratios of magnetization
contrast to density contrast of .013 to .015 emu/gm obtained
from the gravity to magnetic field transformation agree very well

with the value of .014 emu/gm derived from the mean susceptibility

value of .0051 emu/cm^3 multiplied by the earth's magnetic field

strength of .57 oersted and divided by an estimated density contrast

of 0.2 gm/cm^3 between the gabbroic anorthosite (2.9 gm/cm^3) and

the surrounding granitic gneisses and migmatites (2.7 gm/cm^3).

The directions of the total magnetization vectors do not differ

significantly from the direction of the induced magnetization vector

at the 95% confidence level but the direction obtained from

trial 92 differs at the 67% level. If we know, or assume a

value of the Koenigsberger ratio, the direction of the remanent

magnetization vector can be obtained by subtracting the induced

magnetization vector from the total magnetization vector. The

length of the induced magnetization vector with respect to the

length of the total magnetization vector is determined by whatever

value is assigned to the Koenigsberger ratio and is equal to the

length of the total magnetization vector divided by the quantity

$$\cos(b) \pm (Q^2 + \cos^2(b) - 1)^{\frac{1}{2}}$$

where Q is the Koengisberger ratio and b is the angle between the

earth's field and the total magnetization vector. At this

juncture it must be pointed out that in this application to the

Sept Iles feature the statistical uncertainty in the direction

and length of the resultant vector is very large because, even

in the best case, the total magnetization vector is barely

significantly different from the induced magnetization vector.

Nevertheless it is still of interest to examine the results.

Directions of remanent magnetization corresponding to a Q
value of 0.25 are given in Table 3.7. These directions clearly
do not correspond to the direction of stable remanent magnetization
in sample 8001 and point too far to the west to be associated with
the stable remanent magnetization in sample 7701. The calculated
directions might explain the first grouping of NRM values obtained
in Table 3.6 but, if so, what is the significance of a nearly
horizontal remanent magnetization pointing westsouthwest at Sept
Iles? Table 3.8 gives virtual palaeomagnetic pole positions from
the directions of remanent magnetization presented in Table 3.7.
These poles lie within a group of poles obtained from 1200 to
1500 my old rocks located elsewhere in the Canadian Shield (Irving
and Park, 1972) therefore the poorly determined direction of
remanent magnetization obtained from the gravity to magnetic field
transformation might represent the magnetization initially acquired
in cooling. Turning the argument around, many of the anorthosites
in the Canadian Shield seem to have crystallized some 1400 to
1500 my ago (e.g. Fahrig et al., 1974) so, if the Sept Iles feature
is typical, one might expect to find a nearly horizontal
magnetization pointing westsouthwest to be present throughout
the intrusion and this, would, for reasonable Q values, deflect
the azimuth of the total magnetization vector some 20° to 30^0 to
the west of the earth's field. Therefore, from this point of
view, the results of the gravity to magnetic field transformation
are not unreasonable but the unfortunate aspect of the application
of the transformation in this case is that the error limits of the

TABLE 3.7

RESULTS OF GRAVITY TO MAGNETIC FIELD TRANSFORMATION

Sept Iles Feature

TRIAL	AZIMUTH deg	INCLINATION deg	M/ρ emu/gm	r^2	DEPTH OF UPPER SURFACE OF PRISMS km
91	−45.4 (28.1)	76.6 (17.3)	.0128 (.0000)	.77	15
92	−53.5 (13.5)	67.2 (09.5)	.0148 (.0010)	.78	25
93	−52.8 (25.7)	74.5 (16.9)	.0131 (.0011)	.71	50

Direction of Remanent Magnetization (Assuming Q = 0.25)

TRIAL	AZIMUTH deg	INCLINATION deg
91	−110.3	66.6
92	−84.4	15.4
93	−105.0	52.1

M/ρ − ratio of magnetization contrast to density contrast

( ) − standard deviation of quantity

TABLE 3.8

VIRTUAL PALAEOMAGNETIC POLES

Sept Iles - Gravity to Magnetic Field Transform (Q=0.25)

TRIAL	LATITUDE deg	LONGITUDE deg
91	26.	-109.
92	10.	-155.
93	16.	-124.

Sept Iles - Cleaned Samples

SAMPLE	LATITUDE deg	LONGITUDE deg
7701	23.	145.
8001	1.	-26.

1200 to 1500 my Rocks from Other Areas in North America

FEATURE	LATITUDE deg	LONGITUDE deg
Michikamau Anorthosite (1500 my)	-1.	-145.
Crocker Is. Complex (1475 my)	5.	-143.
Sherman Granite (1410 my)	-8.	-151.
Abitibi Dykes (1230 my)	27.	-134.

NOTE: for Cambro-Ordovician poles see Figure 7.6 in Chapter 7.

The standard deviation of a virtual pole from the transformation varies according to the trial but is of the order of $30°$ of latitude.

direction of total magnetization are so large.

One final comment in connection with the rock magnetism data is that virtual poles (Table 3.8) obtained from the stable directions of magnetization in samples 7701 and 8001 group together with Cambro-Ordovician poles rather than the older Grenville (1100 my) and Elsonian (1400 my) poles (Hicken et al., 1972). Noting that the Sept Iles feature lies very close to the Appalachian Front (see Figure 7.4 in Chapter 7), it may be that these stable magnetizations were developed in the margins of the intrusion just prior to and/or during the Taconic (Ordovician) Orogeny.

3.8 APPLICATION OF NON LINEAR OPTIMIZATION TO MODELLING GEOPHYSICAL DATA

3.8.1 Non-linear optimization

Non-linear optimization is the process of numerically determining the maximum or minimum of a function of several variables. One of the first applications to the study of magnetic and gravity anomalies was by Al-Chalabi (1970). Its use has been well documented in the literature and is not repeated here; a paper by Hjelt (1973) is of particular interest in this respect. The application of non-linear optimization typically consists of minimizing the root mean square of the residuals between the observed and computed anomaly values by varying some or all of the coordinates used to define the shape of an anomalous source. Other parameters such as the density or magnetization contrast of

the source body and/or the form and level of the regional back-
ground anomaly can also be varied.

.. . I have exclusively used a method which is due to Rosenbrock
(1960) and based on the method of steepest descent (e.g. Westlake,
1968). The computer subroutine was supplied to the Department of
Geological Sciences by Imperial Chemical Industries, Ltd. A
simplified description of the method follows:

In order to minimize a function, f, of several variables x_1;
x_2 etc.

(1) increment the first argument x_1 by an amount e. If
the function decreases in value, make the size of the
next increment to be applied after all other arguments
are incremented equal to αe where $1<\alpha$. If the function
increases in value set the size of the next increment
equal to βe where $-1<\beta< 0$. This procedure constitutes
an inner loop, I, and provides a way to obtain a
reasonable size of increment, not too large or too
small, in the correct direction.

(2) Increment the second argument, x_2, by an amount e. Set
the size of the next increment to be used after all
of the remaining arguments are incremented by αe or
βe as is required.

(3) repeat the procedure until all arguments have been
incremented once. This completes an intermediate loop,
M.

(4) repeat the cycle (1) to (3) until a "success", i.e. an

increment has been multiplied by α at least once, is

obtained for all the arguments followed by a "failure"

i.e. the step size is multiplied by β, for one parameter.

(5) at this point the vector $\underline{x}$ of arguments is transformed

into a new coordinate system whose axes are u_1, u_2, ...

u_m by means of the Gram-Schmidt orthogonalization process

(e.g. Westlake, 1968); this ensures that an increment

in the u_1 direction will produce the greatest decrease

in the value of f, an increment in the u_2 direction will

produce the next greatest decrease in the value of f,

.etc. This completes an outer loop, O.

The process is repeated using loops I,M and O as before

except f is a function of u_1, u_2, ... u_m instead of

x_1, x_2,...x, . The iterative process is terminated when

there is no significant decrease in the value of f.

I find that Rosenbrock's method usually converges exponent-

ially to a minimum but the problem with this and other

optimization methods is that the user is never certain at the

outset whether a procedure will converge and if it does converge,

whether it converges to a local or a global minimum. A local

minimum is a minor, unwanted minimum, a global minimum is the

overall, desired minimum. A related problem is that the optimized

values of the variable parameters depend upon the starting point

of the calculation. In spite of these basic uncertainties

Rosenbrock's optimization method seems useful in geophysical

applications and it eliminates the drudgery of trial and error

computation where the analyst takes part in each iterative step.

3.8.2 Application to first-arrival seismic travel-time data

In order to reinterpret the available crustal seismic first-arrival travel time data over the Scotian Shelf, I wrote a simple program to calculate the travel time of a seismic wave travelling through a model consisting of n horizontal layers. This program, which is combined with the optimization subroutine, is based on the expression for the travel time of a wave which penetrates the nth layer:

$$t = \frac{x}{V_n} + \sum_{j=1}^{n-1} 2h_j \frac{(V_n^2 - V_j^2)^{\frac{1}{2}}}{V_n V_j}$$

where t is the travel time of the seismic wave

x is the horizontal distance between the seismic source and receiver

V_n is the compressional wave velocity in the nth layer

V_j is the compressional wave velocity in the jth layer.

and selects, at a given observation point, the earliest arrival. The seismic velocities, V_j, are the parameters varied by the optimization routine in order to minimize the r.m.s. difference between the observed and computed travel times.

Tests on simple theoretical models indicated that the procedure worked adequately except that some of the derived models had low-velocity layers which were not in the original models. The

procedure was applied to the crustal seismic data on the southern Scotian Shelf (Chapter 5) with the view that although the model obtained is not unique, it at least provides a possible velocity-depth structure which could produce the observed travel-time vs. distance curve.

CHAPTER 4

THE NORTHERN SCOTIAN SHELF

4.1   INTRODUCTION

The northern portion of the Scotian Shelf is of considerable
geophysical interest as the geological relations between the
structures of southern and eastern Newfoundland and those of Cape
Breton Island have long been a source of discussion (e.g. King, 1951;
Weeks, 1954). The southeastward extension of the Precambrian rocks of
the Burin and Avalon peninsulas (Figure 4.1) and their possible
correlation, or lack of it, with the formations on Cape Breton Island,
is of particular interest because it was first pointed out by Williams
(1964) that the Palaeozoic mobile belt of central Newfoundland is
bounded on either side by Precambrian platforms and that this two-
sided nature of the Appalachian geosyncline is in contrast to the
asymmetrical nature of the geosyncline further to the southwest where
it lacks a well defined Precambrian platform on its southeast side.
Studies of the asymmetrical portion of the Appalachians led to the
classical concept of a geosyncline (Schuchert, 1925; Kay, 1951) and
of continental accretion (e.g. Wilson, 1954). However, because the
geology of Newfoundland does not fit these classical ideas, Wilson
(1966) suggested that the Appalachian mountains were formed as a
result of the closure of an ocean which culminated in collisions of
its bounding continents during the Palaeozoic era and that the south-
eastern part of Newfoundland and adjacent continental shelf is a
continental remnant which was left behind as the European and African

Figure 4.1:   Simplified geological map of southern

Newfoundland and Cape Breton Island.

Data from the Geological Map of the

Island of Newfoundland (Williams, 1967)

and from the Geological Map of the

Province of Nova Scotia (Nova Scotia

Department of Mines, 1965).

80

Simplified Geological Map of Southern Newfoundland & Cape Breton Island

PLUTONIC ROCKS

DEVONIAN & EARLIER GRANITE, GRANODIORITE

GABBRO, DIORITE, PYROXENITE

FAULTS

Areas of Mainly VOLCANIC ROCKS
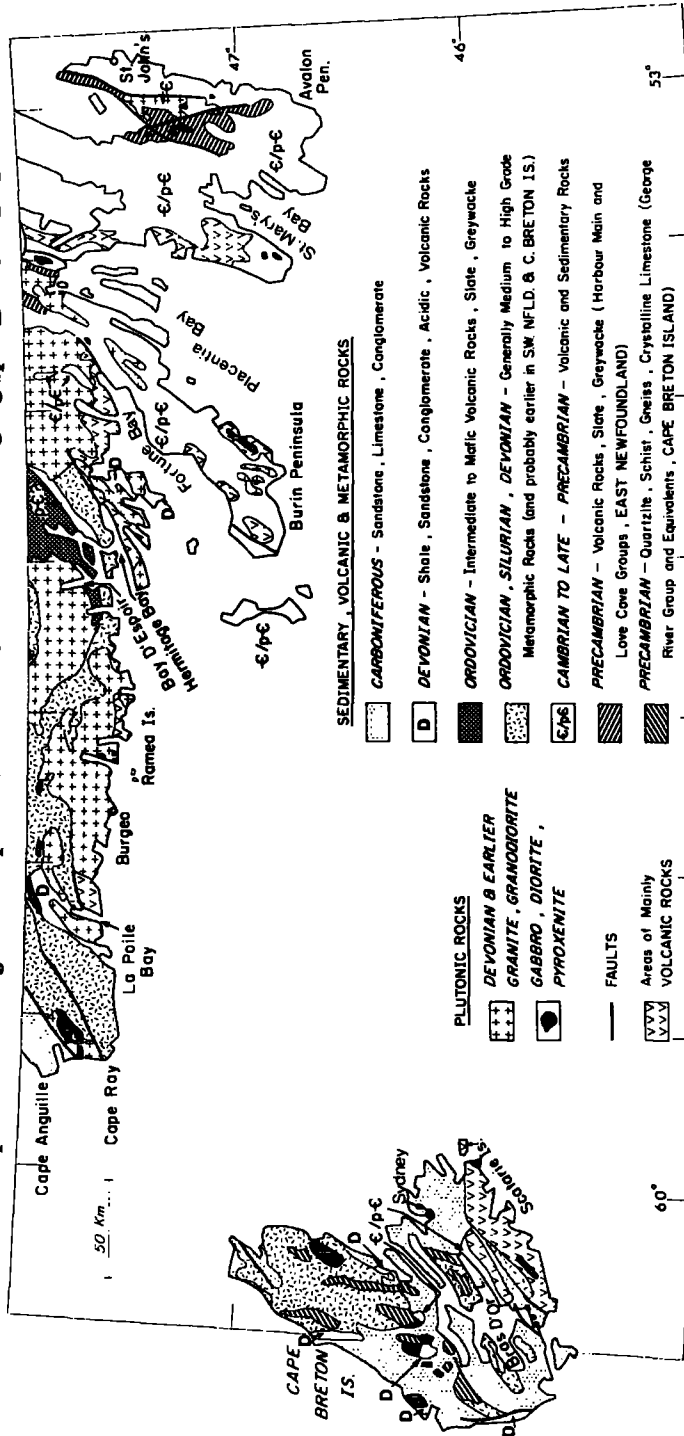
SEDIMENTARY, VOLCANIC & METAMORPHIC ROCKS

CARBONIFEROUS - Sandstone, Limestone, Conglomerate

D DEVONIAN - Shale, Sandstone, Conglomerate, Acidic, Volcanic Rocks

ORDOVICIAN - Intermediate to Mafic Volcanic Rocks, Slate, Greywacke

ORDOVICIAN, SILURIAN, DEVONIAN - Generally Medium to High Grade Metamorphic Rocks (and probably earlier in S.W. NFLD. & C. BRETON I.S.)

CAMBRIAN TO LATE - PRECAMBRIAN - Volcanic and Sedimentary Rocks

PRECAMBRIAN - Volcanic Rocks, Slate, Greywacke (Harbour Main and Love Cove Groups, EAST NEWFOUNDLAND)

PRECAMBRIAN - Quartzite, Schist, Gneiss, Crystalline Limestone (George River Group and Equivalents, CAPE BRETON ISLAND)

continents split apart and moved away from the North American continent during the Mesozoic era. Wilson's scheme has since been reinforced by current theories of plate tectonics (e.g. Morgan, 1968) and subsequent, more detailed models of the evolution of the Appalachians have been proposed by Bird and Dewey (1970), Rodgers (1970) and others.

The main goals of the geophysical analysis of the Northern Scotian Shelf are to study the extent and thickness of Carboniferous and younger sedimentary rocks and to outline structures in the pre-Carboniferous basement, paying particular attention to the underwater extent of Precambrian basement rocks.

4.2 GEOLOGICAL SETTING OF SOUTHERN NEWFOUNDLAND AND CAPE BRETON ISLAND

4.2.1 Geology of southern Newfoundland

The geological formations in Newfoundland that are pertinent to the northern Scotian Shelf are described working from east to west; the main sources of information are Poole (1970); Williams et al. (1972); and the Geological Map of the Island of Newfoundland (Williams, 1967).

On the Avalon Peninsula (Figure 4.1) a basal group of predominantly subaerial andesites, rhyolites and intercalated sandstones (Harbour Main Group) is conformably overlain by an intermediate assemblage of about 2 km of mainly siliceous slates and greywackes (Conception Group). These are, in turn, overlain in places by an upper assemblage of 3 to 5 km of arkosic and red sandstones and

conglomerates (Cabot, Hodgewater and Musgravetown Groups). The latter

group is underlain by a thick (2.5 km) formation of predominantly

basic and intermediate volcanic rocks and volcanic breccia (Bull Arm

Formation). These late Proterozoic assemblages are overlain in places

by thin beds of distinctive white quartzite (e.g. Random Formation)

which have equivalents elsewhere in the Maritimes.

To the west on the Burin Peninsula (Figure 4.1), the rocks are

probably equivalent to the Love Cove Group to the north and its

correlative assemblage, the basal Harbour Main Group to the east on

the Avalon Peninsula. The volcanic rocks are overlain in places by

equivalents of the intermediate and upper assemblages of the Avalon

Peninsula.

There are very few exposed intrusive rocks in the Avalon and

Burin Peninsulas. The notable intrusion in the Avalon Peninsula is

the Holyrood Granite, lying southwest of St. John's and dated radio-

metrically (Rb-Sr) at 574 m.y.; this body intrudes the Harbour Main

volcanics and is overlain by lower Cambrian shales. In the Burin

Peninsula there are several scattered granite outcrops whose ages

are Devonian or earlier. Small outcrops of gabbro and related mafic

rocks occur on the southeast side of the Burin Peninsula, on several

islands in Placentia Bay and at the head of the Bay and at the

southern tip of the peninsula which separates Placentia Bay and

St. Mary's Bay.

North of Fortune Bay (Figure 4.1), rocks which are probably of

late-Precambrian age and which consist mainly of silicic volcanic flows

and interbedded conglomerates, etc., are cut extensively by granites of varying ages ranging from late-Precambrian to Devonian. The largest batholith, probably of Siluro-Devonian age, cuts across a major fault zone which extends in arcuate fashion from the north side of Bonavista Bay (not shown in Figure 4.1) south and west to the south and west to the south side of Hermitage Bay; this fault separates the formations of the Avalon and Burin Peninsulas (Zone H in Figure 4.2) from those to the west.

At Bay d'Espoir (Figure 4.1), just to the north of the Hermitage Bay Fault, basement gneisses and migmatites and overlying complexly folded slates and phyllites (Bay d'Espoir Group) are part of a narrow curvilinear belt of metamorphic rocks which extends southeast from Cape Freels on the northeast coast of Newfoundland to Bay d'Espoir and west from Bay d'Espoir to La Poile Bay (Figure 4.1).The age of metamorphic basement in this zone (Zone G in Figure 4.2) was previously thought to be early to middle Palaeozoic but it is now considered to be early to middle Proterozoic (Williams et. al., 1972). The basement in the northern part of Zone G (Figure 4.2) is covered by an approximately 3 km thick monotonous sequence of psammitic and semi-pelitic schists. The metamorphic belt is cut by numerous granitic bodies of various pre-Carboniferous ages and scattered intrusions of gabbro, diorite, etc. The metamorphic belt separates the Precambrian volcanic-sedimentary rocks of the Avalon and Burin Peninsulas from the younger central mobile belt of Newfoundland.

Figure 4.2:   Map showing main tectonic zones bordering

the Nova Scotian continental shelf (after

Williams et al., 1972). The zones are

discussed in the text and summarized in

the caption of Figure 1.2.
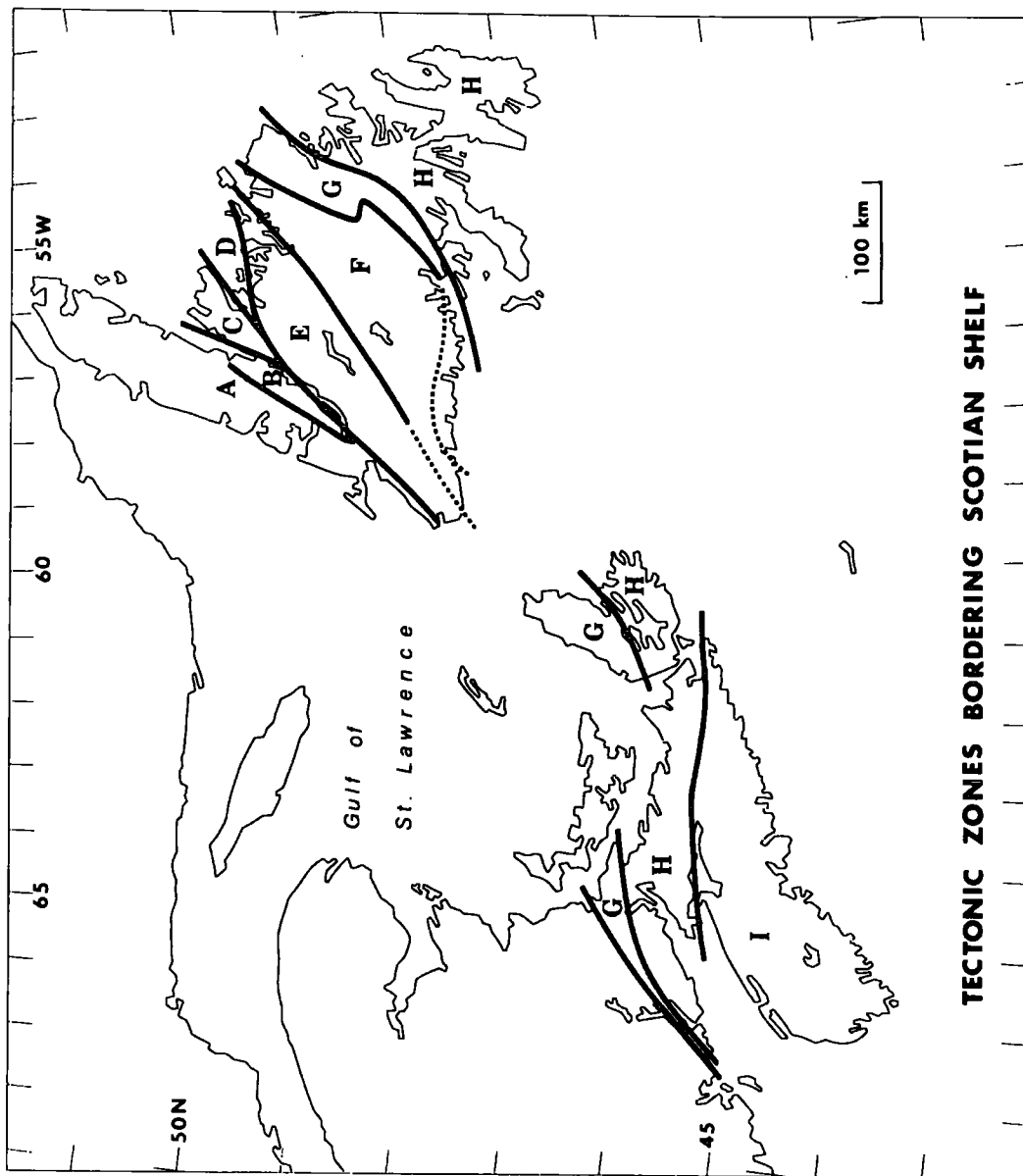
TECTONIC ZONES BORDERING SCOTIAN SHELF

The central mobile belt (Zones E and F in Figure 4.2) consists largely of Ordovician slates, argillites and mafic pyroclastic rocks and pillow lavas overlain in places by Silurian greywackes, conglomerates and sandstones. These rocks are interrupted by extensive areas of acidic to basic igneous and metamorphic bodies and significant linear belts of ultramafic rocks. Although the central mobile belt is some 200 km wide in northern and central Newfoundland, it pinches out and is only about 50 km wide in southwestern Newfoundland.

North of Cape Ray (Figure 4.1) a major, northeast, trending, linear fault zone separates the central mobile belt from a 7 km thick sequence of Carboniferous siltstones, sandstones, and conglomerates which probably overlie Precambrian anorthosite and gneiss.

4.2.2 Geology of Cape Breton Island

On southeast Cape Breton Island (Figure 4.1), a northeast trending belt of mainly silicic to intermediate pyroclastic rocks and lavas, occasionally interbedded with minor shale sequences, (Fourchu Group) is overlain on its northwestern flank by Cambrian shales and sandstones which include, near the base, a distinctive white quartzite member within the Morrison River Formation. Weeks (1954) points out that the Fourchu Group has features in common with the Harbour Main Group on the Avalon Peninsula, but he also demonstrates convincing similarities between the geological setting of the Fourchu Group and younger Morrison River Formation and the characteristics of the mainly volcanic Bull Arm Formation and overlying sedimentary rocks of the Musgravetown Group; he favours the latter correlation.

Further to the north, the Cambrian strata that overlie the Fourchu Group also overlie, with marked angular unconformity, quartzite, marble, schist and gneiss (George River Group). The George River Group (Figure 4.1) and its probable equivalents elsewhere in Cape Breton Island predate the Fourchu Group and exhibit a lithological similarity to basement rocks of the Grenville Geological Province. Several small lenses of anorthosite, a rock characteristic of the Grenville Province, are found near the northern tip of Cape Breton Island within a band of northeast trending metavolcanic rocks; the presence of anorthosite reinforces the assignment of a Precambrian age for much of the basement gneiss and schist of Cape Breton Island.

Several granitic bodies ranging in age from Devonian to late Proterozoic (and possibly older) occur throughout Cape Breton Island. Basic intrusions are not abundant; these are generally Devonian or older although some gabbro intrusives of Carboniferous or possibly Triassic age occur a few kilometers to the southwest of the Fourchu volcanics (Figure 4.1).

With minor exceptions, Ordovician, Silurian and Devonian sedimentary rocks are lacking in Cape Breton Island but Carboniferous and Permian sandstones, siltstones and conglomerates occur widely. The Carboniferous and Permian sedimentary formations relevant to the northern Scotian Shelf are those of the Sydney Basin (in the vicinity of Sydney, N.S.; Figure 4.1) which on land reach a total stratigraphic thickness of about 2 km and include coal seams and evaporites.

4.2.3 Structure and Metamorphism

Williams et al. (1972) have subdivided the Canadian

Appalachians into eight distinctive structural zones (Figure 4.2):

seven of these occur in Newfoundland, the eighth is restricted to

southern Nova Scotia. Of the seven zones in Newfoundland, five are

represented in the southern part. Following their notation, the most

easterly zone, Zone H, includes the mainly Precambrian, volcanic and

sedimentary rocks of the Avalon and Burin Peninsulas in Newfoundland

(Figure 4.1). These rocks exhibit northerly trending upright folds:

the folding is open in the eastern section and tight in the western

part. The age of the folding in the eastern section is clearly

Precambrian as overlying Cambro-Ordovician shales, limestones and

other sedimentary rocks are undeformed, however, Cambro-Ordovician

rocks in the western part have been deformed along with the older

formations during the Devonian period. Metamorphic rocks are of low

grade, ranging from slate in the Harbour Main Group in the eastern

part to greenschist in the Love Cove Group in the west. Major north-

northwest and north-northeast trending faults occur throughout the

region, notably in the vicinity of the Holyrood Granite to the south-

west of St. John's (Figure 4.1).

In Zone G, immediately to the west of Zone H, the gneisses,

migmatites and slates exhibit a complex history of folding which

extends back in time from the Devonian period to probably the middle

Proterozoic. The Devonian deformation is pervasive and is characterised

by the S-shaped bend, called the Hermitage Flexure (Williams et al.

1970), which pinches out the adjacent rocks in Zone F. Metamorphism in

Zone G is variable, often rising to the amphibolite facies and locally
to the granulite facies (e.g. near La Poile Bay). Except for the
major fault zone between Zones G and H, faults do not seem to be wide-
spread within Zone G. Where mapped, they generally trend northeast and
are probably pre-Carboniferous in age.

The Ordovician slates, argillites and mafic pyroclastic rocks
and pillow lavas and the Silurian greywackes, conglomerates and
sandstones in Zones E and F in southwestern Newfoundland are
intensely deformed by Devonian movements and structural trends are
oriented generally northeast. Significant linear belts of mafic and
ultramafic rocks occur throughout Zones E and F and medium to high
grade metamorphic rocks occur in the southwestern parts of Zone E
and F. The type and location of the boundary between Zone F and
Zone G is unknown but the northwest side of Zone E is clearly marked
by a northeast trending, high-angle fault. Williams et al. (1972)
do not show the boundary between Zones E and F in southwestern New-
foundland but I arbitrarily locate it along a fault extending north-
east from Cape Ray as this fault lies on-strike with a major fault
zone that separates Zones E and F further to the northeast.

In the southwestern tip of Newfoundland, the Permo-Carboniferous
siltstones, sandstones and conglomerates in Zone A show varying
degrees of folding with the older rocks more steeply folded than the
younger ones. The rocks are essentially unmetamorphosed and only
occasionally cut by northeast trending faults.

In Cape Breton Island the silicic to intermediate pyroclastic rocks and lavas and occasional interbedded shales of the Fourchu Group, which is assigned to Zone H, exhibit varying degrees of metamorphism and have been subjected to two phases of early to mid-Palaeozoic folding which have produced a northeasterly structural trend.

The Precambrian George River quartzite, marble, schist and gneiss are highly contorted and indicate an intermediate degree of metamorphism.

As in Zone A in southwestern Newfoundland, Carboniferous and younger sandstones, siltstones and conglomerates exhibit folding but little or no metamorphism and the older beds are generally more steeply folded than the younger ones.

Faults in Cape Breton Island generally trend northeast, occasionally northwest. In southeastern Cape Breton Island strike-slip motion appears to have been common in the Devonian period and vertical movement prevalent in the Carboniferous. An interesting exception to the latter is a thrust fault which affects Carboniferous rocks to the south of Bras d'Or Lake.

4.2.4 Brief resume of the tectonic history of southern Newfoundland

The gneissic basement rocks of Zone A (Figure 4.2) were formed or reworked in mid-Proterozoic time and intruded by granitic plutons and swarms of basic dikes. At about the same time or perhaps somewhat later, the gneissic basement rocks of Zone G were formed or reworked and intruded by granite. The rocks in these two zones may or may not

have been part of a single tectonic unit in mid to late-Proterozoic time. In late Proterozoic time the volcanic and sedimentary rocks in Zone H were formed in an island-arc environment, perhaps similar to that presently seen in Indonesia, and the rocks were subsequently folded, metamorphosed and, in one locality, intruded by granite.

In early Palaeozoic time, Zones A and H were stable areas covered by shallow Cambro-Ordovician seas. Whether or not these two zones were once in close proximity, they were, at this time, separated by an intervening ocean which was shrinking in size as its bounding continents converged.

The rocks in Zones E and F were obviously formed in a very active environment which, broadly speaking, changed from marine in the Ordovician to terrestrial in the Silurian. Slices of ultramafic rocks were emplaced mainly at the northwestern margin of Zone F during the middle Ordovician. At some subsequent time large, allocthonous masses of eugeosynclinal Cambro-Ordovician sedimentary rocks and Ordovician ultramafic rocks in central Newfoundland were thrust over the mio-geosynclinal Cambro-Ordovician sedimentary cover rocks in Zone A lying to the west.

The Devonian period was one of extensive deformation, metamorphism and intrusion throughout Zones E, F and G and in the western part of Zone H. This activity marks the collision which culminated the closing of the oceanic region lying between the North American and European lithospheric plates. Subsequent tectonic activity was confined mainly to the narrow, northeast trending zone of Permo-Carboniferous rocks overlying the Precambrian gneissic basement of Zone A. Within this zone generally non-marine deposition and vertical movement of fault-bounded blocks were predominant.

4.3 GEOPHYSICAL DATA

In addition to the uniform regional underwater gravity coverage,
data from several shipborne gravity and magnetic profiles and
scattered seismic profiles are available (Figure 4.3)

The seismic data from the northern Scotian Shelf and the Gulf
of St. Lawrence (Sheridan and Drake, 1968; Hobson and Overton, 1973)
show the typical increase of compressional wave velocity with depth
of the refracting medium (Figure 4.4). The velocities show gaps at
about 4.5 km/s and 5.6 km/s; these gaps provide convenient markers to
subdivide the depth results and this has been done by Hobson and
Overton (1973). Their seismic structure maps which include data from
Sheridan and Drake (1968), show (Figure 4.5) a broad sedimentary
basin underlying the area to the north and east of the Sydney-Glace
Bay region of Cape Breton Island. A prominent feature is the east-
west trending basement ridge (Figure 4.5) bounding the south side of
the basin. As Hobson and Overton ·(1973) show (Figure 4.6) a definite
correlation between compressional wave velocity and rock type is
uncertain but they conclude that the seismic structure map showing
the depths of layers in which the compressional wave velocity exceeds
4.5 km/s outlines accumulation of sedimentary rocks whose ages range
from Recent to Pennsylvanian. Interpretation of their second seismic
structure map (Figure 4.5) is more difficult as rocks ranging in age
from Lower Carboniferous to Precambrian could all exhibit velocities
in excess of 5.6 km/s if a correction for pressure is applied to the

Figure 4.3:   Location of Bedford Institute surface gravity

and magnetic data (Haworth et al., 1972) and

Geological Survey of Canada (Hobson and Overton,

1973) and Lamont Observatory (Sheridan and Drake,

1968) shallow seismic data.

94
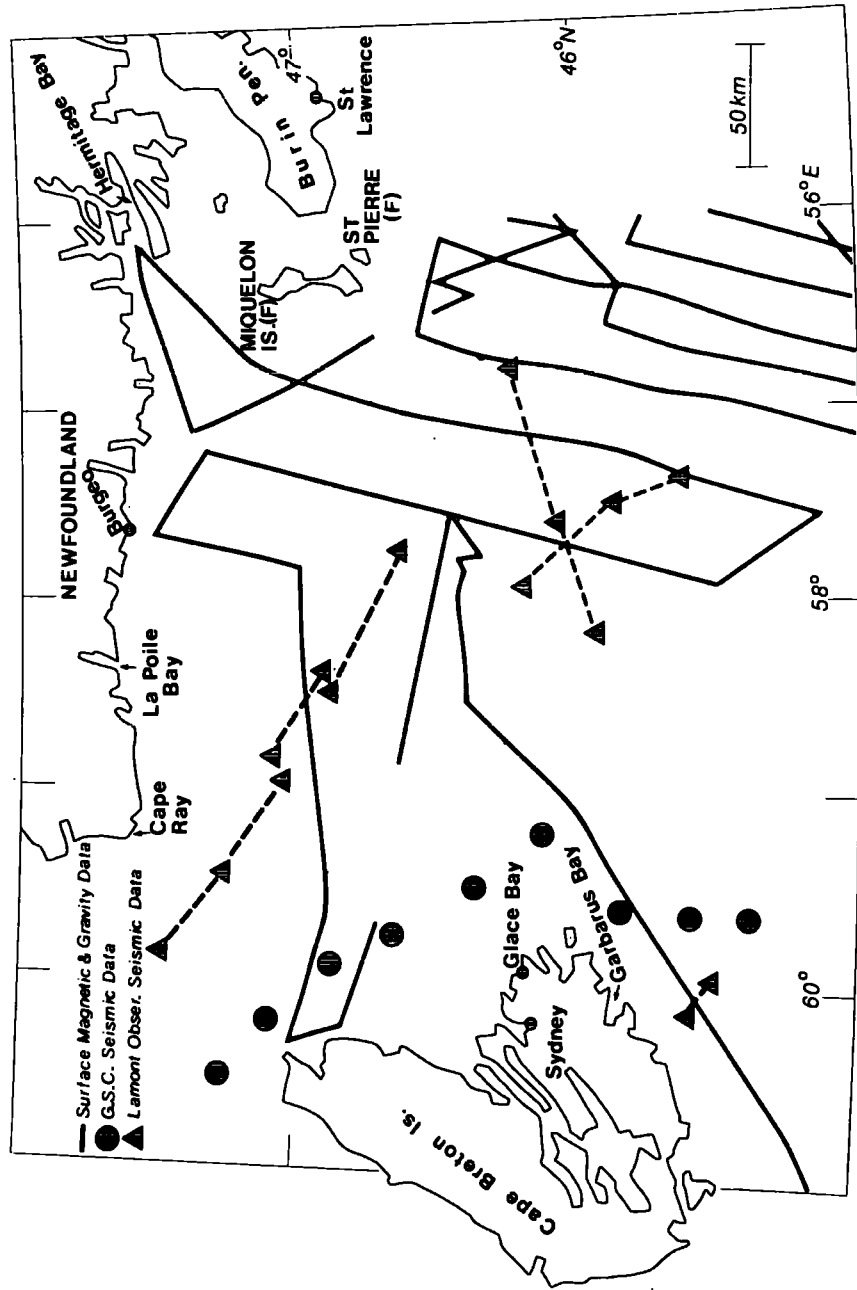
Figure 4.4:   Plot of compressional wave velocity in a

given refractor versus the depth of the

top of the refractor. Data extracted

from Sheridan and Drake (1968).

Figure 4.5:   Map of the depth at which the compressional

wave velocity exceeds 5.6 km/sec.   Taken

from Hobson and Overton (1973).

SEISMIC STRUCTURE MAP-(Basement Velocity ≥ 5.6 km/sec.)
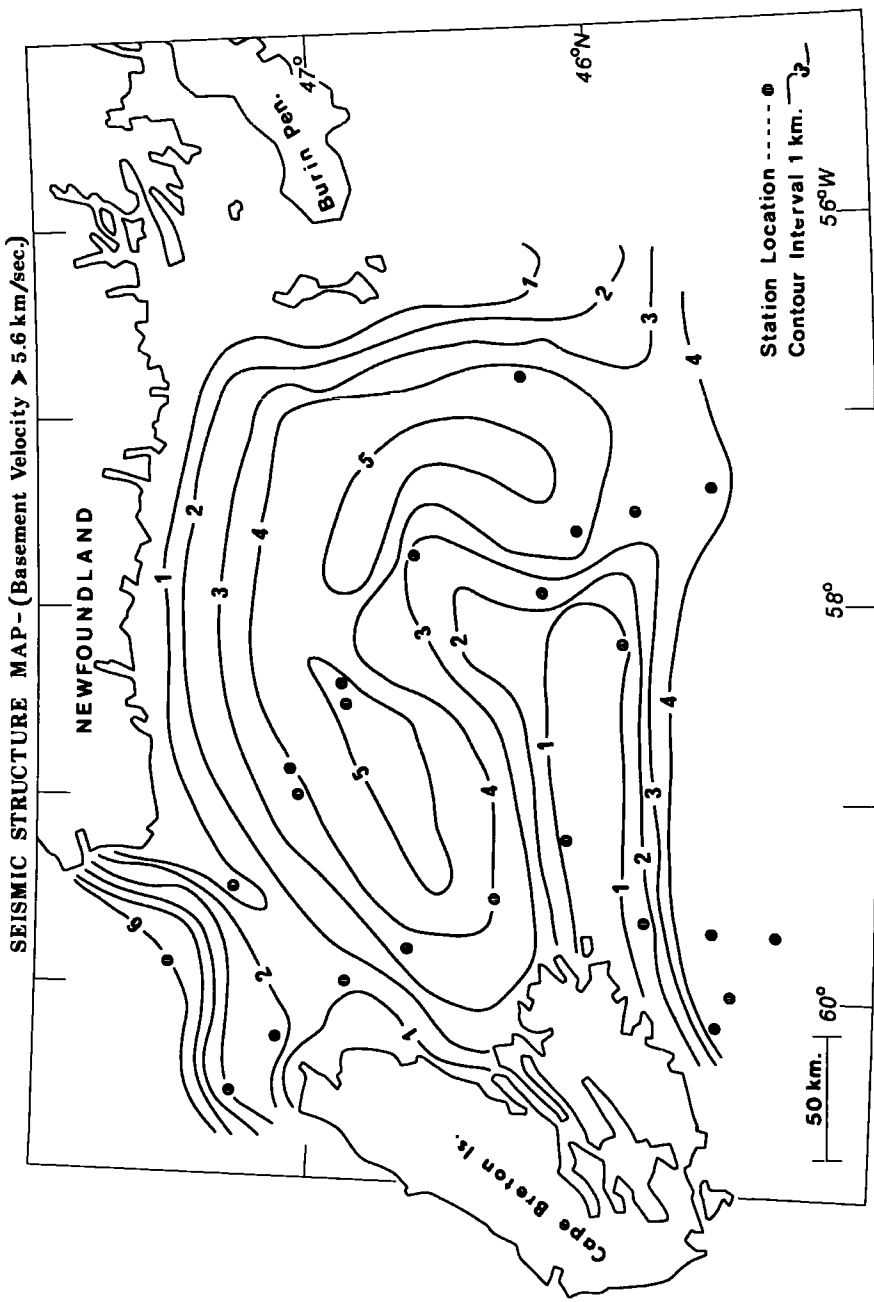
Figure 4.6:   Compressional wave velocities in sedimentary

(and plutonic) rocks at selected sites in

Newfoundland.   Figure from Hobson and

Overton (1973).

VELOCITY KM./SEC.
1 2 3 4 5 6 7

DRIFT

CARBONIFEROUS

SILURIAN

ORDOVICIAN, WESTERN

ORDOVICIAN, CENTRAL

ORDOV. TO DEVONIAN

ORDOV; SILUR; DEV; & EARLIER

ORDOV. & CAMBRIAN UNDIV.

ORDOV. OR EARLIER

CAMBRIAN

CAMBRIAN OR EARLIER

HADRYNIAN

PLUTONIC DEV. & EARLIER

PALEOZOIC

PRECAMBRIAN
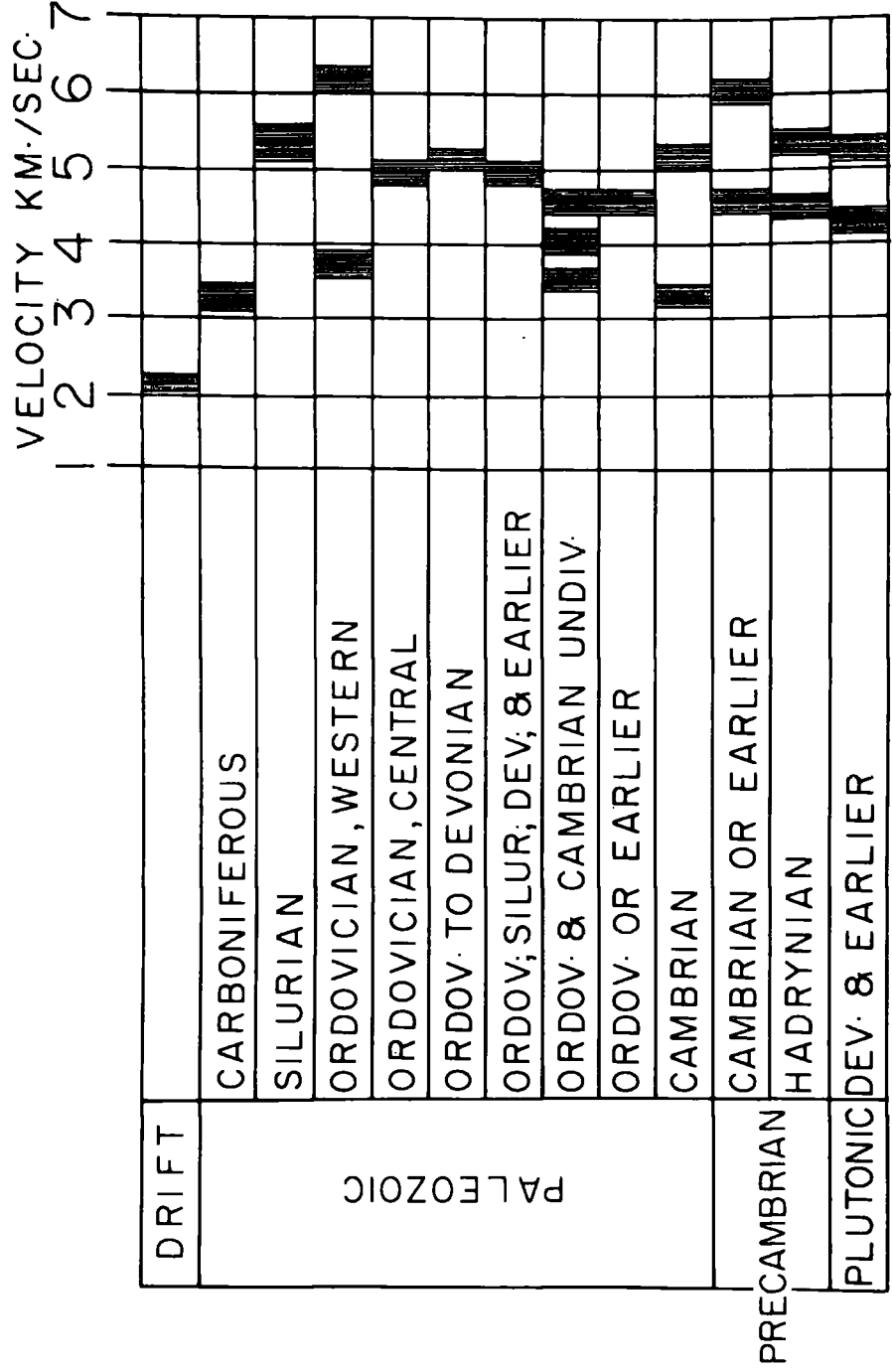
data in Figure 4.6 but Figure 4.5 also shows that there is a broad

basement depression, ie. the Sydney Basin (Jansa and Wade, 1975),

under the northern Scotian Shelf.

A multiple linear regression analysis of the gravity and

shallow seismic data over the northern Scotian Shelf and in the

Gulf of St. Lawrence showed no systematic relation between Bouguer

anomaly magnitude (Figure 4.7) and the compressional wave velocity

within any layer or the thickness of a layer. We cannot, therefore,

use the magnitude alone of the gravity data to predict the extent

and depth of sedimentary basins in this region.

The magnetic data (Haworth et al., 1972) show several intense

large-scale anomalies (Figure 4.8) that generally trend east to

northeast. These probably reflect pre-Carboniferous crystalline

basement structures. There is a generally good correlation between

the belt of linear magnetic highs which extends eastward from

southeast Cape Breton Island and the corresponding gravity and

seismic basement highs. However, the relations between magnetic,

gravity and seismic features over the shelf to the north are more

complex as will be subsequently discussed.

4.4 ST. PIERRE HIGH

The St. Pierre High (Figure 4.7) is a large region of positive

gravity anomaly which extends in a somewhat arcuate fashion westward

from the St. Pierre and Miquelon Islands (Figure 4.3) toward Cape

Breton Island. The northward, convex side of the anomaly is marked

Figure 4.7:   Simplified Bouguer anomaly map of the

northern Scotian Shelf. For more detail

see map in pocket.

BOUGUER ANOMALY MAP – NORTHERN SCOTIAN SHELF
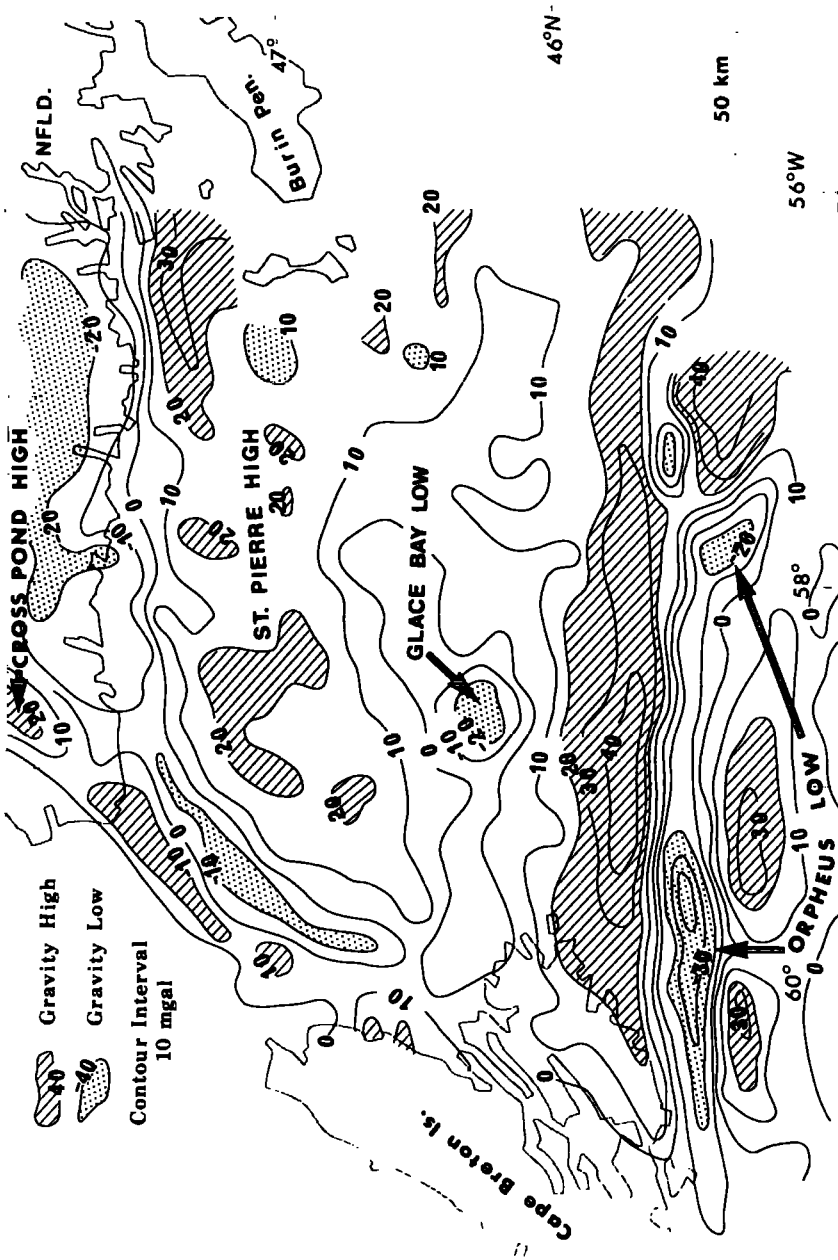
Figure 4.8:   Simplified total magnetic field anomaly map

of the northern Scotian Shelf. Data obtained

from Sheridan and Drake (1968) and Haworth et al.,

(1972). The contours are based on a limited

amount of data as can be seen from the distri-

bution of profiles in Figure 4.3

SIMPLIFIED TOTAL MAGNETIC FIELD ANOMALY MAP - NORTHERN SCOTIAN SHELF

Magnetic High

Magnetic Low

Contour Interval
200 gammas
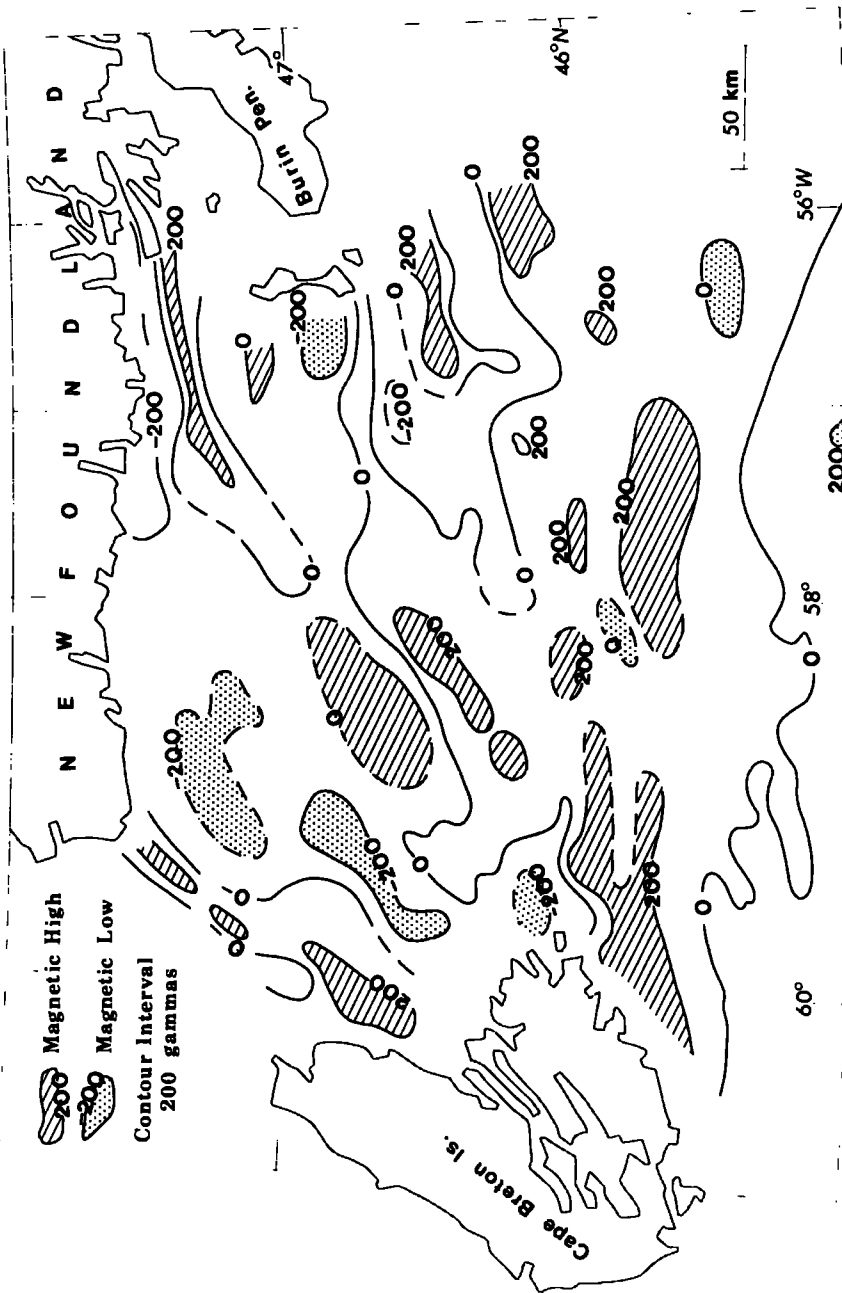
by a steep gravity gradient which, in the vicinity of Hermitage
Bay, marks the seaward extension of the major fault zone which
separates the Proterozoic .volcanic rocks and sedimentary rocks
of the Avalon platform (Zone H) from metamorphic rocks of Zone G.
Associated with the steep gradient are gravity and magnetic highs
over Proterozoic (?) basic lava flows (Figure 4.9) (see location
of profile in Figure 4.10).

In the area to the south and east of the Ramea Islands (Figure
4.1), both the gravity and magnetic anomalies exhibit east-west
trending features that clearly represent seaward extensions of
structures observed on the Burin Peninsula and on the St. Pierre
and Miquelon Islands. Examination of the gravity and magnetic
anomaly maps shows spatial coincidence in two cases of east-west
trending linear highs; these highs probably represent belts of
basic lava. About 20 km west of Grand Miquelon Island there is
an interesting example of the coincidence of a magnetic high and
a gravity low. A similar inverse correlation occurs on the Burin
Peninsula in an area intruded by granitic rocks (southeast end
of profile A-A' in Figure 4.9) and therefore the gravity low west
of Grand Miquelon Island probably outlines another magnetic granite.

A series of seismic refraction profiles (Sheridan and Drake,
1968) along the axis of the Laurentian Trough (Figure 4.11) show
that, with the exception of the prominent northeast trending ridge
situated between Cape Breton Island and southwestern Newfoundland
the crystalline basement rocks are buried at depths of 2 km or more,

Figure 4.9:   Total magnetic field, Bouguer anomaly and

geology along profile A-A' North Bay –

St. Lawrence Harbour, Newfoundland.   See

Figure 4.10 for location of profile.

NORTH BAY - ST. LAWRENCE HARBOUR
(A-A¹)

NW   SE

Total Magnetic Field

Suggested Regional

Bouguer Anomaly

Rhyolite, schist, granite
Granite
Bay d'Espoir Gp.
Gneiss
F
Meta-volcanics, diorite
F?
Volcanic rocks
Granite
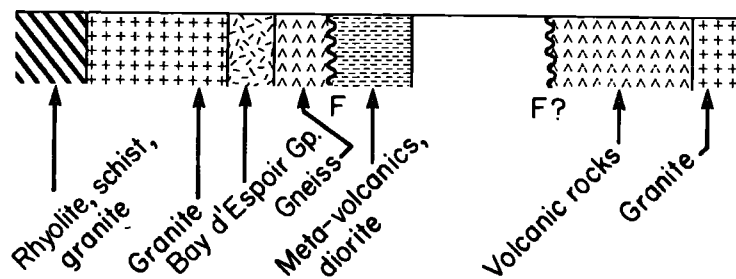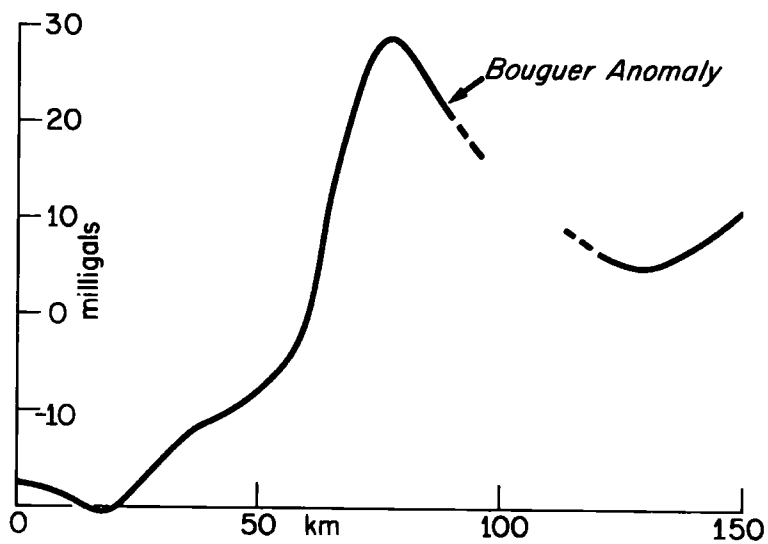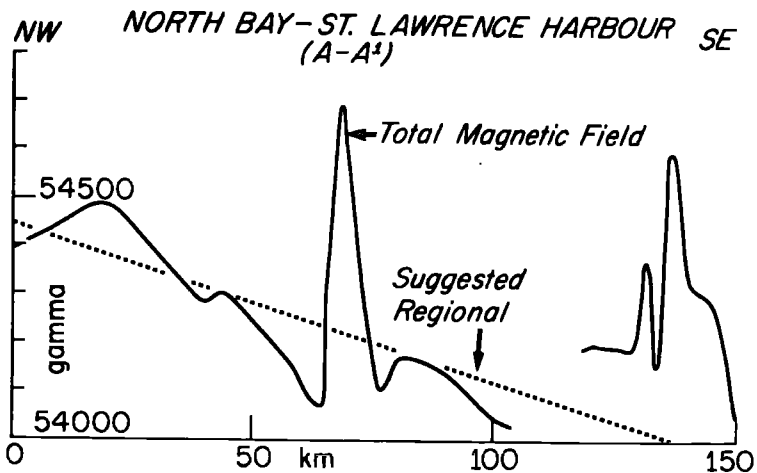
Figure 4.10:   Location of profiles discussed in Chapter 4.
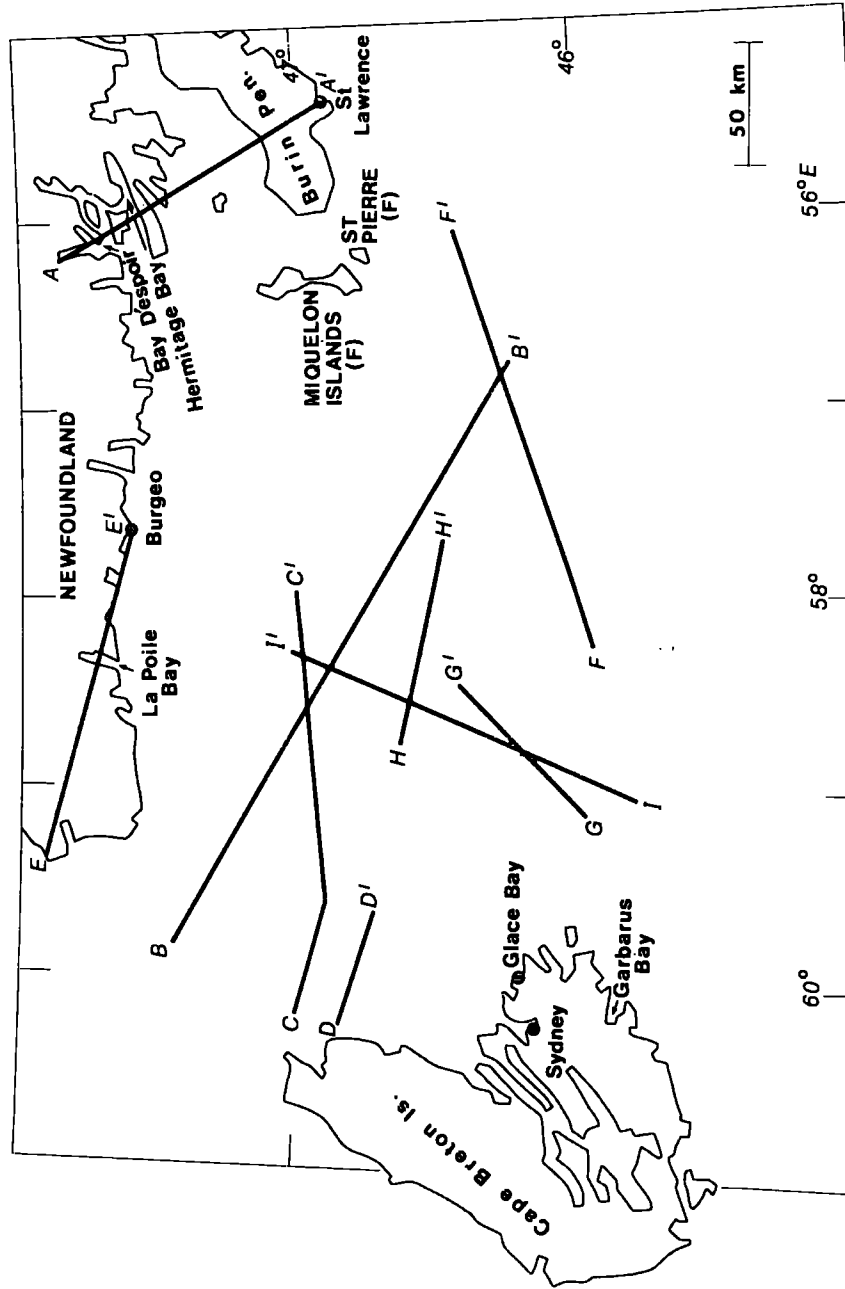
Figure 4.11:   Magnetic and gravity anomalies and seismic

structure along profile B-B' (profile runs

from northwest to southeast). Seismic data

from Sheridan and Drake (1968). Figure taken

from Goodacre et al. (1973). The letters C-D

in the reproduced diagram correspond to B-B'

in Figure 4.10. The profile runs from northwest

to southeast.

C

MAGNETIC PROFILE

GRAVITY PROFILE

ST.PIERRE HIGH
CROSS POND HIGH
GLACE BAY LOW
MAGDALEN LOW

GRAVITY IN BOUGUER ANOMALIES

REFRACTION SEISMIC PROFILE (AFTER SHERIDAN AND DRAKE, 1968)

VELOCITIES IN km/sec.

D

400 300 200 100 Km

400 300 200 100 Km

18W

400
200
0
-200

GAMMAS

40
20
0
-20
-40

M GAL

0
2
4
6
8
10
12

KILOMETERS
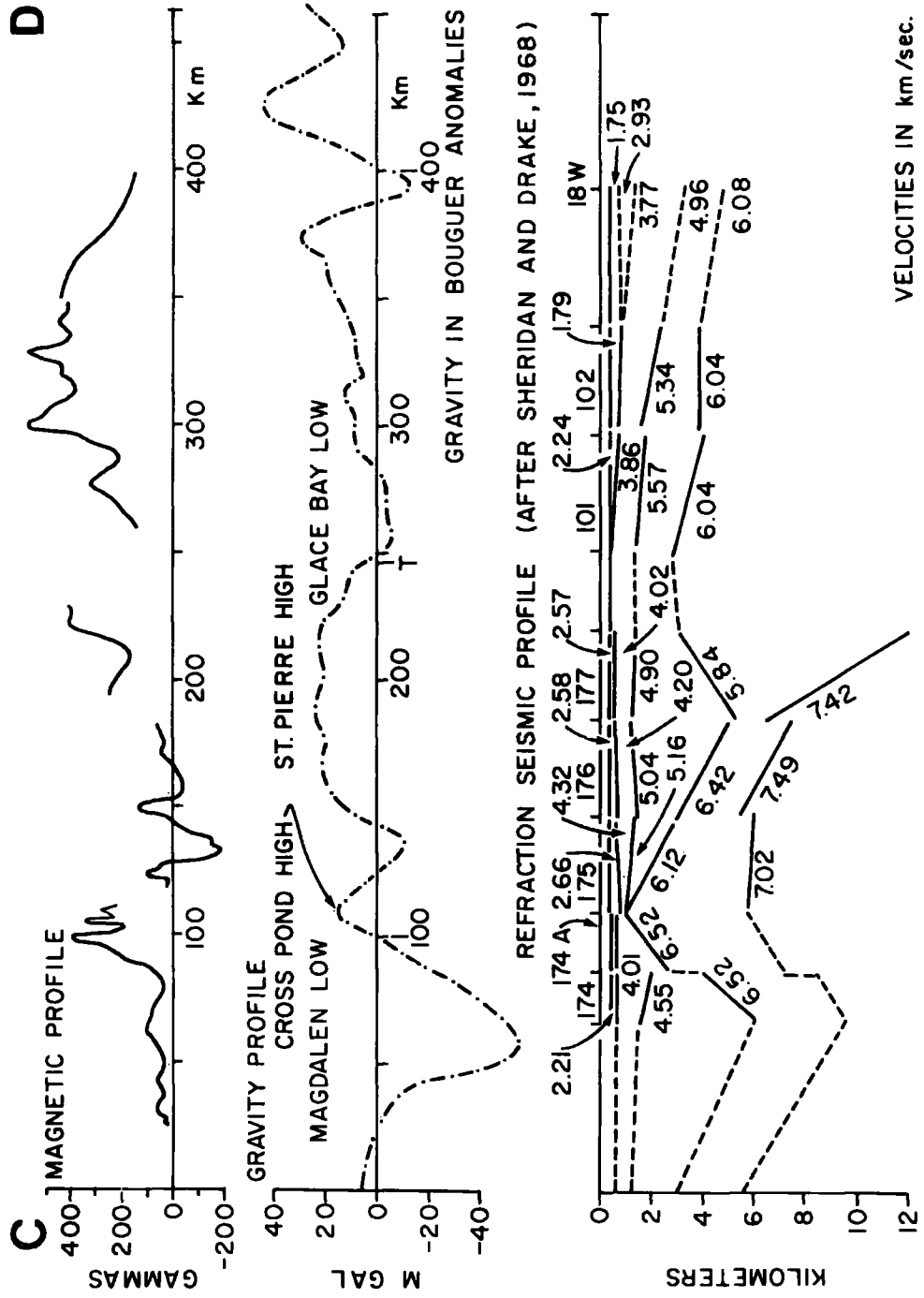
Figure 4.12:   Magnetic and gravity anomalies and pseudo-

gravity anomalies along profiles B-B' and

C-C'. m/d is the rate of magnetization

contrast to density contrast, Inc is the

inclination of the total magnetization

vector and r is the coefficient of linear

correlation between the gravity and pseudo-

gravity anomalies.

SE LAURENTIAN CHANNEL NW
(B-B¹)

Pseudo-Gravity Anomaly
Gravity Anomaly
Magnetic Anomaly

m/d=.013emu/gm
Inc =-30°(N)
r =.77

WSW ST PIERRE BANK ENE
(C-C¹)

Pseudo-Gravity Anomaly
Gravity Anomaly
Magnetic Anomaly

m/d=.029emu/gm
Inc =-40°(N)
r =.77

80 km 120 160
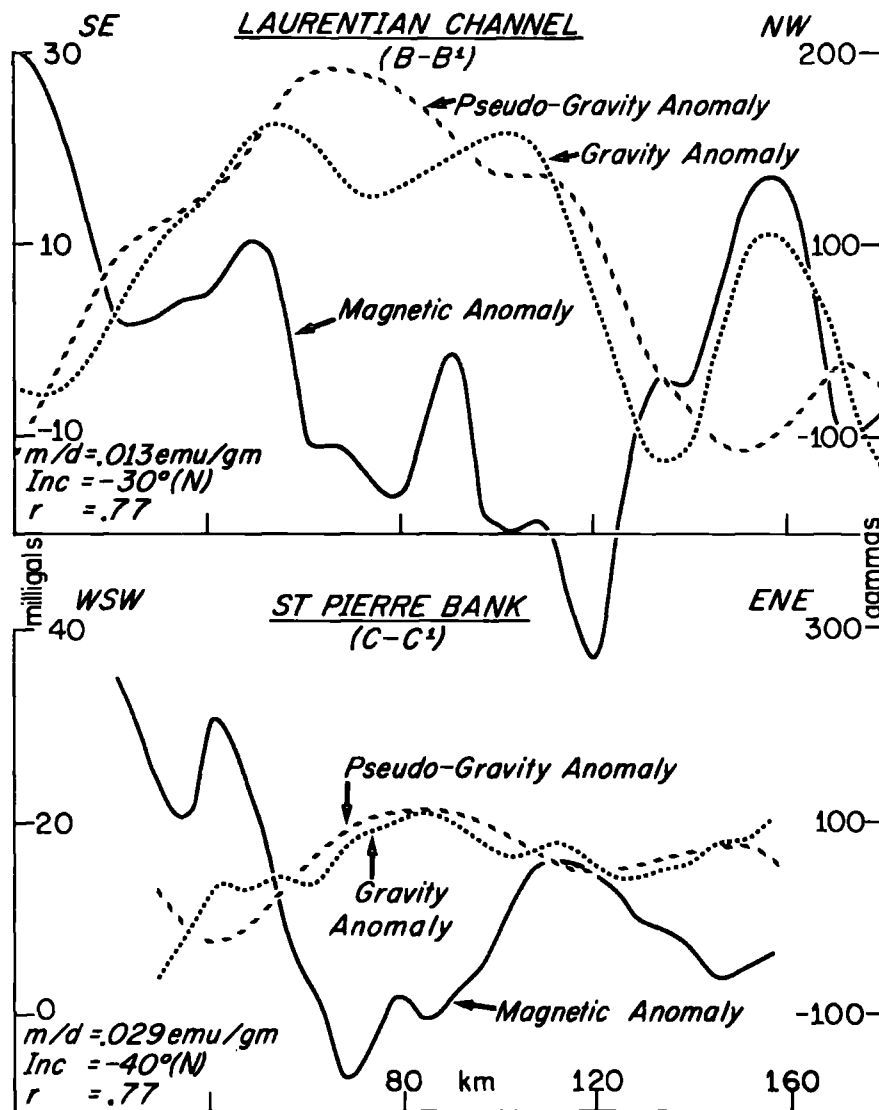
and as Goodacre et al. (1973) point out, there is no simple relation between the seismic results and the gravity and magnetic data. In fact, the gravity high lies near the deepest part of the seismically determined depression and if a correction were made for the mass deficiency of the sedimentary column, the gravity anomaly would be even more positive. From a classical point of view, the generally positive anomalies might reflect, at least in part, crustal thinning beneath the Palaeozoic sedimentary basin but it should be noted that in the Gulf of St. Lawrence, some 300 km to the west where there is a well developed Palaeozoic sedimentary basin (e.g. Sheridan and Drake, 1968), the generally positive Bouguer anomalies are associated with a crust which is thicker, and not thinner, than the crust beneath Nova Scotia and Anticosti Island (Ewing et al., 1966) (See Figure 1.1 for location). Therefore, in the Gulf of St. Lawrence the positive gravity anomalies probably reflect heavy rocks within the crustal column and the same may be true of the St. Pierre High.

Two-dimensional combined analyses of gravity and magnetic profiles B-B' and C-C' (Figure 4.12) over the western portion of the St. Pierre High suggest that the basement in this region is highly magnetic and that a considerable degree of remanent magnetization may be present although this will be discussed more fully in the next section. It is significant that the gravity high marks a region where unusually high compressional wave velocities of 7 km/s are observed at the relatively shallow depth of about

6 km. In Figure 4.11 the area where seismic velocities in excess

of 7 km/sec are observed seems to be shifted to the northwest of

the St. Pierre High but when the original travel-time curves are

consulted and the position where the seismic rays penetrate the

high-velocity refractor is determined, there is good agreement

between the appearance of the 7 km/sec material and the northwest

edge of the gravity high. It must be stressed, however, that

the evidence for velocities in excess of 7 km/sec is somewhat

marginal and depends in the case of each profile (175, 176 and 177

from Sheridan and Drake, 1968) on only two or three data points

and the high apparent velocities might be due to basement

structure rather than a mafic rock composition. The seismic, gravity

and magnetic data are all consistent with the presence of gabbroic

or possibly even more mafic basement rocks but the reason for inverse

correlation between the gravity and magnetic anomalies is not clear.

The mafic basement may be reversely magnetized but it is more likely

that the magnetic highs reflect normally magnetized acidic phases

in the basement or possibly serpentinization of the mafic basement

rock (Saad, 1969). In this latter case the serpentinized rocks

would exhibit a negative density contrast and a positive magneti-

zation contrast and they would be normally magnetized. It is

tempting to equate the high-density, high-seismic velocity basement

underlying the western St. Pierre High with oceanic(?) basic to

ultrabasic rocks from the northwestern part of the Newfoundland

central mobile belt (Zone D, Figure 4.2), as some of these rocks

exhibit densities of 2.8 to 3.2 g/cm^3 and compressional wave

velocities of 6.6 to 7.4 km/s (Petersen et al., 1974). In addition,

there is a suggestion in the magnetic compilation that the linear

positive anomaly extending westward from Hermitage deflects to the

southwest in the vicinity of the Ramea Islands and that the magnetic

lows to the west in the area presently being discussed are

consistent with the depressed field in the eastern part of the

central mobile zone. However, deep magnetic lows also occur over

the Avalon Zone (see for example Figure 7.2) and geological

evidence (Williams et al., 1970) suggests the eastern marginal

metamorphic zone (Zone G) runs westward along the south coast of

Newfoundland rather than turning southwest near the Ramea Islands.

In addition, the oceanic rocks in Zone D appear to be normally

magnetized and compressional wave velocities of 6.6 to 7.4 km/s

could also be produced by mafic granulites and schists (e.g.

Goodacre, 1972). As such, there is no strong evidence for

Palaeozoic oceanic rocks to the southwest of this marginal zone.

4.5 THE SIGNIFICANCE OF DIRECTIONS OF TOTAL MAGNETIZATION OBTAINED FROM THE COMBINED ANALYSIS OF GRAVITY AND MAGNETIC ANOMALIES

The directions of magnetization obtained from the combined

analyses of the gravity and magnetic anomalies along profiles B-B'

and C-C' are nearly at right angles to the earth's field which dips

north-northwest at an angle of 74°. This result is surprising as

It implies that there is quite a strong remanent magnetization in
the underlying basement rocks. It is interesting to note that
Bhattacharyya and Raychaudhuri (1967) analysed the magnetic field
over southeastern New Brunswick and the western part of central
Nova Scotia and found several areas where the direction of
magnetization differed significantly from that of the earth's
field. Although their computed directions are generally scattered,
in one area near $45.5^{\circ}N$; $66.5^{\circ}W$ which is characterized by Devonian
granites, directions of magnetization calculated from four positive
magnetic features cluster together and have a mean azimuth and
inclination of about 150° and 60° respectively (the azimuth and
inclination of the earth's field is about -25° and 75° in this
area). The main weakness in their approach probably is that the
causative body is assumed to have the form of a vertical
rectangular prism (Bhattacharyya, 1966) and the resulting directions
of magnetization may merely be artefacts of the vertical orient-
ation of the prism. Nevertheless, it is possible that some of the
anomalies in their study area are produced by sources which possess
a significant degree of remanent magnetization. In addition to the
Devonian granites mentioned previously, southwestward directed,
downward dipping magnetizations are calculated by Bhattacharyya and
Raychaudhuri (1967) from magnetic highs over Devonian mafic
volcanics near $47^{\circ}5N$; $66.5^{\circ}W$ and from the magnetic high over the
pre-Carboniferous Cobequid basement complex (see Figure 6.2 for
location) centered at approximately $45.5^{\circ}N$; $63.5^{\circ}W$. Because the

problem of obtaining directions of total magnetization which
appear to be significantly different from the earth's field arises
several times in this and subsequent chapters, it seems appropriate
to discuss the problem rather fully here and, where necessary,
refer to this discussion later on. The questions raised by the
combined analysis of profiles B-B' and C-C' are: (1) is the
application of the combined analysis of the gravity and magnetic
anomalies valid and (2) if it is, under what conditions are rocks
likely to exhibit a large amount of remanent magnetization which is
oriented in a direction that is considerably different from the
earth's field?

Although the correlation between the pseudo-gravity anomaly
and the observed gravity anomaly is not high (0.77) along either
of the intersecting profiles B-B' and C-C', the results of the
combined analysis seems to be more or less consistent; the
inclinations of the total magnetization vector (projected into
the vertical plane containing the earth's field) only differ
by about 10° and the ratios of magnetization contrast to density
contrast are of the same order of magnitude although the value
obtained from profile C-C' is about twice as large as the value
obtained from profile B-B'. In profile B-B', it is clear that there
is almost zero, or even a negative, correlation between the pseudo-
gravity anomaly and the observed anomaly at the northwest end of
the profile (at a distance of about 160 km in Figure 4.12) but
the fit is good elsewhere. If the northwest end of the profile

were omitted from the combined analysis a somewhat different result might be expected but the direction of magnetization probably would still differ significantly from the direction of the earth's field.

It is unlikely that the unusual directions of magnetization are the result of some sort of systematic error in the data such as in the positioning of the profiles because the gravity and magnetic information along each profile was obtained by different agencies. The underwater gravity data along profile B-B' was obtained by the Earth Physics Branch (Stephens et al., 1971) and the magnetic information by Lamont Geological Observatory (Sheridan and Drake, 1968). The sea-surface gravity and magnetic data along profile C-C' were collected by the Bedford Institute (Haworth et al. 1972). There seems to be no technical difficulty in the application of the two-dimensional magnetic to gravity field transformation. A modified version of the program by Bott and Ingles (1973) works well on artificial data and, unlike the three-dimensional transform, there is no problem of having to use an insufficient number of data points or equivalent layer prisms due to a lack of computer space. In each application of the two-dimensional transformation, pseudo-gravity anomalies are calculated for a wide range of inclinations of magnetization and the angle which gives the best fit is accepted. To summarize, the unusual directions of magnetization do not seem to result from problems with the data or the computer program and therefore the inclinations are either real or they are the result

of one or more of the assumptions made not being fulfilled.

The three assumptions made are (1) the gravity and magnetic sources have an infinite strike length (2) the direction of magnetization is uniform throughout the source and (3) the ratio of magnetization contrast to density contrast is constant throughout the source. In the case of profiles B-B' and C-C' the gravity and magnetic anomalies tend to have a two-dimensional character inasmuch as the gravity and magnetic contours trend northeast-southwest (Figures 4.7 and 4.8) but there is, in fact, insufficient magnetic information (see the distribution of profiles in Figure 4.3) to adequately delineate the magnetic anomalies and do a three dimensional gravity to magnetic field transformation in order to try to answer the question of how well the assumption of two-dimensionality is fulfilled. The question of whether the direction of magnetization is uniform and the ratio of magnetization contrast is constant throughout the sources along profiles B-B' and C-C' can not be answered directly, but in general, the presence of a reasonably good correlation between an observed gravity anomaly and a calculated pseudo-gravity anomaly tends to support, but does not prove, the validity of these two assumptions. In the case of profiles B-B' and C-C' the correlation is marginal and the results of the magnetic to gravity field transformation should not be regarded as highly significant although it does seem as if some remanent magnetization may be present in the source rocks. In some cases, to be discussed subsequently in this and following chapters, the results of two-dimensional magnetic to gravity field

transformations are supported by two-dimensional magnetic modelling but, of course, it must be stressed that compatible results of the magnetic modelling process are not proof of the validity of the combined analysis.

If, in those situations where there is nothing obviously wrong with the results of a combined analysis of magnetic and gravity anomalies we accept that the source rocks possess some remanent magnetization, what are the source rocks likely to be? The obvious thing to do is to measure the magnetic properties of rocks in areas where there is a reasonably good correlation between the observed gravity and the calculated pseudo-gravity anomaly and where remanent magnetization appears to be present in the source. Unfortunately, rock magnetism studies in the Canadian Appalachians have mainly been done for palaeomagnetic purposes on relatively weakly magnetized sedimentary formations which do not generate magnetic anomalies that are large enough to be usable to attempt a combined analysis and, with the one exception at Sept Iles mentioned in Chapter 3, the magnetic properties of rocks have not been measured in the few areas where geophysical anomalies suggest the presence of some remanent magnetization. We can however, indirectly estimate to what extent the total magnetization vector could be deflected away from the direction of the earth's field by noting that average Koenigsberger ratio for rocks in southern New Brunswick (Figure 4.13) is about 0.2 (McGrath et al., 1973) and that, as will be discussed further in Chapter 7, the earth's

magnetic field was nearly horizontal during the Devonian and
Carboniferous periods. Directions of remanent magnetization from
Carboniferous rocks in the Canadian Maritime Appalachians are
nearly horizontal and seem to invariably point south. Devonian
directions are inclined somewhat more steeply and are mixed with
some pointing down to the south, others up to the north.

Any stable remanent magnetization acquired during these times
would be nearly at right angles to the present-day earth's field
and therefore, be effective in deflecting the total magnetization
vector. The deflection would be about 12° for a Koenigsberger ratio
of 0.2 and about 23° for a value of 0.4, which is high but not
unreasonable. We can conclude therefore, that computed directions
of total magnetization which differ by more than, say, 15 or 20°
from the earth's field are unlikely and results such as those from
profiles B-B' and C-C' where the correlation is marginal are
probably spurious for some uncertain reason. Directions of
magnetization which differ by less than about 15 or 20° might
reasonably be expected, however.

One last comment is that the present direction of permanent
magnetization in rocks may be controlled by some means other than
the direction of the earth's field at the time of cooling (or
deposition in the case of sedimentary rocks). For example, the
direction of permanent magnetization might be controlled by any
lineation that is present in metamorphic rocks or the source rocks
could have been tilted, rotated or folded since the permanent

Figure 4.13:   Frequency distribution of Koenigsberger ratios

for rock cores obtained in southern New

Brunswick (McGrath et al., 1973). Figure made

from a negative kindly supplied by P. McGrath.

$$Q = \frac{NRM}{IM}$$

Mean = 0.22

Mode = 0.15

Frequency

Q-factor
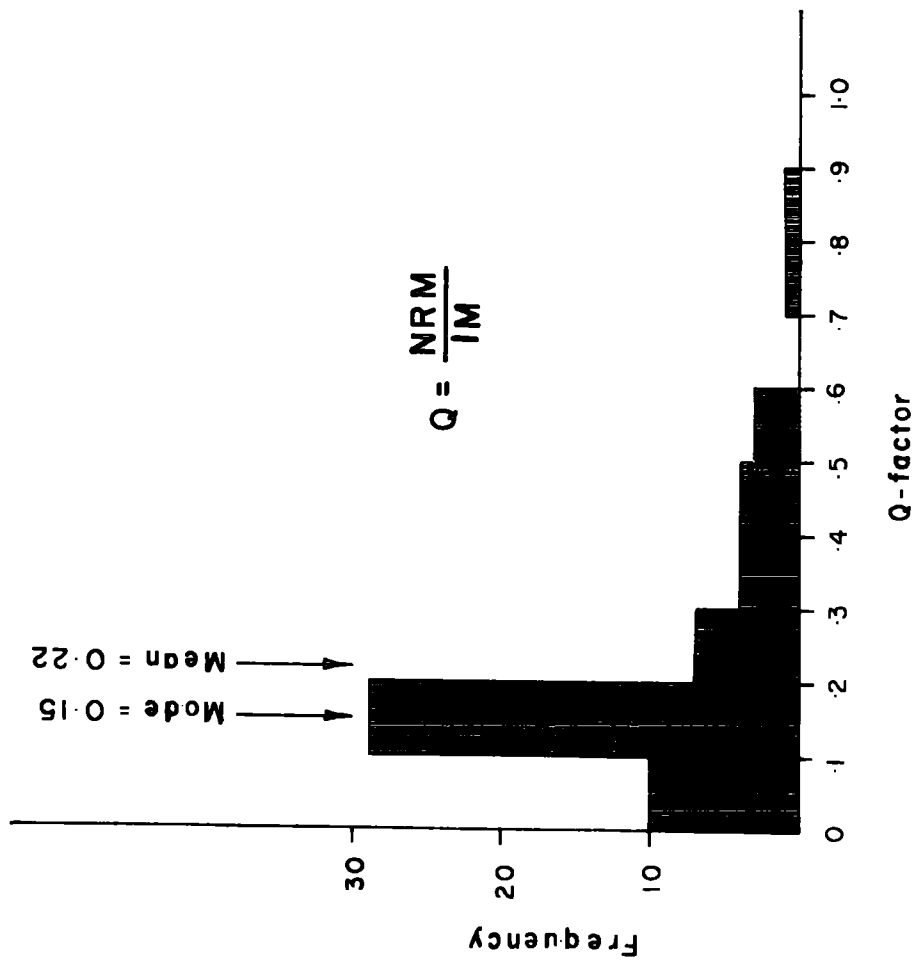
magnetization was acquired. In such a case, a direction of permanent magnetization inferred from the combined analysis of gravity and magnetic data would not accurately reflect the time when the source rocks acquired their magnetization.

4.6 CROSS POND HIGH-GRANITE LAKE LOW EXTENSION

The St. Pierre High is flanked on its western side by a linear, southwest-trending gravity low which appears to be an extension of the Granite Lake Low (Weaver, 1967) centered near $48^{\circ}N$; $57^{\circ}W$ in southern Newfoundland. To the west of the gravity low is a linear gravity high which seems to be an extension of the Cross Pond High (Figure 4.7) and which probably represents either pre-Carboniferous basement complex similar to those found in Cape Breton Island (Goodacre et al., 1969) or a basic Devonian intrusion (Weaver, 1967) or a combination of these sources.

The linear negative gravity anomaly is characterised at its southern end by a magnetic high (Figure 4.14). Since there is no seismic evidence that the negative gravity anomaly is due to a narrow, deep sedimentary basin (Figure 4.5), the anomaly probably outlines a zone of magnetic, low-density gneiss similar to that found about 20 km west of Burgeo (Figure 4.15). Simple models of the gravity low and associated magnetic high (Figure 4.16) have several features in common: both models are wider at the bottom than at the top, their sides dip at angles of 30° or more and they both extend to depths of 10 to 15 km. On the other hand, the sides

Figure 4.14:   Magnetic and gravity anomaly and pseudo-

gravity anomaly along profile D'-D which crosses

the southwesterly extension of the Cross Pond

High-Granite Lake Low in southwestern

Newfoundland (Weaver, 1967). Note that the

direction of profile D'-D is from eastsoutheast

to westnorthwest so that the gravity high

is on the right side of the diagram; the low

to the left.

CROSS POND HIGH
(D¹-D)
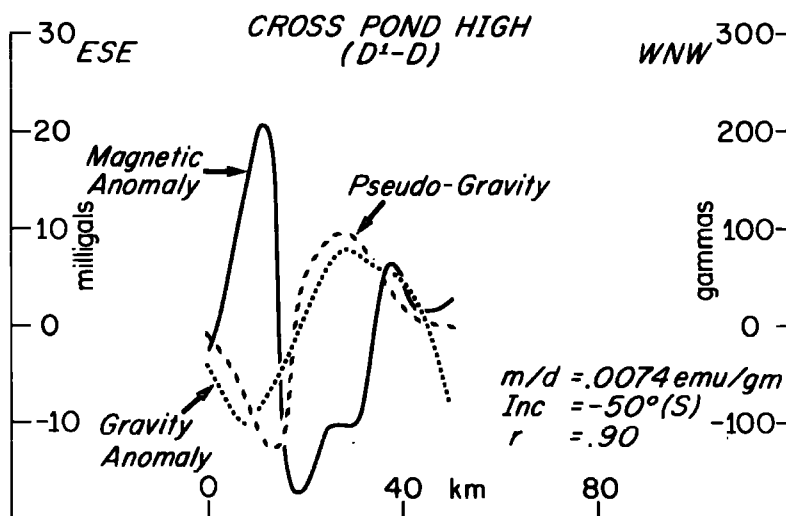
Figure 4.15:   Total magnetic field, Bouguer anomaly and

geology along profile E-E' from Cape

Anguille to Burgeo, Newfoundland.   See

Figure 4.10 for location of profiles.

CAPE ANGUILLE - BURGEO
(E-E¹)

W

E

—55500

—55000

gammas

←Total Magnetic Field

Suggested
Regional

50   km   100   150

—20

—10

milligals

←Bouguer Anomaly

—-10

—-20

Cape Ray
Fault

Bay du Nord

La Poile Gr.

Sandstone,
shale, greywacke

Slate, quartzite,
greywacke

Rhyolite, tuff,
schist, paragneiss

Granite
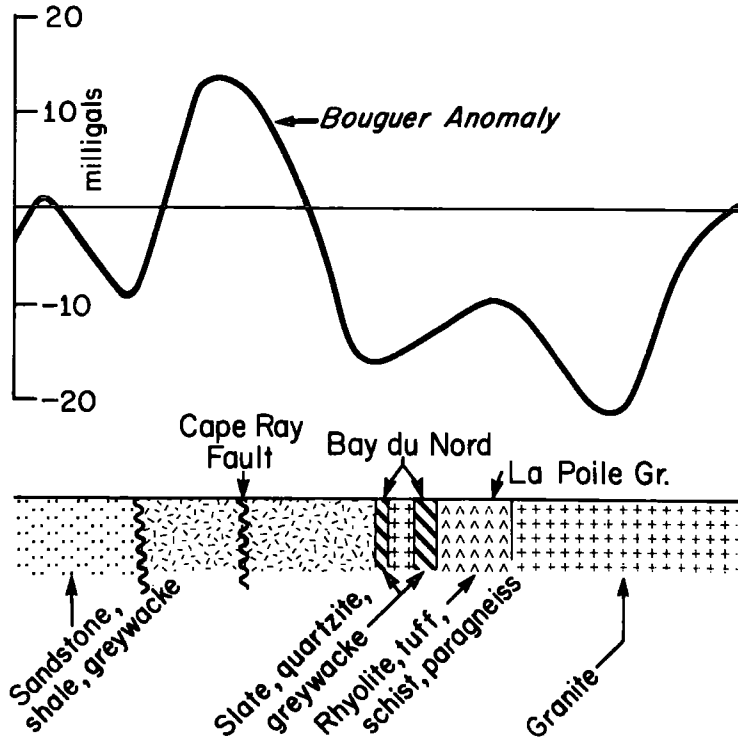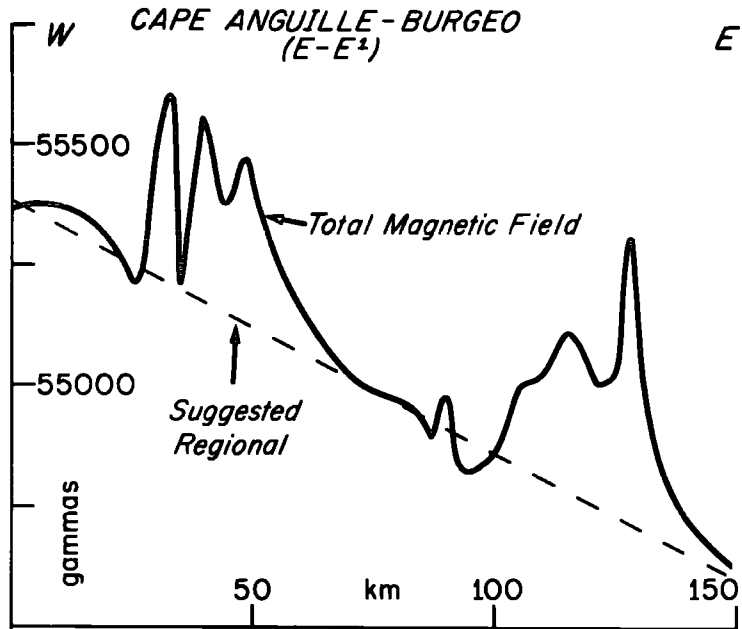
Figure 4.16:   Observed gravity and magnetic anomalies over
a portion of profile D'-D, interpretative
gravity and magnetic models and calculated
anomalies. The Cross Pond High is the gravity
high on the northwest side of the extension of
the Granite Lake Low. The models shown here
relate to the gravity low and the associated
magnetic high.

CROSS POND HIGH
(D^{1}-D)

30 ESE milligals

WNW 300 gammas

Calculated Magnetic Anomaly

Observed Magnetic Anomaly

Magnetic

Gravity

Observed Gravity Anomaly

Calculated Anomaly

Magnetic Model
m=+.001 emu/cm^3
Inc.=89°(S)

Gravity Model
d=−0.1 gm/cm^3
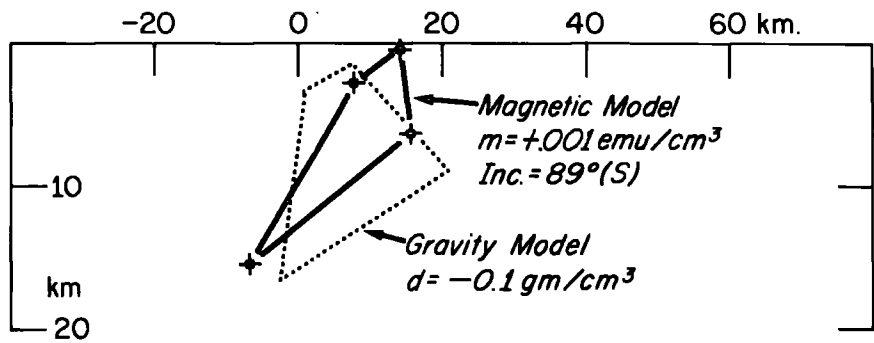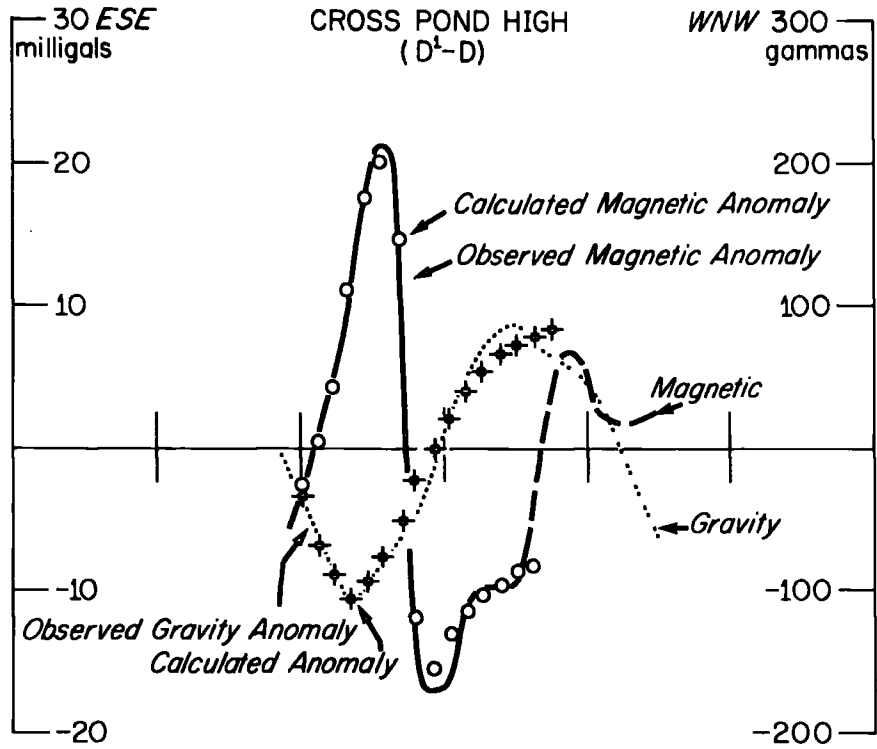
of the gravity model are not parallel with the corresponding sides of the magnetic model. In general, the models are consistent with the presence of a granitic body which is magnetic but possibly not uniformly magnetic, being more highly magnetized on the western margin than elsehwere.

The models in Figure 4.16 are determined by non-linear optimization and provide the best fit from a set of several gravity and magnetic models that were obtained using different initial configurations, density and magnetization contrasts, angles of magnetization etc. No attempt was made to force one model to fit another because I wanted to compare the angle of magnetization obtained for the magnetic model in Figure 4.16 with the results of a magnetic to gravity field transformation. In particular, the nearly vertical inclination of magnetization in the model did not compare well with the value of 50° (N) obtained from the analysis of profile D'-D (Figure 4.13). However, the model was constructed to fit only the easterly portion of profile D'-D so a magnetic to gravity field transformation was applied to the same portion and a maximum correlation of 0.95 between the observed gravity and the pseudo-gravity anomaly was achieved for an angle of inclination of 85° (S). This value is in much better agreement with that obtained from the model and confirms the validity of the two-dimensional magnetic to gravity field transformation when a high degree of correlation is obtained between observed and calculated anomalies but it also highlights

how important and difficult it is to properly isolate an anomaly

for interpretation. In this case, halving the length of the

profile changed the angle of magnetization by 45°.

A nearly vertical angle of total magnetization in the posulated

granitic gneiss is not unreasonable in view of the discussion in

Section 4.5 where it was pointed out that the total magnetization

vector might reasonably be displaced up to 15 degrees or so away

from the direction of the earth's field. As will be discussed

further in Chapter 7, a southerly directed remanent magnetization

could have been produced in the source body during the Devonian

or Carboniferous Period.

An interesting aspect of profile E'-E in Figure 4.15 is that

west of La Poile Bay there is a positive correlation between the

gravity and magnetic field whereas to the east there is a negative

correlation. This suggests the presence of a structural

discontinuity which might be the boundary between the eastern

marginal metamorphic Zone G and Zone F of the central mobile belt.

4.7 GLACE BAY LOW

The Glace Bay Low (Figure 4.7) is a negative anomaly belt which

extends eastward from Cape Breton Island towards St. Pierre and

Miquelon Islands. The gravity field reaches a minimum about 100 km

east of Glace Bay where a nearly circular low of about -20 mgal

amplitude is superimposed on a broader east-west trending low

of about 0 to -5 mgal. These anomalies are referred to a regional

level of about 5 mgal. This value is consistent with regional

levels determined by Weaver (1967) for Newfoundland and by

Goodacre and Nyland (1966) for the Gulf of St. Lawrence. The

broader low almost certainly reflects a basement depression

because seaward dipping Carboniferous sedimentary rocks are

exposed in the Sydney-Glace Bay region (Figure 4.1) and the broad

gravity minimum along profile F-F' (Figure 4.17) at the eastern

end of the anomaly correlates well with a depression in seismic

basement. The broad low is similar, in a general way, to the

broad gravity low over eastern Prince Edward Island defined by

Goodacre et al. (1969) (see map in Pocket, or Figure 7.1) and the

two lows together appear to outline an east-west trough of

Palaeozoic and possibly younger sedimentary rocks that is

interrupted by the uplifted pre-Carboniferous basement complexes

which form Cape Breton Island.

The nearly circular gravity minimum might reflect an accumula-

tion of low-density sedimentary rocks within the broader sedimentary

basin but a strong magnetic high associated with the gravity low

suggests this is probably not the case. Although the magnetic

anomaly might be due to reversely magnetized basement enclosing a

basin of non-magnetic, low-density sedimentary rocks, it seems

more likely that the anomaly source is a magnetic, low-density

granite surrounded by high-density basement rocks. The nearest

exposed example of such a situation is the magnetic granite at

the head of Gabarus Bay (Figure 4.3) in Cape Breton Island.

Figure 4.17:   Magnetic and gravity anomaly, pseudo-gravity

anomaly and seismic structure along profile

F-F'. Seismic structure from Sheridan and

Drake (1968).

LAURENTIAN TROUGH
(F-F')

WSW ... ENE

Magnetic Anomaly

Pseudo-Gravity

Gravity Anomaly

m/d = .099 emu/gm
Inc = -5(N)
r = .77

Distance km

3.7-4.0 km/sec

5.2-5.3 km/sec

6.0-6.3 km/sec

Depth km
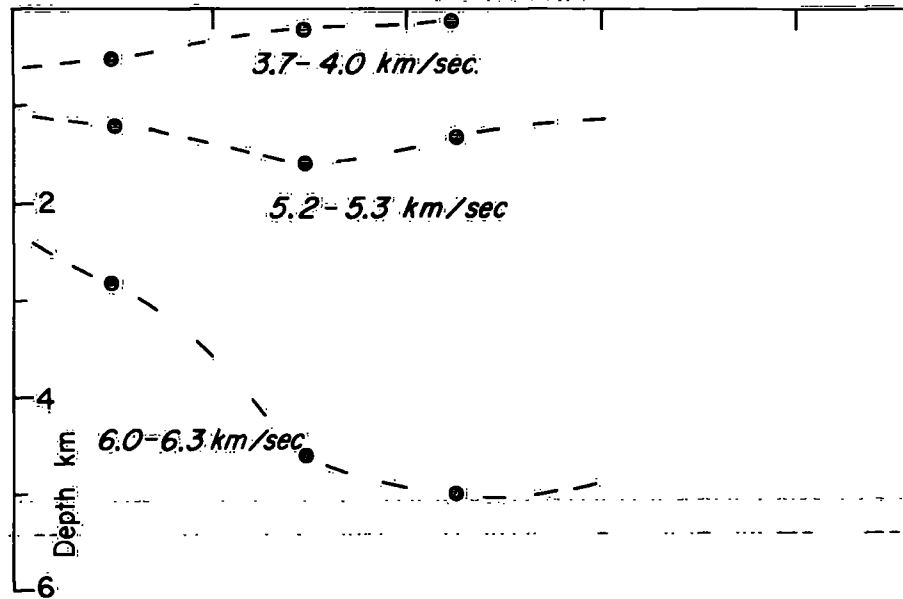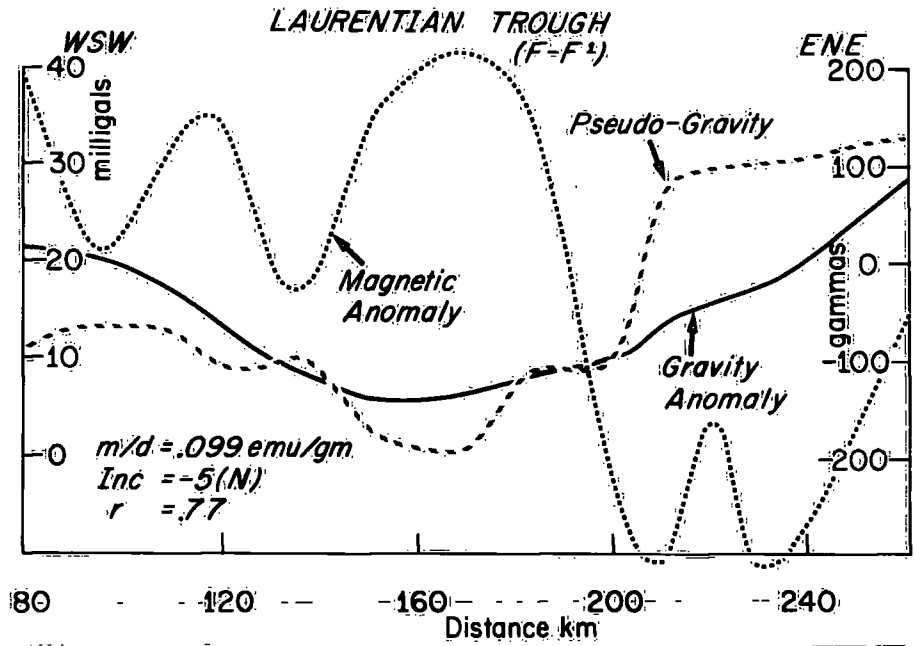
Figure 4.18:   Magnetic and gravity anomalies and pseudo-

gravity anomalies along profiles G-G' and

H-H'.

GLACE BAY FEATURE
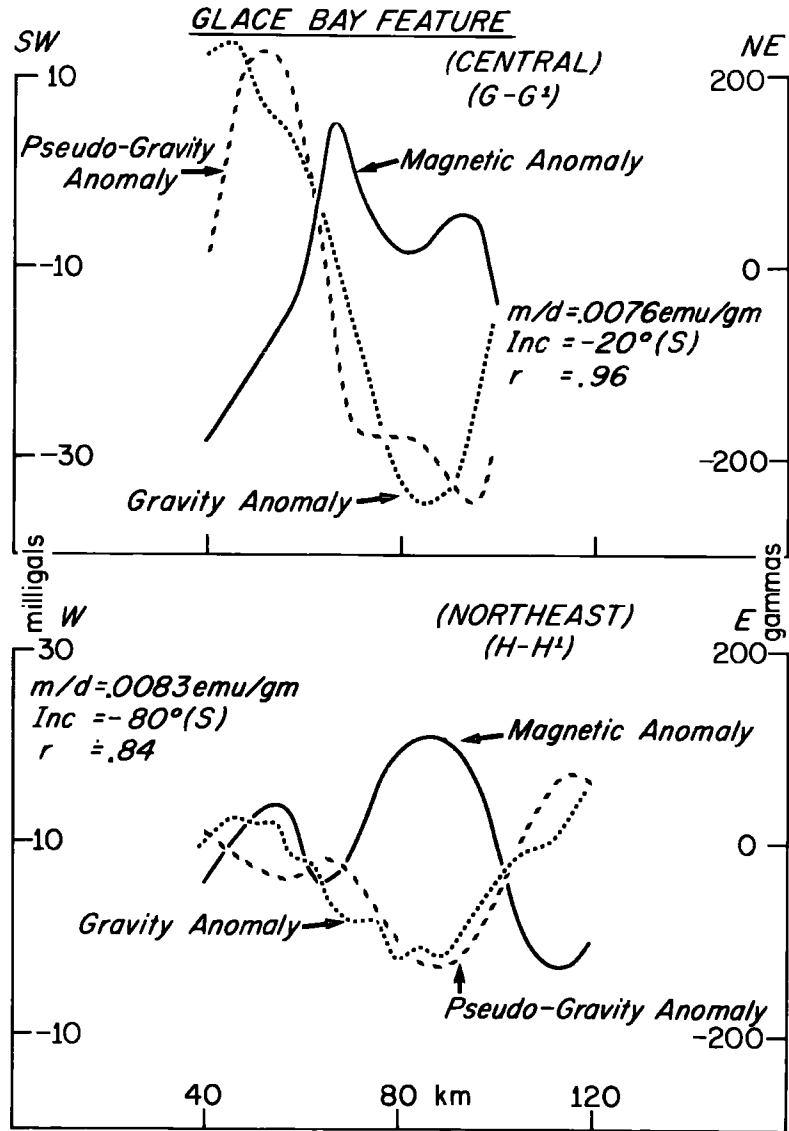
Figure 4.19:   Range of in-situ magnetic susceptibility

values from rocks in New Brunswick

(McGrath et al., 1973).   Figure made from a

negative kindly supplied by P. McGrath.
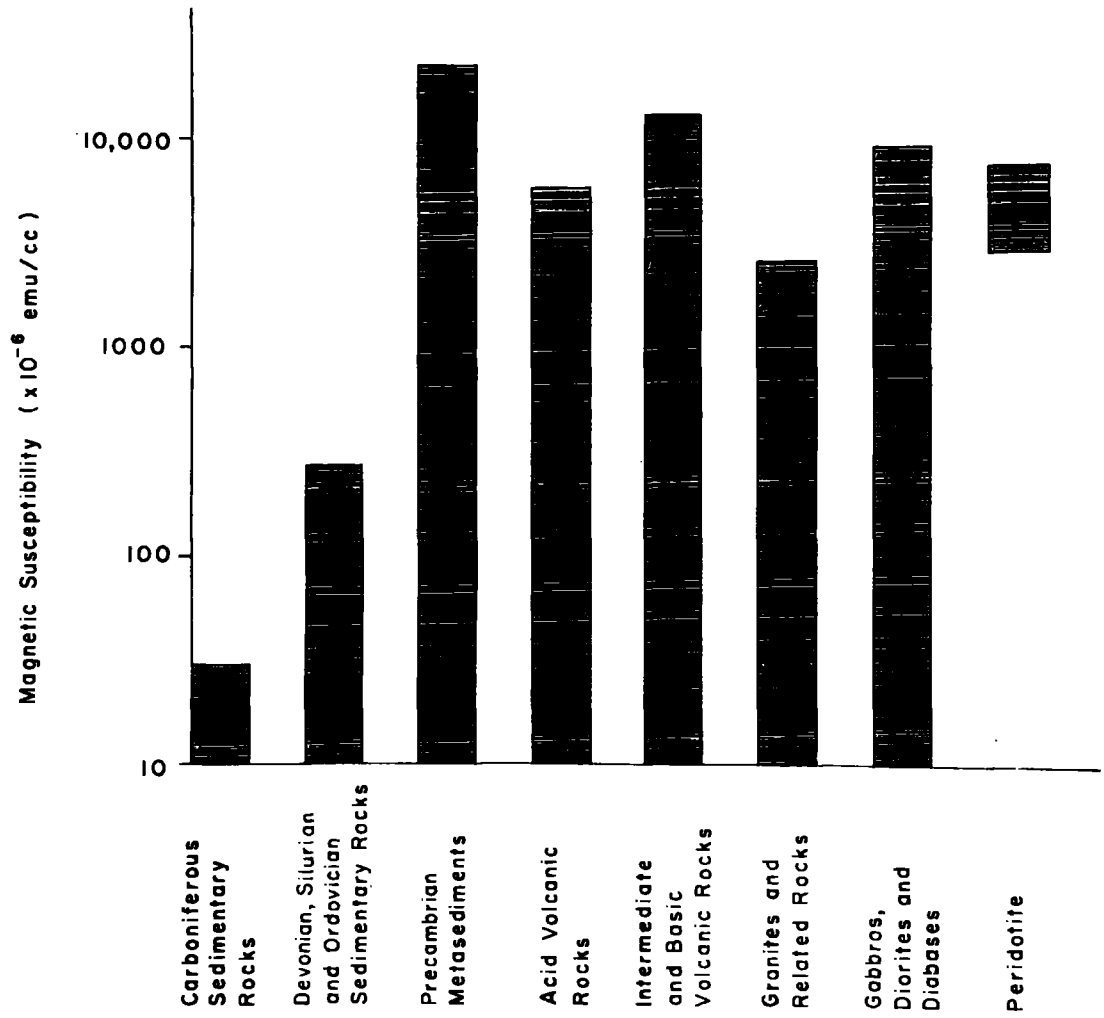
Figure 4.20:   Observed Bouguer anomaly, gravity model and

calculated gravity anomaly for profile I-I'

over the Glace Bay Low. The insert shows the

r.m.s. difference between observed and

calculated anomaly as a function of density

contrast of the source body and the depth of

the highest portion of the model.

GLACE BAY LOW

d=-0.2 gm/cm³
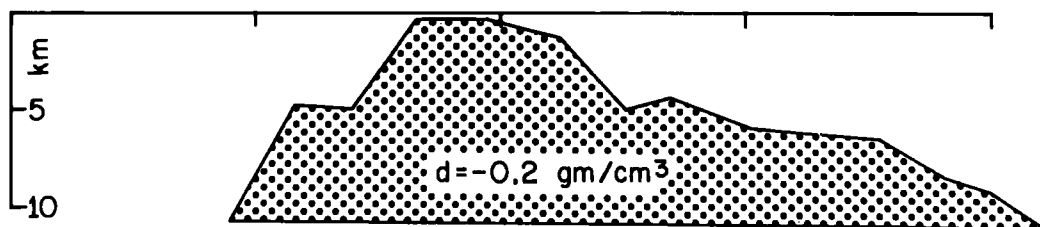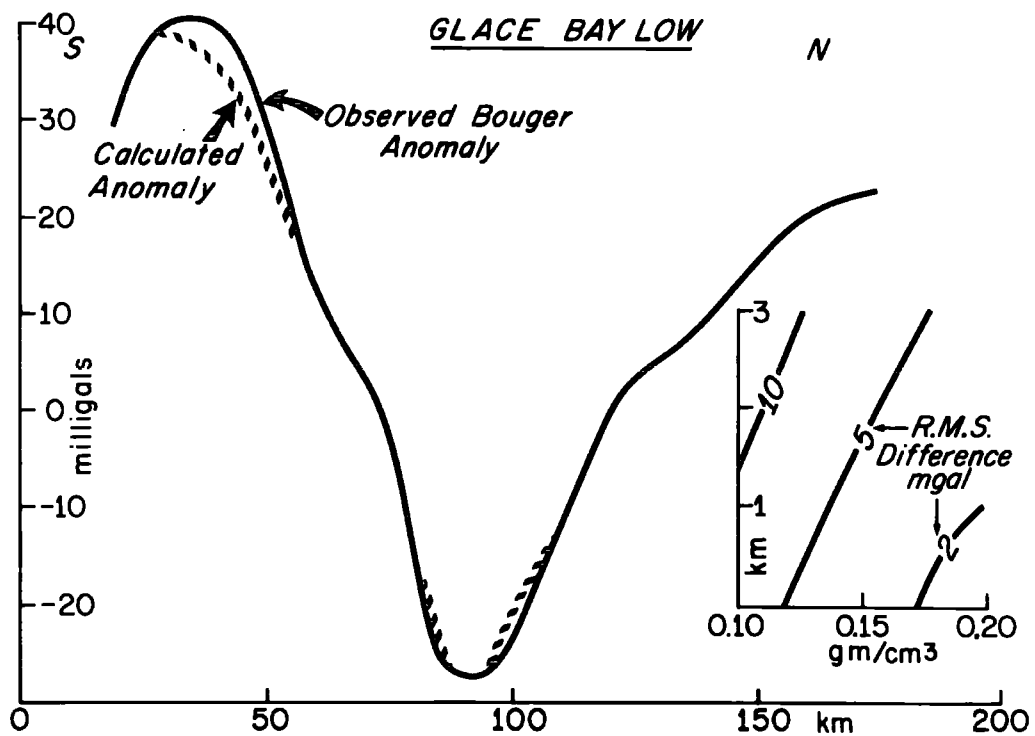
The relation between the gravity and magnetic anomalies is not simple, however, as the local gravity low is nearly circular whereas the magnetic high is elongate in a southwest-northeast direction. As mentioned in the caption of Figure 4.8, the magnetic anomaly field is not particularly well defined but it is clearly not what one would expect if the ratio of magnetization contrast to density contrast were uniform throughout the source. However, the main portion of the Glace Bay Low and the northeast-trending arm both seem to be associated with magnetic highs. Notwithstanding the differences in the gravity and magnetic anomaly patterns, both the gravity and magnetic data suggest the presence of a northeast-trending structural boundary dividing the rocks which produce the St. Pierre High from the rocks which cause the northeastern arm of the Glace Bay Low. Combined analysis of two profiles (Figure 4.18), one profile (G-G') crossing the circular gravity low and the other (H-H') crossing the tip of the northeast arm of the gravity low, shows apparently good correlation between the gravity and magnetic fields in each case. However, the directions of magnetization deduced for profiles G-G' and H-H' do not agree very well with each other and this tends to confirm the observation that the gravity/magnetic properties are not uniform throughout the postulated magnetic, low-density granite. In particular, the magnetization appears to be enhanced at the margins of the intrusion underlying the central portion of the Glace Bay Low and the rocks associated with the western arm seem to be non-magnetic.

The similar ratios of magnetization contrast to density

contrast of .008 emu/gm obtained from profiles G-G' and H-H' coupled

with the minimum density contrast value of about 0.2 gm/cm^3 derived

for the gravity source (see insert in Figure 4.20) indicate a

minimum magnetization values of about .0016 emu/cm^3 for the

causative magnetic rocks. Such rather high values are not

inconsistent with the postulated presence of granitic rocks since

magnetizations of this order (see Figure 4.19) are observed in some

granitic rocks in New Brunswick (McGrath et al., 1973) but the

magnetization value is by no means diagnostic as similar values

are found in a wide range of metasedimentary and acidic to basic

volcanic rocks (e.g. McGrath et al., 1973).

Figure 4.20 shows a gravity model obtained for profile I-I'

which crosses north-south across the central portion of the Glace

Bay Low. The model is calculated with respect to a regional

background of 40 mgal. It should be pointed out that the model in

Figure 4.20 is oversimplified because it does not take into account

the sedimentary column indicated by the seismic data in Figures

4.5 and 4.11. However, the broad low that the sedimentary basin

would be expected to produce is only of the order of 5 to 10 mgal,

at most, due to the relatively high seismic velocities encountered

in the sedimentary column (e.g. Figure 4.11); a correction for the

mass deficiency of the sedimentary basin would make the model

thinner but not change the main aspects. Another problem with the

model is that it comes too close to the surface to be compatible

with the seismic data in Figure 4.11 which suggest that the basement is buried about 2 to 3 km deep.. However, as the insert in Figure 4.18 shows, the depth of the top of the model (the vertical axis of the insert) can be increased to 2 km or so without markedly increasing the r.m.s. difference between the calculated and observed Bouguer anomaly. A third comment concerning the model in Figure 4.20 is that although other shapes are possible, the model exhibits the typical outward sloping contacts often associated with granitic intrusions (Bott, 1962) and is consistent with the sharp curvature of the anomaly in the vicinity of the gravity minimum. Therefore, the combination of gravity, magnetic and seismic data indicates the presence of a generally, but not uniformly, magnetic granite surrounded by high-density basement rock and overlain by 2 to 3 km of Palaeozoic and younger sedimentary rocks.

4.8 SUMMARY AND DISCUSSION OF THE STRUCTURE OF THE NORTHERN SCOTIAN SHELF

Although the shallow refraction seismic data indicate that much of the northern Scotian Shelf is underlain by an extensive, somewhat kidney-shaped basin trending approximately east-west and filled with late-Palaeozoic and possibly younger sedimentary rocks, most of the gravity and magnetic anomaly features appear to originate from within the crystalline basement. For example, the linear highs trending westward from the vicinity of the Burin Peninsula probably outline belts of volcanic rocks which are related to the basalts

and andesites of the Bull Arm Formation on the Avalon Peninsula and several gravity lows are associated with magnetic highs (e.g. the Glace Bay gravity low) and seem to outline magnetic granites similar to those found on the Burin Peninsula or at the head of Gabarus Bay on Cape Breton Island.

The general trends of the gravity and magnetic anomalies indicate that there is a broad-scale structural continuity between the late-Precambrian rocks of the Avalon and Burin Peninsulas and similar formations in the eastern part of Cape Breton Island. The structural boundary between the sedimentary and volcanic rocks of the Avalon and Burin Peninsulas (zone H) and the metamorphic rocks (zone G) on the eastern flank of the central mobile zone of Newfoundland is interpreted to pass in an arcuate fashion beneath Hermitage Bay and run parallel to the south coast of Newfoundland at least as far as the Ramea Islands (Figure 4.1). Its continuation is uncertain because magnetic data (Figure 4.8) suggest the boundary may turn to the southwest in the vicinity of the Ramea Islands whereas the gravity data (Figure 4.7) indicate that the boundary continues westward to approximately to the La Poile Bay area where it then swings southwest towards Cape Breton Island. Because the magnetic data are sparse and the gravity data more abundant, the latter path is favoured.

If the boundary between Zones G and H runs approximately along a line drawn between La Poile Bay, Newfoundland and Sydney, Nova Scotia, as opposed to a line drawn between Ramea Islands,

Newfoundland and Sydney, Nova Scotia, the linear, southwest trending gravity low lying to the west of the St. Pierre High probably represents a belt of low-density rock which is part of zone G and similar to the gneiss near Burgeo (Figure 4.14). This interpretation is consistent with the way the tectonostratigraphic zones are drawn in Figure 4.2 and seems reasonable but the following points should be noted. First, the negative anomaly area north of Burgeo is more characteristic of zone F than zone G so that the negative belt west of the St. Pierre High might represent zone F rocks. Second, it may be that not all of the Precambrian rocks in the western part of Cape Breton Island belong to zone G; the anorthosites in northwestern Cape Breton are characteristic of zone A. Third, because the rocks underlying the western portion of the St. Pierre High, immediately to the northwest of the Glace Bay Low (Figure 4.7), exhibit unusually high seismic velocities and seem to be highly magnetic, they might be remnants of Palaeozoic oceanic material trapped between two Precambrian continental blocks rather than late-Proterozoic to early Cambrian basic igneous rocks. Therefore this part of the northern Scotian Shelf may be very complicated structurally and may have undergone very severe deformation as the North American and European continental blocks collided in the Palaeozoic era.

CHAPTER 5

THE SOUTHERN SCOTIAN SHELF

5.1   INTRODUCTION

The southern Scotian Shelf (see Figure 1.3 for an outline of the area considered) is of interest because it is adjacent to southern Nova Scotia which seems to be geologically distinct from northern Nova Scotia and separated from this latter area by the major Minas Basin-Chedabucto Bay fault zone. It is possible that southern Nova Scotia (that is the part south of this fault zone) was once part of the African lithospheric plate (e.g. Schenk, 1971) and if so, paleomagnetic evidence (Hicken et al., 1972) suggests that it had been brought into its present position from some considerably distant place. Important questions, therefore, are whether the southern Scotian Shelf and southern Nova Scotia form a single structural unit and whether there is any palaeomagnetic evidence that it was separated from northern Nova Scotia and the northern shelf in early Palaeozoic times.

5.2   GEOLOGICAL SETTING OF SOUTHERN NOVA SCOTIA

5.2.1. Sedimentary, volcanic and metamorphic rocks

The oldest rocks in southern Nova Scotia are contained in the Cambro-Ordovician Meguma Group which consists primarily of greywacke, slate and schist (Figure 5.1). The Meguma Group is made up of two formations; the lower one, the Goldenville Formation, is made up chiefly of thinly laminated grey slate with small amounts of siltstone and argillite. Where observed, the contact between the

two formations is conformable and generally gradational.

The thickness of the Halifax Formation varies from about 3.5 km near the Minas Basin (Figure 5.1) to about 0.5 km near the southern tip of Nova Scotia but Taylor (1969) points out that thickness determinations of the Halifax Formation are virtually meaningless as the rocks have been closely folded and crumpled. The total thickness of the older Goldenville is unknown as its base is no where exposed but some 5.5 km of Goldenville rocks are observed in three widely separated locations. The total thickness of the Meguma group is therefore in excess of 9 km.

Whereas the exposures of the Cambro-Ordovician Meguma Group are widespread throughout southern Nova Scotia, outcrops of upper Ordovician, Silurian and Devonian sedimentary and volcanic rocks are restricted to a narrow, discontinuous belt which is subparallel to the Bay of Fundy coastline (Figure 5.1). Contained within this belt are the upper Ordovician and/or Silurian (?) White Rock Formation, the Silurian Kentville and New Canaan Formations and the Devonian Torbrook Formation. The White Rock Formation exhibits an extremely diverse lithology consisting of quartzite, slate, siltstone, rhyolite, basalt, andesite and hornblende-feldspar gneiss. Slate in the White Rock Formation is indistinguishable from the slate of the Halifax Formation; on the other hand there is a distinctive massive, light-coloured quartzite in the White Rock Formation that occurs in no other rock unit in southwestern Nova Scotia. Near Yarmouth, N.S. the formation is nearly 5 km thick and over half of it consists of mafic volcanic rock. This is of considerable interest as no evidence of

Figure 5.1:   Simplified geological map of Nova Scotia. Data

from the Geological Map of the Province of Nova

Scotia (Nova Scotia Department of Mines, 1965).

Simplified Geological Map of Nova Scotia

NEW BRUNSWICK

BAY OF FUNDY

P.E.I.

Cape Breton Island

Chedabucto Bay

Sable Is.

Halifax
St. Margaret's Bay
Mahone Bay
La Have Is.
Liverpool Bay
Shelburne
Pubnico
Yarmouth
St. Mary's Bay
Digby
Kingston
Minas Basin

Ꮼ/pꞓ

45°N
44°

66°W
64°
62°
60°

TRIASSIC DIKE

50 Km.

SEDIMENTARY , VOLCANIC & METAMORPHIC ROCKS

TRIASSIC - Basalt / Conglomerate , Sandstone

CARBONIFEROUS - Sandstone , Limestone , Conglomerate

SILURIAN, DEVONIAN - Shale , Sandstone, Conglomerate
Quartzite, Volcanic Rocks

SD

DEVONIAN & EARLIER - Gneiss Complex (includes
Granite , Gabbro , Diorite)

CAMBRIAN, ORDOVICIAN - Volcanic & Sedimentary Rocks

CAMBRIAN, ORDOVICIAN - Greywacke, Quartzite, Slate, Schist

PRECAMBRIAN - Volcanic, Breccia, Tuff, Lava ; Greywacke,
Shale, Schist

Ꞓ/pꞓ

PRECAMBRIAN - Quartzite, Schist , Gneiss, Crystalline
Limestone

PLUTONIC ROCKS

DEVONIAN - Granite

DEVONIAN, CARBONIFEROUS -
Gabbro, Diabase

FAULTS

Areas of Mainly
VOLCANIC ROCKS

extensive pre-Triassic basic volcanism is preserved elsewhere in southern Nova Scotia.

The upper Silurian Kentville formation consists of up to 1 km of siltstone and slate that overlie the White Rock Formation; the Kentville Formation is conformably overlain by the upper Silurian New Canaan Formation near Wolfville, N.S. and by the lower Devonian Torbrook Formation near Digby and Kingston (Figure 5.1), N.S. The New Canaan Formation consists of andesite and breccias with volcanic fragments, siltstone, slate and limestone. The Torbrook Formation is made up of 2 to 3 km of shale, siltstone, quartzite and some quartzitic iron formation.

Carboniferous rocks are, with the exception of minor exposures (not shown in Figure 5.1) around Mahone Bay and St. Margaret's Bay, confined to the area immediately to the south of the Minas Basin and to the vicinity of the Minas Basin-Chedabucto Bay fault zone (Figure 5.1). In these areas the Mississippian Horton, Windsor and Canso Groups and the Pennsylvanian Riversdale Group are mapped. The rocks forming these groups are predominantly sandstone, limestone, shale and conglomerate and the Windsor rocks are generally of marine origin while those of the other groups are continental. The total thickness of the Carboniferous rocks south of the Minas Basin is about 3 km.

Except for isolated patches around Chedabucto Bay, Triassic rocks in southern Nova Scotia are confined to the shores of the Bay of Fundy and the Minas Basin. The Annapolis Formation consists of up to 1 km of heterogeneous sedimentary rocks which range from

coarse conglomerate through sandstone to shale; these rocks are conformably overlain along the Bay of Fundy by the tholeiitic North Mountain Basalt which is about 250 m thick. Its radiometric age is about 200 my (Carmichael and Palmer, 1968).

5.2.2. Intrusive rocks

Nearly one half of southern Nova Scotia is occupied by intrusive rocks that are generally of granodioritic composition but which commonly attain a more acidic composition. These rocks, which are usually of batholithic proportions and generally discordant, exhibit Devonian ages as determined by radiometric methods.

Whereas acidic intrusions are well represented in southern Nova Scotia, the areal exposures of intermediate and basic intrusive rocks are very small. Following Taylor (1967) and subdividing these latter rocks on the basis of whether they are pre-granitic or post-granitic in age, several small bodies, primarily sills, of diorite and gabbro are mapped mainly to the west and north of the discontinuous belt of Ordovician, Silurian and Devonian rocks. The ages of these sills are uncertain but as they generally cut the Halifax Formation but not the granitic rocks they are probably mid-Ordovician to early Devonian in age. A few examples of basic intrusives cutting the granitic rocks area observed (Taylor, 1969) but the most distinctive post-granitic intrusive is a long diabase dike that extends some 110 km from near Pubnico, N.S. northeast to the LaHave Islands (Figure 5.1). Samples of this dike give a radiometric age of 192 ± 32 my. (Larochelle and Wanless, 1966) very close to that of the North Mountain Basalt.

Ultramafic rocks are represented by only one exposure of peridotite at Liverpool Bay, N.S. (Figure 5.1). Unfortunately the geological relationship of the peridotite, which exhibits a Devonian radiometric age, to the surrounding Cambrian Goldenville Formation is unknown but its presence is of considerable interest in view of association of peridotite with orogenic activity.

5.2.3 Structure and metamorphism

The trend of folds in the Cambro-Ordovician greywackes, slates and schists of the Meguma Group varies from northerly near Yarmouth and St. Mary's Bay (Figure 5.1) to northeasterly in the northeastern part. The rocks in this latter district are more tightly folded than those in the central region (Malcolm, 1912). Throughout the area, the folding seems to have completed before the culmination of regional metamorphism (Taylor and Schiller, 1966) during the Acadian Orogeny in the Devonian period. The synclines and anticlines generally exhibit shallow plunges and steeply dipping axial planes. Although no general rules can be made, the axial planes tend to dip steeply northwestward (Malcolm, 1912).

In the younger, Carboniferous, sandstones, limestones, shales and conglomerates south of the Minas Basin the primary folds developed during the Appalachian Orogeny are open and trend generally northeast to east-northeast but locally the fold pattern is extremely complex.

Triassic conglomerates and overlying tholeiitic basalts along the Bay of Fundy are unfolded but dip a few degrees to the

northwest.

The fault pattern of southern Nova Scotia is very complex (e.g. Cameron, 1956) but, broadly speaking, the major fault trend is southeast-northwest except near Yarmouth and St. Mary's Bay where the trend is north-south and in the region south of the Minas Basin where east-west and minor southwest-northeast trends occur in addition to the widespread southeast-northwest trend. North and east of Halifax, the northwest-trending faults (Figure 5.1) cut the Meguma Group and often show left-handed displacements which exceed a kilometer; on the other hand, faults of similar orientation in the Meguma in the area southwest of the Minas Basin (Figure 5.1) are right-handed (Malcolm, 1912). Northwest faults cut Carboniferous rocks south of the Minas Basin and on the northeast coast of Mahone Bay so it is clear that some of these faults were active in Carboniferous, or more recent, times.

Except along the Minas Bay - Chedabucto Bay fault zone, east-west faults are confined mainly to the Carboniferous rocks south of the Minas Basin. In one location in this region the last period of movement along these faults is post-Triassic and Boyle (1963) believed that the east-west set of faults is younger than the northwest-southeast set but he pointed out that there is no direct geological evidence to support this idea.

Metamorphism in southern Nova Scotia is largely confined to the Cambro-Ordovician Meguma Group but it also affects the Ordovician-Silurian White Rock Formation which is made up of quartzite, slate, gneiss and mafic volcanic rocks. The regional

metamorphic grade is generally of the greenschist facies or lower

except in the Pubnico-Shelburne area where the almandine-amphibolite

facies is recognised (Taylor, 1967 and 1969). Contact metamorphism

of Meguma rocks associated with the intrusion of Devonian granite,

occurs throughout Southern Nova Scotia and postdates the regional

metamorphism (Taylor and Schiller, 1966).

5.2.4 Brief resume of the tectonic history of southern Nova Scotia

In Cambro-Ordovician times the Goldenville Formation was laid

down in a marine, possible deep-sea, environment in which turbidity

currents were active. The depositional environment changed, probably

rapidly, to one of quiet, shallow-water deposition as the Halifax

Formation was laid down. The composition of the Meguma Group and

palaeocurrent information indicate that a source area of gran-

odioritic composition lay to the southeast (Taylor and Schiller,

1966). This area possibly now lies in northwest Africa. Tectonic

activity was subsequently initiated in the discontinuous belt

running from Yarmouth to the Minas Basin (Figure 5.1) as great

thicknesses of andesite and basalt were extruded in White Rock

Ordovician-Silurian time. Perhaps contemporaneously, or somewhat

later during the Devonian period, the entire region was folded by a

compressive force oriented roughly southeast-northwest and

subsequently metamorphosed by heat and pressure as the African

and North American lithospheric plates converged (e.g. McKerrow

and Ziegler, 1972). The northwest fracture system may have been

initiated about this time. The effect of the collision of the

lithospheric plates culminated with the intrusion of large masses

of granitic material in the middle Devonian. The region then

stabilized and was subjected to erosion with generally continental

deposition occurring mainly in the Minas Basin region. Faulting

and subsequent east-west and vertical movements became important

in the Minas Basin in the Carboniferous period and renewed movement

occurred in some areas along the northwest trending faults.

The next recorded phase of tectonic activity occurred in the

Triassic period with deposition of sedimentary and volcanic rocks

along the Bay of Fundy and in the Minas Basin and with the

injection of the long, linear diabase dike in southern Nova Scotia.

These latter events were possibly in response to the initial

stage of break-up of the present-day North America and African

lithospheric plates.

5.3 GEOPHYSICAL DATA

A considerable amount of shipborne and airborne magnetometer

data, scattered shallow and deep crustal refraction seismic profiles

(Figure 5.2) and some drill-hole data (McIver, 1972; Jansa and Wade,

1975) are available to complement the underwater gravity data.

A simplified gravity map (Figure 5.3) shows that, in addition to

the characteristic rise in the Bouguer anomaly field as the

continental margin is approached, the two primary anomalous gravity

features are the Middle Bank Low and the Emerald High.

The simplified magnetic anomaly map of the southern Scotian

Shelf (figure 5.4) made from a Geological Survey of Canada
compilation kindly supplied by P.J. Hood, does not exhibit the
detail of the original map which clearly outlines the seaward
extension of the Meguma rocks (Hood, 1966) but it does show magnetic
highs over, and to the west of Sable Island and an intense local
low on the eastern margin of La Have Bank (see Figure 1.1 for
location).

Figure 5.5 which is adapted from Sherwin (1972), is based
mainly on unpublished seismic data which consist of profiles spaced
from about 25 to 50 km apart according to Jansa and Wade (1975).
The seismic data show that the southern Scotian Shelf is separated
from the northern Scotian Shelf by a deep, elongate sedimentary
basin which lies on strike with the Minas Basin - Chedabucto Bay
fault zone. This basin will be discussed further in the next
chapter. The sedimentary rocks on the southern Scotian Shelf form
a wedge which thickens more or less uniformly from the shoreline
to the continental margin and the maximum basement depression
occurs east of Sable Island. Some northeast-trending faults in
the basement are inferred (Jansa and Wade, 1975) about 70 km north
of Sable Island and in the area south of Emerald Basin (Figure 1.1).

5.4 CRUSTAL SEISMIC RESULTS

In order to provide some background for an interpretation of the
"Halifax Profile" in the next section, and for a discussion of long
wavelength magnetic anomalies, in the next chapter, I would like

Figure 5.2:   Southern Scotian Shelf - location of deep and

shallow seismic lines and gravity and magnetic

profiles J-J', K-K' and L-L'.

161
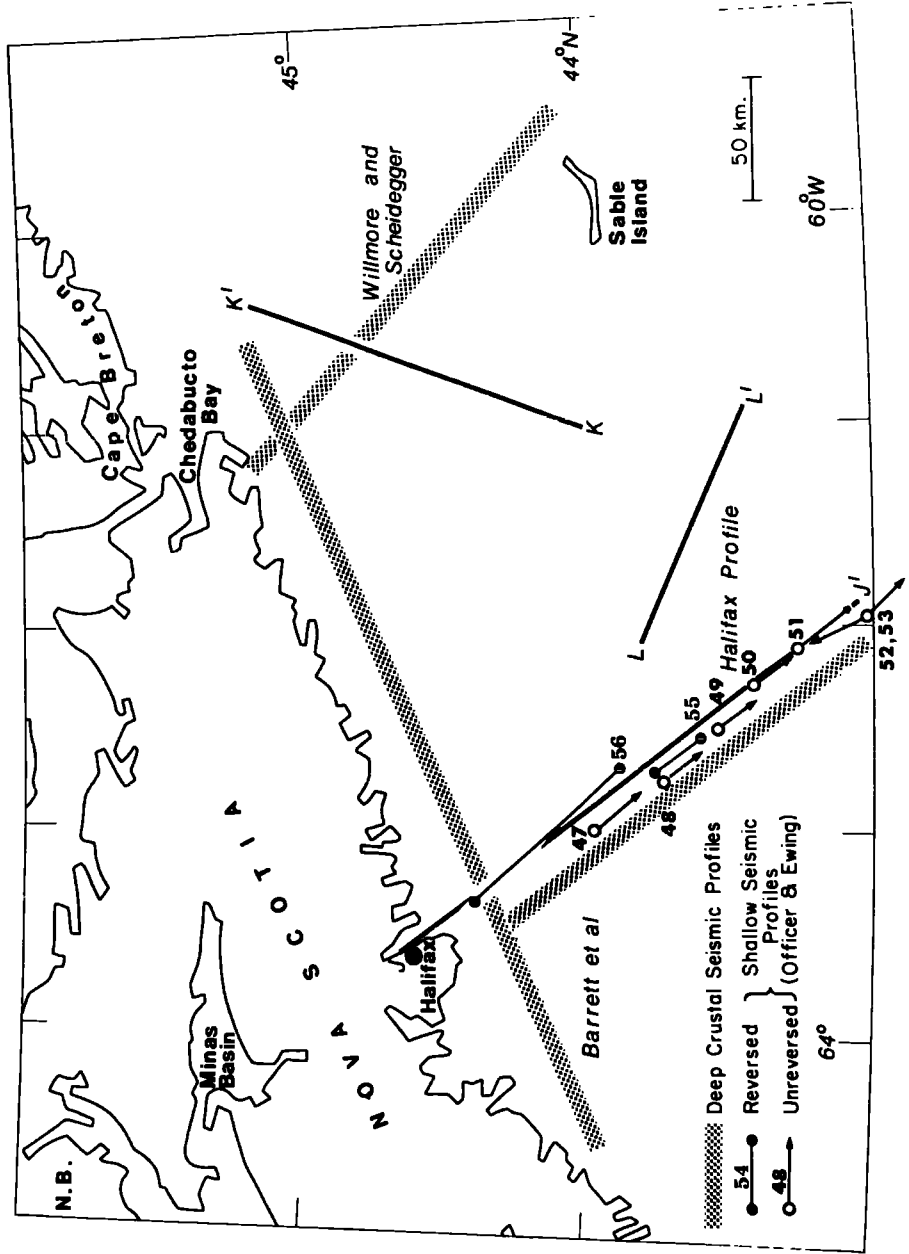
Figure 5.3:   Simplified Bouguer anomaly map of the southern

Scotian Shelf - for more detail see map in pocket.

BOUGUER ANOMALY MAP - SOUTHERN SCOTIAN SHELF
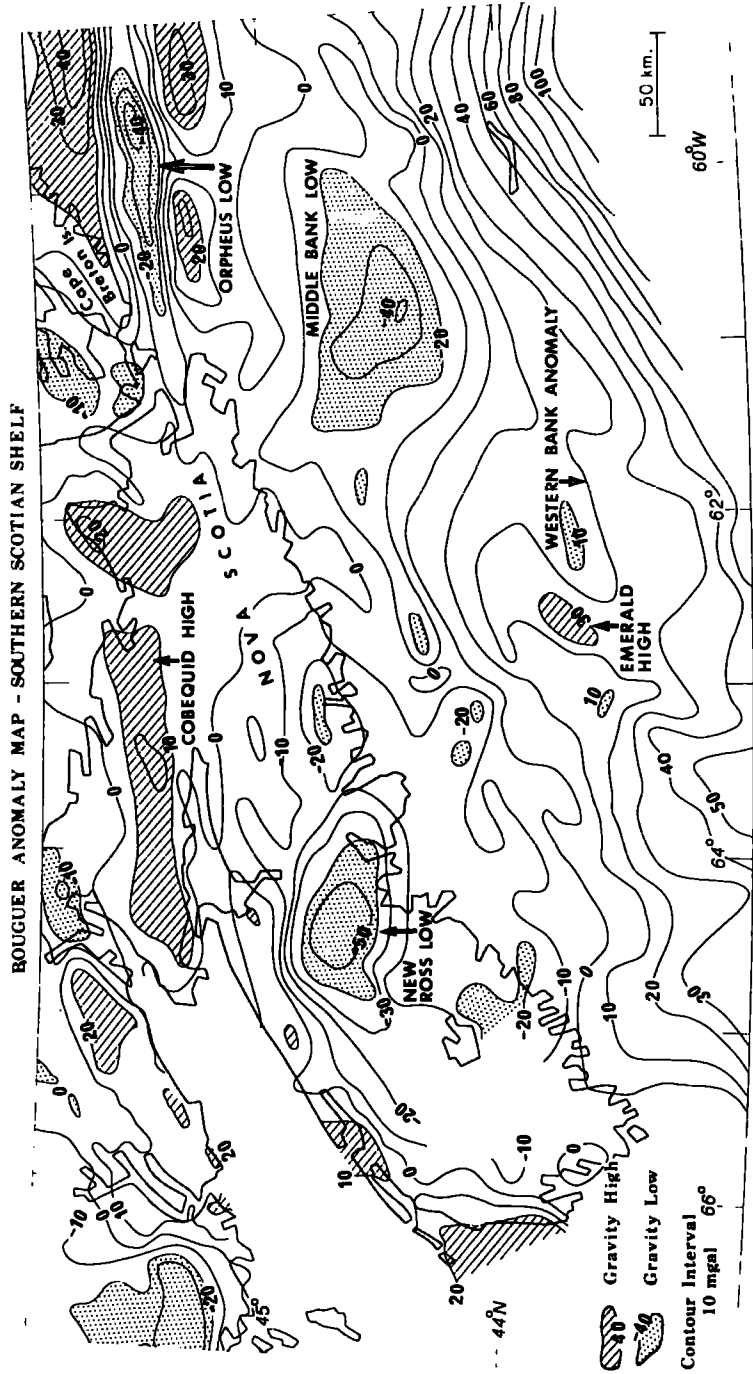
Figure 5.4: Simplified total magnetic field anomaly map of the Southern Scotian Shelf. Data obtained from a 1:1,000,000 compilation by P.J.Hood of the Geological Survey of Canada.

SIMPLIFIED TOTAL MAGNETIC FIELD ANOMALY MAP – SOUTHERN SCOTIAN SHELF
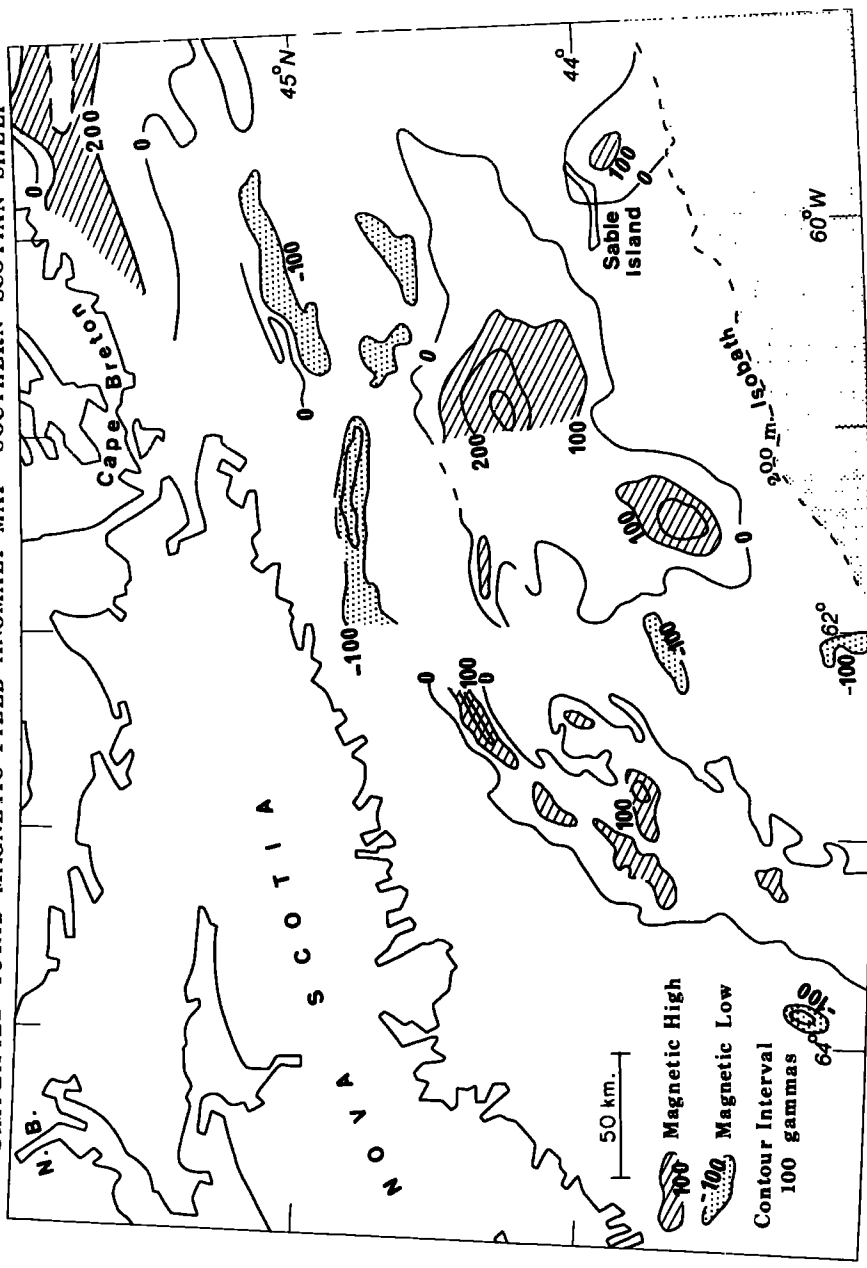
Figure 5.5:   Depth of seismic basement on the southern

and central Scotian Shelf. The diagram is

based on a figure from Sherwin (1972) and is

based mainly on unpublished seismic profiles

spaced from 25 to 50 km apart. The main

features, as named by Jansa and Wade (1975)

are the Sable subbasin near Sable Island

(44°N; 60°W) and the east-west trending

Orpheus Graben (about 46°N).

TOTAL BASIN FILL - SOUTHERN SCOTIAN SHELF (after Sherwin, 1972)
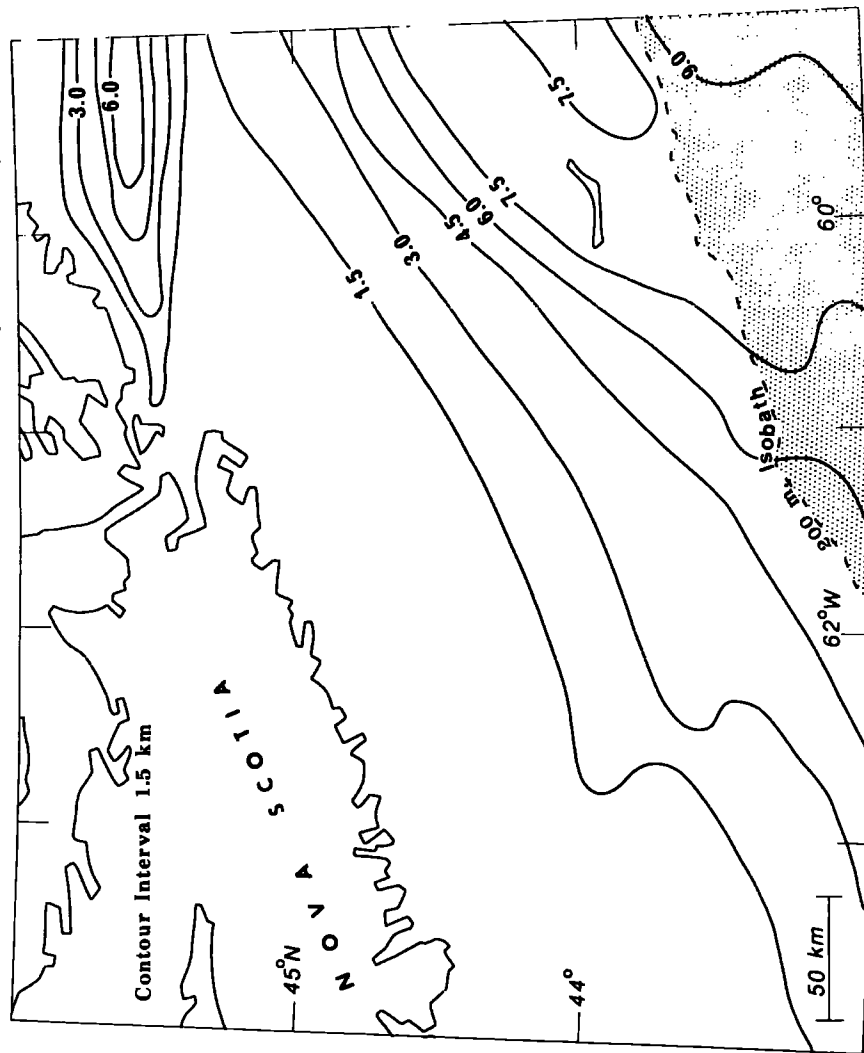
to discuss the available crustal seismic data which are available

unfortunately, only on the southern section of the Scotian Shelf.

Willmore and Scheidegger (1956) carried out the first crustal

seismic investigation of the Scotian Shelf as part of a study of

the Gulf of St. Lawrence. Their profile, which runs from

Chedabucto Bay to Sable Island, was subsequently complemented by

the investigations of Barrett et al., (1964) and Berger et al.

(1965). Figure 5.2 shows the locations of the deep crustal seismic

profiles and Figure 5.6 summarizes the travel-time results of

Willmore and Scheidegger (1956) and the data of Barrett et al.

(1964) along the profile perpendicular to the coast line (Figure

5.2); their data from the profile parallel to the coastline and the

shorter range, unreversed data of Berger et al. (1965) are omitted

for clarity. Travel-time corrections of 1 sec have been applied

to Willmore and Scheidegger's data in three cases (open circles

in Figure 5.6). In the first two cases the redundancy of data

at a distance of 170 km clearly shows that one of the station

times is in error by 1 sec. In the third case, the general shape

of crustal seismic travel-time curves (e.g. Goodacre, 1972)

strongly suggests that the shot which provides arrivals at distances

of 60 to 70 km was mistimed by 1 sec.

In Canada, the regional Bouguer anomaly level is, in general,

a function of crustal thickness and compressional wave velocity in

the upper mantle (Goodacre, 1972). In this respect the travel-

time data in Figure 5.6 indicate that the crust along the south-

Figure 5.6: Reduced travel-time data from crustal seismic

investigations by Willmore and Scheidegger (1956)

and by Barrett et al. (1964). See Figure 5.2

for the locations of the profiles.
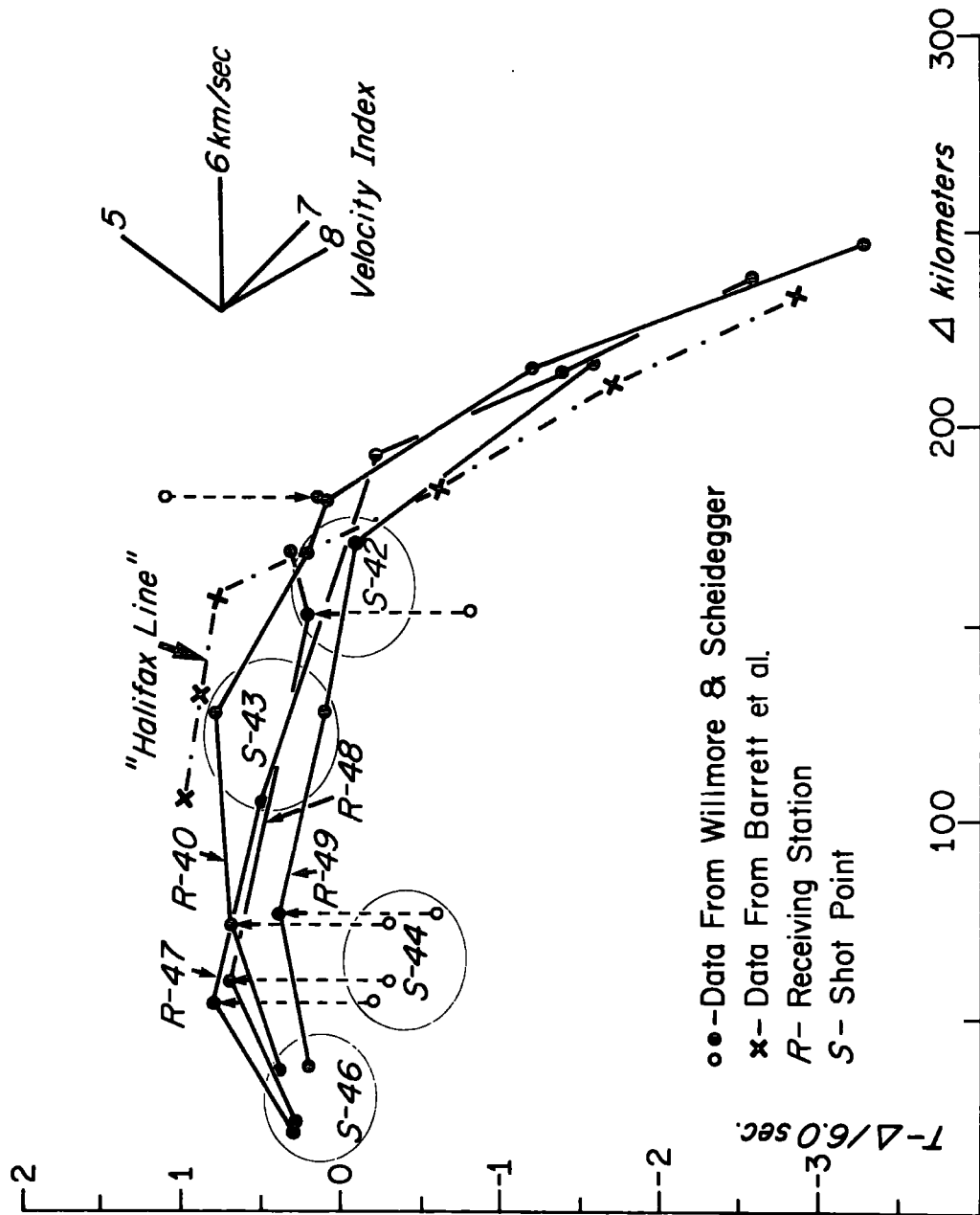
Figure 5.7:   Velocity-depth models of the crust obtained
              by applying a non-linear optimization technique
              to the data in Figure 5.6.

Port Herbert—
Cole Harbour

Chedabucto Bay
— Sable Is.
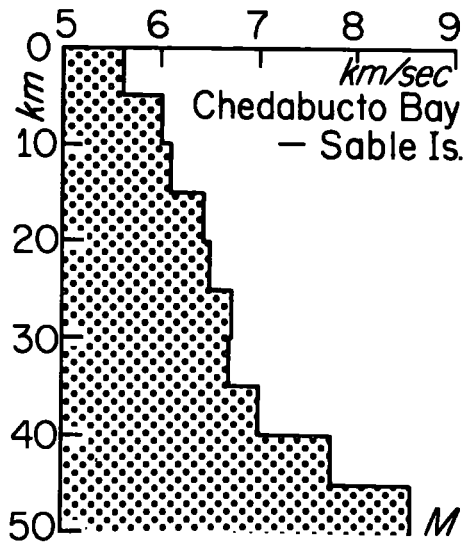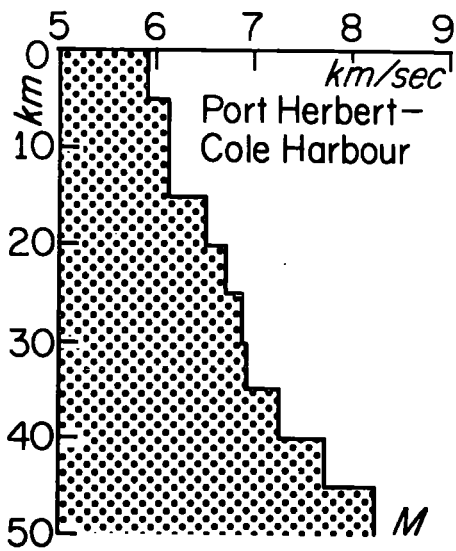
eastern coast of southern Nova Scotia is normal for an area where

the regional Bouguer anomaly is about 0 to -10 mgal and the upper

mantle velocity is about 8.1 km/sec. Barrett et al. (1964)

obtained a value of 32 km for the thickness of the crust along

the profile parallel to the coastline (Figure 5.2) using a single

layer crustal model. Their model, although a good first approx-

imation, is not consistent with the general increase of compressional

wave velocity with depth in the crust in Canada (Goodacre, 1972) so

it seemed appropriate to fit multi-layer crustal models to the

available seismic data. Velocity-depth curves (Figure 5.7) were

derived for two long profiles over the Scotian Shelf using the

non-linear optimization routine described in Chapter 3 to adjust,

in each case, the crustal model until first-arrival travel-time

calculated for the model agreed reasonably well with the observed

travel-time. No claim of uniqueness is made for the method but

it does provide plausible models which indicate that the crust in

the vicinity of southern Nova Scotia is about 45 km thick. This

value is some 15 km greater than the value obtained by Barrett

et al. (1964) due to the presence, in the models derived here, of

high seismic velocity layers immediately above the Mohorovicic

Discontinuity. The significance of these high velocity layers

is not clear but they may represent rocks of amphibolite composition

(Goodacre, 1972). The seismic velocities in the upper 10 to 15 km

of the crust are consistent with the presence of rocks of siliceous

chemical composition such as the Meguma shales, slates and quartzites

31
30

Figure 5.8: Magnetic and gravity anomalies and shallow seismic

structure along Halifax Line (profile J-J' in Figure

5.2) Seismic data are from Officer and Ewing (1954).
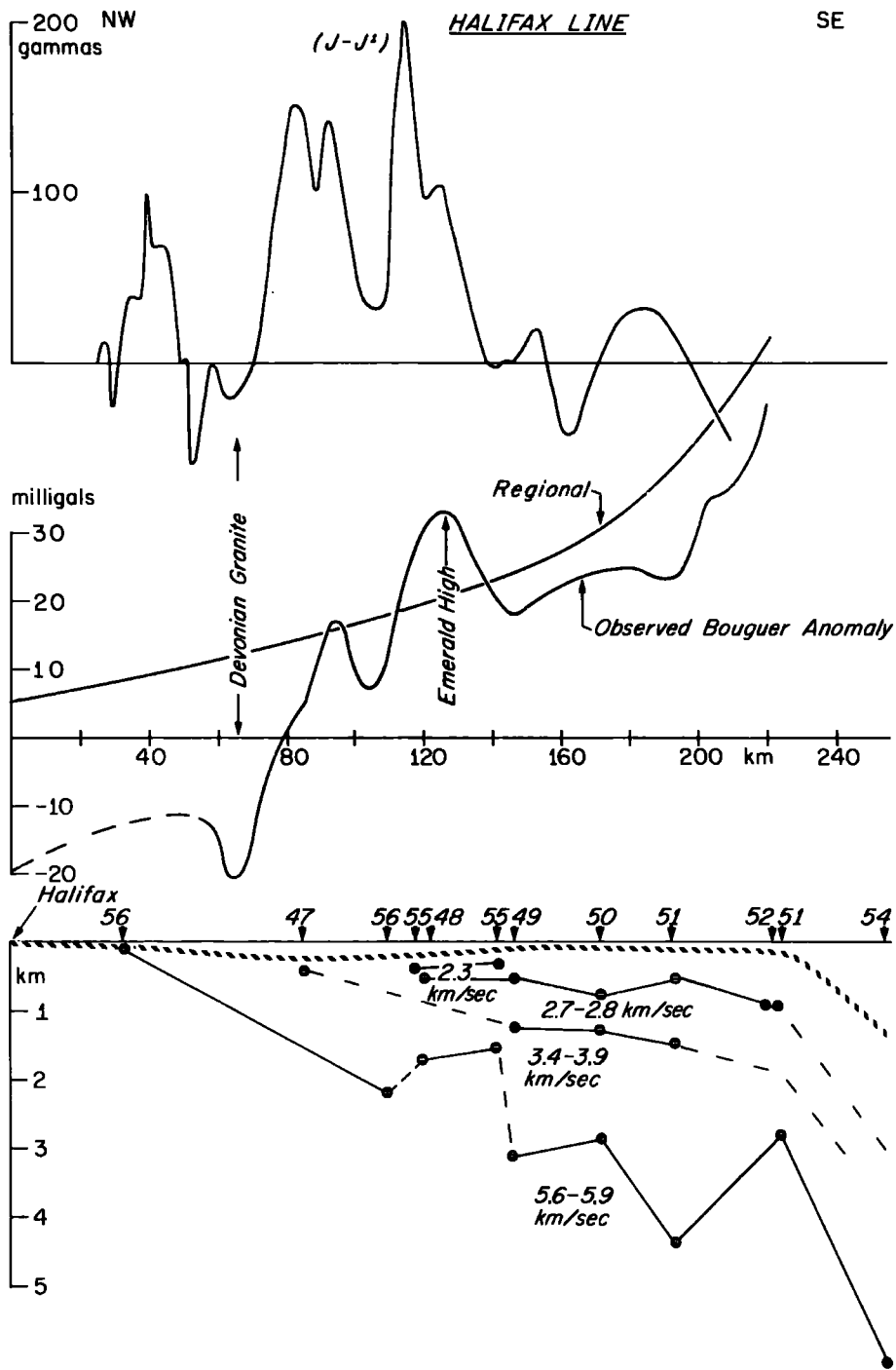
HALIFAX LINE

and the intrusive Devonian granites.

5.5 THE HALIFAX LINE AND EMERALD HIGH

5.5.1 Seismic and magnetic results

The Halifax Line (J-J' in Figure 5.2) is a profile perpendicular to the shore line along which oceanographic measurements have been repeated at regular intervals throughout the years. The line has also been used to locate geophysical measurements and Figure 5.8 displays the available gravity, magnetic and shallow seismic data along the profile. The seismic data are from Officer and Ewing (1954) and provide a typical example of a fractured, downwarped continental shelf basement covered by a thick wedge of sedimentary rocks.

The total field magnetic anomaly profile was constructed from 1:250,000 scale Geological Survey of Canada aeromagnetic maps which have had the regional variation removed. The northwestern half of the profile exhibits short-wave length variations superimposed on large-amplitude, long-wavelength anomalies whereas on the southeastern half of the profile the anomalies are smoother and smaller in amplitude. This difference probably reflects a change in basement structure and/or thicker sediments as one goes towards the continental margin (Figures 5.5 and 5.8). The magnetic signature of the northwestern portion of the Halifax Profile is typical of that obtained over the Meguma Group where narrow, intense

magnetic highs correlate with magnetic units within the Halifax Formation and localized flat, featureless areas (Figure 5.9) overlie Devonian granite intrusions (McGrath et al., 1973) so it appears that the Meguma Basement can be traced some 75 km out from the shoreline near Halifax where it is no longer recognizable.

5.5.2 The regional gravity trend

The gravity profile, constructed from the underwater gravity data, shows, in addition to local features such as the Emerald High, the typical increase in Bouguer anomaly as the continental margin is approached. The suggested regional variation in Figure 5.8 is calculated on the assumption that the mass deficiency of sea water is compensated, at depth, by the rise of the Mohorovicic Discontinuity from a depth of 45 km under southern Nova Scotia (Figure 5.7) to a depth of about 12 km under the deep ocean and that the topography on the crust-mantle interface is a mirror image of the bathymetry. In other words, it is assumed that isostasy prevails according to the Airy hypothesis. The "zero level" of the calculated regional curve, i.e. its value at large distances away from the continental margin, was set at -5 mgal as this is the average sea-level Bouguer anomaly value over the Gulf of St. Lawrence (Goodacre et al., 1969). This zero level could be in error by a few milligals so the relative amplitudes of the positive and negative residual anomalies obtained by subtracting the regional trend from the Bouguer anomaly are not highly significant but the

Figure 5.9: Comparison of an aeromagnetic anomaly over the

Scotian Shelf (right-hand box) with an anomaly

which is typical of those over Devonian granites

in southern Nova Scotia (left-hand box). Figure

is from McGrath et al. (1973).
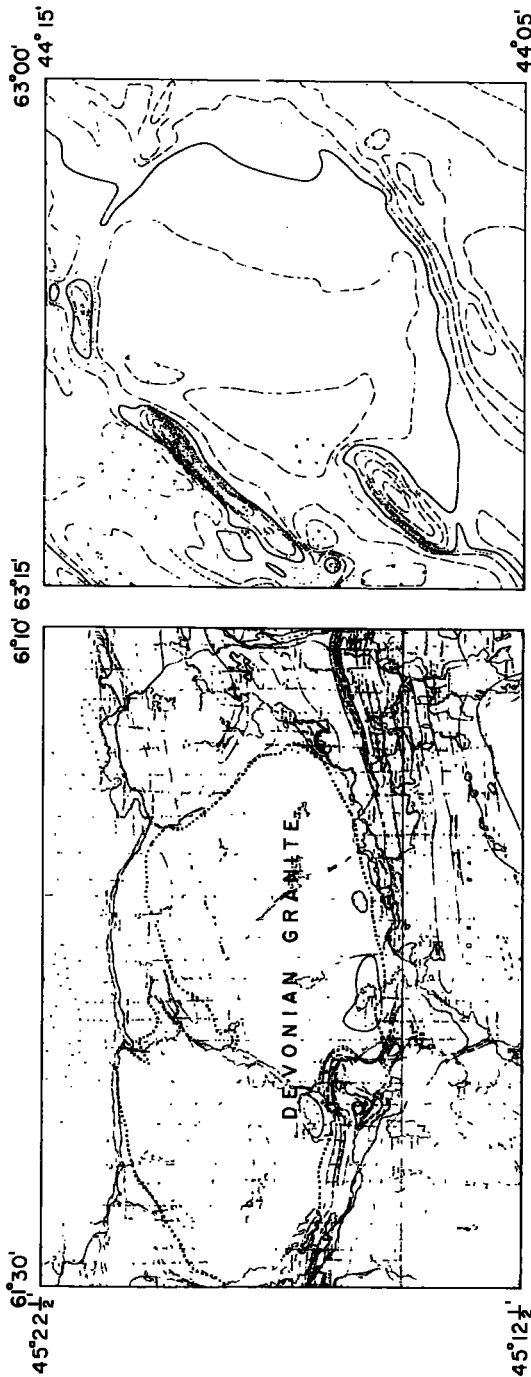
PORTION OF GSC
AEROMAGNETIC MAPS
231G & 237G

PORTION OF SCOTIA SHELF
MAD SURVEY
1962

DEVONIAN GRANITE

0 1 2 3 4
nautical miles

.... 10 gammas
– – – – 20 gammas
———— 100 gammas

1000 ft. ◄——— SURVEY ALTITUDE ———► 200 ft.

63°00'
44°15'

61°10' 63°15'

61°30'

45°22½'

45°12½'

44°05'

interesting aspect is that the seaward rise of the observed gravity

field can be adequately explained by a simple isostatic model.

5.5.3 The geologically corrected gravity field

The residual Bouguer anomaly field has been corrected for the

mass deficiency of the sedimentary rocks by converting the

compressional wave velocities shown in Figure 5.8 to densities with

the aid of seismic results (Berger et al., 1965) and drill-hole

results (McIver, 1972) near Sable Island and assuming the seismic

structure to be two-dimensional in character. The resulting anomaly

(Figure 5.10) still shows some residual correlation with the

basement depth over, and to the southeast of, the Emerald High but

this could be diminished by the choice of a slightly higher density

contrast between the 5.6-5.9 km/sec basement and the 2.4-3.9 km/sec

sedimentary layer. The main feature of the gravity profile in

Figure 5.10 is the more or less step-like rise from -20 mgal to

+20 mgal at a distance of about 80 km from Halifax. Superimposed

on this change in gravity level are local highs and lows which will

be discussed in the next sub-section.

A simple, two-dimensional gravity model which has a density

contrast of 0.1 gm/cm^3, its upper surface buried at a depth of

about 2 km and a steeply sloping face extending to a depth of

about 12 km explains the main step-like change in the anomaly

level. This model is by no means unique and, in fact, several

other models, each having a different density contrast, all fit

the observed anomaly about as well as the model in Figure 5.10 does.

Figure 5.10: Halifax Line- (a) the observed Bouguer anomaly

minus the adopted regional curve (Figure 5.8) and

corrected for the mass deficiency of the sedimen-

tary layers (Figure 5.8), (b) the anomaly due to a

semi-infinite slab as shown in the bottom part of

the diagram, (c) the pseudo-gravity anomaly obtained

from the northwestern half of the magnetic profile

in Figure 5.8; m/d is the ratio of magnetization

contrast to density contrast, Inc is the inclina-

tion of the total magnetization vector, r is the

coefficient of linear correlation between the

observed and pseudo-gravity anomaly. (d) the gravity

low in the region marked: Devonian Granite - area B

coincides spatially with an aeromagnetic anomaly

similar to,and adjacent to,the one shown in the

right-hand box in Figure 5.9. Area B is outlined

in Figure 5-12.

Figure showing Halifax Line (J–J') gravity anomaly profile and basement surface cross-section.
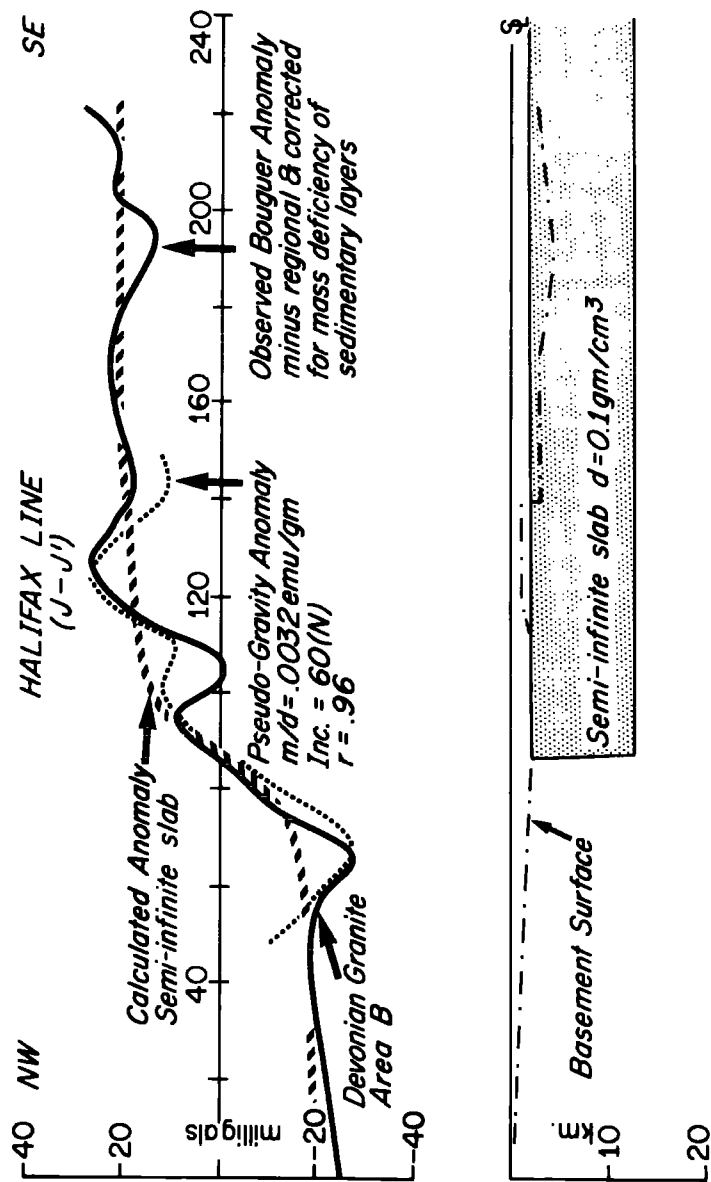
Common features of the models are that their top surfaces are buried 1 to 3 km deep and their faces dip more than 45° from the vertical. The main difference is that a given model is thicker or thinner depending upon the density contrast used. The smallest density contrast that will produce an acceptable fit is about 0.05 gm/cm^3. and for this case the model extends to a depth of 24 km. The models all point to a fairly abrupt transition in the upper portion of the crust from the typical shales, slates and quartzites of the Cambro-Ordovician Meguma Group (d=2.70 to 2.75 gm/cm^3) and intrusive Devonian granites (d=2.60 to 2.65 gm/cm^3) to a slightly heavier, more basic, type of basement rock that occupies an area which includes the Emerald High and lies approximately to the south of the +10 mgal contour in Figure 5.3. How far this heavier basement extends on either side of the profile is not clear but it may extend to the southwest as far as the gravity coverage goes and to the northeast at least as far as the Middle Bank Low (Figure 5.3).

5.5.4 The Emerald High

In view of the foregoing discussion, in particular the correlation between the Bouguer anomaly profile and the seismically determined basement topography (Figure 5.8), it appears that the Emerald High (Figure 5.3) which is a local, isolated, quite prominent high about 60 km long and 15 km wide, reflects an uplifted basement block, in a terrain which is somewhat more dense than the typical Meguma Basement. In fact, the character of the

gravity and magnetic anomalies suggests that the block producing

the Emerald feature may locally contain phases which are even more

dense and magnetic than elsewhere. The local gravity and magnetic

lows immediately to the north of the Emerald High might represent

a low-density granitic intrusion in the same way that the gravity

low at a distance of 65 km from Halifax (Figure 5.8 and 5.10)

almost certainly reflects a granitic intrusion because it

correlates spatially with the magnetically smooth area in the right

hand box in Figure 5.9 but the gravity and magnetic lows on the

south flank of the Emerald feature are more elongate and hence

suggestive of a narrow sedimentary basin.

5.5.5 Correlation between the gravity and magnetic data

Since there is some correlation between the gravity and

magnetic variations on the northwest half of the Halifax Profile

(Figure 5.8) it seemed appropriate to perform a two-dimensional

magnetic to gravity transformation even though some of the anomalies

tend to be three-dimensional in character and it is not clear

whether we are dealing with a single suite of anomalies. The

interesting result is that the maximum correlation between the

observed and pseudo-gravity anomaly (Figure 5.10) is obtained for

an angle of magnetization which is close to the inclination of the

earth's field so there is no evidence of any significant amount of

remanent magnetization in the basement rocks over, and on the

northwest side of the Emerald High.

5.6 THE MIDDLE BANK LOW

The most prominent gravity anomaly on the southern Scotian

Shelf is the widespread Middle Bank Low (Figure 5.3) which reaches

a minimum value of -40 mgal over the Middle Bank bathymetric

feature (Figure 1.1). The main portion of the anomaly is somewhat

kidney-shaped with the convex side pointing south. The main

portion has two off-shoots or arms; one arm extends southwest from

the western side of the anomaly and the other, less prominent,

arm extends northeast from the eastern side. The local low at the

tip of the southwesterly trending arm (Lat. 44.4°N; Long. 62.8°W)

coincides spatially with a magnetically smooth area which is

partially surrounded by a magnetic halo. The magnetic anomaly

pattern closely resembles those in Figure 5.9 and it is likely

therefore, that this local gravity low is produced by an intrusion

of low-density, non-magnetic granitic material into the Meguma

basement rocks. There are insufficient aeromagnetic data over the

local gravity low immediately to the northeast to make a similar

interpretation but there is no reason to suspect that this second

local low is not also produced by low-density granite,

particularly as the basin fill map (Figure 5.5) indicates relatively

shallow basement near the coastline of southern Nova Scotia.

The lack of a pronounced sedimentary basin anywhere on the

southern Scotian Shelf (Figure 5.5) indicates that the main portion

of the Middle Bank Low is due to a low-density granite batholith but

it seemed appropriate to confirm this interpretation by modelling the gravity anomaly. A study of several two-dimensional models of the gravity field along profile K-K' (see Figure 5.2 for location) using non-linear optimization (Al - Chalabi, 1970) and iterative procedures using matrix methods (Laving, 1971) gave good results for a body which has its top surface buried at a fairly shallow depth, has outward sloping sides and offers a density contrast of about -0.15 gm/cm^3 with the surrounding rocks (Figure 5.11). Although a complicated model with inward dipping sides might also fit the gravity anomaly, the model in Figure 5.11 is consistent with the sharp curvature of the gravity field over the centre of the anomaly and the more gentle curvature on the flanks. The characteristics of the gravity field and the model therefore support the interpretation that the central portion of the Middle Bank Low is produced by a batholith of Devonian (?) granite.

An interesting aspect of the main portion of the Middle Bank Low is that it is associated with a large magnetic anomaly. This is clearly shown along profile K-K' (Figure 5.11) and in Figure 5.12 where a magnetic high occurs on the southern flank of the gravity low and a series of lows occur on the northern flank. Studies of a large suite of two-dimensional models of the magnetic anomaly (Figure 5.11) along profile K-K' (see Figure 5.12 for location) show that the best fit is obtained for a model which has its upper surface at a depth of 2 km, has outward sloping sides and has a magnetization contrast of at least 0.001 emu/cm^3. The depth

Figure 5.11:   Observed gravity and magnetic anomaly profiles

over the Middle Bank feature, interpretative

gravity and magnetic models and their computed

gravity and magnetic anomalies. The inclination

of the total magnetization in the, magnetic

model is 40°(N) in the vertical plane containing

the earth's field. The inclination of the earth's

field is 74°(N).

MIDDLE BANK ANOMALY
(K–K²)

SW — NE

Inclination of Magnetization 40°(N)

Computed Magnetic Anomaly

Observed Magnetic Anomaly (Total Field)

Computed Gravity

Observed Bouguer Anomaly

Gravity Model d=-0.15 gm/cm³   Magnetic Model m=.002 emu/cm³
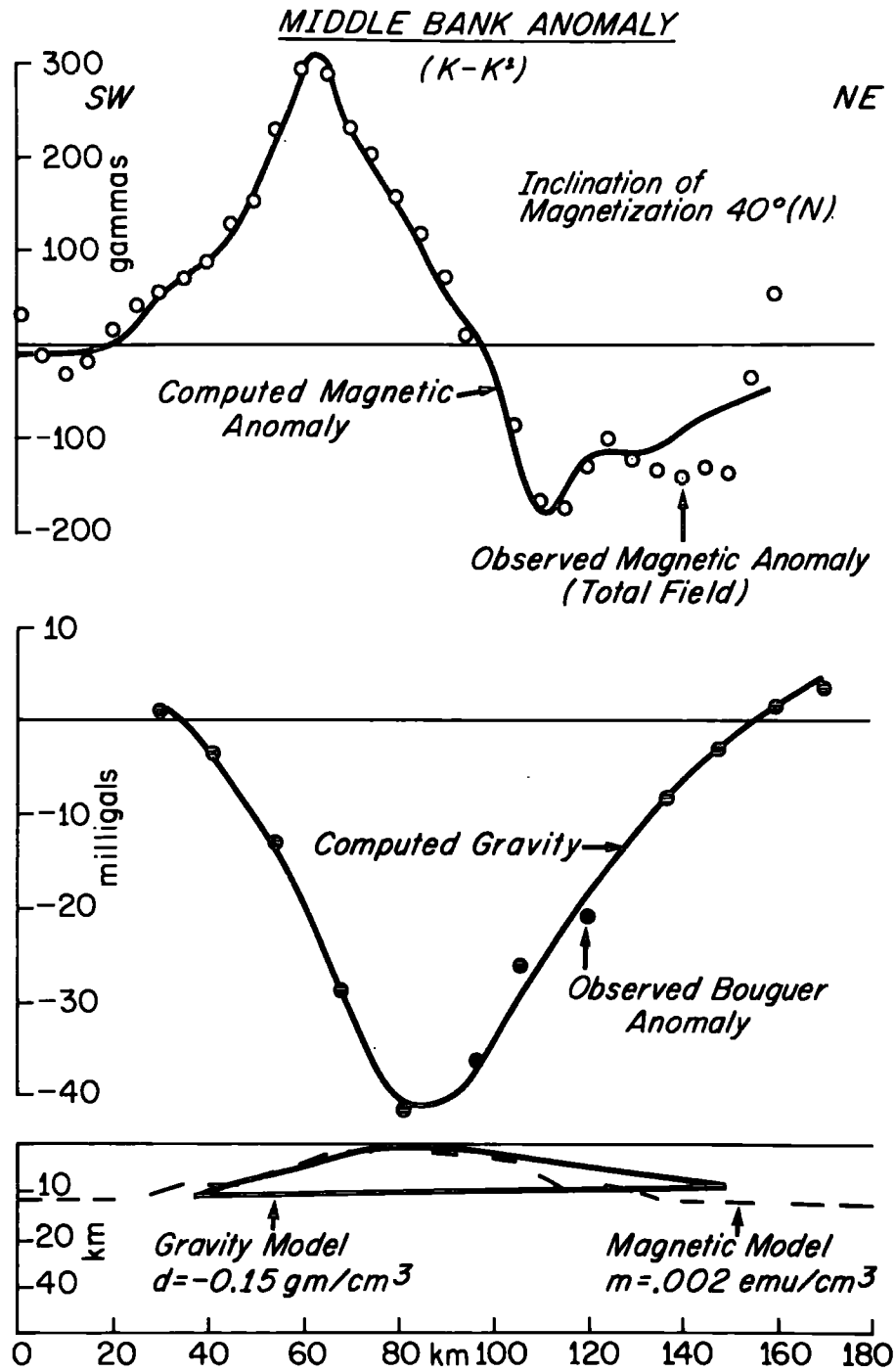
of the top of the model is quite closely determined and agrees

with the basement depth indicated in Figure 5.5. The shapes of

the gravity and magnetic models are quite similar and, since no

attempt was made to force one model to fit another, it seems

reasonable to assume that there is a close relationship between

the magnetic and gravity anomalies. There is, in fact, a high

degree of correlation between the observed gravity anomaly and the

pseudo-gravity anomaly calculated from the magnetic anomaly

(Figure 5.13) and the inclination of total magnetization of 28^{o}(N)

which is obtained from the two-dimensional magnetic to gravity

field transformation differs by only 12° from that obtained by

the modelling procedure. It could be argued that a two-dimensional

study of a feature that is three-dimensional in plan view is

subject to serious error but since the thickness and depth of

burial of the causative body are small compared to its lateral extent,

the error should not be too serious. A three-dimensional joint

analysis of the gravity and magnetic fields within the area

outlined by the box in Figure 5.12 was made and will be discussed

further in Chapter 7. The results give a somewhat shallower

inclination of magnetization of 14^{o}(S) when the three-dimensional

result is projected on to the vertical plane containing the earth's

field. The direction of magnetization from the three-dimensional

study will be discussed further in Chapter 7 but it should be

pointed out here that there may be a significant component of

remanent magnetization in the body producing the magnetic anomaly.

Figure 5.12:   Bouguer gravity anomaly contours superimposed on

total field magnetic anomaly contours over the

Middle Bank Area of the southern Scotian Shelf.

This figure was constructed using the information

in Figures 5.3 and 5.4. Notice the east-west

trending magnetic anomaly lows (wide-spaced dots),

lying at a latitude of 44.8°N along the -20 mgal

contour on the north side of the Middle Bank

gravity low (close-spaced dots) and the positive

magnetic anomaly region (horizontal lines) on the

south side of the gravity low. A two-dimensional

analysis of the gravity and magnetic field was

made along profile K-K'; a three-dimensional study

in the rectangular region labelled "Area of Actual

Study". Boxes marked "A" and "B" refer to the

left and right-hand boxes, respectively of Figure

5.9.

191

GRAVITY & MAGNETIC ANOMALIES - MIDDLE BANK AREA
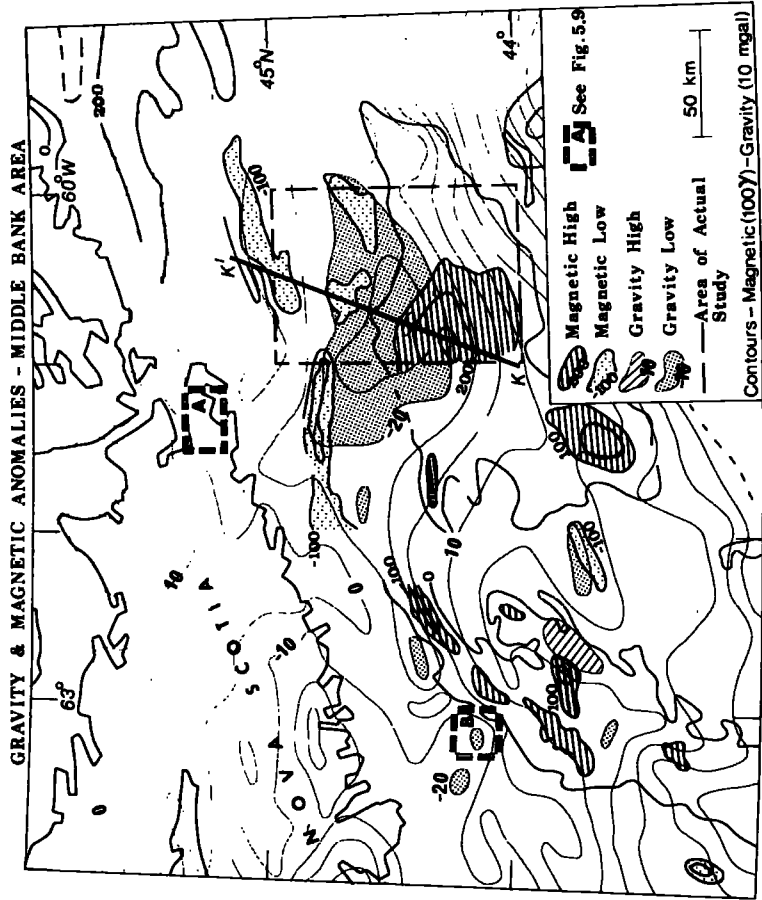
Figure 5.13:   Observed magnetic and gravity anomalies and

calculated pseudo-gravity anomaly along profile

K-K '. m/d is ratio of magnetization contrast to

density contrast, Inc is inclination of total

magnetization vector, r is the coefficient of linear

correlation between the observed gravity and the

pseudo-gravity anomalies.
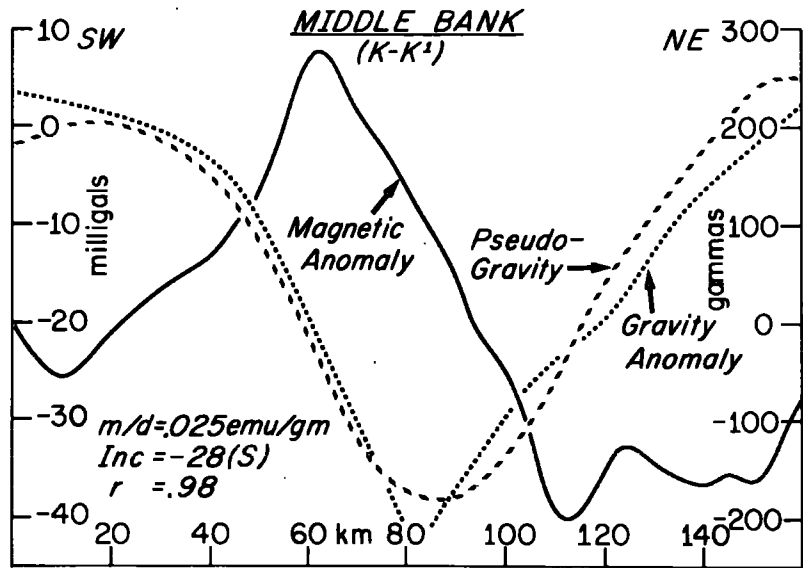
MIDDLE BANK
(K-K¹)

The source of the main portion of the Middle Bank Low is probably a Devonian (?) granite which is magnetic, unlike the Devonian granites of southern Nova Scotia. Magnetic, low-density granites of Devonian age are found in New Brunswick; a good example of one is the Pokiok intrusion (McGrath, 1970) which produces a gravity low (see map in pocket) and a magnetic high (Figure 5.14). McGrath (1970 and personal communication) finds that in some parts of the Canadian Maritime Appalachians there is a correspondence between the magnetic properties of granitic intrusions and the degree to which they have undergone alteration. Fresh, pale-gray granites, such as those in southern Nova Scotia, are non-magnetic whereas some moderately altered pink granites, such as the eastern portion of the Pokiok intrusion in New Brunswick have magnetite developed within them. The magnetite, which is revealed both in chemical analyses of the rocks and by Curie temperature determinations (McGrath, personal communication) is accompanied by chlorite; these minerals indicate the probable breakdown of micas in the granite (Turner, 1968). The magnetic anomaly associated with the Middle Bank Low may indicate, therefore, a moderate degree of alteration of the postulated granite batholith. This postulated situation is contrasted with that of the granites of southern Nova Scotia where, if any magnetic anomaly is present, it takes the form of a halo at the margin of the intrusion (e.g. Figure 5.9) and the anomaly source is magnetite which has been developed from pyrrhotite (in the Halifax Formation

of the Meguma Group) during the intrusion of the granite

(P. McGrath, personal communication).

Although it seems reasonable to assign a Devonian age to the

postulated Middle Bank Granite, the batholith could be older inasmuch

as Devonian Granites are generally non-magnetic whereas the older

Avalonian (late Proterozoic) and Taconic (Ordovician) granites tend

to be magnetic (W. Poole, personal communication). Of course, there

are exceptions to this rule and the Devonian Pokiok Granite is one

of them. There is also the possibility, which will be discussed in

Chapter 7, that the Middle Bank Granite was intruded during Permo-

Carboniferous times and is a counterpart of the Hercynian granites

of Devon and Cornwall in England (e.g. Bennison and Wright, 1969).

There are two reasons why this might be so. Firstly, one would expect

on the basis of a continental reconstruction (e.g. Bullard et al.,

1965) that the Scotian Shelf might have been affected by the Hercy-

nian orogeny and secondly, Carboniferous radiometric age dates are

obtained from some of the basement samples drilled in the southern

Scotian Shelf (M. Given, personal communication). However, the main

portion of the Middle Bank batholith is still unusual in that it is

magnetic ; the granites in southwest England are non-magnetic although

marginal magnetic haloes are quite well developed in some cases as can

be seen on Sheet 2 of the Aeromagnetic Map of Great Britain

(Bullerwell, 1965).

An alternative, but unlikely, explanation of the magnetic

Figure 5.14:   Magnetic anomaly over the Pokiok granite intrusion

in southwestern New Brunswick. Diagram is from

McGrath et al. (1973) and made from a negative

kindly supplied by the authors. The coincident

gravity low may be seen on the map in pocket.
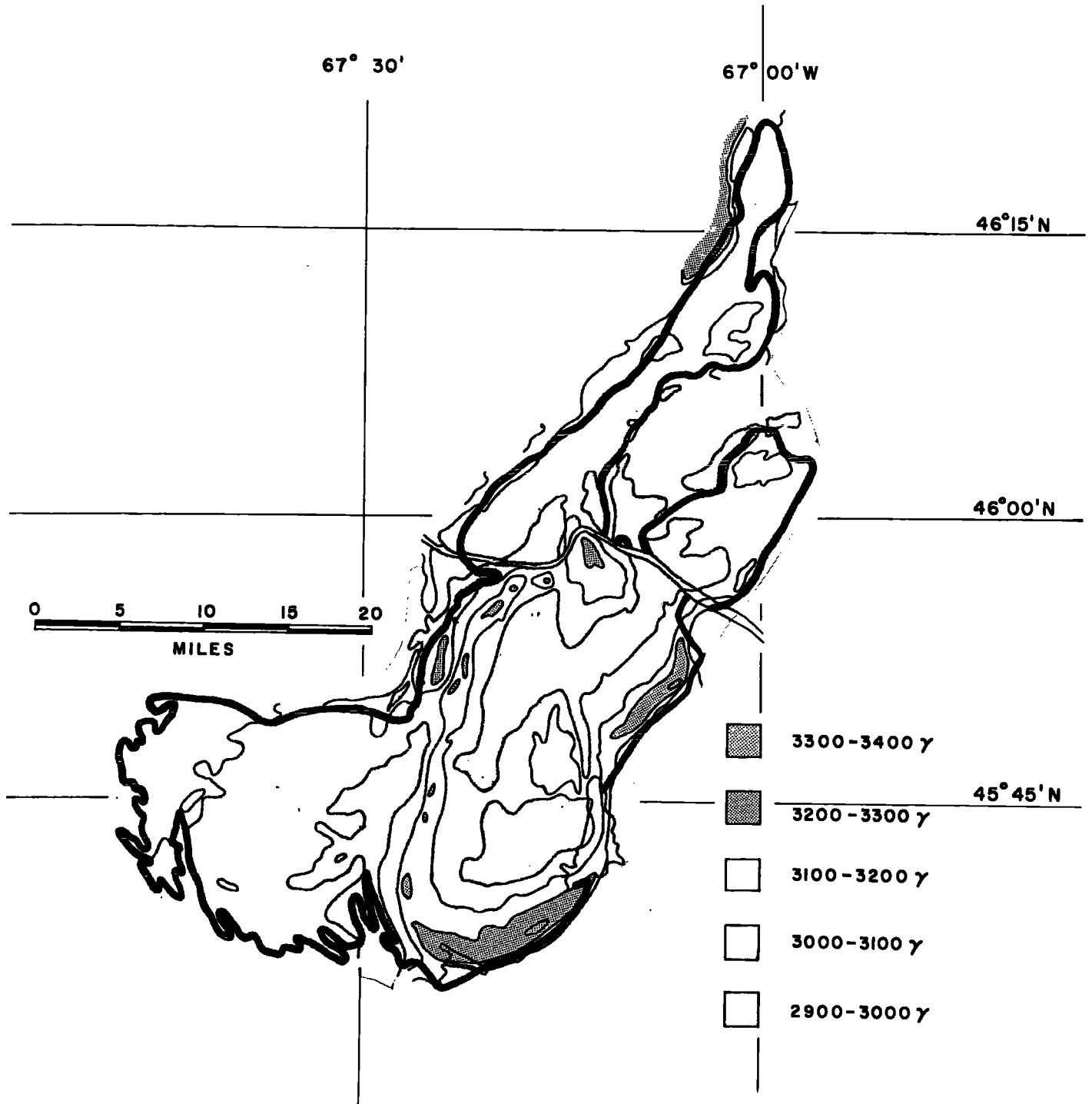
Figure 5.15: Observed magnetic and gravity anomalies and

calculated pseudo-gravity anomaly over Western

Bank. Symbols as explained for Figure 5.13.

WESTERN BANK
(L¹-L)

m/d = .026 emu/gm
Inc = 0°(N)
r = .61

Magnetic Anomaly
Gravity Anomaly
Pseudo-Gravity

gammas
milligals
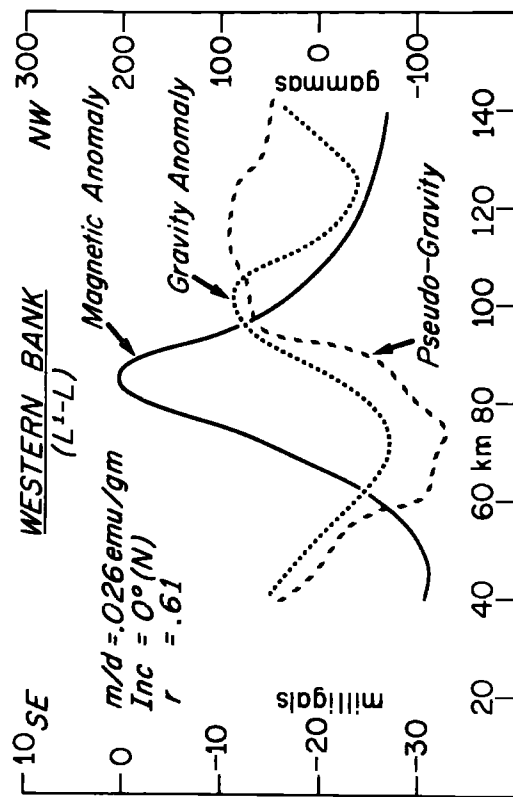
anomaly is that the source of the gravity low is non-magnetic and that the basement rocks are reversely magnetized. They may have acquired their magnetization due to metamorphic effects associated with the intrusion of the granite in Devonian (?) times or the basement may have been "soaked" with magnetic basaltic magma during continental collision and break-up in Permo-Triassic times. The difficulty with this concept is that the basement rocks would have to have a strong component of remanent magnetization oriented more or less opposite to the earth's field and, as mentioned in Chapter 4, such a situation is not found on land. Nevertheless, the idea may not be completely unrealistic as magnetic anomalies in the Atlantic suggest the presence of strong, reverse magnetizations in oceanic basalts of various ages dating back to the opening of the Atlantic Ocean in Triassic times and the majority of the directions of remanent magnetization in rocks, particularly Permo-Carboniferous rocks, from the Canadian Maritimes are in opposition to the earth's field. However, the combined analysis of the gravity and magnetic data on the northwestern portion of the Halifax Line gives no evidence for reversely magnetized rocks and, in the absence of any independent evidence of reversely magnetized rocks, the more conservative interpretation, supporting the existence of magnetic granite, is favoured.

Although the eastern arm of the Middle Bank Low may delineate a spur of granitic rock, Stephens and Cooper (1973) pointed out that diapiric structures (King and MacLean, 1970) near Sable Island

suggest that this portion of the low may outline a basin containing

Mesozoic and Tertiary sedimentary rocks and salt deposits. Their

interpretation is strengthened by Jansa and Wade's (1975)

recognition of the Abenaki sub-basin in this area. It is interesting

to note that the northeasterly trending arm lies on strike with the

coincident, elongate gravity and magnetic lows (Figure 5.12) which

are situated southeast of the Emerald High (at about 43.8^{o}N; 62°W)

and probably reflect a second local sedimentary basin.

5.7   WESTERN BANK AND LA HAVE BANK ANOMALIES

Western Bank (Figure 1.1) is characterized by a smooth oval

magnetic high (Figure 5.4) which is produced by a source about

7 km deep (McGrath et al., 1973). Seismic evidence in the adjacent

region suggests that the source is associated with the crystalline

basement and may be an intrusion or an up-faulted block similar

to that which is thought to cause the Emerald High. Two-dimensional

combined analysis of the gravity and magnetic anomaly fields

(Figure 5.15) along profile L'-L shows little correlation and

indicates that there is no simple relation between the two fields.

The intense, apparently circular magnetic low (Figure 5.4) on

the eastern margin of La Have Bank (near 43.2N, 63.8W) is defined

by only one profile. The anomaly may merely be a manifestation

of a magnetic disturbance as this profile was not corrected for

diurnal variation (R.T. Haworth, personal communication) but if

the anomaly is real, it probably represents a compact intrusion

which cooled during a time when the earth's field was reversed. The magnetic low shows no obvious relation to the gravity field.

5.8 SUMMARY AND DISCUSSION OF THE STRUCTURE OF THE SOUTHERN SCOTIAN SHELF

The general geophysical picture of the southern Scotian Shelf is one of the eroded top of a southeasterly dipping basement complex overlain by a wedge of late Palaeozoic and younger sedimentary rocks which reach their maximum thickness east of Sable Island. Throughout most of the area, the gravity and magnetic anomalies generally reflect variations of density and magnetization within the pre-Carboniferous basement rocks except near the continental margin where the sedimentary column depresses the gravity field by some 40 to 50 mgal and local gravity and magnetic features such as the Emerald High and flanking lows may reflect fault-bounded horsts and sedimentary basins produced as a result of stresses imposed during continental break-up (e.g. Stephens and Cooper, 1973). A large portion of the southern Scotian Shelf appears to be underlain by a batholith of low-density granite. This granite differs from those in southern Nova Scotia in that it appears to be magnetic and possess a significant amount of remanent magnetization whereas the granites of southern Nova Scotia are conspicuously non-magnetic. The basement rocks in the vicinity of the Emerald High are denser than, and hence different from, the Meguma basement rocks to the northwest.

The structure of the crust along the southeastern coastline
of Nova Scotia is normal when compared to other regions in Canada
which are characterized by approximately the same regional Bouguer
anomaly level and upper mantle compressional wave velocity. The
southern Scotian Shelf is approximately in isostatic equilibrium
and the increase in Bouger anomaly level as the continental margin
is approached is probably largely due to the rise of the Mohorovicic
Discontinuity from a depth of 45 km under southern Nova Scotia to
depths of 10 to 15 km beneath the deep ocean.

The question of whether southern Nova Scotia and the southern
Scotian Shelf form a single structural unit is difficult to answer.
There is no obvious structural feature separating the two areas
in the same way that there is one separating the northern and
southern Scotian Shelf and so there is no reason to suspect that
the typical Meguma slates, shales and quartzites and the intrusive
Devonian granites of southern Nova Scotia do not underlie most of
the southern Scotian Shelf. One area where they probably do not
occur, however, is in the vicinity of the Emerald High where the
denser basement probably forms a distinctly different structural
unit. Because the presumed granite batholith to the northeast is
magnetic, unlike the ones on land, it is possible that this
different structural unit extends northeast to encompass the main
portion of the Middle Bank Low. If so, the southwestern edge of
the Meguma basement would run approximately parallel to the
coastline north of Halifax at a distance of some 50 to 75 km

offshore but there is, admittedly, no strong evidence that the

Meguma rocks terminate along such a line.

Without trying to draw any close parallel between the age and

history of the two areas, it is interesting to note that the

horst and graben type of structure postulated to occur within the

dense basement underlying the Emerald High region is reminiscent of

the uplifted, dense Precambrian basement blocks and flanking

Carboniferous sedimentary basins which occur in the Antigonish-

Cape Breton Highlands area. The basement in the vicinity of the

Emerald High may be a remnant of one of the late Precambrian

basement nuclei found in northwest Africa, or, alternatively,

the basement rocks could have been formed or reworked during

Permo-Carboniferous times. Further discussion of this will be

left until Chapter 7.

CHAPTER 6

THE CENTRAL SCOTIAN SHELF

6.1   INTRODUCTION

The central Scotian Shelf and adjacent land region of central
Nova Scotia (see Figure 1.3) is of considerable interest because the
available geological and geophysical information indicate the presence
of a major discontinuity of crustal proportions which separates the
rocks of the southern Scotian Shelf and southern Nova Scotia from
those of the northern Scotian Shelf and central Nova Scotia. As men-
tioned in the introductory chapter, this discontinuity is thought to
be related to the convergence and/or separation of lithospheric plates
in the Palaeozoic Era. An important aim of the geophysical investi-
gation described in this chapter is to determine, if possible, the
structure of the discontinuity which cuts the Scotian Shelf.

6.2   GEOLOGICAL SETTING OF CENTRAL NOVA SCOTIA

6.2.1   Sedimentary, volcanic and metamorphic rocks

The two main pre-Carboniferous basement features of central
Nova Scotia (Figure 6.1) are the Cobequid Highlands and the Antigonish
Highlands (Figure 6.2). A large portion of the Cobequid Highlands is
made up of granite, granite gneiss, diorite and metamorphosed sedimen-
tary and volcanic rocks consisting of grey to black fine-grained
sedimentary rocks or volcanic ash beds, grey and red shale, light grey
to white quartzite or silicified tuff, chlorite schist and fine-
grained conglomerate or volcanic breccia. This complex is cut by
Devonian granitic batholiths and diabasic dykes and is bounded, in

Figure 6.1:   Simplified geological map of Nova Scotia.

Faulting in central Nova Scotia is shown

in more detail in Figure 6.2.

Simplified Geological Map of Nova Scotia

SEDIMENTARY, VOLCANIC & METAMORPHIC ROCKS

TRIASSIC – Basalt / Conglomerate, Sandstone

CARBONIFEROUS – Sandstone, Limestone, Conglomerate

SILURIAN, DEVONIAN – Shale, Sandstone, Conglomerate
Quartzite, Volcanic Rocks

DEVONIAN & EARLIER – Gneiss Complex (includes
Granite, Gabbro, Diorite)

CAMBRIAN, ORDOVICIAN – Volcanic & Sedimentary Rocks

CAMBRIAN, ORDOVICIAN – Greywacke, Quartzite, Slate, Schist

PRECAMBRIAN – Volcanic, Breccia, Tuff, Lava; Greywacke,
Shale, Schist

PRECAMBRIAN – Quartzite, Schist, Gneiss, Crystalline
Limestone

PLUTONIC ROCKS

DEVONIAN – Granite

DEVONIAN, CARBONIFEROUS –
Gabbro, Diabase

FAULTS

Areas of Mainly
VOLCANIC ROCKS

Figure 6.2:   Map of central Nova Scotia and the central

               Scotian Shelf showing: major topographic

               features in central Nova Scotia, seismic

               data on the central Scotian Shelf,

               location of profiles discussed in text

               and Bouguer anomaly contours.

209
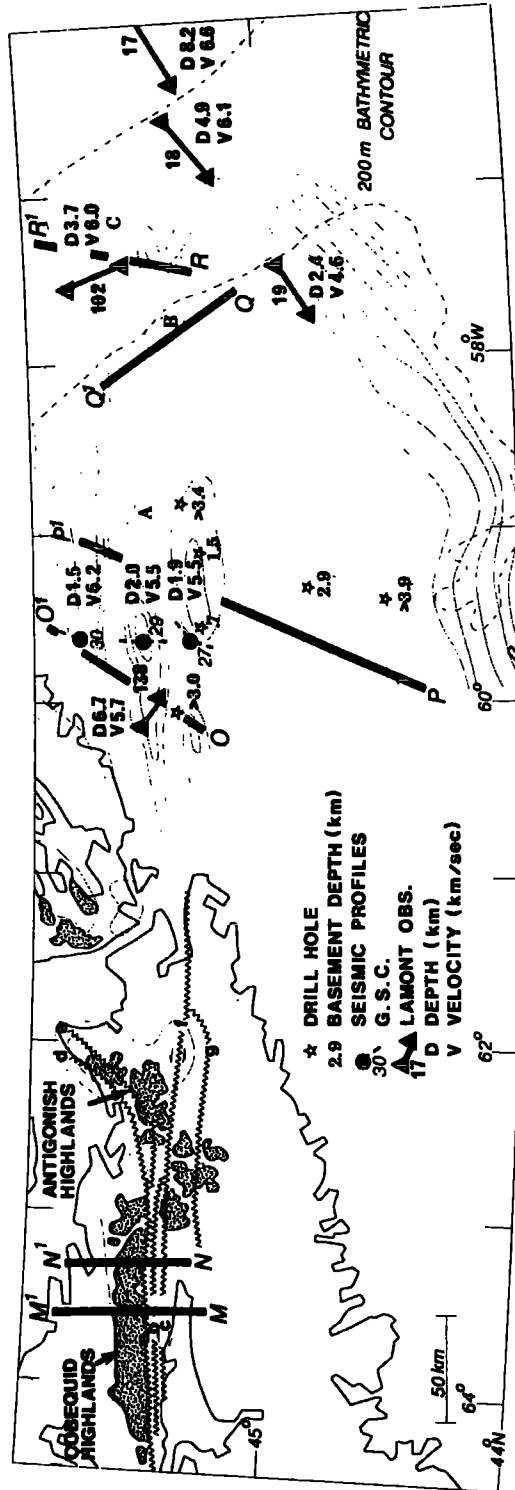
some places, on the south side by a black, graphitic schist which is thought to mark a zone of considerable shearing (Weeks, 1948). The age of the basement complex is uncertain but recent radiometric age dating of some of the older granitic rocks provides ages of about 600 m.y. (W.H. Poole, personal communication). Sedimentary rocks of probable Silurian age are found mainly in the southwestern Cobequid Highlands. These rocks generally consist of unfossiliferous, grey, slightly sandy shale and resemble rocks of the Silurian Arisaig Group (Weeks, 1948) which lie some 100 km to the east in the Antigonish Highlands.

The lowermost exposed rocks of the Antigonish Highlands (Figure 6.1) are made up of about 6 km of volcanic, and sedimentary rocks of the Cambro-Ordovician Brown's Mountain Group. This group is subdivided into four formations, the basal Keppoch Formation, consisting of porphyritic leucodacite to rhyolite and minor breccia and tuff, the Baxter Brook Formation, consisting of laminated tuffaceous siltstone, shale and argillite, crystal tuff, shale and silty shale, The Brierly Brook Formation, consisting of leucoandesite porphyry , lapilli crystal tuff, andesite, and agglomerate, breccia and greywacke, and the uppermost Little Hollow Formation consisting of siltstone, quartzite and minor wacke (Benson, 1974). The basal volcanics have been dated at 531 ± 27 my (Cormier, 1974).

The Cambro-Ordovician rocks of the Brown's Mountain Group are unconformably overlain in several localities by the generally sedimentary rocks of the Silurian Arisaig Group. This group has been of particular interest to palaeontologists because of "its completeness, fossil contents and decided European affinities" (Williams, 1912).

The Arisaig Group is made up of five formations which generally con-
sist of shale and limestone and have a total preserved thickness of
about 1 km. The lower formations contain some tuff beds.

The pre-Carboniferous basement rocks of the Cobequid and Anti-
gonish Highlands are overlain by Carboniferous shale, slate and sand-
stone of the Mississippian Horton and Windsor Groups and the Pennsyl-
vanian Canso, Cumberland and Pictou Groups. In many places the
Carboniferous rocks lie unconformably on the older basement rocks but
in some places (for example south of the Cobequid Highlands and north-
west of the Antigonish Highlands) the Carboniferous rocks are separated
from the basement by faults.

Triassic conglomerate, sandstone and shale, the Annapolis
Formation, and scattered outcrops of basalt occur on the north shore
of the Minas Basin; patches of rocks similar to those of the Annapolis
Formation occur west and north of Chedabucto Bay (Stevenson, 1959).

6.2.2   Intrusive rocks

Large masses of granitic to granodioritic rocks intrude the
older gneisses and volcanic sedimentary rocks of the Cobequid High-
lands. Radiometric age dates of about 580 my are found in granite
rocks in the Cape Breton and Antigonish Highlands (Benson, 1974) and
perhaps they are contemporaneous with the older (as opposed to the
younger) granitic rocks in the Cobequid Highlands. According to Weeks
(1948) the more basic phases of the granite in the Cobequid Highlands
probably result from the assimilation of pre-existing basic volcanic
material. The younger granitic rocks intrude fossiliferous Silurian

to lower Devonian sedimentary rocks and granite remnants occur in nearby Carboniferous clastics so their age is well established. Acid porphyries found in the Cobequid Highlands in regions underlain by Silurian shale may have been emplaced in the Carboniferous Period.

Diabasic intrusive rocks are rather evenly distributed throughout the Cobequid complex; their age is uncertain but is probably Carboniferous (Weeks, 1948). Several exposures of diabase and gabbro occur to the east of the Cobequid complex and immediately to the north of the Minas Basin – Chedabucto Bay fault zone (Figure 6.1). The age of these intrusives is uncertain but is probably Permo-Carboniferous (Schiller, 1961).

6.2.3   Structure and metamorphism

In the Cobequid Higlands, the structures in the volcanic-sedimentary complex are generally obscure but where mapped in one location, they are discordant with those in the Silurian (?) shales which exhibit a relatively shallow, uniform dip to the south. The Cambro-Ordovician slate, greywacke and andesite in the Antigonish Highlands are folded and exhibit steep dips. The unconformably over-lying Silurian shales and limestones also exhibit similar but somewhat less intense folding.

Folds in Carboniferous shale, slate and sandstone vary from open to tight and the pattern is complex. Folds generally trend northeasterly but locally they trend northerly near Chedabucto Bay and easterly north of the Minas Basin.

Large-scale faulting exists throughout central Nova Scotia. A major discontinuity is the Cobequid Fault (labelled "a" in Figure 6.2)

which separates the pre-Carboniferous Cobequid volcanic-sedimentary complex from the Carboniferous rocks lying to the south. At the eastern end of the Cobequid Mountains the fault divides into two branches. The northerly branch curves northeastward and joins up with the Hollow Fault ("d") (e.g. Cameron, 1956) which separates the pre-Carboniferous rocks of the Antigonish Highlands from Carboniferous rocks lying to the northwest. The other branch links up with the Brown's Mountain Fault ("e") (Benson, 1974) which cuts lower Devonian rocks but not Carboniferous sedimentary rocks. To the south of the Cobequid Fault lie two east-west trending faults, the Portapique Mountain - North River Fault ("b") and the Gerrish Mountain-Riversdale Fault ("c"). Further east, these faults join together into a fault zone which links up with an east-west trending portion of the Chedabucto Fault ("f"); the latter fault extends into the sea along the south side of Chedabucto Bay (King and McLean, 1970). Where mapped, the West River St. Mary's Fault separates Carboniferous sandstone, shale, conglomerate, etc. from the Cambro-Ordovician quartzite, greywacke, etc. of the Meguma Group (Figure 6.2).

Faults "b", "c" and "f" make up a major zone of east-west faulting which extends from the Minas Basin to Chedabucto Bay. In the west the fault zone cuts Carboniferous and Triassic rocks, in the central portion it defines the southern boundary of the Antigonish Highlands and in the east it separates the Cambro-Ordovician Meguma Group of southern Nova Scotia from the Carboniferous sedimentary rocks of central and northern Nova Scotia. A most interesting aspect of this east-west fault is that there are no known outcrops of

Precambrian rocks on the south side.

South of the Antigonish Highlands, the St. Mary's River Graben (Benson, 1974) is bounded on its north side by the Riversdale-Chedabucto Fault zone ("c" and "f") and on its south side by the West River St. Mary's fault ("g"). The graben is about 15 km wide and characterized by a featureless aeromagnetic anomaly field. To the east, the graben structure is either truncated or offset to the north. The latter interpretation is favoured because an east-west trending topographic lineament marked by the Guysborough River (not shown) which empties into the head of Chedabucto Bay lies some 15 km north of the Chedabucto Fault and may mark the northern edge of a graben-type structure. Note, however, that in the vicinity of Chedabucto Bay the Chedabucto Fault marks the south, not the north side of the graben.

The general sense of vertical motions associated with the faults running from the Minas Basin to Chedabucto Bay is such that younger rocks are down-faulted against older rocks. The direction and extent of lateral motion is not clear. Benson (1974) indicated left-lateral motion along the Chedabucto Fault ("f") whereas Weeks (1948) mapped a right-handed movement affecting Triassic rocks along the Gerrish Mountain Fault ("c") which seems to be a westerly continuation of the Chedabucto Fault. Boyle (1963) mapped left-lateral movements in east-west trending faults which cut Triassic rocks south of the Minas Basin. Movement along the Cobequid-Hollow Fault zone is right-handed (Eisbacher, 1969).

Although there are some areas in northern Cape Breton Island

215

where high-grade metamorphic rocks occur, metamorphism in central Nova

Scotia is generally low grade, only reaching the greenschist facies in

parts of the Cobequid and Antigonish Highlands. An interesting excep-

tion is the presence of the few scattered, isolated outcrops of amphi-

bolite and composite gneiss of unknown age (Schiller, 1961) east of

the Antigonish Highlands and just to the north of the Minas Basin-

Chedabucto Bay fault zone.

6.2.4   Brief tectonic history of central Nova Scotia (and Cape Breton
        Island)

The oldest rocks in Cape Breton Island appear to be the George

River Group which consists of quartzite, marble, schist and gneiss.

These rocks and possibly the isolated patches of amphibolite and com-

posite gneiss found to the north of the Minas Basin - Chedabucto Bay

fault zone and the older granitic rocks in the Cobequid Highlands

represent Precambrian basement fragments which have survived a com-

plicated, uncertain history.

The oldest, clearly defined period of volcanic activity is

recorded in Cape Breton Island in the Fourchu volcanic-sedimentary

rocks where volcanic activity in this area commenced or extended into

the early Cambrian when a change-over to a miogeosynclinical environ-

ment occurred.

The next recorded period of eugeosynclinical activity occurred

in Cambro-Ordovician times in the Antigonish Highlands where andesite

volcanism occurred in an island-arc environment (Benson, 1974).

Sedimentation, continuing into the Silurian Period, indicates a

progression towards a shallow-water environment. Fossils in the upper

Silurian rocks of Arisaig are closely related to those of western

Europe but not to those of North America (McLearn, 1924) so this part

of Nova Scotia may have been a part of the European lithospheric plate

at this time and the andesitic volcanism probably reflects generation

of magma by means of processes associated with lithospheric under-

thrusting as the European and North American plates converged.

As in Newfoundland, the Devonian Period saw an end to large-

scale extrusion of acidic to intermediate magma and initiated wide-

spread intrusion of granitic magma. In addition, the Devonian Period

was one of extensive folding, faulting and regional metamorphism; this

presumably reflects, in this region the end of, or at least the marked

reduction of, the convergence of the European and North American plates.

In the Carboniferous Period the environment was mainly contin-

ental and the areas occupied by the Cobequid, Antigonish and Cape

Breton Highlands were positive fault-bounded regions flanked by subsid-

ing sedimentary basins. Considerable vertical and possibly some

horizontal differential movement took place along major fault zones.

In particular, the Minas Basin - Chedabucto Bay fault zone was an

important tectonic feature because "differences in Carboniferous Fault

indicates that these basins were not all inter-connected as suggested

by their present form" (Benson, 1974).

At some time, or times, during the Carboniferous and/or Permian

Periods the rocks on the north side of the Minas Basin-Chedabucto Bay

fault zone were intruded by diabasic rocks. This activity may have

been   the result of the action of mechanical forces associated

with the Hercynian deformation of a broad band extending from northern

Africa to southern England (e.g. Burrett, 1972).

The final period of volcanism occurred in the late Triassic with the appearance of basaltic flows in the Bay of Fundy region. These flows were probably in response to stresses present during the opening of the present-day Atlantic ocean. In contrast to Newfoundland, Cape Breton Island and most of southern Nova Scotia; the Minas Basin-Chedabucto Bay region is unique in that it records significant Permo-Triassic tectonic activity.

6.3 GEOPHYSICAL DATA

The underwater gravity coverage is uniform over the central Scotian Shelf except near the mouth of the Laurentian Channel at about $45.5^\circ N$; $56.6^\circ W$ where a small gap exists in the underwater gravity station distribution (see map in pocket). The underwater gravity data are supplemented by several surface gravimeter profiles made by the Bedford Institute, Dartmouth, N.S. The main gravitational feature on the central Scotian Shelf is the linear, east-west trending, Orpheus Low and its flanking highs (Figure 6.3). In the vicinity of the mouth of the Laurentian Channel two small oval lows occur adjacent to an elongate high which is ill-defined due to the gap in the underwater gravity station distribution. On land, the dominant features in central Nova Scotia are gravity highs over the Cobequid and Antigonish Highlands (Figure 6.2).

Magnetic coverage of the central Scotian Shelf is provided by several reconnaissance-type surface magnetometer profiles which reveal generally negative anomalies south of latitude $45.5^\circ N$ and positive

Figure 6.3:   Bouguer anomaly map of the central

Scotian Shelf.

219

BOUGUER ANOMALY MAP – CENTRAL SCOTIAN SHELF
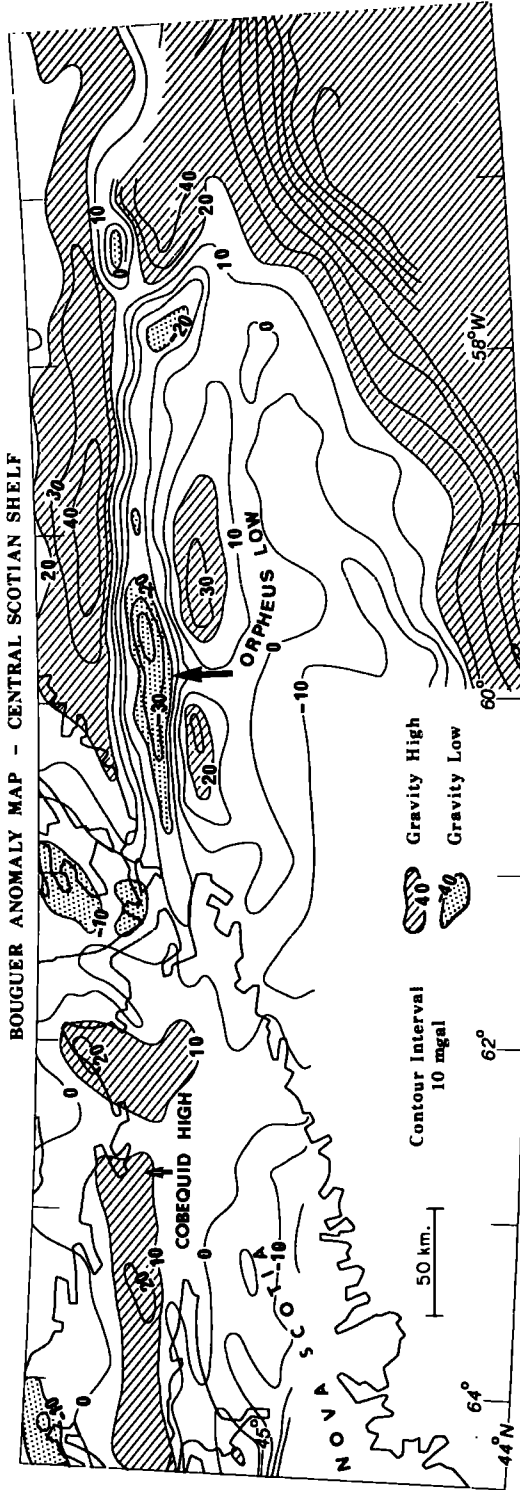
Figure 6.4   Total field magnetic anomaly map of

the central Scotian Shelf. Map derived

by subtracting a linear regional gradient

from Natural Resource Maps 15056-C and

15058-C (Canadian Hydrographic Service, 1974).

MAGNETIC ANOMALY MAP - CENTRAL SCOTIAN SHELF
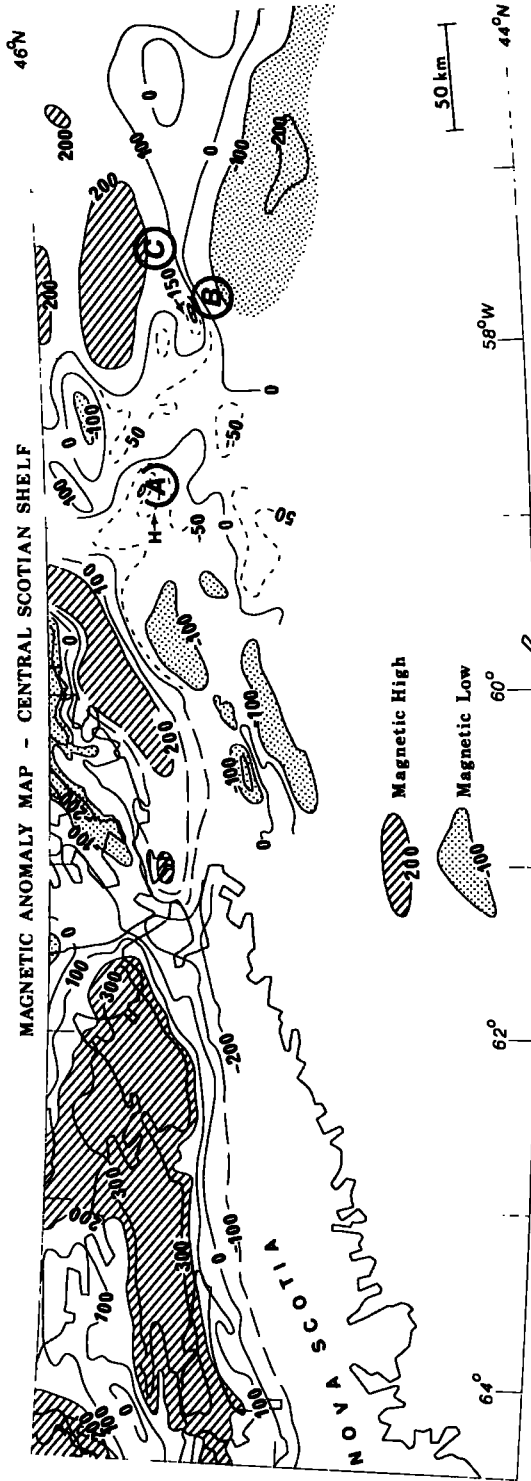
anomalies to the north (Figure 6.4). Whereas the gravity trends are east-west the magnetic trends are often northeast-southwest (45.5°N; 60°W) or northwest-southeast (45.5°N; 57°W). On land there is excellent aeromagnetic coverage which shows that the Cobequid and Antigonish Highlands (Figure 6.2) are characterized by magnetic highs.

Several shallow seismic refraction profiles are available on the central Scotian Shelf (Figure 6.2). They indicate the presence of a fairly thick sedimentary sequence in the vicinity of Orpheus low and shallow basement benath the flanking gravity highs. To the east, near the mouth of the Laurentian Channel, the basement beneath the gravity highs is more deeply buried. Of particular interest are two drill holes over one of the southern flanking gravity highs which confirm the presence of shallow basement consisting of rocks which appear to be typical Meguma schist and Devonian granite but which exhibit Carboniferous radiometric ages (M. Given, personal communication).

The investigation of the central Scotian Shelf and the adjacent part of Nova Scotia is done from west to east, first attempting to relate the geological and geophysical data on land and then working eastward over the shelf.

6.4 THE COBEQUID AND ANTIGONISH HIGHS

As Garland (1953) pointed out in his discussion of the gravity field over the Cobequid Highlands, the positive anomaly "is thrown into striking contrast by the negative areas over the Minas Basin to the south and the Cumberland Basin to the north". As may be seen from the previous section, there is reasonably good correlation between the exposures of pre-Carboniferous basement rocks in the Cobequid Highlands

Figure 6.5:   Magnetic,gravity and pseudo-gravity profiles

along profiles M-M' and N-N' over the

Cobequid Highlands.

GLENHOLME TO MIDDLEBORO
(M-M¹)

S

N

-25

700-

m/d=.0091emu/gm
Inc=85(S)
r =.81

-20

500-

Pseudo-Gravity

-15

300-

-10

100-

Magnetic
Anomaly

-5

-100-

Bouguer
Anomaly

milligals

gammas

TRURO TO TATAMAGOUCHE
(N-N¹)

S

700-

-20

N

m/d=.020emu/gm
Inc=85(S)
r =.88

-15

500-

Observed Gravity

300-

-10

100-

-5

Pseudo-
Gravity

Magnetic Anomaly

-100-

-0

20

40 km

60
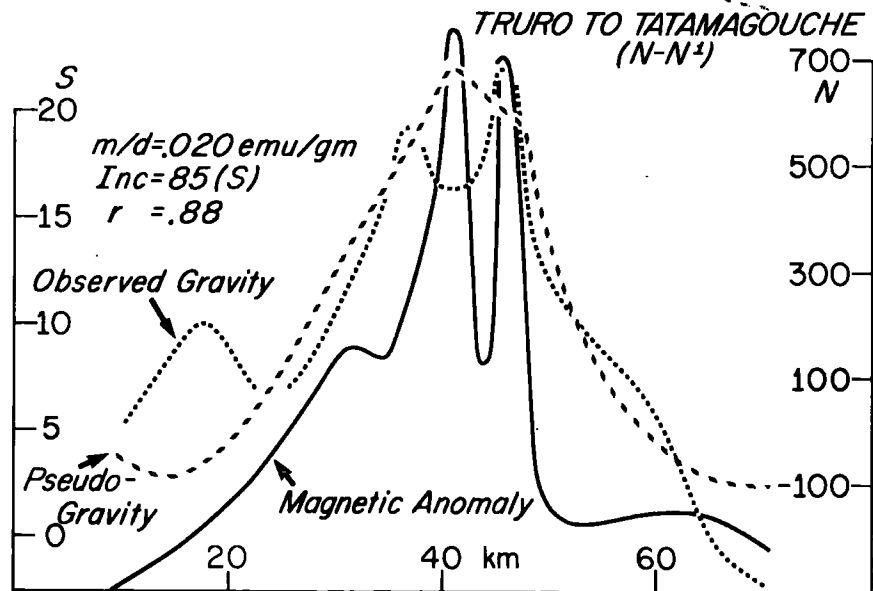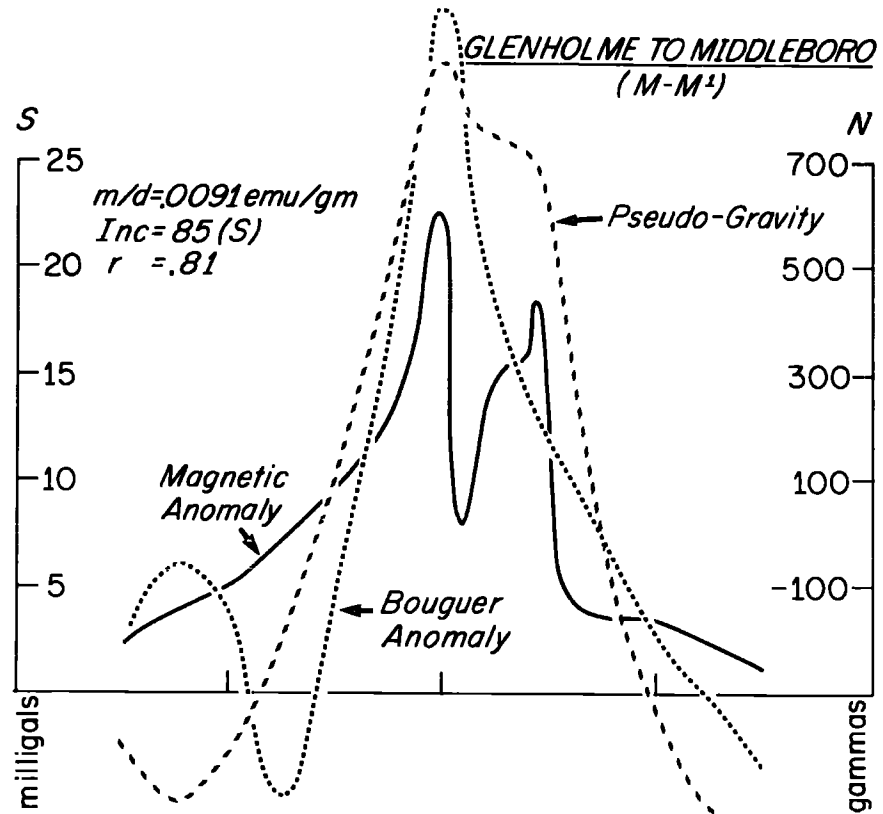
and the elongate gravity and magnetic highs. The gravity and magnetic

highs over the Cobequid Highlands are typical of anomalies over other

fault-bounded, pre-Carboniferous basement complexes in this part of

the Canadian Atlantic Provinces (e.g. Goodacre and Nyland, 1966).

Detailed gravity profiles made by the Nova Scotia Research Foundation

supplement the available magnetic and geological information over the

Cobequid Highlands and provide an opportunity to obtain a fairly

accurate model of the crustal discontinuity along the south side of

the Cobequid complex.

The first step made in studying the geophysical data was to do

a two-dimensional combined analysis of the gravity and magnetic fields

along profiles M-M' and N-N' (Figure 6.2). The elongate nature of the

anomalies justifies the use of a two-dimensional analysis. In both

cases quite good correlation was obtained between the observed gravity

and the "pseudo-gravity" for a direction of magnetization of 85°(S) in

the vertical plane containing the earth's magnetic field (Figure 6.5).

Since the inclination of the earth's field is 74°(N), the direction of

total magnetization of 85°(S) indicates the possibility of some remanent

magnetization in the magnetic source and, as mentioned in Chapter 4,

a deflection of the earth's field by some 10 to 20° can be produced

for reasonable values of 0.2 to 0.4 for the Koenigsberger ratio. On

the other hand, the validity of the two-dimensional magnetic to gravity

field transformation depends upon the fulfillment of all the assump-

tions. The fact that the pseudo-gravity anomaly is somewhat wider than

the observed anomaly along profile M-M' (Figure 6.5) indicates that,

in this case, the ratio of magnetization contrast to density contrast

is not everywhere constant (e.g. the distribution of anomalous magnetization may be wider than the density excess). However, the results of the two profiles taken together suggest the presence of a southerly directed remanent magnetization in the source rocks.

The second step in studying the magnetic high was to model the magnetic anomaly along each of the two profiles M-M', N-N' using a suite of two-dimensional, homogeneous sources in order to determine which inclination of magnetization gives the best fit between the observed and calculated anomaly and to find out what is the minimum allowable value of magnetization contrast. Laving's (1971) matrix method programs were used and models with both inward and outward dipping sides were tried. The results, displayed in Figure 6.6, show that the best fit is obtained for models with outward-dipping sides and for an inclination of magnetization of about 80°(S). This value is probably determined to within about plus or minus five degrees. Of course, it might be possible to find other homogeneous, or heterogeneous, bodies magnetized in a different direction which would provide a fit equally as good, or better, than the fits obtained here, nevertheless, this angle is consistent with that derived from the two-dimensional combined analysis and provides further evidence of remanent magnetization in the source rocks. The modelling also showed that the mininum magnetization contrast of the source is of the order of 0.001 emu/cm^3. This value coupled with a ratio of 0.01 emu/gm derived from the combined analysis (Figure 6.5) indicates a minimum density contrast of about 0.1 gm/cm^3 for the source of the gravity anomaly. This value is not inconsistent with the expected density contrast, which, according to Garland (1953), is of the order of 0.15 to 0.20 gm/cm^3.

Figure 6.6:   Root mean square residual plotted as a
              function of inclination of magnetization
              and magnetization contrast for models of
              the magnetic anomalies along profiles M-M'
              and N-N'.

GLENHOLME TO MIDDLEBORO

TRURO TO TATAMAGOUCHE
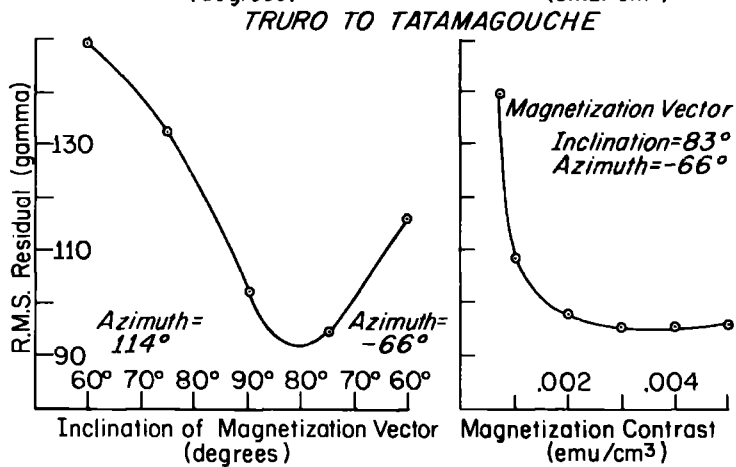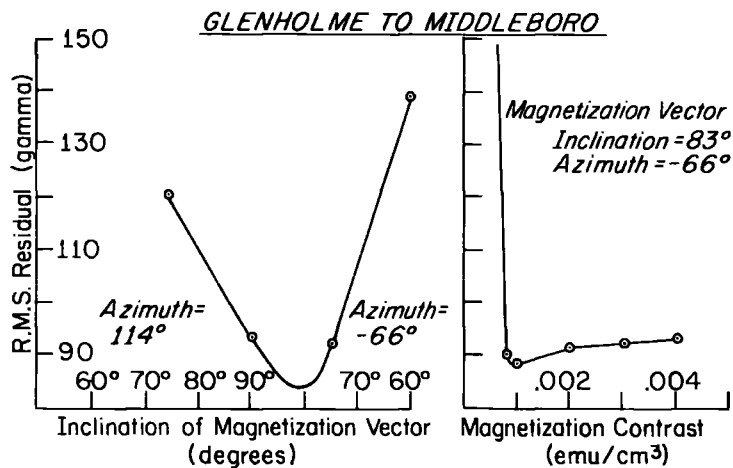
Figure 6.7:   Observed and computed magnetic anomalies

and interpretative model along profile

M-M' using a magnetization contrast of

0.002 emu/cm^3.

GLENHOLME TO MIDDLEBORO
(M-M±)

Observed Magnetic Anomaly

Computed Magnetic Anomaly
(m=.002emu)

R.M.S. Residual 92 Gamma
Inclination of Magnetization
83° (S)

Cobequid Highlands

m=.002emu

m=.001emu
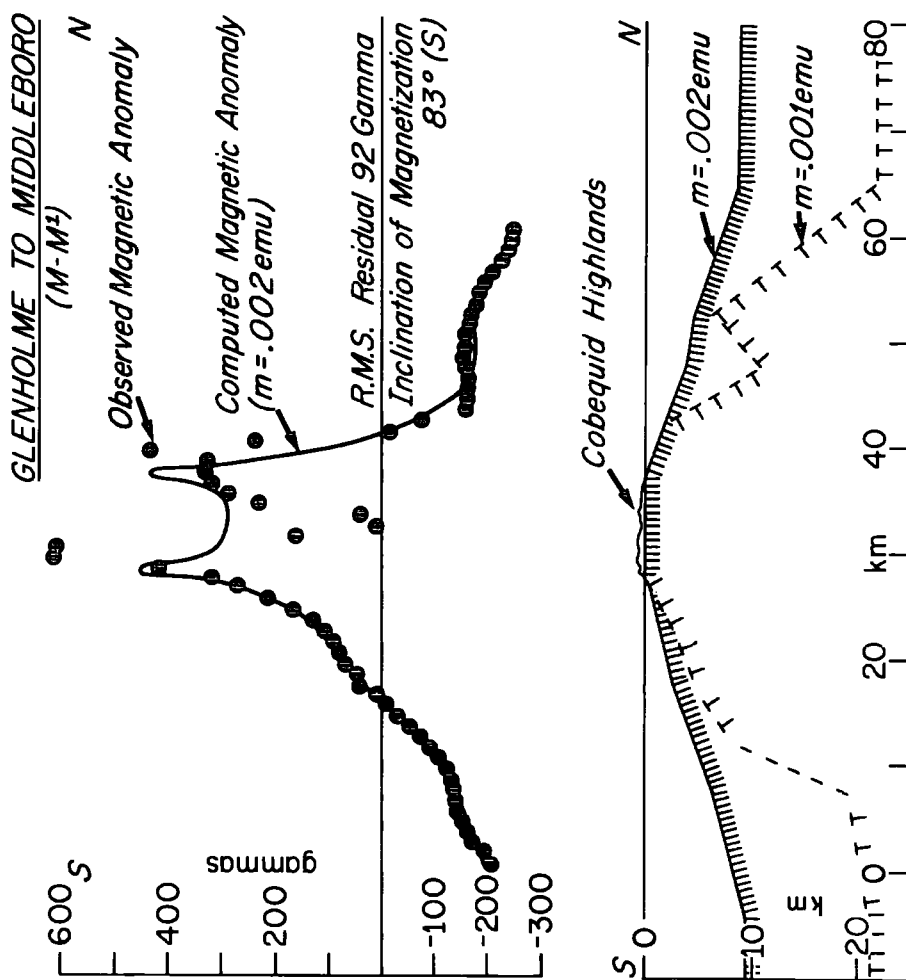
Figure 6.7 shows a magnetic model derived (using Laving's (1971) matrix method programs) from the Glenholme to Middleboro profile (M-M' in Figure 6.2) for a magnetization contrast of 0.002 emu/cm^3. A second model which has a magnetization contrast of 0.001 emu/cm^3 is shown by dashed lines. The latter model provides an upper limit of about 30° for the angle at which the southern face of the magnetic source dips. The gravity anomaly was also modelled with a view towards determining the characteristics of the geophysically defined contact along the south side of the Cobequid Highlands. A suite of simple models was obtained using non-linear optimization methods (Al-Chalabi, 1970). All of the models exhibited approximately the same characteristics: trapezoidal shapes with outward sloping sides, thicknesses of about 6 to 8 km and dips of the southern face of 30 to 40°. The shapes of the gravity models generally coincide with that of the magnetic model but the gravity models tend to be somewhat narrower and their sides tend to dip somewhat more steeply. In order to get a satisfactory fit it was necessary to use a density contrast of at least 0.15 gm/cm^3. This is somewhat larger than the minimum value derived from the magnetic to gravity field transformation but is consistent with Garland's (1953) estimate mentioned earlier.

It should be pointed out that in modelling the gravity and magnetic anomalies over the Cobequid Highlands (and in doing the combined analyses) it is assumed that the background, or regional, level of either anomaly is zero over the flanking sedimentary basins so that the resulting anomalies can be modelled using a single, positive magnetization or density contrast. A more complete interpretation,

particularly in the case of the gravity anomalies, would assume a

slightly higher regional level and would require using sources which

have a negative density contrast to model the gravity lows over the

sedimentary basins and sources which have a positive density contrast

to model the highs over the Cobequid Complex but the aim here is to

model the boundary between the dense, magnetic rocks in the Cobequid

Highlands and the light, essentially non-magnetic rocks to the south.

In order to relate the source of the magnetic and gravity highs

to the geology of the Cobequid Highlands, the author obtained rock·

samples on a traverse along part of the Glenholme to Middleboro (M-M')

profile. The measurements of density and susceptibility given in Table

6.1 suggest that the causative body is composed of heavy, magnetic

dioritic to gabbroic rock and that the gravity and magnetic anomalies

outline the contact between this rock and the lighter, less magnetic

metasedimentary rocks to the south. If the boundary between the meta-

sedimentary rocks and the dioritic gabbroic rocks is a fault, it was

probably formed under compression, not tension, because of the rela-

tively low angle of dip. The geophysically defined boundary may have

been developed during the formation of the mylonite zone (samples 24,

31,41 in Table 6.1) by dextral strike-slip motion during the Devonian

period (Eisbacher, 1969) and, if so, may predate the Cobequid Fault.

It is interesting to note that the geophysical boundary does not coin-

cide exactly with the Cobequid Fault ("a" in Figure 6.2) which lies

about 1 km further south and is marked by a thin zone of phyllite

(sample 23) that separates the Carboniferous conglomerate and sandstone

from the pre-Carboniferous metasedimentary rocks.

TABLE 6.1

DENSITIES AND SUSCEPTIBILITIES OF ROCK SAMPLES FROM FOLLY LAKE AREA
OF COBEQUID HIGHLANDS.

Sample No.	Approx.dist. north of Glenholme N.S. km	Description	Density gm/cm^3	Susceptibility x10^{-6} emu/cm^3
11	37.0	Conglomerate	2.48	120
12	37.0	Sandstone	2.57	
23	37.4	Phyllite	2.76	
24	37.4	Brecciated impure quartzite	2.70	30
31	37.7	Quartzite	2.64	40
41	38.1	Sheared quartzite	2.60	10
51	38.5(?)	Gabbro	2.98	80
61	38.8	Metasiltstone	2.74	30
71	39.0	Dolerite	2.80	1800
82	42.0	Gabbro	2.90	110
91	42.5	Gabbro	2.99	5620
101	42.8	Syenite	2.79	110

			Koenigs- berger ratio (Q)	Remanent Magnetization x10^{-6} emu/cm^3
71			0.1	200
91			0.3	1800

The Cobequid Fault might be expected to show up in the gravity
data since the Carboniferous conglomerate and sandstone are somewhat
less dense than the quartzite, etc. but there is no evidence of it in
the anomaly profile. In addition neither the Portapique Mountain –
North River Fault nor the Gerrish Mountain – Riversdale Fault ("b" and
"c" in Figure 6.2) are reflected in the presently available gravity or
magnetic data. This indicates that, if the Cobequid Fault and the
other faults ("b" and "c") to the south cut the shallow-dipping
geophysical boundary, no extensive vertical movement has taken place
on any one fault otherwise it would show up in the gravity and magnetic
fields. On the other hand, the net vertical motion on all the faults
might be significant. However, in the case of the Cobequid Fault, the
significant movement was probably strike-slip (Eisbacher, 1969) rather
than dip-slip.

The upper surface of the model in Figure 6.7 dips to the north
as well as the south. Since no large-scale faults are mapped along
the northern edge of the Cobequid Highlands, the model probably repre-
sents pre-Carboniferous basement dipping under the Carboniferous sedi-
mentary cover. The model indicates that the sedimentary column may be
nearly 10 km thick in the vicinity of the Cumberland Strait between
Nova Scotia and Prince Edward Island (see Figure 1.1 for location).
This is probably overestimated to some extent as only 7 km of Carboni-
ferous sedimentary rocks are reported in the Cumberland Basin lying
between the westernportion of the Cobequid Highlands and the Cumberland
Strait (Garland, 1953) and some 6 km are present beneath the eastern
part of Prince Edward Island (e.g. Goodacre and Nyland, 1966).

Nevertheless, the pre-Carboniferous basement to the north of the Cobequid Highlands is probably more deeply buried than the pre-Carboniferous basement lying to the north of the Orpheus gravity feature (Figures 6.3 and 4.5).

Although the gravity and magnetic highs over the Antigonish Highlands seem to be related to each other and are probably due to heavy, magnetic rocks, possibly the Cambro-Ordovician basic volcanics of the Brown's Mountain Group, the magnetic anomaly seems to be more widespread than the gravity anomaly and, on the southeast side of the Antigonish Highlands, the magnetic contours (Figure 6.4) exhibit a distinct northeast trend not apparent in the gravity field. These northeast trending magnetic contours may define a fault which is parallel to the Hollow Fault ("d") and the Brown's Mountain Fault ("e") on the opposite side of the Antigonish Highlands. No major fault is shown on the geological map on the southeast side of the Highlands but minor faults cutting Carboniferous rocks are mapped by Benson (1970) in the vicinity of the postulated fault.

6.5 THE ORPHEUS GRAVITY FEATURE

6.5.1 Introductory Remarks

The Orpheus gravity low was discovered in 1964 by members of the Bedford Institute of Oceanography who were operating a surface gravity meter while on the way from Halifax to make a ceremonial visit to Charlottetown, P.E.I. Several reconnaissance surface meter profiles were subsequently made and the resulting feature was modelled as a trough filled with sedimentary rock (Loncarevic and Ewing, 1967) in

accordance with results from shallow refraction seismic data (Ewing and

Hobson, 1966). The underwater work described here complements the

surface meter data and provides uniform regional coverage over the area.

In addition, a close spaced profile of underwater stations was made

along profile O-O' (see Figure 6.2 and map in pocket). Sheridan and

Drake (1968) subsequently reported a refraction seismic profile done

some eight years earlier by Lamont Geological Observatory (No. 138 in

Figure 6.2) which suggested that a rather thick sequence of sedimentary

rocks was present further to the west where the negative anomaly is less

intense. In recent years seismic work by the oil exploration industry

had added some detail to the seismic picture and the Orpheus feature

is now termed the Orpheus Graben and is known,through drilling, to

contain Jurassic and younger sedimentary rock (Jansa and Wade, 1975).

The graben is about 40 km wide and at least 150 km long.

6.5.2   Seismic Results

The original travel-time and distance values (Ewing and Hobson,

1966; Sheridan and Drake, 1968) were obtained and plotted in Figure 6.8.

There is no noticeable difference between the first-arrival travel-time

data from profile 29 and the data from profile 138 but, for a given

distance, the times from these two profiles which lie over the Orpheus

Low are significantly longer than those obtained from profile 30 which

lies to the north. Velocity-depth profiles obtained by non-linear

optimization indicate that the compressional wave velocity in the upper

2 to 3 km of the crust is about 1 km/sec less beneath the Orpheus low

than it is beneath the flanking gravity high to the north. It is not

Figure 6.8: Observed and calculated travel-times

for profiles 29,30 and 138 (Figure 6.2).

Inset shows velocity-depth profiles

obtained from the travel time data. First

arrivals are obtained only from those

portions of the curves above the dotted

lines. The velocity-depth values at the

bottom of each curve were obtained by the

original workers on the basis of second

arrivals.

ORPHEUS FEATURE
Travel-Time Data

Observed Values
● Profiles 29,138
○ Profile 30

Calculated Time-Distance Curve

Calculated Curve

Time sec

Distance km

Velocity km/sec.

Depth km

Profile 29, 138
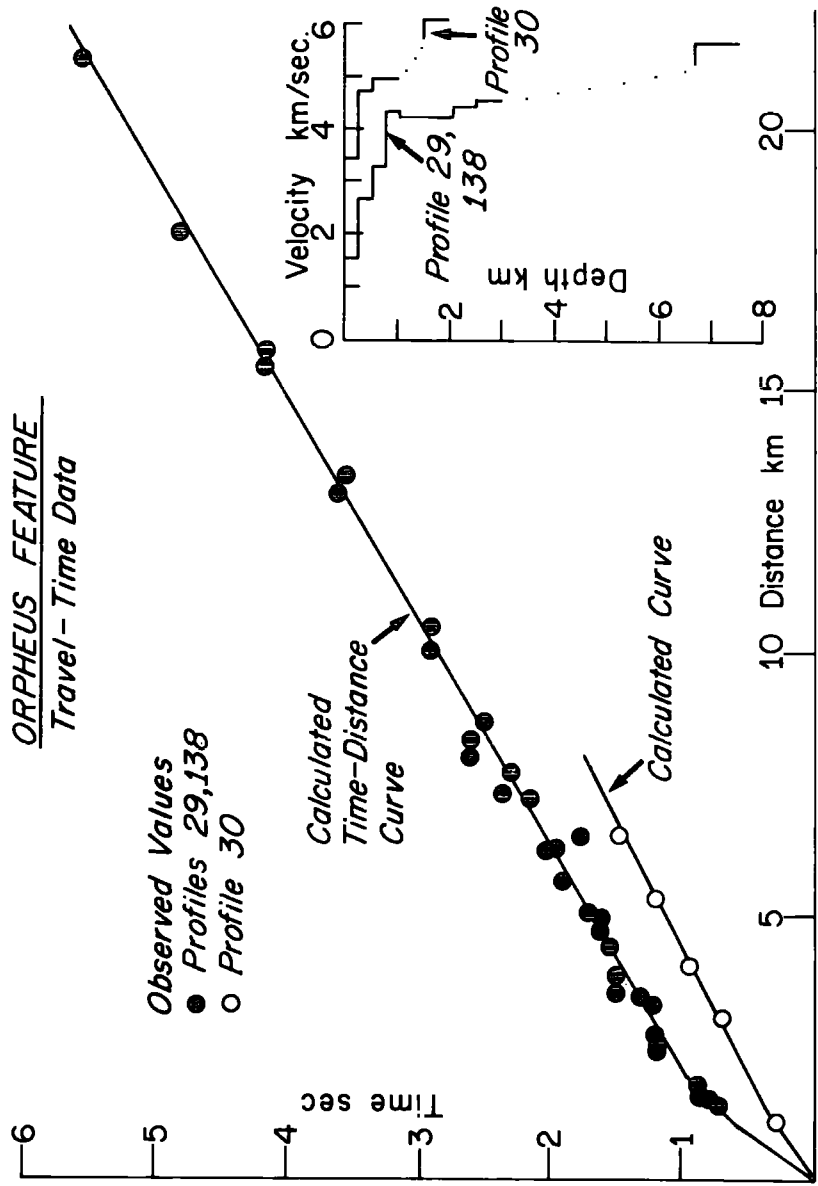
Profile 30

clear how far down this velocity difference extends however, because no first arrivals from basement, that is a refractor in which the velocity exceeds about 5.5 km/sec, were obtained on any of the profiles. Basement velocities and depths were obtained by the workers on the basis of second arrivals. In the case of profile 29 the second arrivals were observed only on the north leg where Ewing and Hobson (1966) pointed out a distinct offset in the first arrivals which might represent a fault. There is no evidence that decreased values of compressional wave velocity do not exist down to depths of the order of 5 km or so beneath the southern part of profile 29 and beneath profile 138. If they do, the mass deficiency expected from typical velocity-density relationships would be sufficient to account for the Orpheus gravity low.

6.5.3   Gravity and Magnetic Models

Figure 6.9 shows a basin-type model (indicated by tick marks) constructed using a density contrast of 0.4 gm/cm^3 which explains the gravity low. The density contrast is about the minimum value which will allow a homogeneous model to reproduce the observed segments of sharp curvature in the gravity anomaly. The density contrast is consistent with a velocity contrast of about 1 km/sec. The density contrast is large partly because some of the sedimentary rocks may have a low density (for example, Jansa and Wade (1975) mention that about 1 km of salt was penetrated by the drill hole on profile 0-0' (Figure 6.2)), and partly because the adjacent basement rocks may have a high density as suggested by the positive flanking gravity anomalies. It is gratifying to find that the gravity model is consistent with the

Figure 6.9:   Observed and calculated gravity and

magnetic anomalies and interpretative

models along profile 0-0'. The dashed

line shows an alternative model for

a different inclination of magnetization

as explained in the text.

ORPHEUS ANOMALY (O-O¹)
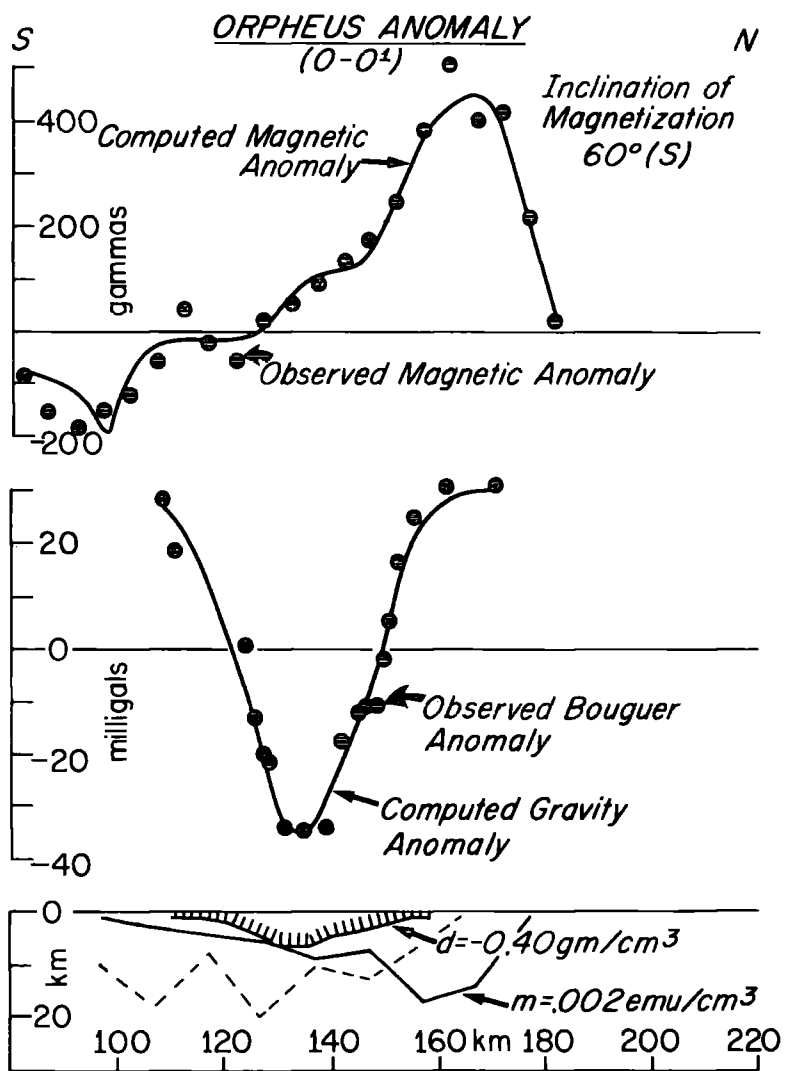
seismic and drill hole results since the gravity model was constructed

independently of these other data.

The sides of the model dip inwards at a shallow angle of about

15°. If each side were due to only a single fault, a compressional

source would be indicated but it seems more likely, judging from cross-

sections given by Jansa and Wade (1975), that the basement trough is

bounded on either side by a series of step-faults such as are often

associated with grabens.

There seems to be no simple relationship between the gravity

and magnetic data over the Orpheus feature. Whereas the Bouguer anom-

aly pattern is more or less symmetrical and the contours trend east-

west, the total field magnetic anomaly pattern tends to be asymmetrical

and, where the pattern is not too irregular, the contours exhibit a

northeast-southwest trend. Profile O-O' is not particularly suitable

for studying the magnetic anomaly because it cuts across the magnetic

trends at an angle of about 45° and there is some evidence of a compact,

very intense magnetic high and associated low just to the east of

profile O-O' and this may interfere with the magnetic anomaly profile.

It is clear from Figure 6.9 and the gravity and magnetic anomalies map

in Figures 6.3 and 6.4, respectively, that the source of the gravity

high on the south flank is only weakly, if at all, magnetic whereas

the rocks producing the northern flanking high are generally strongly

magnetic. An important exception, to be discussed later is the area

between 58.0°W and 59.5°W where the magnetic anomaly intensity is

diminished. This area coincides approximately with the peak values of

the gravity high on the north flank of the Orpheus Low.

In order to determine the nature of the discontinuity between the magnetic and non-magnetic rock, the magnetic anomaly along profile 0-0' was modelled using simple step models with sloping faces but none of these gave particularly good fits so more complicated models were constructed using computer programs developed by Laving (1971). The model outlined by the solid line in the bottom portion of Figure 6.9 produces a good fit to the observed magnetic anomaly for an angle of magnetization of $60^{\circ}(S)$. This angle was determined by trial and error to obtain the fit and is broadly consistent with an angle of $75^{\circ}(S)$ obtained by a combined analysis of the gravity and magnetic anomalies over the north side of the Orpheus feature (Figure 6.10). The magnetization contrast of 0.002 emu/cm^3 is consistent with the minimum density contrast value of about 0.4 gm/cm^3 coupled with the value of 0.0044 emu/gm obtained from the combined analysis for the ratio of magnetization contrast to density contrast. In spite of the good fit, the model seems unrealistic because it overlaps the gravity model and it is unlikely that sedimentary rocks would offer a magnetization contrast of the order of 0.002 emu/gm. The dashed line outlines the upper surface of another model which has an inclination of magnetization of 30° (N); this gives a poorer fit but does not overlap the proposed sedimentary sequence. Noting that the surface magnetometer profiles used to construct the map in Figure 6.4 are scattered and uncorrected for diurnal variation and magnetic storms it may be that improved magnetic data can be reconciled with the gravity data but, for the time being, the two sets of data do not appear to give compatible results along profile 0-0'.

Figure 6.10:   Magnetic,gravity and pseudo-gravity
                anomaly over the north half of the
                Orpheus feature on profile O-O'.

ORPHEUS FEATURE (NORTHSIDE)
(O-O¹)

m/d = .0044 emu/gm
Inc = 75 (S)
r = .97
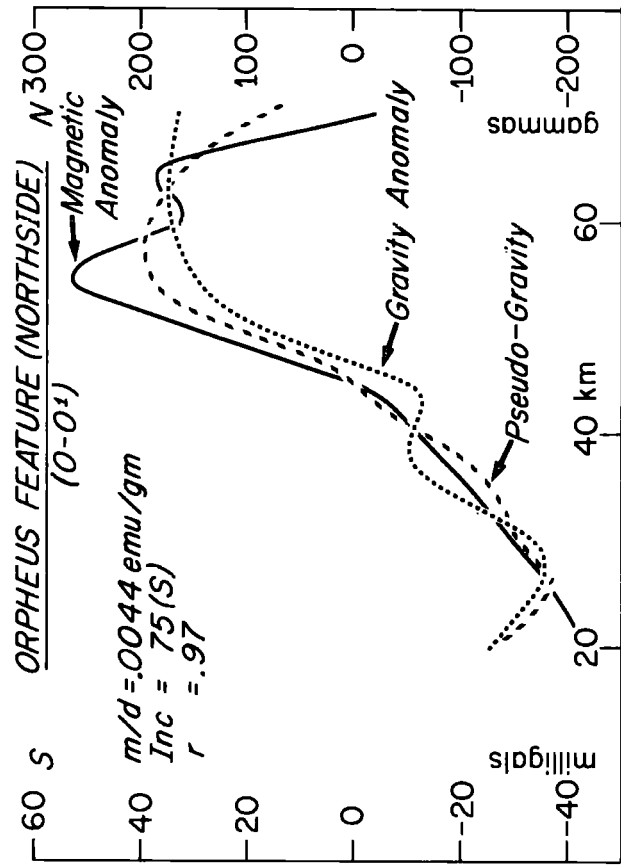
6.5.4   Possible Deep-Seated Source of the Gravity Highs

An important point to note is that, except for the typical
rise of the Bouguer anomaly field as the continental margin is
approached, all of the gravity anomaly variations thus far encountered
can be explained in terms of density variations in approximately the
upper 10 km of the crust.   However, the Orpheus gravity feature might
represent an example of a near-surface mass deficiency (low-density
sedimentary rocks) compensated isostatically at depth by a mass excess.
The concept of an isostatically compensated geological feature has
often been advanced (e.g. Weber and Goodacre, 1966; Bott and Smithson,
1967; Tanner, 1969) so profile P-P' was selected, in conjunction with
I-I' (Chapter 4) to study this idea.   The profile was chosen to empha-
size the more or less symmetrical, "dipolar" nature of the gravity
anomaly (Figure 6.11).   The magnetic anomaly along profile P-P' will
not be discussed except to point out that, unlike profile O-O', there
is no obvious magnetic high associated with the positive gravity peak
on the north side of the Orpheus low.   The four drill holes along the
south flank of the Orpheus feature suggest that there is a basement
uplift which correlates with and might partly explain the high that is
crossed by profile P-P'.   But three reasons for suspecting that the
sources of the two gravity highs on the south side may be deep-seated
are (1) no typically dense gabbros, amphibolites, etc. were found in
either of the two drill-holes which penetrated basement over the
gravity high,   (2) the basement velocity of 5.5 km/sec observed on
profile 27 is typical of an acidic rather than a basic rock and (3)
the source appears to possess little or no magnetization and therefore

Figure 6.11:   Observed Bouguer anomaly and calculated

gravity anomalies for models a and c.

The anomaly due to model b is omitted for

clarity.

ORPHEUS FEATURE
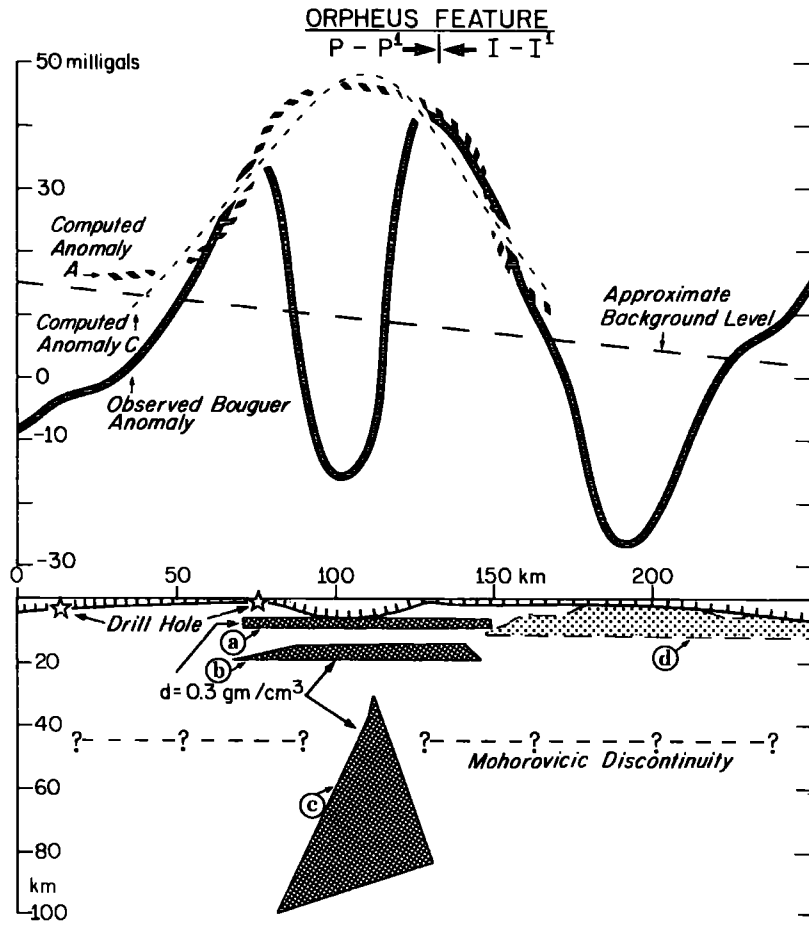
might be buried below the Curie point isotherm. In a similar manner, a deep-seated, dense, non-magnetic source might be contributing to the elongate positive peak on the north side.

Figure 6.11 shows three different models (a, b, and c) which produce anomalies which are approximately the same as the observed anomaly might be if it were corrected for the mass deficiency of the sedimentary basin. In other words, if we could replace the low-density sedimentary rocks by basement rocks which have a normal (or slightly greater than normal) density, we would be left with a single positive anomaly rising above the background level. The background, or regional, level was obtained by assuming that the shelf topography is an isostatic equilibrium as discussed in Chapter 5. The gravity lows (relative to the adopted background level) on either side are thought to be due primarily to low-density granites plus the overlying late-Palaeozoic and younger sedimentary rocks and it is assumed that these lows could be removed by an appropriate correction for the mass deficiency of the source rocks. Model(d), representing a low-density granite, is taken from Figure 4.19 and the configuration of the basement surface is shown schematically by the tick-marked line. Model (d) was calculated using a background level of about 40 mgal because it was interpreted in the context of being a low-density granite intruded into high-density basement rocks. As such, the model is not consistent with the lower regional level adopted here but it serves to show the general extent of the interpreted granite.

The best fit to the overall gravity high is given by model (a) which represents a slab of material about 3 km thick that has its

upper surface buried at a depth of about 7 km. Models (b) and (c) give

significantly poorer fits and do not reproduce the observed horizontal

gradients very well at approximately the 75 and 125 km points on the

profile. The anomaly from (b) is omitted for clarity. As mentioned

previously, models (a) and (b) are calculated assuming the background

level shown in figure 6.13. Model (c) was calculated assuming a

regional level of about -30 mgal. There is no real justification for

assuming such a low value but it was done to see whether the overall

rise of the gravity field from the minimum values over the Middle Bank

and Glace Bay Lows to maximum values over the highs flanking the

Orpheus Low could be caused by an upwarp in the Mohorovicic Discontin-

uity or by some other source in the lower crust and/or upper mantle

rather than by near-surface geological features. For example, it might

reasonably be expected that any deep-seated basaltic magma in the axial

zone of a rift-type structure would solidify in the eclogite facies and

offer a positive density contrast with respect to the surrounding lower

crustal and/or upper mantle rocks (e.g. Goodacre, 1972). Model (c) may

seem artificial but a simple four-sided form was used to overcome in-

stabilities encountered in trying to model the overall positive anomaly

by undulations in the Mohorovicic Discontinuity. The model could be

considered as representing both an upwarp in the Mohorovicic Discon-

tinuity and heavier than normal rocks in the upper mantle, but in view

of the arbitrary choice of -30 mgal for the regional level and the

generally shallow gradients produced by such a deep-seated feature it

seems most likely that the sources of the Orpheus gravity low and the

flanking highs all lie within the upper part of the crust. This

conclusion is consistent with the results of a downward continuation of the gravity field along profile 0-0' which indicated a maximum source depth of about 8 km. However, it should be pointed out that even though the sources of the gravity anomalies are probably not deep-seated, the Orpheus feature may still be an example of an iso-statically compensated geological feature but the compensating mass probably lies in the upper part of the crust and not at, or below, the crust-mantle boundary.

It was noted before that the magnetic anomaly field is gener-ally positive to the north of the Orpheus Low but its intensity is diminished where the flanking positive gravity anomaly attains its highest values. It seems, therefore, that the rocks producing the gravity anomly on the north side may be less magnetic than the adja-cent basement rocks. The rocks producing the southern flanking gravity high are essentially non-magnetic. It is not clear what the signifi-cance of these heavy, essentially non-magnetic rocks might be but it is interesting to point out a similar situation in the Gulf of St. Lawrence east of the Gaspé Peninsula (see Figure 1.1) where the arcuate belt of heavy rocks producing the Gaspé High (see Figure 7.1) is not accompanied, at least where magnetic data are available, by a corres-ponding magnetic high. Goodacre and Nyland (1966) suggest that the gravity high is due to ultrabasic rocks emplaced in the upper part of the crust as a result of thrusting during the Taconic (Ordovician) Orogeny. It is not intended, however, to draw any close parallel between the inferred geological structure east of the Gaspé Peninsula and the Orpheus feature but only to point out the possibility, in this

latter area, of near-surface basic to ultra-basic rocks brought into
position by tectonic activity.

6.5.5 Comparison of the Orpheus feature with some other continental
       grabens.

Two continental grabens which have dimensions similar to the
Jurassic (or older) Orpheus Graben (which is about 40 km wide and at
least 150 km long) are the Permian Oslo Graben in southern Norway and
the Eocene Rhine Graben which cuts through Germany and France. The
Oslo Graben is about 40 km wide and some 200 km long and characterized
by generally positive gravity and magnetic anomalies (see Figure 6.12
taken from Ramberg (1972)). The Rhine Graben is also about 40 km
wide but somewhat longer, about 300 km, and characterized by generally
negative gravity anomalies (Lecolazet, 1970) and an irregular, but
often negative, magnetic anomaly pattern (Bosum and Hahn, 1970).
Gravity and magnetic profiles discussed by Mueller (1970) are shown
in Figure 6.13. Noting that the Orpheus Graben is characterized by a
central negative gravity anomaly and flanking positives and by an
asymmetrical magnetic anomaly pattern which is generally more positive
to the north than to the south, it can be seen that, although the
physical dimensions, particularly the widths, of the Oslo, Rhine and
Orpheus Grabens are similar, their gravity and magnetic characteris-
tics are different. Nevertheless, some parallels can be drawn between
the Orpheus Graben and the other two features. Firstly, the magnetic
anomalies on either side of the Rhine Graben, and some anomalies within,
seem to outline pre-existing Hercynian basement features (Bosum and
Hahn, 1970) in much the same way that the northeast or northwest

Figure 6.12: Observed magnetic and gravity anomalies,

calculated gravity anomaly and structural

models of the Oslo Graben (Ramberg, 1972).
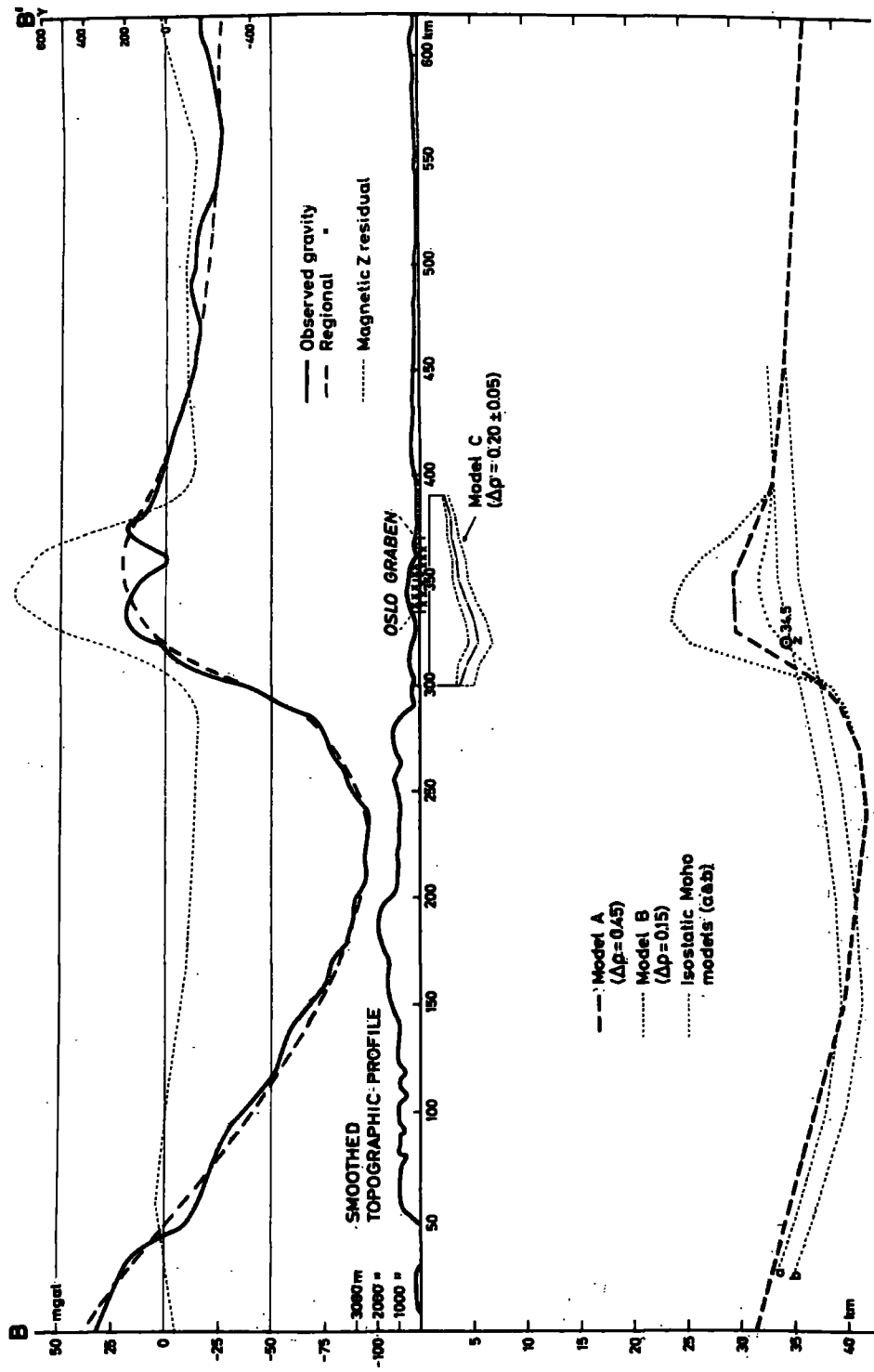
Figure 6.13:   Temperature, Bouguer anomaly and total
                field magnetic anomaly profiles and
                geological section of the Rhine Graben
                (Meuller, 1970).

(a) 100°C-Geoisotherme nach ILLES, [1965]

(b) Bouguer – Schwere nach MUELLER et al. [1967]

(c) Magnetisches Profil in ΔT nach ROCHE und WOHLENBERG [1969]

Geographische Lage der Messpunkte, B4=Bezugspunkt

(d) Geologischer Grabenschnitt nach BOIGK und SCHÖNEICH [1968]
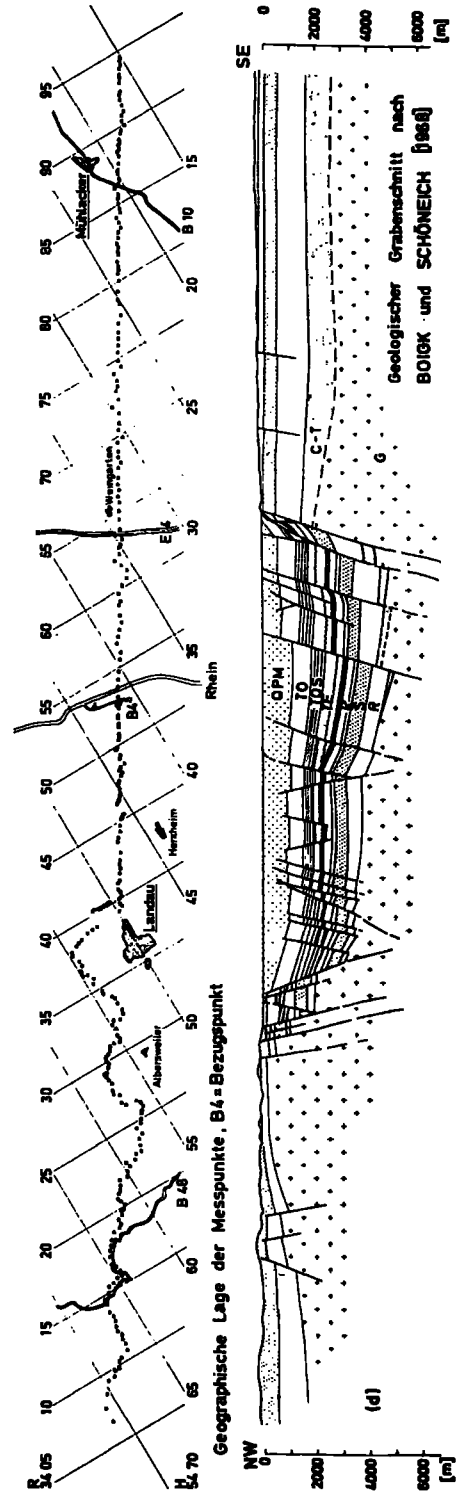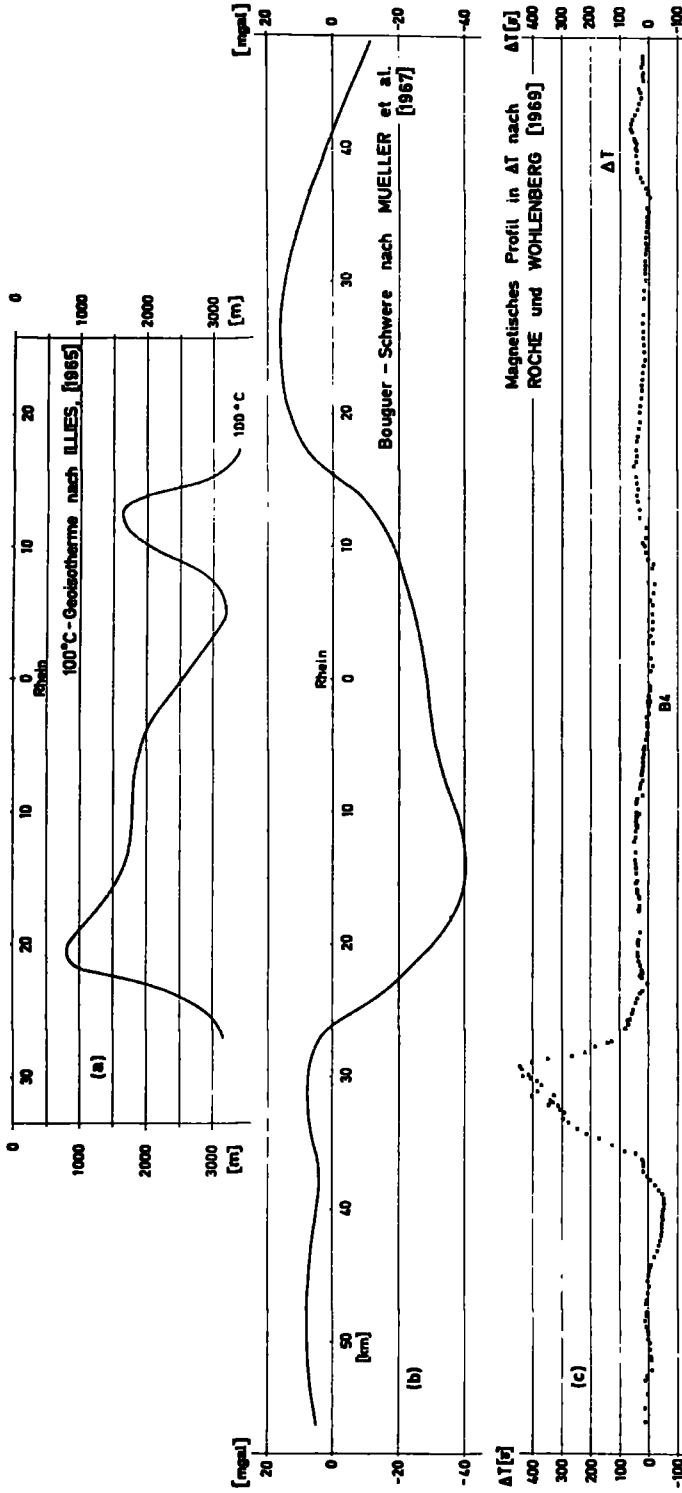
trending magnetic anomalies to the north of the Orpheus Graben (Figure 6.4) seem to reflect structure in the late-Proterozoic(?) basement and secondly, the negative gravity anomalies over both the Orpheus and Rhine Grabens are clearly due to the infill of low-density sedimentary rocks. On the other hand, the source of the flanking positive gravity anomalies over the Orpheus Graben and the source of the broad positive over the Oslo Graben is not clear in either case.

According to Ramberg (1972), the igneous rocks collected from within the Oslo Graben have a mean density of 2.66 gm/cm^3 which is less than the mean density of 2.74 gm/cm^3 of the rocks from the surrounding Precambrian shield so the positive anomaly source must be deep-seated. Ramberg (1972) suggests that the anomaly may be due to an upwarp in the Mohorovicic Discontinuity beneath the graben but points out that the seismically determined depths (about 35 km) of this discontinuity are about the same beneath the graben as they are elsewhere and that, consequently, at least part of the anomaly source must lie within the lower crust. Certainly, if the positive magnetic anomaly is produced by the same source which causes the gravity high, the source rocks must lie above the Curie Point isotherm. Intermediate seismic velocities of 7.2 to 7.3 km/sec have been detected further to the south in the Skagerrak (e.g. Ramberg and Smithson, 1975) at depths of about 20 km and these imply the presence of amphibolites, mafic granulites, or other heavy, possibly magnetic, rocks which, as Ramberg and Smithson (1975) point out, could produce the observed anomalies over the Oslo Graben if they were restricted to the axis of the graben. Seismic velocities of the order of 7.6 to 7.7 km/sec are also found

near the base of the crust in the vicinity of the Rhine Graben but,
since they are found up to 100 km on either side (Ansorge et al., 1970),
they can't be considered as being peculiar to the Rhine Graben itself.
Unfortunately, no deep seismic data are available over the Orpheus
Graben but, as mentioned in the previous subsection, it seems unlikely
that the positive gravity anomaly sources are situated at the base of
the crust.

6.6 THE MOUTH OF THE LAURENTIAN CHANNEL

As mentioned earlier, the mouth of the Laurentian Channel (see
Figure 1.1) is characterized by two oval gravity lows and an ill-
defined high. At first glance these gravity lows seem to be related to
the Orpheus Low and reflect an eastward continuation of the low density
sedimentary rocks filling the Orpheus Graben. However, the oval gravity
lows, labelled B and C in Figure 6.2 and the small low some 50 km to
the west, labelled A, all correlate spatially with magnetic highs as
can be seen from the magnetic map (Figure 6.4) and on profiles Q-Q'
and R-R' (Figure 6.14). This strongly suggests that the gravity lows
reflect intrusions of magnetic granite and the magnetic highs repre-
sent magnetic minerals formed at their margins during their emplace-
ment or produced within the granites by subsequent metamorphism. The
strong magnetic high on the south side of the gravity low in profile
Q-Q' may represent enhanced magnetization at the margin of a granitic
intrusion as does the partial magnetic halo around the anomaly marked
(A) in Figures 6.2 and 6.4. The magnetization in the source producing
the anomaly along profile R-R' may be more uniformly distributed since

Figure 6.14:   Observed gravity and magnetic anomaly

along profile Q-Q'.   Observed magnetic and

gravity anomaly and calculated pseudo-

gravity anomaly and seismic structures

along profile R-R'.

LAURENTIAN CHANNEL
(Q - Q¹)
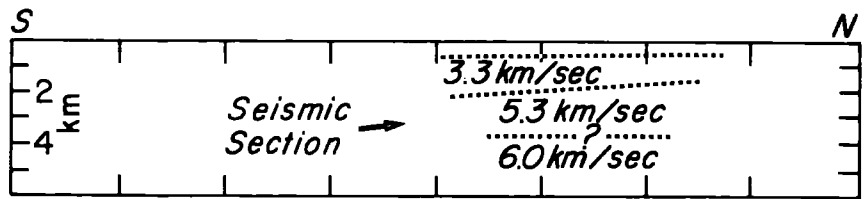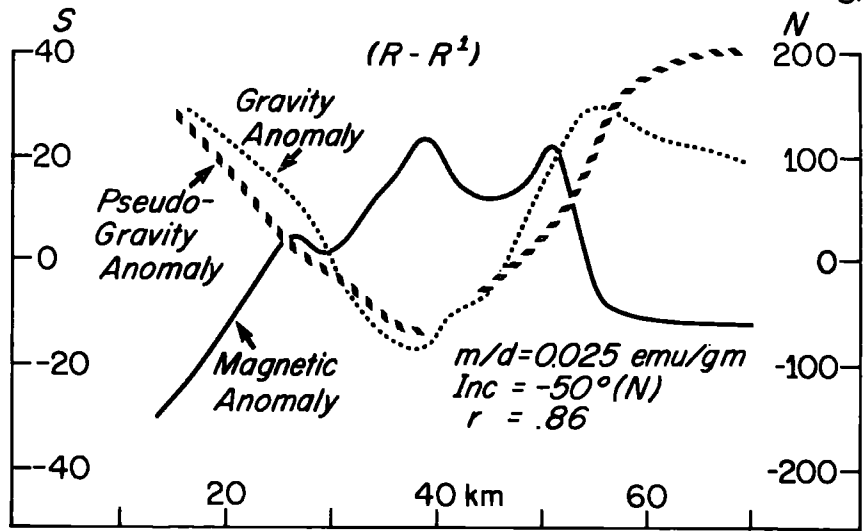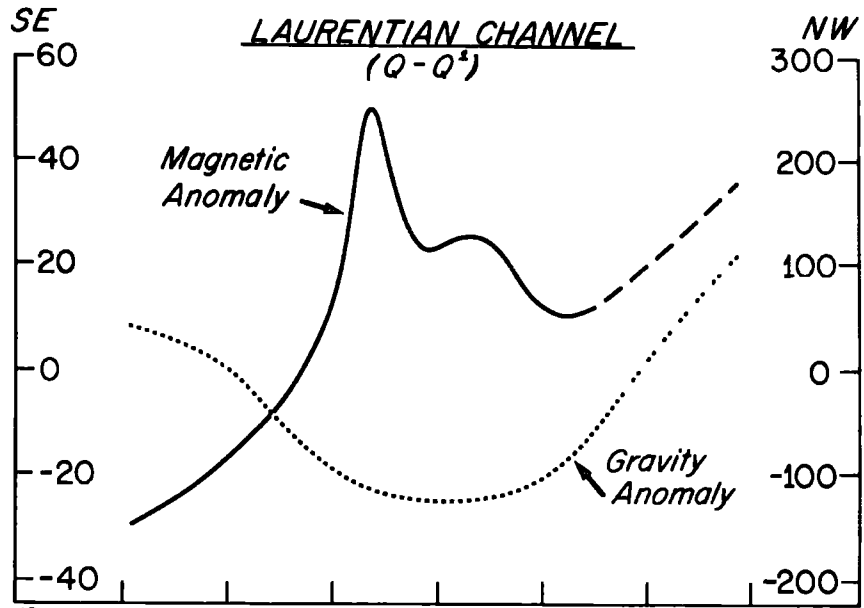
there is a fairly good correlation between the observed gravity anomaly

and the calculated pseudo-gravity anomaly derived from the magnetic

anomaly. It is interesting to note that the inclination of the total

magnetization vector, which is about 50^{O}(S) if we assume the source is

normally magnetized, is significantly different from that of the earth's

field (74^{O}(N)) and suggests the possibility of a southerly directed

component of remanent magnetization.

The seismic refraction data near profile R-R' (Figure 6.12)

indicate that the postulated magnetic granite is buried under about 4

km of sedimentary rocks. Further to the east, the basement is buried

even more deeply in accordance with the general seaward plunge of the

basement rock beneath the sedimentary cover. In this area there may

be faults associated with those bounding the Orpheus Graben but there

seems to be no strong graben-type structure. The seismic velocities

in the basement rocks beneath profiles 17, 18 and 102 are 6.0 km/sec

or greater and suggest that the rocks in this area are more closely

related to the basement rocks on the north side of the Orpheus low

than to those on the south side where velocities of only 5.5 km/sec

are measured. This suggestion is supported by the magnetic anomaly

map (Figure 6.4) which, as mentioned earlier, indicates generally

magnetic basement rocks to the north of the crustal discontinuity and

non-magnetic rocks to the south. In fact, the magnetic anomalies

clearly indicate a northwest-southeast trending basement discontinuity

in the vicinity of the mouth of the Laurentian Channel. A composite

magnetic profile (Figure 6.15) of five, approximately north-south,

profiles in this area (see Figure 4.3 for their location) shows a rise

in the magnetic anomaly field from -200 γ to 100 γ as one goes from

Figure 6.15:   Observed total field magnetic anomaly

averaged from five profiles near the

mouth of the Laurentian Channel, calculated

magnetic anomaly and interpretative model.

LAURENTIAN CHANNEL (COMPOSITE)

Calculated Anomaly

Observed Total Magnetic Field Anomaly

m=.0008emu/cm³
Inc=84°(S)
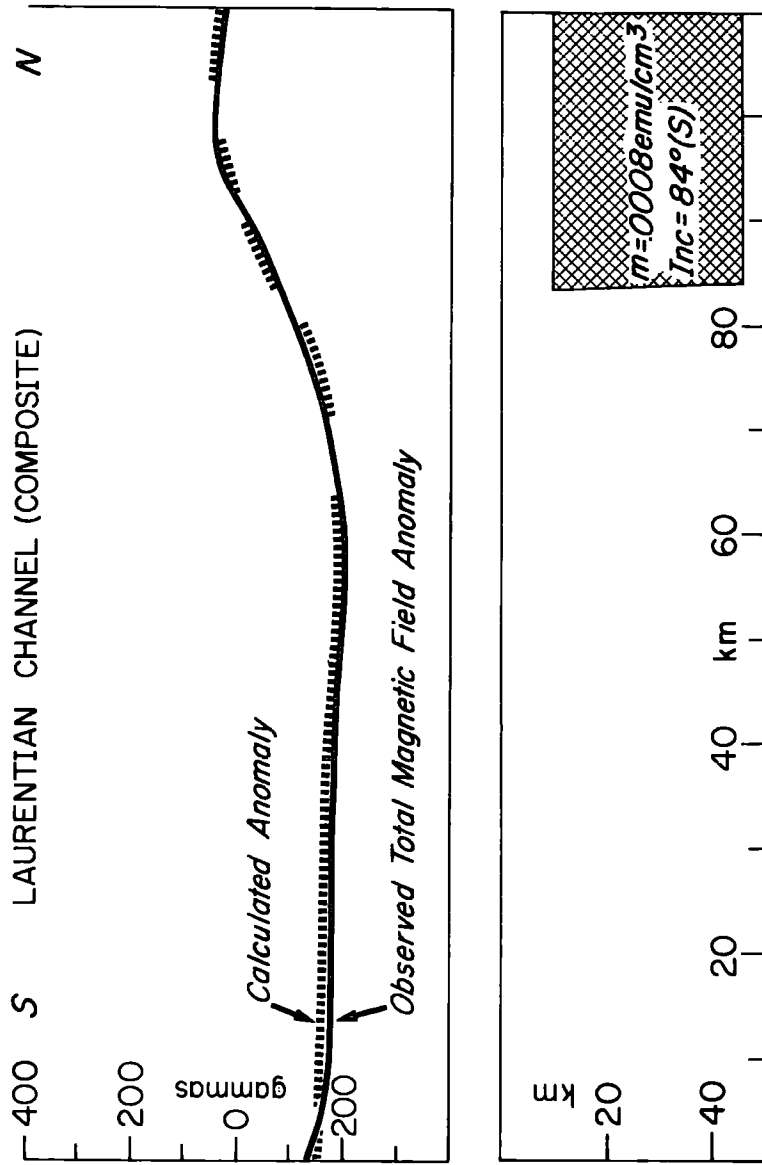
south to north across the 45°N parallel. Except at the extreme northern ends of the five profiles, the composite profile accurately reflects the variation of the magnetic field and this seems to be one of the few locations where the long-wavelength portion of a major magnetic anomaly is not obscured by other anomalies.

The significant aspect of the magnetic model in Figure 6.15 and several others which were made are (1) the nearly vertical discontinuity (2) the large thickness and great depth of burial of the magnetic body and (3) the steeply dipping, southward-directed magnetization of 84°(S). The model rules out a shallow thrust fault as the source of the discontinuity in this region. The large depth of the upper surface of the model is consistent with a thick wedge of overlying sedimentary rocks at the continental margin and the great thickness of the model indicates that Curie Point isotherm may be quite deep if the magnetization of the rocks is as low as the modelling procedure suggests. It would be interesting to know whether the base of the model coincides with the Mohorovicic Discontinuity because in area where temperatures are sufficiently low, the Mohorovicic Discontinuity could mark a dividing line between magnetic gabbroic and amphibolitic rocks of the lower crust and relatively non-magnetic (unserpentized) peridotites of the upper mantle. The Mohorovicic Discontinuity under the southern Scotian Shelf may be as deep as 45 km but it is unwise to extrapolate these seismic results northwards across the major crustal discontinuity which transects the Scotian Shelf.

6.7   SUMMARY AND DISCUSSION OF THE STRUCTURE OF THE CENTRAL SCOTIAN
       SHELF

It is clear from the geological and geophysical evidence that

there is a major crustal discontinuity which transects central Nova

Scotia and the central Scotian Shelf. The geological evidence lies

in the presence of several east-west trending faults in the region

between the Minas Basin and Chedabucto Bay and in the absence of Pre-

cambrian rocks to the south of the fault zone. The geophysical evidence

lies in the presence of mainly magnetic, medium-velocity basement

rocks to the north of the fault zone and generally non-magnetic, low-

velocity basement rocks to the south. The asymmetrical aspect of

these geophysical data is contrasted with the presence over the

western part of the central Scotian Shelf of a pronounced, symmetrical

east-west trending gravity feature consisting of the Orpheus Gravity

low and its flanking gravity highs. The structure reflected by this

major gravity features dies away to the west near Chedabucto Bay and

to the east near the western margin of the Laurentian Channel.

Gravity and magnetic models of Cobequid complex indicate that

crustal discontinuity dips south at a shallow angle, suggesting its

formation by thrusting or strike-slip motion. There is some diffi-

culty in reconciling gravity and magnetic models over the Orpheus

feature but these models, in conjunction with seismic and drill-hole

data, show that the Orpheus Low outlines a graben structure filled

with lower Jurassic and younger sedimentary rocks. In this area the

discontinuity between magnetic and non-magnetic rocks either dips

south at a shallow angle or more probably occurs as a series of step-

faults such as are often observed at the boundaries of continental

grabens. The origin of the more or less non-magnetic rocks producing the flanking gravity highs is not clear but they were probably emplaced during the formation of the graben in such a manner as to approximately maintain isostatic equilibrium. The graben is clearly a pre-Jurassic feature but just how early it was formed is uncertain. This will be discussed more fully in the next chapter where the Scotian Shelf is discussed in terms of paleomagnetic results and plate tectonics.

There is no particular reason why the east-west discontinuity was formed everywhere at the same time, but, if it were, it could have been formed by a scissors movement with an opening under tension of the Orpheus graben, strike-slip motion along the discontinuity at the mouth of the Laurentian Channel and a closing, with compressive forces operative, along the south side of the Cobequid Highlands. If this were the case, and if southern Nova Scotia and the southern Scotian Shelf acted as a competent block, thrusting would be expected in the Bay of Fundy region and strike-slip motion somewhere to the southeast of Nova Scotia, possibly in the vicinity of Yarmouth, N.S. or further out in the Gulf of Maine. Unfortunately, these areas are covered by water and geological evidence to refute or confirm this idea is currently lacking but it should be pointed out that, topographically, the Bay of Fundy, which is about some 60 km wide and bifurcates into the Minas Basin to the east and Chignecto Bay to the northeast, has the appearance of a typical graben and therefore was probably formed under tension rather than compression. It seems more likely that faults were initiated in different areas at different

times and were probably reactivated intermittently at different times, particularly as both right and left-handed movements are mapped along faults within the Minas Basin-Chedabucto Bay fault zone. In general, the right-handed movements probably result from continental collision during the early Palaeozoic Era and the left-handed movements from continental separation in the late Palaeozoic and Mesozoic Eras. The possibility that the Orpheus Graben was formed along an older zone of weakness has an interesting parallel in the area between the Orkney and Shetland Islands where a postulated basin of Mesozoic sedimentary rocks (Bott and Browitt, 1975) has formed along one side of the pre-existing Great Glen Fault.

One of the most interesting aspects of the Orpheus graben structure is that it appears to be confined to the western part of the central Scotian Shelf and does not extend eastward with any great degree of intensity across the Laurentian Channel. In this latter area the local oval gravity lows appear to outline acidic phases within the crystalline basement rocks rather than show accumulations of low-density sedimentary rocks. Although not conclusive, this interpretation is strongly indicated by the association of magnetic highs over or at the margins of the oval gravity lows. In this respect, the combination of gravity and magnetic data has been most helpful in trying to distinguish between magnetic granite and low-density sedimentary rocks.

CHAPTER 7

GENERALIZED STRUCTURE AND HISTORY OF THE NOVA SCOTIAN
CONTINENTAL SHELF

7.1   INTRODUCTORY REMARKS

In the preceding three chapters, the main emphasis has been on

structural interpretations of the major geophysical anomalies occurring

on the Scotian Shelf. In each chapter the interpretations were local

in nature inasmuch as they were made in the context of the nearby land

geology. In this final chapter the main points of the interpretations

are reviewed and brought together in the context of possible litho-

spheric plate motions during the Palaeozoic and early Mesozoic Eras.

In preview, the gravity and magnetic anomalies commonly seem

to reflect structures in the pre-Carboniferous basement rocks and many

of these structures on the Scotian Shelf are probably products of

continental convergence and collision. In trying to unravel the pre-

Mesozoic history of the Scotian Shelf the main difficulty is to achieve

a reasonable timing of the proposed events and to explain such problems

as how southern Nova Scotia relates to the remainder of the Canadian

Maritime Appalachians and why there is seemingly little evidence of the

Hercynian Orogeny in Nova Scotia and Newfoundland.

7.2   REVIEW OF MAJOR GEOPHYSICAL ANOMALIES AND THEIR INTERPRETATION

7.2.1   Bouguer gravity anomalies

Working from southwest to northeast on the Scotian Shelf, the

major gravity anomalies are: The Middle Bank Low, the Orpheus Low and

its flanking highs, the Glace Bay Low and the St. Pierre High (Figure

Figure 7.1:   Simplified Bouguer anomaly map of the Canadian

Maritime Appalachians. Compiled from Weaver (1967)

and Stephens and Cooper (1973).

7.1). Other important anomalies, not named in Figure 7.1, are the

Emerald High (Figure 5.3) lying to the southwest of Middle Bank Low,

the local gravity lows (A,B,C in Figure 6.2) to the east of the Orpheus

Low and the linear gravity low lying on the western flank of the St.

Pierre High (Figure 4.7). This latter gravity low separates the St.

Pierre High from the southwesterly trending extension of the Cross

Pond High. An interesting aspect of the compilation in Figure 7.1 is

the general east-west trend of the gravity anomalies over the Scotian

Shelf and the adjacent land areas of southern and central Nova Scotia.

This east-west trend is in contrast to the northeasterly Appalachian

trend of gravity anomalies in Newfoundland and southern New Brunswick.

On land, the gravity anomalies generally reflect structures in pre-

Carboniferous basement rocks with gravity lows, such as the New Ross

Low and the Granite Lake Low, overlying Devonian and older(?) granite

and gravity highs, such as the Cobequid High and the Kingston High,

outlining uplifted pre-Carboniferous basement complexes. Some nega-

tive anomalies, such as the small negative to the northwest of the

Cobequid High, the negative on the northwest flank of the Cross Pond

High (Figure 7.1) and, of course, the Orpheus Low, reflect the presence

of thick sequences of Carboniferous and possibly younger sedimentary

rocks but, in general, geologically and seismically determined sedi-

mentary basins (Howie and Cumming, 1963; Hobson and Overton, 1973) do

not show up particularly well in the gravity field. The reason for

this lack of correlation is not clear but may be due in part because

the sedimentary basins are more or less isostatically compensated and

because any pre-Carboniferous sedimentary rocks which are present over

offer little or no density contrast to the crystalline basement rocks.

7.2.2   Total field magnetic anomalies

Total field magnetic anomalies are displayed in Figure 7.2.
In this diagram red indicates a magnetic low; blue a high so the
colour scheme is opposite to that in Figure 7.1. Working southwest
to northeast, some interesting points to note are: (1) the lack of
any magnetic anomaly associated with the granite outlined by the New
Ross Low (Figure 7.1) but a large magnetic anomaly associated with the
Pokiok granite about 50 km west-northwest of Saint John, N.B. (Figures
7.2 and 5.4), (2) the curvature of the magnetic anomalies which outline
the folded Cambro-Ordovician Meguma rocks. The Meguma rocks appear to
have been folded, or re-folded, about a vertical axis situated some-
where near the outer edge of the Scotian Shelf, (3) the contrast
between magnetic basement to the north of the Minas Basin-Chedabucto
Bay-Orpheus fault zone and relatively non-magnetic basement to the
south. On the Scotian Shelf, the general asymmetry of the magnetic
field provides one of the strongest pieces of geophysical evidence of
a major crustal discontinuity, (4) the general continuity of magnetic
trends between eastern Cape Breton Island and southeastern Newfound-
land, (5) the association of a depressed magnetic field with the
mainly sedimentary rocks of tectono-stratigraphic Zone F of Newfound-
land and a somewhat "granular" positive field with the mainly volcanic
rocks of Zone E.

Although exceptions can be found, magnetic lows within the
Appalachian geological province generally seem to outline areas of
predominantly sedimentary rocks whereas magnetic highs generally occur

Figure 7.2:   Simplified total field magnetic anomaly map of the

               Canadian Maritime Appalachians. Photographed from

               the Magnetic Anomaly Map of Canada (Geological

               Survey of Canada, 1970). Data over the northern

               Scotian Shelf added from Haworth et al. (1972).

               Colour scheme - blue - greater than 200 gamma,

               red - less than -400 gamma, intermediate contour

               interval is 200 gamma.

metamorphic and volcanic terrain. The magnetic anomalies, by them-selves, are not diagnostic of granitic intrusions as the granites range from being completely non-magnetic to highly magnetic. It is for this reason that negative gravity anomalies are particularly helpful in outlining magnetic, granitic intrusions which might otherwise be mistaken for intermediate to basic igneous or metamorphic rocks. On the other hand, it is difficult to know, a priori, whether a negative gravity anomaly outlines a granitic body or a basin filled with low-density sedimentary rocks. If a magnetic high coincides with a gravity low, a granitic source is probably indicated.

Although local correlations can often be found between magnetic and gravity anomalies sometimes there is little or no correlation. For example, there is poor correlation on the Avalon Peninsula between the gravity and magnetic data and generally no clear-cut relation between the geophysical and geological data. On a broader scale, the gravity and magnetic fields tend to show different features because the regional Bouguer anomaly tends to reflect variations in topographic elevation whereas the magnetic field does not. A good example of this is on the Scotian Shelf where the increase in Bouguer anomaly as the continental margin is approached is not reflected in the magnetic field.

7.2.3   Interpretative basement geological map

Figure 7.3 shows the major basement features on the Scotian Shelf as deduced from gravity, magnetic and seismic data. Only selected geological features are shown on land. The basement features

Figure 7.3:   Interpretative basement geological map of Nova

                  Scotian continental Shelf.   Only selected features

                  shown on land.   The term basement covers a broad

                  range of pre-Carboniferous, crystalline rocks.   The

                  letters A to I refer to the tectonostratigraphic zones

                  of Williams et al. (1972) and are explained in the

                  caption of Figure 1.2.   The Hermitage Flexure

((Williams et al., 1970) is outlined by the sinuous

                  trace of zone G and Hermitage Bay is identified in

                  Figure 4.1.

INTERPRETATIVE BASEMENT GEOLOGICAL MAP OF THE NOVA SCOTIAN CONTINENTAL SHELF

BASEMENT COMPLEX

VOLCANIC ROCKS

HEAVY, GENERALLY MAGNETIC ROCK

HEAVY, IRON OR WEAKLY MAGNETIC, ROCK

GRANITE OR GRANITIC GNEISS

FAULTS

GEOLOGICALLY DEFINED
INTERPRETED
NORMAL

TECTONIC ZONE BOUNDARY

Gulf of
St. Lawrence

Approximate limit of
the MEGUMA GROUP

200 Meters

Sable Is

Dike

200 km

48°N

44°N

56°W

60°W

64°W

N.B.

P.E.I.

N.S.

NFLD.
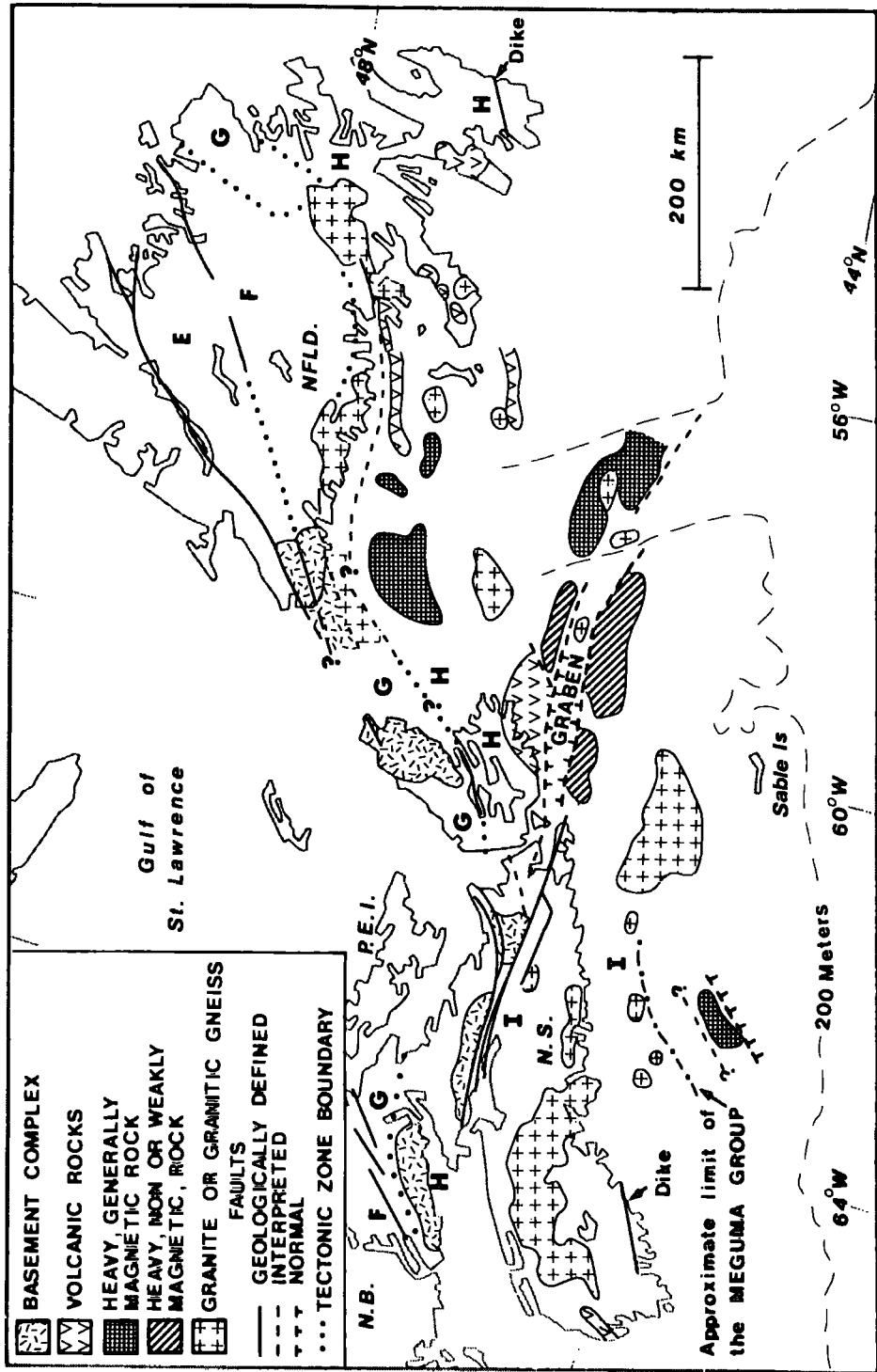
are covered, for the most part, by late-Palaeozoic and possibly younger sedimentary rocks whose seismic thickness is outlined in Figures 4.5 and 5.5.

On the northern Scotian Shelf, belts of typical late-Proterozoic volcanic - sedimentary rocks strike out southwest from the vicinity of the Burin peninsula. Interspersed between these belts are intrusions of magnetic, low-density granite. Other intrusions of magnetic, low-density granite are thought to occur northeast of Cape Breton Island (i.e. beneath the Glace Bay Low) and to the east of the Orpheus Graben. The ages of these granites could range from late-Precambrian (e.g. the Holyrood granite near St. John's, Nfld.) to Devonian, an age typical of many granites in the Appalachians. Proterozoic volcanic rocks, similar to the Fourchu Group, are interpreted to lie off the east coast of Cape Breton Island.

Halfway between Cape Breton Island and southern Newfoundland and near the mouth of the Laurentian Channel are occurrences of heavy, generally magnetic rock (Figure 7.3). It is difficult to relate these features to geological formations on land because the overall correlation between geological and geophysical data in Zone H in Newfoundland is poor, but the relatively high seismic velocities of the order of 7.0 km/s in the basement beneath the western part of the St. Pierre Gravity High (Figure 7.1) suggest the presence of rocks such as amphibolite or basic granulite. The somewhat lower seismic velocities (6.0 to 6.5 km/s) in the basement rocks near the mouth of the Laurentian Channel suggest a dioritic to gabbroic composition of these latter heavy, magnetic rocks.

The essential large-scale structural feature of the northern
Scotian Shelf is the sigmoidal trend of the Avalonian geological fea-
tures running between Cape Breton Island and southeastern Newfoundland.
The trend is typified by the Hermitage Flexure (Williams et al., 1970)
which outlines the sinuous trace of the boundary between Zones G and H
(Figure 7.3). Even though the exact location of the boundary between
Zones G and H is uncertain beneath the water-covered area, the
Hermitage Flexure is best reflected in the magnetic anomaly pattern
(Figure 7.2). Williams et al. (1970) consider the Hermitage Flexure
to be very important in terms of Newfoundland geology and its signifi-
cance in connection with the Scotian Shelf will be discussed later.

The western part of the southern Scotian Shelf appears to be a
continuation of the Meguma block of southern Nova Scotia consisting of
folded Cambro-Ordovician sedimentary rocks intruded by low-density,
non-magnetic Devonian granite. As originally pointed out by Hood
(1966), the Meguma trends seem to terminate at the dashed line shown
in Figure 7.3. Because of generally sparse magnetic coverage the
existence of such a line is somewhat uncertain except where shown in
Figure 7.3 where it is quite clear from both the gravity data and
detailed, low-level aeromagnetic data. To the southeast of the dashed
line in Figure 7.3 lies a region of heavier basement rock. In the
vicinity of Emerald Bank a basement block appears to be uplifted and
bounded on its southeast side, and possibly on its northwest side, by
a fault. To the northeast of Emerald Bank, beneath Middle Bank (Figure
1.1), lies a large granite batholith similar in extent to the nearby
New Ross batholith in southern Nova Scotia but different in that the

the Middle Bank Granite appears to be strongly magnetic, as is the Pokiok Granite in New Brunswick, whereas the New Ross Granite is conspicuously non-magnetic. The Middle Bank Granite was probably emplaced during the Devonian Period but could possibly be younger as Carboniferous radiometric ages have been obtained from basement rocks drilled on the southern Scotian Shelf (M. Given, personal communication). Alternatively, the area near the continental shelf could consist of Meguma rocks reworked during Permo-Carboniferous times.

Two important structural features in southern Nova Scotia and the southern Scotian Shelf appear to be the curvature, in plan view, of the folds in the Meguma group and the possible termination of the Meguma rocks along a northeasterly trending line offshore.

Perhaps the most outstanding structure on the Scotian Shelf is the Orpheus Graben which is part of a major crustal discontinuity that cuts east-west across central Nova Scotia and the Scotian Shelf and separates late-Precambrian to early Palaeozoic Avalonian formations of the northern Scotian Shelf from Cambro-Ordovician and possibly younger basement rocks of the southern shelf. The discontinuity is particularly apparent in the magnetic field and is characterized geologically by the apparent lack of any Precambrian rocks on the south side. The Orpheus Graben (Figure 7.3) is filled with a fairly thick sequence of Jurassic and possibly younger sedimentary rocks whereas the flanking basement rocks are only thinly covered. The Orpheus feature seems to be a typical continental graben but the explanation of the heavy rocks on either side is not clear. They do not appear to be deep-seated and have no obvious counterpart in nearby Nova Scotia.

Before discussing the main structural elements of the basement beneath the Scotian Shelf, the late-Palaeozoic setting of the Scotian Shelf will be described and palaeomagnetic evidence of early Palaeozoic plate motions presented.

7.3 LATE PALAEOZOIC SETTING OF THE SCOTIAN SHELF

Figure 7.4 shows the Scotian Shelf and the adjacent Canadian Maritime Appalachians in relation to the Spanish Sahara, Morocco, Portugal, France and the British Isles according to the reconstruction of Bullard et al.(1965). According to Francheteau (1970) the closest grouping of palaeomagnetic poles based on this reconstruction occurs for the Permian period. On the other hand, Roy's (1972) treatment suggests that a somewhat earlier, lower Carboniferous, age is more appropriate. However, the main point is that the reconstruction appears to be valid for the late Palaeozoic era.

Line A-A' indicates the approximate northern limit of Palaeozoic deformation in the Northern Appalachians and in the Scottish Caledonides. Line B-B' indicates the approximate northern limit of late Precambrian to early Palaeozoic Avalonian-Baltic type basement remnants found at scattered locations in New England, southern New Brunswick, central Nova Scotia and Cape Breton Island, southeastern Newfoundland and parts of Wales and southern England. These late Precambrian rocks and the somewhat older Grenville and Lewisian rocks to the north of A-A' formed the "jaws of the vice" (Rodgers, 1970) which came together during the early Palaeozoic era to telescope and, in part, destroy by subduction the intervening oceanic volcanic and

Figure 7.4:   Late Palaeozoic setting of the Nova Scotian contin-

ental shelf.   Reconstruction after Bullard et al.

(1965).   Line A-A' indicates northwesterly limit of

Palaeozoic deformation.   Line B-B' shows the north-

westerly limit of late-Precambrian Acado-Baltic base-

ment complexes.   Line C-C' shows the approximate

northern limit of the Alleghany (Hercynian) Orogeny

in the central Appalachians.   Line D-D' delineates

the Hercynian structural front in southern England

and southern Ireland.   Line E-E' shows the approxi-

mate southern limit of the Hercynian Orogeny in

northwest Africa.   SAF-South Atlas Fault, HBF-

Highland Boundary Fault, SUF-Southern Uplands Fault,

GFZ-Gibbs Fracture Zone, NFZ-Newfoundland Fracture

Zone, KS-Kelvin Seamounts, BF-Bay of Fundy, MB-Minas

Basin, CB-Chedabucto Bay, GB-Georges Bay, WB-White

Bay, NYC-New York City, SJ-Saint John.
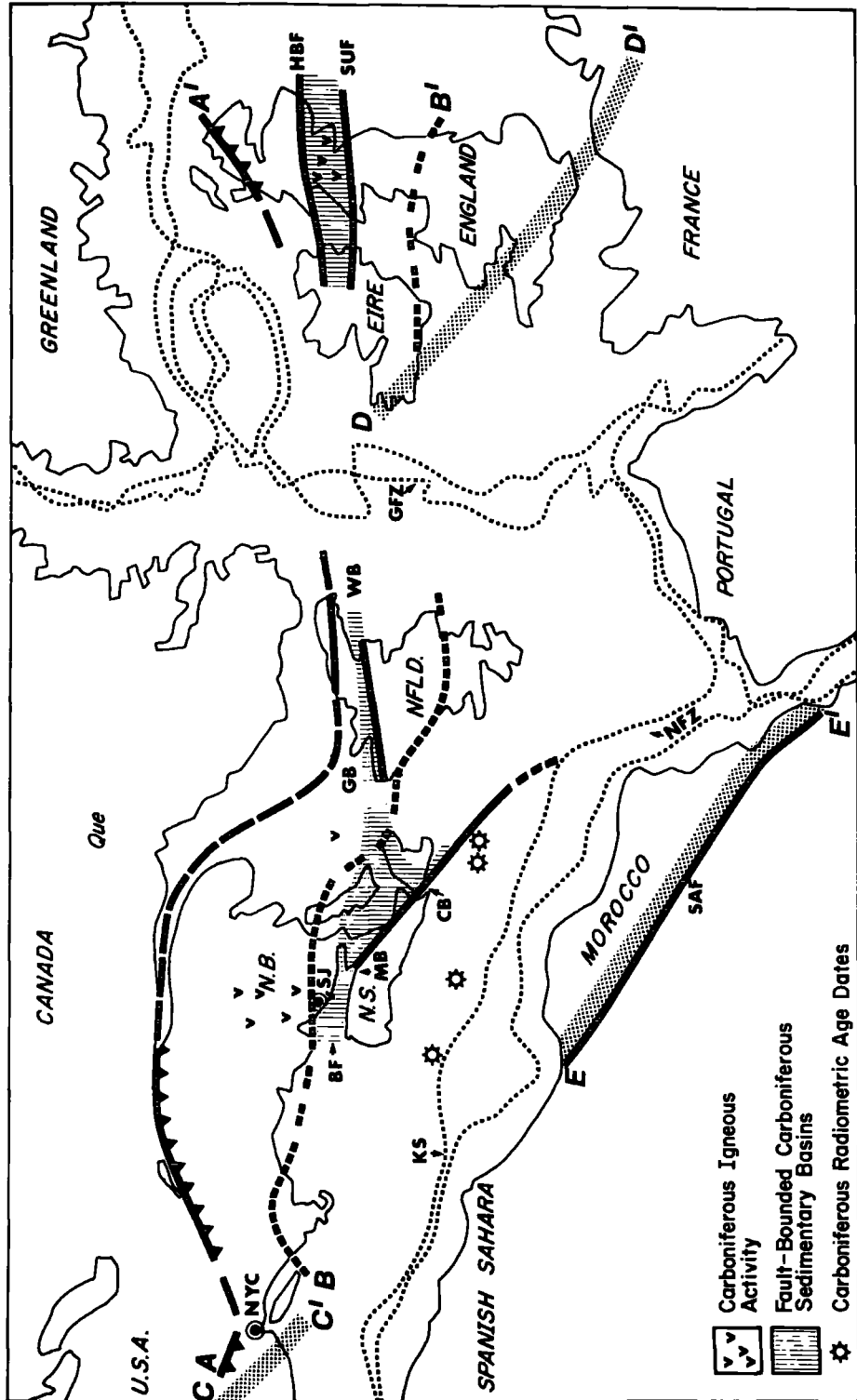
sedimentary rocks. As mentioned in the introductory chapter, this convergence and collision is manifested in the Northern Appalachians by the Taconic (Ordovician) Orogeny and the Acadian (Devonian) Orogeny and in the British Isles by the Caledonian (Silurian) Orogeny. The ages in brackets are only approximate as peak orogenic activity occurred in different areas at different times.

The next period of tectonic activity in the Canadian Appalachians was the "Maritime Disturbance" (Poole, 1967) which occurred during the Carboniferous Period and was mainly confined to a zone running from the Bay of Fundy northeast across the Gulf of St. Lawrence and through the Georges Bay - White Bay area of west central Newfoundland (shaded area in Figure 7.4) and to a second east-west trending zone from Minas Basin to Chedabucto Bay. The Maritime Disturbance was not severe enough to be termed an orogeny but it would seem to be related to the major Hercynian Orogeny which affected a wide area between the lines D-D' and E-E' in western Europe and to its North American counterpart, the Allegheny Orogeny, which affected the Southern and Central Appalachians, approximately south of the line C-C' near New York City. These late-Palaeozoic orogenies probably resulted from the collision of Gondwanaland and Laurasia during the Permo-Carboniferous Period (e.g. McKerrow and Ziegler, 1972).

As mentioned previously, the continental masses are probably shown in the correct spatial relationship for the Permo-Carboniferous Period and it is interesting to note that, on a purely geometrical basis, the northeasterly trending rift zone through the Bay of Fundy-Georges Bay-White Bay area seems to link up with the Midland Valley of Scotland (lying between the Highland Boundary Fault and the Southern

Uplands Fault, Figure 7.4).

These areas in the Canadian Maritimes *and* Scotland
may, therefore, have been part of an intracontinental, Permo-Carboniferous rift zone which lay to the north and west of the main
Alleghenian-Hercynian orogenic belts.

One of the puzzling features of Permo-Carboniferous tectonic
activity in the area shown in Figure 7.4 is the large offset in the
northern margin of the Hercynian Front between Europe and North America
and the apparent lack of Hercynian folding, faulting and igneous
activity in southern Nova Scotia and eastern Newfoundland. However,
before discussing this and other problems in connection with the
structure and history of the Scotian Shelf, palaeomagnetic data from
most of the areas shown in Figure 7.4 will be discussed as these data
provide some constraints on the early Palaeozoic geometry of the land
masses.

7.4 PALAEOMAGNETIC EVIDENCE OF EARLY PALAEOZOIC PLATE MOTIONS

7.4.1 New Brunswick and Western Newfoundland

Virtual geomagnetic pole positions (Figure 7.5) derived from
directions of stable remanent magnetizations in rocks from the Canadian Atlantic Provinces generally show a systematic northward migration
from the area east of the Philippine Islands in the Cambrian period to
the Arctic coast of Siberia in the Triassic period. The displacement
of the Cambrian and Devonian pole positions from New Brunswick westward with respect to those from western Newfoundland led Nairn et al.
(1959) to suggest that the displacement could be explained by a

Figure 7.5:   Palaeomagnetic pole positions from rocks in the

                Canadian Maritime Appalachians. Precambrian results

                from Nairn et al. (1959), Ordovician pole from eastern

                Newfoundland from Deutsch and Rao (1970). Ordovician

                pole from western Newfoundland from Beales et al.

                (1974), Cambrian and Devonian poles from western

                Newfoundland and southern New Brunswick from Black

                (1964), the remaining poles are taken from Hicken et

                al. (1972).
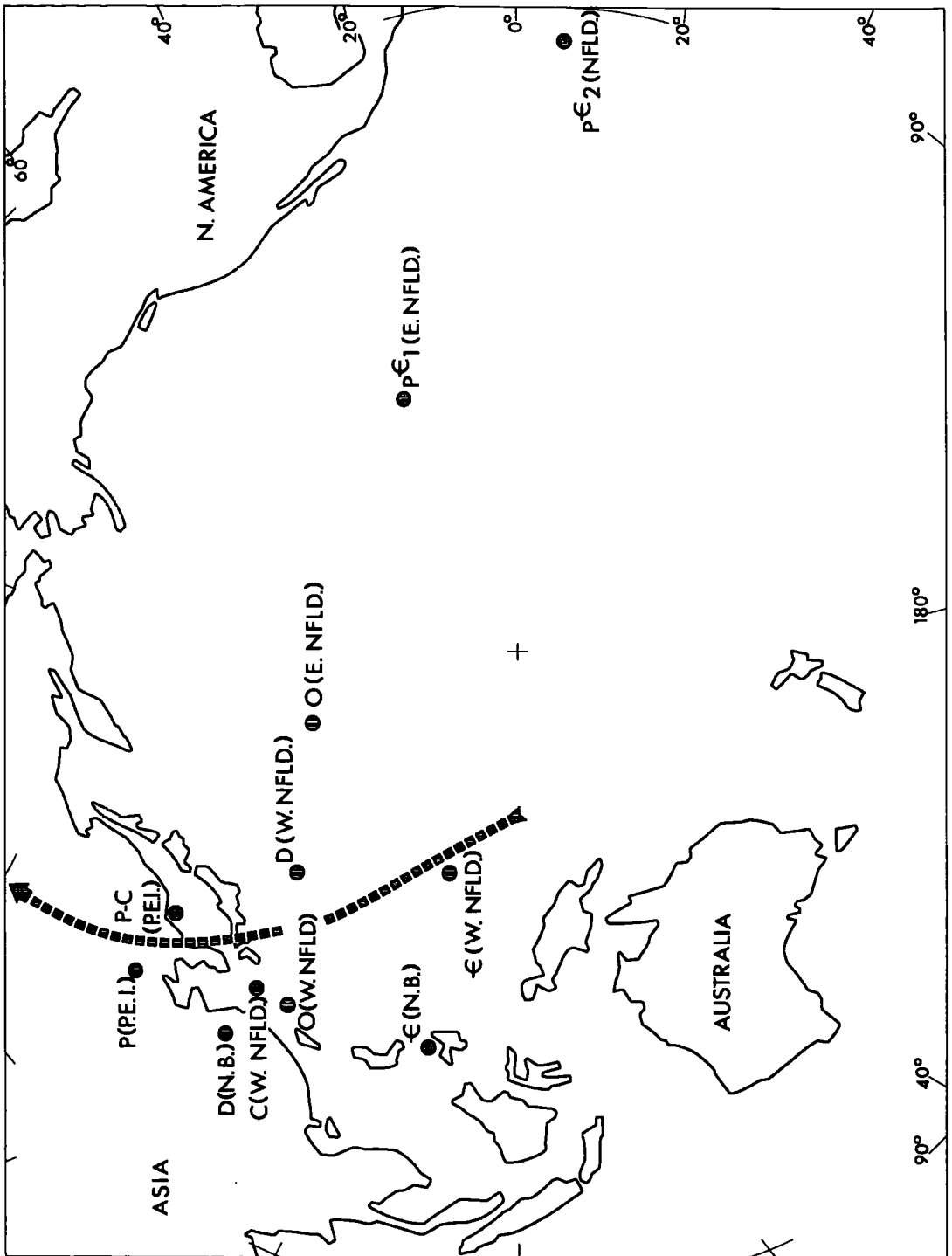
counter-clockwise rotation of Newfoundland. Du Bois (1959) concluded

that if such a rotation took place, it took place prior to the Carboni-

ferous period. Subsequent work by Black (1964) supported the earlier

palaeomagnetic results. It is unlikely, however, that Newfoundland has

rotated with respect to the remaining Atlantic Provinces because there

is no geophysical evidence (e.g. Goodacre et al.,1969; Haworth, 1975)

of an incipient Red Sea-type rift structure in the northeastern part

of the Gulf of St. Lawrence. As Deutsch (1969) has pointed out, an

alternative explanation for the displacement of the Cambrian and

Devonian pole positions is that southeastern New Brunswick lay somewhat

to the east of its present position during early Palaeozoic time.

This is an important point because it means that, within the context

of the palaeomagnetic data, we can regard western Newfoundland as

being fixed with respect to the North American (Grenville) plate and

ascribe the differences in the Cambrian and in the Devonian palaeo-

magnetic poles to a westerly movement of southeastern New Brunswick at

some time between the lower Devonian and the lower Carboniferous. The

palaeomagnetic poles from the two areas can be brought together into

remarkably good agreement by moving southeastern New Brunswick more or

less due east to approximately $45^{o}N$; $50^{o}W$ (just outside the lower

right-hand side of Figure 7.3). A westerly movement of southeastern

New Brunswick during the Devonian Period is broadly consistent with

the present-day en-echelon arrangement of the late-Precambrian rocks

in Zones G and H (Figure 7.3) if we assume that the Avalon Peninsula

was approximately in its present position during the Devonian Period.

289

7.4.2 . Eastern and Western Newfoundland

Figure 7.6 shows Palaeozoic palaeomagnetic pole positions from rocks on opposite sides of the Atlantic Ocean plotted according to the continental reconstruction shown in Figure 7.4. The palaeomagnetic data are from Hicken et al. (1972). A puzzling aspect of Figure 7.6 is that the Ordovician palaeomagnetic poles from eastern New-foundland, Portugal and northwestern Eire are quite different from Ordovician poles from western Newfoundland, other parts of North America and western Europe. Deutsch (personal communication) and Briden et al. (1973) suggest that the anomalous Ordovician result from Eire may be due to tectonic rotation of the Mweelrea rocks. In a similar fashion, the palaeomagnetic data from eastern Newfoundland and Portugal suggest that these two areas have been rotated counter-clockwise some 50° and 110° respectively since the Ordovician Period. In the case of eastern Newfoundland, such a rotation would be broadly consistent with the formation of the Hermitage Flexure (Williams et al., 1970), which is the bend in tectonostratigraphic zones G and H at Hermitage Bay (Figures 7.3 and 4.1), at some time subsequent to the lower Ordovician. The anomalous Ordovician poles from Portugal and northwestern Eire can be brought into coincidence with the "normal" poles from western Europe and North America by merely rotating Portugal and northwestern Eire; no translation of either area seems necessary in view of the probable errors inherent in the palaeomagnetic pole positions. On the other hand, an unresolved difficulty with the palaeomagnetic result from eastern Newfoundland is that it

Figure 7.6:   Cambro-Ordovician palaeomagnetic poles from North

America, Europe and Africa based on a continental

reconstruction and plotted with respect to the

present-day coordinates of North America.
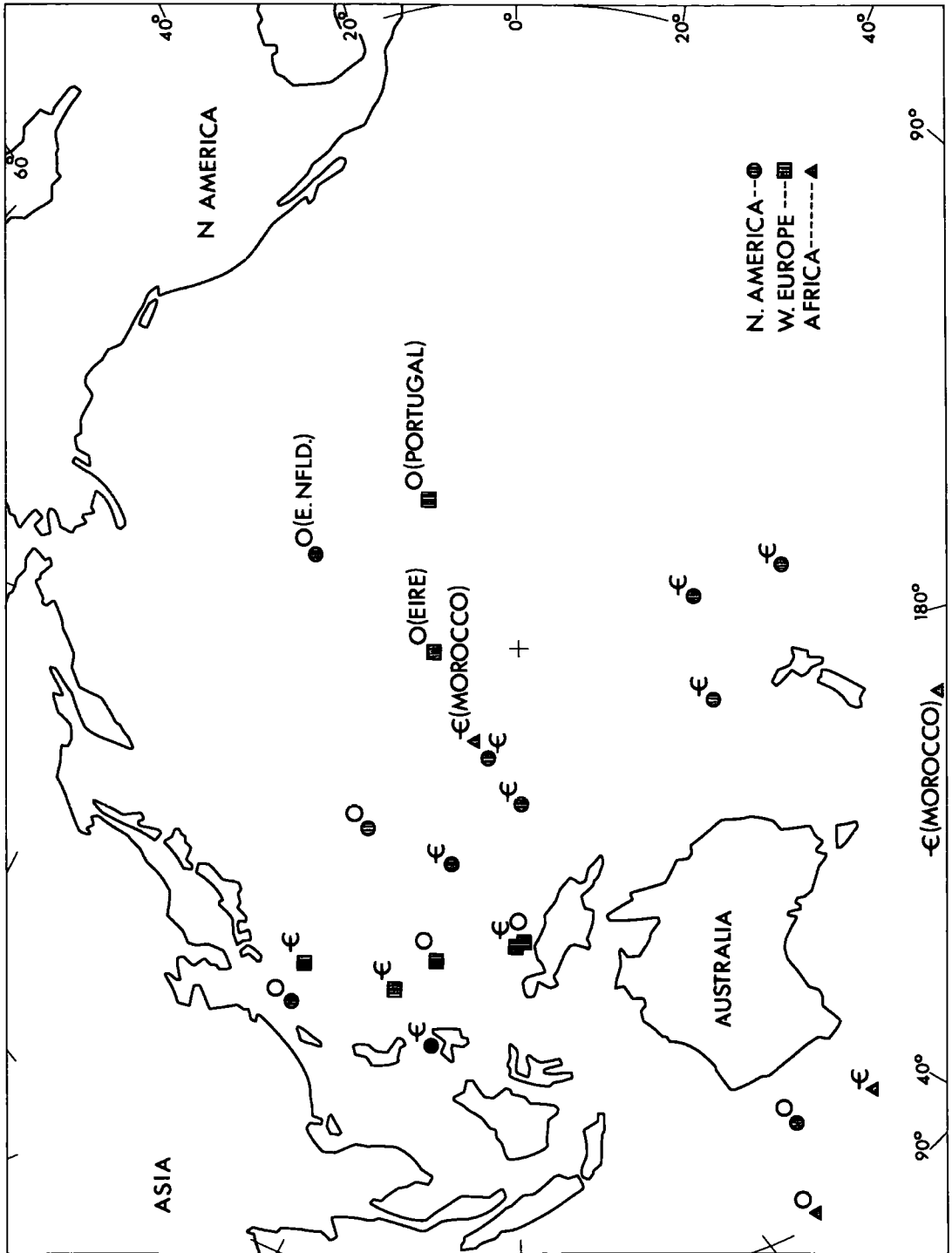
places this latter area some 20° (in palaeolatitude) away from western Newfoundland and it is difficult to reconcile this in any reasonable continental reconstruction.

In summary, therefore, the Ordovician palaeomagnetic results broadly indicate that eastern Newfoundland and at least parts of Portugal and Eire were portions of tectonic blocks which underwent a considerable rotation during, or after, the Ordovician Period but the extent and detailed location of these tectonic units is not clear.

7.4.3 Southern Nova Scotia and Morocco

The Cambro-Ordovician pole positions in Figure 7.6 indicate that Africa, with the possible exception of a part of Morocco, was located a considerable distance away from North America during those times. Palaeoclimatic data (e.g. Fairbridge, 1970; Schenk, 1972) are consistent with the palaeomagnetic evidence which indicates that during the Cambrian Period the eastern margin of North America lay near the palaeoequator and northwest Africa lay near the pole. Because northwest Africa and the Canadian Maritime Provinces collided during the Palaeozoic Era it is reasonable to suppose that remnants of one continent may now be attached to the other, and vice versa. The problem is to decide whether southern Nova Scotia once belonged to Africa or to the Acado-Baltic province of western Europe (which includes the Avalon Platform), as this affects the interpretation of the Minas Basin - Chedabucto Bay-Orpheus fault zone. There is geological evidence that southern Nova Scotia was once in close proximity to northwest Africa (Schenk, 1971) and subject to glaciation during

the Ordovician Period (Schenk, 1972). Additional evidence for south-
ern Nova Scotia's being an African remnant would be the discovery of
nearly vertical stable permanent magnetization in the Meguma rocks,
because it would be consistent with deposition in high latitudes.

Parts of Morocco may have once belonged to the Acado-Baltic
province as Tarling and Sutton's (1967) data suggest that Cambrian
red beds in west central Morocco were deposited in equatorial lati-
tudes. If so, southern Nova Scotia and the southern Scotian Shelf
could also have been in equatorial latitudes and formed a part of
the Acado-Baltic province. An alternative explanation of the Moroccan
results is that the stable magnetization was acquired in these red
beds at a later time, perhaps during the Hercynian orogeny. The
problem of how southern Nova Scotia and Morocco fit into the contin-
ental mosaic of Figure 7.4 will be discussed further in the last
section.

7.5   INTERPRETATIONS OF DIRECTIONS OF TOTAL MAGNETIZATION

7.5.1   Introductory remarks

In this section, directions of total magnetization are inter-
preted in terms of the palaeomagnetic data in Figures 7.5 and 7.8.
The directions of total magnetization are accepted at face value
but, as mentioned in Chapter 4, it must be kept in mind that the
directions of total magnetization derived from the transformation of
gravity and magnetic fields or from magnetic modelling may be spurious
if all of the assumptions of the geophysical analysis are not met.

7.5.2   Relationship between induced, remanent and total magnetization

Magnetic modelling or combined analysis of gravity and magnetic data only defines the direction of the total magnetization vector $\vec{T}$, which is the vector sum of the induced magnetization vector, $\vec{I}$, and the remanent magnetization vector, $\vec{R}$.[*] Although the direction of $\vec{I}$ is known, neither its magnitude nor the ratio of remanent to induced magnetization (Koenigsberger ratio or Q ratio) is usually known and the best that can be done for palaeomagnetic studies is to set limits on the direction of the remanent magnetization vector.

Figure 7.7 gives an example of the possible magnitudes and directions of the vectors $\vec{I}$ and $\vec{R}$ for different values of Q when the direction and magnitude of $\vec{T}$ is given. The solid lines represent the case where the total magnetization dips down 16° toward magnetic north. The diagram is drawn in the plane which contains these vectors; in a two-dimensional case the diagram represents the vector components which lie in the vertical plane containing the earth's field. In the two-dimensional case, the inclination of the total magnetization vector is often specified in the vertical plane perpendicular to the strike of the source but, throughout the thesis, this vector has been projected into the vertical plane containing the earth's field in order to allow comparison of results from features which strike in different directions.

It is readily seen that $\vec{R}$ must lie in the sector bounded by $\vec{T}$ and a vector directed opposite to $\vec{I}$. The intensity of $\vec{R}$ is a minimum when $\vec{R}$ is perpendicular to I; Q is a minimum when $\vec{R}$ is

[*] See subsection 3.5.3 for a discussion of the effect of basement magnetization on the determination of the total magnetization vector.

Figure 7.7:   The vector relationship between induced (I), remanent

(R) and total (T) magnetization. The total magneti-

zation vector is distinguished from the others by a

thicker line. Solid lines refer to the case where

the total magnetization vector of unit length is

dipping down 16° to the north; dashed lines refer

to the case when the total magnetization vector is

pointing in the opposite direction. In either case

vector combination of I and R gives T.
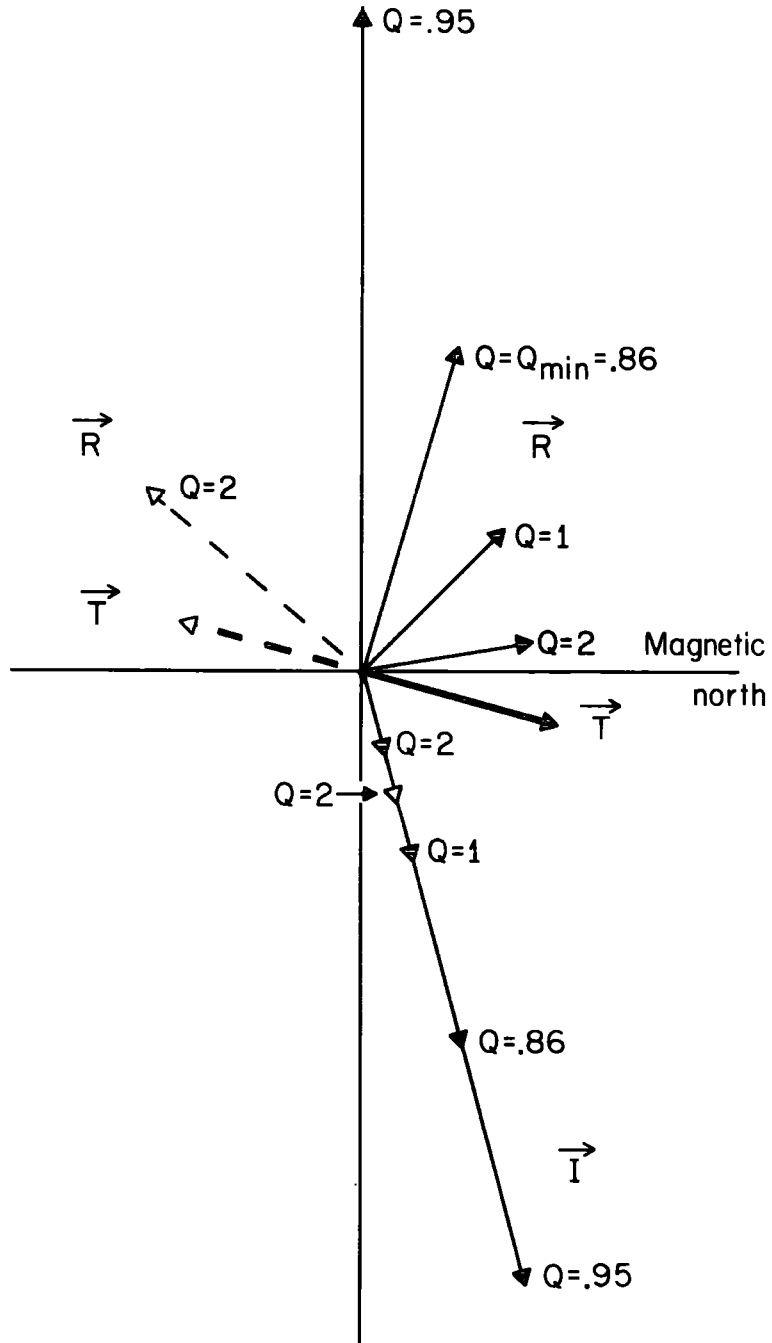
perpendicular to $\vec{T}$. If the angle between $\vec{R}$ and $\vec{T}$ is obtuse, the intensities of $\vec{R}$ and $\vec{I}$ are greater than the intensity of $\vec{T}$ and if $\vec{T}$ is large, very large intensities of $\vec{R}$ and $\vec{I}$ are required if $\vec{R}$ is more or less antiparallel to $\vec{T}$. One problem in the interpretation of magnetic models or the results of the transformation of a gravity anomaly to a magnetic anomaly, and vice versa, is to decide whether the source body is normally magnetized in one direction or the country rock is reversely magnetized in the opposite direction. This latter situation is unlikely but must not be neglected entirely. If the total magnetization vector, $\vec{T}$, were pointing to the direction opposite to that adopted in Figure 7.7 (solid line), the remanent magnetization vector must lie between $\vec{T}$ (dotted line) and a vector antiparallel to the earth's field and the Q values must be greater than unity.

7.5.3   St. Pierre High (west)

Figure 7.8a shows the directions of stable remanent magnetization in the Atlantic Provinces projected onto the vertical plane containing the earth's field. The two Precambrian results (pЄ) are from eastern Newfoundland and, as may be seen in Figure 7.5, are probably not representative of the remainder of the Maritimes. The clockwise rotation with time of the permanent magnetization vector and reversals in its direction are apparent in the data. Assuming that there is an inverse relation between rock density contrast and magnetization contrast (e.g. where the density contrast is negative but the magnetization contrast is positive), the direction of total

Figure 7.8:   (a) Directions of stable remanent magnetization

from selected results from rocks in the Canadian

Maritime Appalachians. The vectors shown here are

the projections of the remanent magnetization vectors

onto the vertical plane containing the earth's field.

This was done to provide an easy comparison with the

results of two-dimensional magnetic to gravity field

transformations. The symbols are as follows: pϾ -

Precambrian;   uϾ - upper Cambrian; 0-Ordovician;

1D-lower Devonian; 1C- lower Carboniferous; P-Permian;

Tr-Triassic.

(b) Directions of total magnetization derived from

selected results of magnetic to gravity field trans-

formations.
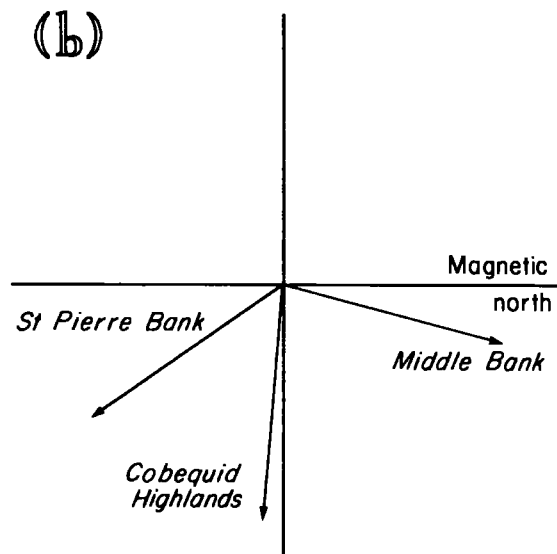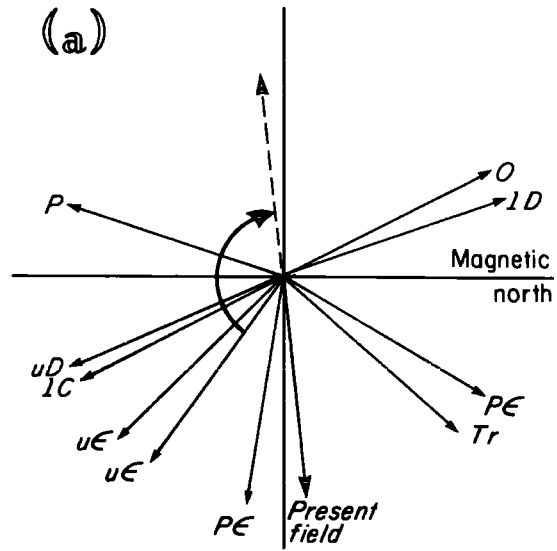
magnetization deduced for the western St. Pierre High are (Figure 7.8b) indicates that the permanent magnetization was acquired no earlier than the Cambro-Ordovician Periods. This result is not highly significant because the angle of total magnetization is only determined to within about plus or minus 20°. If there is a direct relation, the permanent magnetization was acquired no later than during the Ordovician-Silurian-Devonian Periods. However, a direct relation requires higher Q ratios and higher values of induced and remanent magnetization than an inverse relation does, so an inverse relation seems more likely. As mentioned in Chapter 4, an inverse relation could result from serpentinization of basic to ultrabasic rocks. The Cambro-Ordovician age limit is not unreasonable in view of the widespread effects of the Taconic and Acadian orogenies but, as mentioned in Chapter 4, it is not clear how such a large degree of remanent magnetization could be produced and preserved.

7.5.4 Cobequid Highlands and the mouth of the Laurentian Channel

There is little doubt in these cases that there is a direct rather than inverse relation between rock density and magnetization so the presence of a total magnetization vector component dipping at an angle of about 85° ($\pm 5^o$) to the south (Figure 7.8b) indicates that a southerly directed permanent magnetization in the Cobequid Highlands and in the rocks near the mouth of the Laurentian Channel was acquired no earlier than in late Precambrian to Cambrian times. The minimum value of Q (see Section 7.3.1) is about 0.3; since the highest Q factor observed in samples collected in the Cobequid Highlands (Table

6.1) is 0.3 and since the average Q factor for rocks in New Brunswick

is about 0.2 (McGrath et al., 1973) there is a good possibility that

the permanent magnetization in the Cobequid Highlands is nearly

horizontal and was acquired during the Devonian Period.

7.5.5 Middle Bank Area

Sufficiently good magnetic and gravity coverage and a seeming-

ly favourable relation between the gravity and magnetic fields allow

a three-dimensional combined analysis to be made of the Middle Bank

feature. The results of the three-dimensional gravity magnetic field

transformation (Table 7.1) appear to be good inasmuch as there is a

high correlation between the observed and computed magnetic fields but

there are two difficulties with the calculated direction of the total

magnetization vector which is pointing northward and slightly upward.

Firstly, the total magnetization vector is nearly at right angles to

the earth's field and this means that the minimum value of the Koenigs-

berger ratio is about 1. Such a value is extraordinarily high for

typical granitic rocks (McGrath et al., 1973) and appears to be unlikely

in this case. Secondly, the inclination differs by some 40° from the

result obtained from the two-dimensional analysis (Figure 7.8b) des-

cribed in Chapter 5. Although there are undoubtedly some problems in

applying a two-dimensional analysis to a three-dimensional source, one

reason for the rather large discrepancy in the inclinations may be

that the ratio of magnetization contrast to density contrast is not

uniform throughout the Middle Bank Granite. In particular, the mag-

netization may be enhanced at the margins. The results of the three-

dimensional gravity to magnetic field should, therefore, be treated

with caution.

Figure 7.9 shows virtual palaeomagnetic pole positions obtained from the results of the three-dimensional gravity to magnetic field transformation (Table 7.1) for different values of the Koenigsberger ratio, (Q). Pole positions are shown for two cases: (a) solid dots representing north palaeomagnetic poles for the case where there is an inverse relation between magnetization contrast and density contrast (e.g. a positive magnetization contrast and a negative density contrast corresponding to a magnetic granite) and (b) open circles representing south palaeomagnetic poles for the case where there is a direct relation (e.g. a non-magnetic granite surrounded by magnetic rocks). The 67% oval confidence limit around the south pole corresponding to Q=2 is typical of the other confidence limits. ·

The virtual north poles (solid dots) migrate approximately south along the 90°E meridian. This path comes close to the approximate polar wandering curve for Africa (Figure 7.10) but seems to be distinct from the lower Palaeozoic portion of the Maritime polar wandering curve at the 95% confidence interval ($\pm 30^{\circ}$). The results of the gravity to magnetic field transformation are consistent, therefore, with the hypothesis that southern Nova Scotia and the southern Scotian Shelf were once part of Africa but they do not prove it because the virtual south poles (open circles) lie quite close to the Triassic-Jurassic poles from North America (Figure 7.9). The main difficulty, however, in accepting the virtual south poles is to postulate a convincing situation where a non-magnetic granite could be surrounded by magnetic rocks. It might be possible that a Devonian(?)

TABLE 7.1

COMBINED ANALYSIS OF GRAVITY AND MAGNETIC FIELDS

MIDDLE BANK AREA

Gravity to magnetic field transformation

Total Magnetization Vector		Ratio of Magnetization Contrast to Density Contrast emu/gm	Coefficient of Linear Correlation between Observed and Computed Fields
Azimuth deg	Inclination deg		
-157.3	13.7	.0091	.84
(13.7)	(7.7)	(.0014)	

Q value	Remanent Magnetization Vector		Virtual Magnetic Pole	
	Azimuth deg	Inclination deg	Latitude deg	Longitude deg
2	-163.1	-16.0	-50.3	-87.3
4	-160.1	-0.7	-42.0	-87.7
∞	-157.3	-13.7	-33.7	-87.9
2*	30.0	-43.4	14.6	91.7
4*	25.8	-28.0	25.7	91.7

* Calculated for the case where the ratio of magnetization contrast to density contrast is assumed to be negative

( ) Standard deviation of quantity

Note: the standard deviation of a virtual pole varies according to the value of Q adopted but is of the order of $15°$ of latitude

Figure 7.9:   Results of a three-dimensional combined analysis of

                gravity and magnetic anomalies over the Middle Bank

                area (see Figure 5.12) compared with the late

                Palaeozoic and Mesozoic polar wandering curve for

                North America (solid line with tick marks).

                Virtual poles (solid dots and open circles)

                obtained from the three-dimensional gravity to

                magnetic field transformation for various values

                of the Koenigsberger ratio,(Q) are shown, as explained

                in the text, by solid dots if the ratio of magnetization

                contrast to density contrast is assumed to be negative

                and by open circles if positive. The tick marks represent

                mean palaeomagnetic poles taken from Irving and Park (1972)

                for the Carboniferous (C), Permian (P), Triassic (Tr),

                Jurassic (J) and Cretaceous (K) Periods.
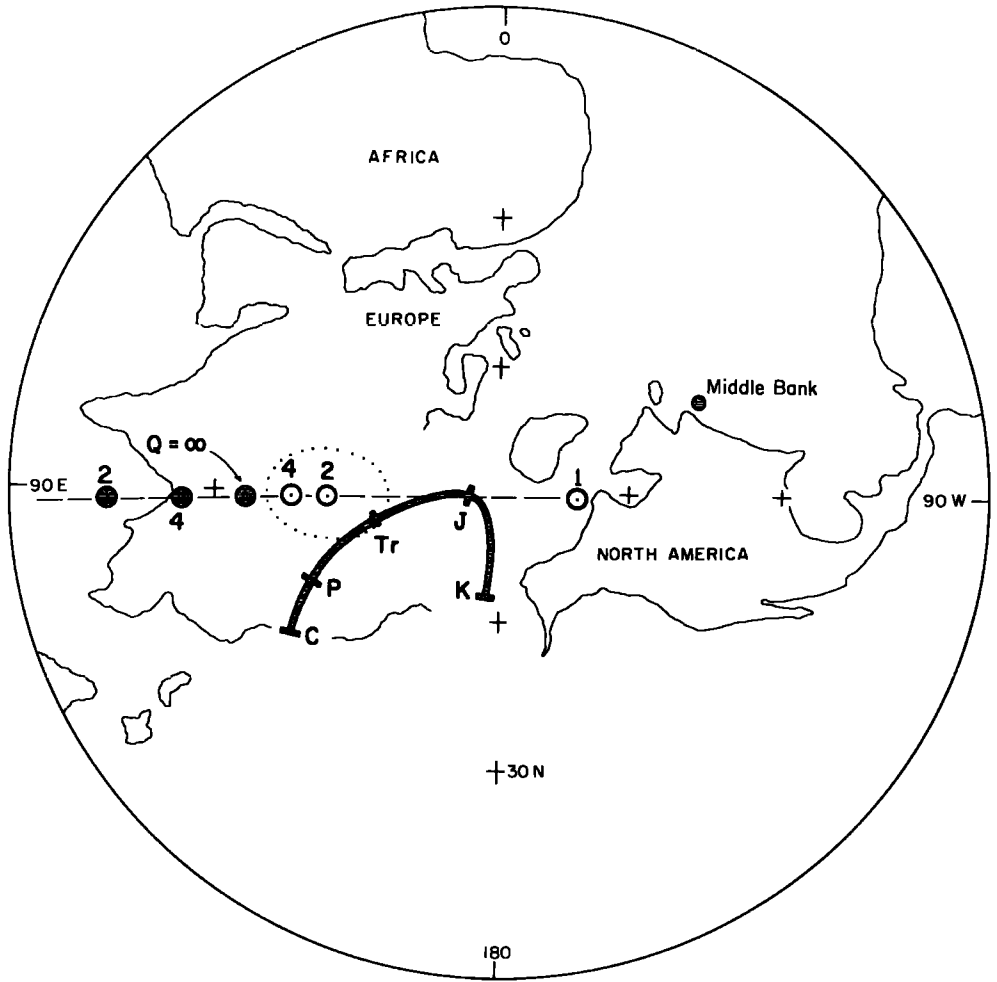
Figure 7.10:   Virtual magnetic poles, as explained in the text and

in the caption of Figure 7.9, obtained from the application

of the three-dimensional gravity to magnetic field

transformation to the Middle Bank area compared with

generalized polar wandering curves for the Canadian

Maritimes and Africa (see Figures 7.5 and 7.6 for

individual locations of palaeomagnetic poles).
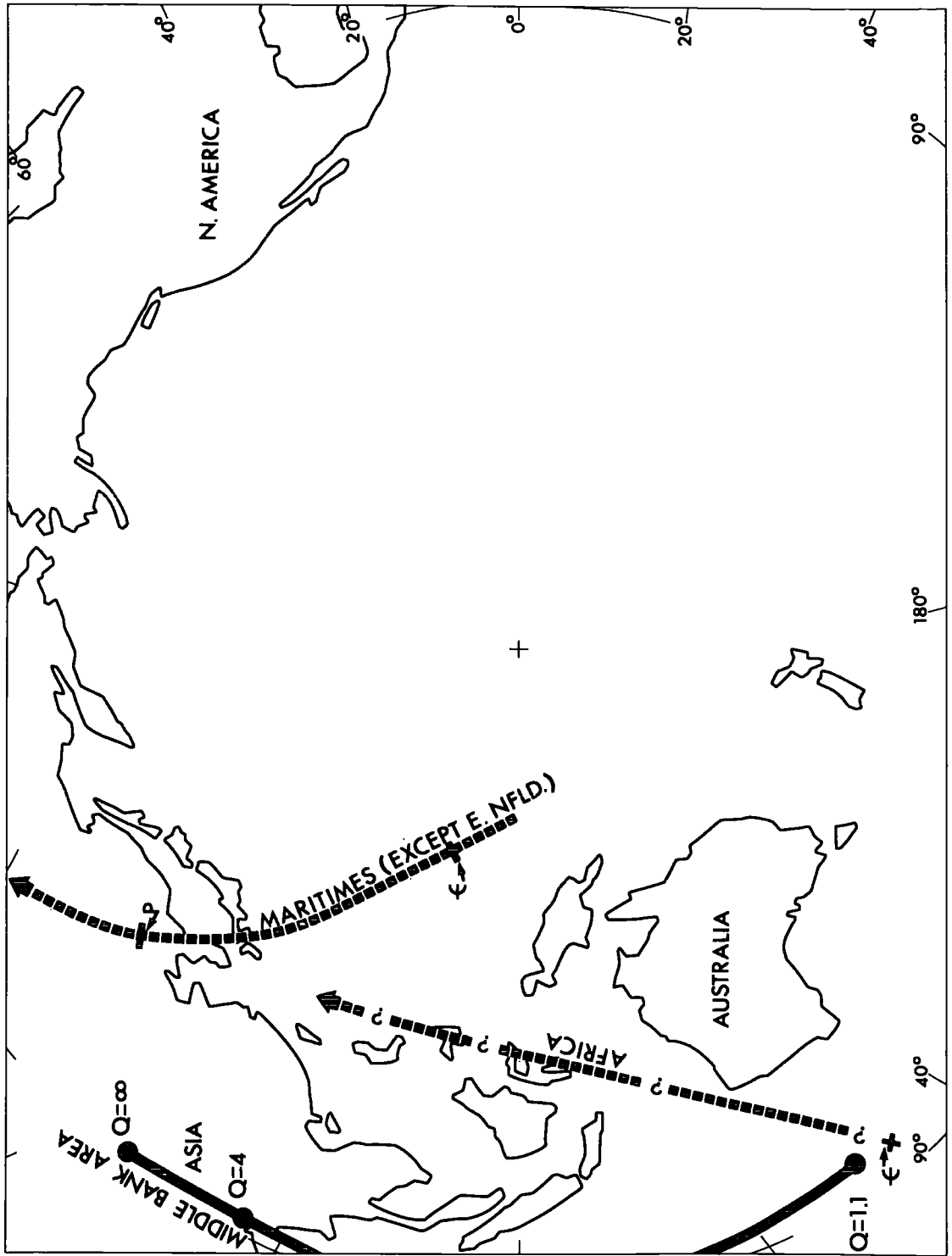
or possibly Permo-Carboniferous(?) granite formed a topographic high and was surrounded by Triassic flood basalts during the opening of the present-day Atlantic Ocean. This configuration might approximate the situation assumed for the gravity to magnetic field transformation where the entire surrounding basement is taken to be magnetic, however this explanation is highly speculative.

As mentioned previously, the results of the three-dimensional gravity to magnetic field transformation must be viewed with caution but it is curious that it gives results which have at least some possibility of being reasonable when we consider that the calculated pole positions might have lain some 90° in longitude away from the Maritimes and African polar wandering curves.

7.5.6   Avalon Peninsula

Considerable effort was put into trying to achieve significant results from combined analysis of gravity and magnetic anomalies over the Avalon Peninsula because the late-Precambrian pole positions determined by Nairn et al. (1959) seem to be at variance with other results from eastern Canada (Figure 7.5). Unfortunately most of the results from the combined analyses are meaningless due to a negligible correlation between observed and calculated fields; those that show some correlation $(r = 0.5)$ give poles well to the east of the polar wandering curve and in very coarse agreement with the poles in Figure 7.5. The best result, one for the southern part of the Avalon Penin-sula gives a pole $(Q = \infty)$ lying part way between pG_1 and pG_2.

7.6 DISCUSSION

7.6.1 Early Palaeozoic structure and history

When considering the major structural trends in the pre-Carboniferous basement rocks of the Scotian Shelf and the adjacent land areas, the Meguma block of southern Nova Scotia seems to be a "nose" which has been thrust into the late Precambrian Avalonian belt, truncated the Avalonian basement along the Minas Basin - Chedabucto Bay - Orpheus fault zone and produced the fractured appearance which the pre-Carboniferous basement complexes such as the Cobequid, Antigonish and Cape Breton Highlands present in plan view (Figures 1.1, 6.2 and 7.1). Such an event might explain the similarity noted many years ago by King (1951) in the amount of offset observed in the Appalachian structures between Newfoundland and the mainland region and in the offset of the continental margin along the southern edge of the Grand Banks of Newfoundland. Of course, whether these large scale structural features are genetically related depends critically upon the timing of the events.

The curvature of the folds in the Cambro-Ordovician Meguma rocks of southern Nova Scotia (shown by the aeromagnetic anomalies in Figure 7.2) seems to be consistent with a thrusting of the Meguma block towards the north and west. For example, Benson (1967) proposed that tectonic features in the Antigonish Highlands were related to the folding and thrusting of the Meguma rocks and Eisbacher (1970) has pointed out that the compressive stress producing the shear zone in the Cobequid Mountains is about the same as that required to produce the folds in the Meguma rocks. According to Taylor and Schiller (1966),

the folding of the Meguma was completed before the culmination of the

regional metamorphism of the rocks and the regional metamorphism pre-

dates the contact metamorphism associated with the intrusion of

Devonian granite. Since the radiometric age dates associated with

the New Ross Batholith and other granites cluster about 375 my, the

folding occurred during or prior to the lower Devonian.

The formation of the sigmoidal trends in the northern Scotian

Shelf also appears to have been during or prior to the lower Devonian.

The sigmoidal trends are epitomized by the Hermitage Flexure (Williams

et al., 1970) and the Hermitage Fault (which separates Zones G and H -

see Figure 7.3) is cut by the Ackley granite which exhibits radio-

metric age dates ranging from 370 to 400 my (W. Poole, personal

communication).

Although the lower age limit for the folding of the Meguma

Group and the formation of the Hermitage flexure are about the same,

it is difficult to establish an exact correspondence of these features

since it is difficult to determine an upper limit for the ages of the

rocks affected in southern Newfoundland. The Siluro-Ordovician (?)

Torbrook Formation of southern Nova Scotia seems to have been deformed

along with the Meguma rocks. The Hermitage flexure appears to pinch

out the Siluro-Ordovician rocks of the central mobile belt (zones E

and F), therefore, a Siluro-Devonian age for the production of the

major features discussed is not unreasonable although a somewhat

earlier, mid to late-Ordovician age might be possible. However,

palaeomagnetic evidence supports a Siluro-Devonian age for their

formation for two reasons. Firstly, the lower Ordovician poles place

eastern and western Newfoundland so far apart that it seems unlikely
that the Hermitage flexure could have been formed in its present
position as early as the middle to late Ordovician (although the Her-
mitage flexure might have been formed elsewhere and brought to its
present position by transcurrent movement along the fault dividing
zones E and F or along some other major fault or faults in central
and western Newfoundland). Secondly, Deutsch's (1969) explanation of
the discrepancies between Cambrian and Devonian poles from southern
New Brunswick and western Newfoundland places a lower Devonian age
limit on the time at which New Brunswick could have been pushed west-
ward.

What is the relationship of the folding of the Meguma rocks
and the formation of the Hermitage flexure to the production of the
recess in the northern Appalachians between Newfoundland and New York
City as outlined by line A-A' in Figure 7.4? Geometrically these fea-
tures would seem to be related and possibly formed simultaneously by a
Himalayan type collision although the recess in the northern Appala-
chians might have been a pre-existing feature in the edge of the
Grenville continental mass (W.H. Poole, personal communication;
Haworth, 1975). The line A-A' shows, in general, the northwest limit
of Palaeozoic deformation of the Appalachians but at several points in
New York State, Quebec and Newfoundland line A-A' coincides with the
boundary between autochthonous, undeformed miogeosynclinal rocks to
the northwest and allochthonous and para-autochthonous eugeosynclinal
rocks to the southeast. An upper age limit of the emplacement of the
transported rocks is set by the fact that lower and/or middle Ordovi-
cian rocks are affected whenever field relations can be determined.

A lower limit is difficult to determine as different allochthons may
have been emplaced at different times, but Silurian sedimentary rocks
overlie thrusts near Lake Aylmer, Quebec (St. Julien and Hubert, 1975),
lower Devonian strata overlie thrusts at one locality in New York State
(Zen, 1968) and middle Ordovician rocks overlie thrusts at Port au
Port, Newfoundland(Rodgers and Neale, 1963). Therefore, although one
might expect geometrically (and cannot disprove geologically) a genetic
relationship between the thrusting of the Meguma block (zone I in
Figure 7.3) into the Avalon platform (Zone H in Figure 7.3) and the
formation of the northern Appalachian recess between New York City
and George's Bay, Nfld. (Figure 7.4), the latter feature probably
predates the former by several tens of millions of years.

As mentioned previously, the middle Ordovician positions of
the northern Scotian Shelf and the southern Scotian Shelf with respect
to the Grenville block are uncertain. The southern Scotian Shelf-
Morocco area may have been attached to the major portion of Africa and
the northern Scotian Shelf-Portugal area (Figure 7.4) may have been
part of the Acado-Baltic plate. The two areas then converged towards
each other and towards the Grenville block to produce the main Siluro-
Devonian features of southeastern Newfoundland, southern Nova Scotia
and the Scotian Shelf. In particular, the Minas Basin - Chedabucto
Bay - Orpheus Fault zone was probably formed at this time and may have
been a part of a transcurrent fault passing along the southern margin
of the Grand Banks and through the Strait of Gibraltar between Morocco
and Spain (Figure 7.4). The thrusting of the Meguma block into the
Avalon platform appears to have been the forerunner of the collision

between Gondwandland and Laurasia which was responsible for the late-Palaeozoic orogenies in Europe and North America.

7.6.2   Late Palaeozoic structure and history

The Maritime Disturbance is confined mainly to the shaded zones depicted in Figure 7.4, although some Carboniferous volcanic activity is also recorded at scattered locations in central New Brunswick and on the Magdalen Islands near the center of the Gulf of St. Lawrence.   One of the puzzling aspects of Canadian Maritime Appalachian geology is the lack of strong, widespread Permo-Carboniferous tectonic activity.   Except possibly along the north shore of the Bay of Fundy where Rast and Grant (1973) provide evidence of a Carboniferous structural front, there seems to be no significant Hercynian folding, thrusting or granitic intrusion similar to that found in southern England or southern Ireland.   Several authors (e.g. Cherkis et al.,1973) have drawn the Hercynian front as passing through central Newfoundland and along the north shore of the Bay of Fundy but in view of the general lack of strong Hercynian activity, it seems more likely that the Hercynian structural front, which is recognized in the southern and central Appalachians south of the line C-C' near New York City (Figure 7.4), continues out to sea and, as will be discussed later, may pass through the Scotian Shelf.

The rift zone of strike-slip faulting which passes northwest through the Gulf of Maine, the Bay of Fundy, Georges Bay and White Bay, Newfoundland may have decoupled southern Nova Scotia and the greater part of Newfoundland from the remainder of the Canadian

Maritime Appalachians and allowed the former areas to act as competent

blocks while being jostled around during the Hercynian orogeny. Central

and eastern Newfoundland, the Grand Banks and possibly Spain and

Portugal (Figure 7.4) probably formed one continental block. Southern

Nova Scotia, the southern Scotian Shelf and possibly Morocco formed a

second block which was decoupled from the first by the fault zone

running eastward from the Minas Basin through Chedabucto Bay and along

the southern margin of the Grand Banks and through what is now the

Strait of Gibraltar. At some time during the Carboniferous Period,

dextral strike-slip motion along the Minas Basin-Chedabucto Bay fault

zone could have brought thrusting to bear along the north shore of

the Bay of Fundy to explain the geological observations by Rast and

Grant (1973) of a structural front in southeastern New Brunswick.

Such movement may have been contemporaneous with dextral motion

along the South Atlas Fault (SAF in Figure 7.4) which produced thrust-

ing in the southern Appalachians (Badham and Halls, 1975).

If Morocco, Portugal, France and southern England and Ireland

were affected by the Hercynian orogeny we would expect at least the

outer edges of the Scotian Shelf and the Grand Banks to show some

evidence of Hercynian deformation. In this respect it is worthwhile

to remember as Hood (1966) pointed out, the Meguma trends appear to

be truncated along the dot-dash line in Figure 7.3 and, probably even

more significantly, Permo-Carboniferous radiometric age dates are

reported from basement rocks drilled on the Scotian Shelf (Figure 7.4)

(M. Given, personal communication).

In view of the general lack of a strong compressional environ-

ment associated with the Maritime Disturbance (Poole, 1967) there seems to be no compelling reason to postulate a Hercynian structural front anywhere in the Canadian Maritimes, but, if one does, it certainly seems more desirable to joint up the Alleghenian Front in the southern Appalachians to the Hercynian Front in southern Ireland and England by passing the front through the southern Scotian Shelf (and the Grand Banks area) rather than through Newfoundland. Such a structural front might run approximately parallel to the continental margin to the northwest of the drill hole sites on the Southern Scotian Shelf (Figure 7.4). If so, the Middle Bank Low could be produced, as mentioned in Chapter 5, by a Hercynian granite similar to those in southwest England but different in that the Middle Bank granite is magnetic whereas the Carboniferous granites in Devon and Cornwall are non-magnetic (although there are well developed magnetic halos at their margins).

Generally speaking, one of the main characteristics of much of the Hercynian tectonic activity in the Canadian Maritime Appalachians is that it seems to have occurred along pre-existing zones of weakness which were formed in Siluro-Devonian times or earlier. This includes the Minas Basin-Chedabucto Bay-Orpheus fault zone which was probably initiated in Siluro-Devonian times and which was subsequently re-activated.

Although the fault zone along which the Orpheus Graben is presently situated was active during the late Palaeozoic it is not clear when the Orpheus Graben itself was created. A Permo-Carboniferous age of formation is not unreasonable in view of the possible link between the Orpheus Graben and the rift zones of the Maritime Disturbance. The scissors-like movement described in Chapter

6 could have taken place at this time, providing tension east of

Chedabucto Bay and compression in the Bay of Fundy but the tensional

forces which produced the Orpheus Graben may have only occurred later

when Africa and North America separated in the Mesozoic Era.

7.6.3   Mesozoic structure and history

The only Mesozoic rocks found on the land areas adjacent to

the Scotian Shelf are the Triassic conglomerates, sandstones and

basalts along the edges of the Bay of Fundy and the Minas Basin, a

small patch of Triassic sedimentary rocks near Chedabucto Bay and a

Triassic dike in southern Nova Scotia.   A second dike, interpreted

from aeromagnetic data over the Avalon Peninsula (Figure 7.3) may also

have been emplaced during the Triassic Period (Papezik et al., 1975).

On the other hand, seismic profiling and drilling have revealed exten-

sive deposits of Mesozoic (and younger) sedimentary rocks on the Scotian

Shelf and an up-to-date review of Mesozoic structure and history of

the Scotian Shelf has recently been presented by Jansa and Wade (1975).

The highlights of their discussion will be given here after first

discussing the Orpheus Graben.

The extrusion of basalt and the formation of dikes indicate a

tensional environment during the Triassic period which may also have

produced the Orpheus Graben.   The Orpheus Graben was almost certainly

in existence during the early Jurassic due to the presence of lower

Jurassic (?) Argo salt (Jansa and Wade, 1975) therefore a Triassic age

of initial formation seems reasonable.   An earlier, Permian or Carboni-

ferous age of initial formation is also possible since Carboniferous

sedimentary rocks may be present at depth but the Orpheus Graben is

distinct from Carboniferous basins in Nova Scotia and New Brunswick in that the mass deficiency of the sedimentary rocks in the Orpheus Graben depresses the gravity field to values of the order of -40 to -50 mgals whereas negative anomalies over known Carboniferous basins (where younger sedimentary rocks were either not deposited or subsequently preserved) are only of the order of -15 to -20 mgals. The more depressed gravity field over the Orpheus Graben is consistent with the presence of lower Jurassic salt and other less compacted, post-Carboniferous rocks. If the Orpheus Graben were formed during Permo-Carboniferous times, active subsidence and deposition must have continued during the Triassic and Jurassic periods. Subsequent tectonic activity seems to have tapered off, however, as only a limited amount of upper Jurassic and lower Cretaceous sedimentary rocks are present in the stratigraphic section in the Orpheus Graben (Jansa and Wade, 1975).

As mentioned in Chapter 4, 5 and 6, the crystalline basement rocks of the Scotian Shelf are overlain by quite thick sequences of sedimentary rocks. The Sydney Basin occupies much of the northern Scotian Shelf, the Orpheus Graben cuts through the central Shelf and the Scotian Basin runs along the southern Scotian Shelf attaining its maximum depth beneath the continental slope. Jansa and Wade (1975) recognized two sub-basins in the southern Scotian Shelf, the Sable Sub-Basin southwest of Sable Island and the Abenaki Sub-Basin to the northeast. According to Jansa and Wade (1975), sedimentation in the deeper basins or sub-basins was more or less continuous since the late Triassic after a late Permian-early Triassic hiatus in deposition.

The thickest Triassic deposits occur in the Bay of Fundy where some

4 km of conglomerate, shale, etc. were laid down. A definite Triassic-

Jurassic boundary has not yet been established but some 3 km of pre-

sumably Jurassic salt and another 3 km of Jurassic carbonates and

clastics occur within the Abenaki Sub-Basin in the area to the south-

east of Profile P-P' (Figure 6.2). The details of the sediment accu-

mulation in the Sable Sub-Basin are not well known but approximately 3

km of Cretaceous sandstone and siltstone occur in both the Sable and

Abenaki Sub-Basins. Tertiary and younger mudstones attain a maximum

thickness of about 1.5 km near the edge of the Scotian Shelf.

Jansa and Wade (1975) point out that the geological history of

the Scotian Basin is very similar to the Essaouira Basin in Morocco

and that these features could have been part of the same basinal system.

The geological and geophysical data from the Scotian Shelf do not allow

an exact dating of the initiation of sea-floor spreading but Jansa and

Wade (1975) favour an early Jurassic age. The Iberian Peninsula and

the Grand Banks region probably remained connected until the early

Cretaceous when a regional uplift of the Grand Banks was followed

by a marine transgression and a change in faunal affinities from

European to Gulf Coast suggests the creation of a waterway between

the Grand Banks and Portugal.

During the separation of Africa from North America, faults

sub-parallel to the continental margin were initiated or reactivated.

One of the main northeast trending fault zones shows up as a basement

hinge zone passing southeast of Emerald Bank, Middle Bank and Misaine

Bank (Figure 1.1). This hinge zone, which shows up in the seismic

section in Figure 5.8, controlled the deposition of lower to middle

Jurassic sediments. Late Cretaceous or possibly Tertiary, faulting occurred on the Scotian Shelf along a sinuous line running southeast of La Have and Emerald Banks somewhat to the seaward side of the basement hinge zone. There are probably several sets of faults between the basement hinge zone and the continental margin but the basement is too deeply buried for these to show up with the presently available seismic data (J. Wade, personal communication).

One final comment in connection with the opening of the present day Atlantic Ocean is that it is interesting to note that the positions of some oceanic structural features seem to be related to pre-existing tectonic features. For example, in Figure 7.4 the Kelvin Seamount Chain (KS) lies on strike with the South Atlas Fault (SAF), the Newfoundland fault zone (NFZ) connects up with the Minas Basin - Chedabucto Bay - Orpheus Fault Zone and the Gibbs Fracture Zone (GFZ) is near the northern limit of the Avalon Platform.

APPENDIX 1

PROGRAM SPECIFICATIONS FOR MGTRAN

'URPOSE: To calculate the direction of total magnetization in an anomalous

body and the ratio of magnetization contrast of density contrast under

the assumptions that the direction of magnetization is uniform throughout

the body and that the magnetization contrast is proportional to density

contrast.

UCTURE: The main program, MGTRAN, is subdivided into four sections:

The first section reads in the required data.

The second section calculates the direction of the total

magnetization vector and the ratio of magnetization contrast to density

contrast and standard deviations of these quantities. It does this by

generating pseudo-magnetic anomalies from the gravity anomaly using an

equivalent layer of matter, for the three cases where the direction of

total magnetization in the equivalent layer is in the x, y and z direction

respectively. The observed magnetic field is then expressed, by the

method of least squares, as a linear combination of the three pseudo-

magnetic anomalies; the direction of magnetization and the ratio of

magnetization contrast to density contrast are then obtained from the

three coefficients multiplying the pseudo-magnetic anomalies.

The third section calculates the same quantities as the second

section but it does it in a reverse manner by generating pseudo-gravity

anomalies from the magnetic field and fitting the pseudo-gravity anomalies

to the observed gravity field. This latter procedure generally does not

give as good results as the one in the second section and could be omitted if desired.

The fourth section checks the results obtained in the second and third sections and calls a subroutine which calculates virtual geomagnetic poles corresponding to the directions of magnetization obtained.

Subroutine COEFF and CG3D calculate the gravitational and magnetic attractions of rectangular prisms according to a suggestion by Goodacre (1973).

It is necessary on several occasions during the execution of the program MGTRAN to express one quantity as a linear combination of other quantities. Subroutine MULREG is a multiple regression (see e.g. Draper and Smith, 1966) program which calculates the required coefficients (and their standard deviations) according to the method of least squares. In order to save computer time and space the program uses a modified Doolittle method (e.g. Goulden, 1952) which makes use of the fact that the matrix of coefficients of the normal equations is symmetric.

Subroutine POLE uses equations from Cox and Doell (1960) to calculate the position of the pole of a dipolar geomagnetic field which would induce a specified direction of magnetization at a given location.

INPUT DATA

DIMENSIONS

distances	= kilometers
density contrast	= grams per cubic centimeter
magnetization contrast	= e.m.u. per cubic centimeter
angles	= degrees
gravity anomalies	= milligals
magnetic anomalies	= gammas

FORMATS

– input mode card –

IP – input parameter specifies whether gravity and magnetic field observation

points are different (0) or the same (1) FORMAT I10

– number of observations and prisms –

for case IP = 0 (locations different) NSG, NBG, NSM, NBM, FORMAT (4I10)

for case IP = 1 (locations same) NSM, NBM, FORMAT (2I10)

NSG = no. of gravity observations

NSM = no. of magnetic observations

NBG = no. of prisms needed to generate gravity field

NBM = no. of prisms needed to generate magnetic field

– gravity and magnetic data cards –

for case IP = 0 (locations different)

NSG cards

GOBS, XG, YG, ZG, INDEX1

FORMAT (4 (F 10.4), 30 X, I10)

NSM cards

MOBS, XM, YM, ZM, INDEX2

FORMAT (4 (F 10.4), 30 X, I10)

for case IP=1 (locations same)

NSM cards

GOBS, MOBS, XM, YM, ZM, INDEX2

FORMAT (5 (F 10.4), 20 X, I10)

explanation of parameters

GOBS = observed gravity anomaly

MOBS = observed magnetic anomaly

XG, YG, ZG = x, y, z coordinates of gravity anomaly

XM, YM, ZM = x, y, z coordinates of magnetic anomaly

INDEX1, INDEX2 = integer labels

- direction of measurements of magnetic field card -

EINC, EAZI

FORMAT (2 (F10.4))

INC = inclination (positive downwards)

AZI = azimuth (with respect to y-axis)

(if total field anomalies are used, these

quantities refer to direction of earth's

field.)

- locations of equivalent layer prisms -

for case IP = 0 (locations different)

NBG cards

CBGX, CBGY, DBGZ, INDEX3

FORMAT (3 (F 10.4), 40X, I10)

CBMX, CBMY, DBMZ, INDEX4

FORMAT (3 (F 10.4), 40X, I10)

for case IP=1 (locations same)

NBM cards

CBMX, CBMY, DBMZ, INDEX4

FORMAT (3 (F 10.4), 40X, I 10)

explanation of parameters

CBGX, CBGY = x, y coordinates of centers of gravitating

equivalent layer prisms

- prism size card -

DELX, DELY, DELZ

FORMAT (3 (F 10.4))

DELX, DELY = length and width of each prism

DELZ = height of prism.

- location of anomaly card -

ALAT, ALONG

FORMAT (2 (F 10.4))

ALAT = latitude of anomaly

ALONG = longitude of anomaly

OUTPUT DATA

The headings in the output listing are self-explanatory but it should be noted that the quantity labeled CORR COEFF is the multiple regression correlation coefficient squared.

325

```
      PROGRAM MGTRAN(INPUT,OUTPUT,TAPE7,TAPE5=INPUT,TAPE6=OUTPUT)
C     COMBINED 3-D ANALYSIS OF GRAVITY AND MAGNETIC ANOMALIES
C     *** IMPORTANT--- NO. OF OBSERVATIONS MUST EXCEED
C     NO. OF BODIES BY AT LEAST ONE ***
C     NO = NO. OF OBSERVATIONS
C     NP = NO. OF BODIES(PRISMS)
      REAL MOBS,MCOMPG,MCOMPM,MCOMPZ,MCOMPX,MCOMPY
      DIMENSION GOBS(100),MOBS(100)
      DIMENSION XM(100),YM(100),ZM(100),XG(100),YG(100),ZG(100)
      DIMENSION CBMX(100),CBMY(100),CBMZ(100),CBGX(100),CBGY(100),
     1CBGZ(100)
      DIMENSION CONSG(4),TTG(4),CONSM(4),TTM(4)
      DIMENSION GCOMPM(100),GCOMPG(100),MCOMPG(100),MCOMPM(100)
      DIMENSION MCOMPZ(100),MCOMPX(100),MCOMPY(100)
      DIMENSION RESG(100),RESG1(100),RESG2(100)
      DIMENSION RESM(100),RESM1(100),RESZ(100),RESX(100),RESY(100)
      DIMENSION TTG2(100),TTM2(100),TTMX(100),TTMY(100),TTMZ(100)
      DIMENSION INDEX1(100),INDEX2(100),INDEX3(100),INDEX4(100)
      DIMENSION GINC(3),GAZI(3)
      DIMENSION BMIN(3),BMAZ(3),BMAGSX(100),
     1BMAGSY(100),BMAGSZ(100),BDENS(100)
C     DIMENSIONS OF BMFMMZ,ETC. BMFMGZ,ETC.ARE NO*NP
      DIMENSION BMFMGZ( 550),BMFMGX( 550),BMFMGY( 550)
      DIMENSION BMFMMZ( 550),BMFMMX( 550),BMFMMY( 550)
C     DIMENSIONS OF CFMGG,CFGMM ARE NO*3
      DIMENSION CFMGG(300),CFGMM(300)
C     DIMENSIONS OF AMAG,RHO MUST BE AS IN SUBR. COEFF
C     DIMENSIONS OF BMAGS,DENS MUST BE AS IN SUBR. COEFF
      DIMENSION AMAG(22,3),RHO(22,3),BMAGS(22,3),DENS(22,3)
C     DIMENSIONS OF BMFMM,BMFMG MUST BE AS IN SUBR. COEFF
      DIMENSION BMFMM(30,22,3),BMFMG(30,22,3)
C     DIMENSION OF BGFGG MUST BE AS IN SUBR. COEFF
      DIMENSION BGFGG(30,22,3)
      DIMENSION VLAT(2),VLONG(2),ALAT(2),ALONG(2),AMIN(2),AMAZ(2)
      COMMON AMAG,RHO,BMFMM,BMFMG
      EQUIVALENCE (BGFGG,BMFMG)
      EQUIVALENCE(BMFMMZ(1),BMFMM(1,1,1)),(BMFMMX(1),BMFMM(1,1,2)),
     1(BMFMMY(1),BMFMM(1,1,3)),(BMFMGZ(1),BMFMG(1,1,1)),
```

```
    2 (BMFMGX(1),BMFMG(1,1,2)),(BMFMGY(1),BMFMG(1,1,3))
      EQUIVALENCE (RHO,DENS)
      EQUIVALENCE(RESM1,RESG1),(TTM2,TTG2),(BMAGSZ,BDENS),(RESG,RESM),
    1 (TTMZ,RESZ),(TTMX,RESX),(TTMY,RESY)
  101 FORMAT(I10)
  102 FORMAT(2I10)
  103 FORMAT(5(F10.4),20X,I10)
  104 FORMAT(4I10)
  105 FORMAT(4(F10.4),30X,I10)
  106 FORMAT(3(F10.4),40X,I10)
  200 FORMAT(1X,3(F15.7))
  201 FORMAT(1X,6(F15.7,1X),I10)
  202 FORMAT(1X,5(F15.7,1X),I10)
  203 FORMAT(1X,(F20.8))
  204 FORMAT(1X,9(F12.6,1X),I10)
  205 FORMAT(1X,10(F11.6,1X),I10)
  206 FORMAT(1X,2(F15.7,1X),I10)
  207 FORMAT(1X,7F15.2,I10)
  208 FORMAT(6(F10.4),10X,I10)
  298 FORMAT(1H1)
  299 FORMAT(1H0)
  900 FORMAT(1X,"RESULTS OF MAGNETIC TO GRAVITY TRANSFORMATION"//)
  901 FORMAT(3X,"OBS.G",6X,"COMP.G",5X,"RES.",5X,"XG",5X,"YG",5X,"ZG",5X
     1,"STN. NO."//)
  902 FORMAT(3X,"COEFFS",5X,"T-VALUES"//)
  903 FORMAT(1X,"CORR COEFF",1X,"F-VALUE",1X,"STD ERROR"/)
  904 FORMAT(1X,"AZIMUTH  INCLINATION  RATIO RHO/MAGN"//)
  905 FORMAT(1X,"DENSITY VALUES  T-VALUES   CBGX CBGY DBGZ*-1  BODY NO."
     1//)
  906 FORMAT(1X,"RESULTS OF GRAVITY TO MAGNETIC TRANSFORMATION"//)
  907 FORMAT(1X,"AZIMUTH  INCLINATION  RATIO  MAGN/RHO"//)
  908 FORMAT(1X,"CHECK GRAVITY TO MAGNETIC TRANSFORMATION"//)
  909 FORMAT(1X,"R.M.S. RESIDUAL GAMMA"/)
  910 FORMAT(1X,"R.M.S. RESIDUAL MILLIGAL"/)
  911 FORMAT(1X,"MAGN-Z,T-VALUE MAGN-X,T-VALUE MAGN-Y,T-VALUE
     1CBMX,CRMY,DBMZ*-1, BODY NO."/)
  912 FORMAT(1X,"OBS.M COMPM-Z,RES COMPM-X,RES COMPM-Y,RES
     1XM YM ZM   STN. NO."//)
```

```
  913 FORMAT(1X,"CHECK MAGNETIC TO GRAVITY TRANSFORMATION"//)
  914 FORMAT(1X,"VALUES ARE FOR Z,X,ANDY-COMPONENTS"//)
  915 FORMAT(3X,"OBS.M",6X,"COMP.M",5X,"RES.",5X,"XM",5X,"YM",5X,"ZM",5X
     1,"STN. NO."//)
  916 FORMAT(1X,"     DELAZ,DELIN,DELRATIO"/)
  917 FORMAT(1X,"ANGLE BETWN. EARTHS FIELD AND TOTAL MAGN. VECTOR"//)
  918 FORMAT(1X,"Q-MINIMUM"//)
  919 FORMAT(1X," MEAN VALUE OF GOBS  MOBS"//)
  920 FORMAT(1X," BACKGROUND GRAVITY "//)
  921 FORMAT(1X," DELX  DELY  DELZ  "//)
  922 FORMAT(1X," OBS.M.  XM  YM  ZM  STN. NO."//)
      ********* THIS PORTION READS IN REQUIRED DATA
      READ(5,101)IP
C
C        IF IP = 0  MAGNETIC AND GRAVITY FIELD POINTS ARE DIFFERENT
C        IF IP N.EQ. 0                           POINTS ARE SAME
      IF (IP) 301,302,301
  301 READ(5,102)NSM,NBM
      NBG = NBM
      NSG = NSM
C        NSM = NO. MAG FIELD PTS  NBM = NO. MAG BODIES
C        NSG = NO.GRAV FIELD PTS  NBG = NO.GRAV BODIES
      DO 305 J=1,NSM
      READ(5,103)GOBS(J),MOBS(J),XM(J),YM(J),ZM(J),INDEX2(J)
      INDEX1(J) = INDEX2(J)
C        INDEX1,INDEX2 = INTEGER LABELS TO IDENTIFY GRAV AND MAG VALUES
  305 CONTINUE
C        GOBS = OBS GRAVITY  MOBS = OBS MAGNETIC ANOMALIES
C        XM , YM , ZM  ARE FIELD POINT COORDINATES  THESE  ARE THE SAME
C                    FOR  BOTH THE GRAVITY AND MAGNETIC ANOMALIES
      DO 306 J=1,NSM
      XG(J) = XM(J)
      YG(J) = YM(J)
      ZG(J) = ZM(J)
  306 CONTINUE
      GO TO 3308
  302 READ(5,104)NSG,NBG,NSM,NBM
      DO 307 J=1,NSG
```

```
      READ(5,105)GOBS(J),XG(J),YG(J),ZG(J),INDEX1(J)
  307 CONTINUE
      DO 308 J=1,NSM
      READ(5,105)MOBS(J),XM(J),YM(J),ZM(J),INDEX2(J)
  308 CONTINUE
 3308 CONTINUE
C
      READ INCL + AZIM OF EARTHS FIELD AND BODY MAGN VECTOR
      READ(5,105)EINC,EAZI,VMIN,VMAZ
      DO 1001 L=1,3
      GINC(L) = EINC
      GAZI(L) = EAZI
 1001 CONTINUE
C     EAZI  =   AZIMUTH     OF EARTHS FIELD
C     VMIN  =   INCLINATION  OF BODY MAGNETIZATION VECTOR
C     VMAZ  =   AZIMUTH     OF BODY MAGNETIZATION VECTOR
C     INCLINATION VARIES FROM -90   TO +90   DEGREES
C     AZIMUTH  VARIES FROM   0   TO 360  DEGREES
C     A POSITIVE INCLINATION MEANS VECTOR IS POINTING INTO GROUND
C     AZIMUTHS ARE TAKEN CLOCKWISE FROM + Y AXIS
C     Y AXIS  CAN POINT IN ANY DIRECTION BUT FOR CONVENIENCE CAN
C            POINT NORTH(TRUE)
C     READ X Y  COORDINATES OF VERTICAL CENTRAL AXES IN PRISMS AND
C            DEPTHS OF TOPS OF PRISMS
      IF (IP) 311,312,311
  311 DO 315 K=1,NBM
      READ(5,106)CBMX(K),CBMY(K),DBMZ(K),INDEX4(K)
      INDEX3(K) = INDEX4(K)
C     INDEX3,INDEX4 = LABELS TO IDENTIFY PRISMS USED TO CONSTRUCT
C     GRAV AND MAG EQUIVALENT LAYERS
  315 CONTINUE
      DO 316 K=1,NBM
      CBGX(K)= CBMX(K)
      CBGY(K)= CBMY(K)
      DBGZ(K)= DBMZ(K)
  316 CONTINUE
      GO TO 3318
  312 DO 317 K=1,NBG
      READ(5,106)CBGX(K),CBGY(K),DBGZ(K),INDEX3(K)
```

```
  317 CONTINUE
      DO 318 K=1,N3M
      READ(5,106)CBMX(K),CBMY(K),DBMZ(K),INDEX4(K)
  318 CONTINUE
 3318 CONTINUE
      DO 319 K=1,N3G
      DBGZ(K) = -DBGZ(K)
  319 CONTINUE
      DO 320 K=1,NBM
      DBMZ(K) = -DBMZ(K)
  320 CONTINUE
C         READ LENGTH WIDTH AND HEIGHT OF PRISMS (ALL PRISMS HAVE SAME
C             DIMENSIONS BUT DIFFERENT LOCATIONS)
      READ(5,106)DELX,DELY,DELZ
      WRITE(6,921)
      WRITE(6,200)DELX,DELY,DELZ
      WRITE(6,299)
      WRITE(6,299)
      DELX = DELX/2.
      DELY = DELY/2.
C         READ CENTRAL LAT AND LONG OF ANOMALY FOR USE IN CALCULATION
C             OF VIRTUAL GEOMAGNETIC POLE
      READ(5,106)ALAT(1),ALONG(1)
C         REGG,REGM = MEAN VALUES OF OBS GRAV AND MAG ANOMALIES
      QNSG = NSG
      REGG = 0.0
      DO 4001 J=1,NSG
      REGG = REGG + GOBS(J)
 4001 CONTINUE
      REGG = REGG/QNSG
      QNSM = NSM
      REGM = 0.0
      DO 4002 J=1,NSM
      REGM = REGM + MOBS(J)
 4002 CONTINUE
      REGM = REGM/QNSM
      DO 4003 J=1,NSG
 4003 GOBS(J) = GOBS(J) - REGG
```

```
      DO 4004 J=1,NSM
 4004 MOBS(J) = MOBS(J) - REGM
      WRITE(6,919)
      WRITE(6,206)REGG,REGM
C     ********** THIS PORTION CALCULATES A ***BEST - FITTING***
C               MAGNETIC ANOMALY FROM THE GRAVITY ANOMALY
C     COMPUTE GRAVITATIONAL ATTRACTION (Z-COMPONENT) OF PRISMS OF
C               UNIT DENSITY
      DO 501 K=1,NBG
      RHO(K,1) = 1.0
      AMAG(K,1) = 1.0
  501 CONTINUE
      BMIN(1)= 90.0
      BMAZ(1)= 0.0
      BMIN(2)= 0.0
      BMAZ(2)= 90.0
      BMIN(3)= 0.0
      BMAZ(3)= 0.0
      CALL COEFF(NSG,NBG,1,CBGX,CBGY,DBGZ,DELX,DELY,DELZ,XG,YG,ZG,GINC,
     1 GAZI,BMIN,BMAZ)
C          TO SAVE SPACE WE USE BMFMGZ INSTEAD OF BGFGGZ
      DO 502 K=1,NBG
      DO 502 J=1,NSG
      JJJ = (K-1)*NSG + J
      BMFMGZ(JJJ) = BGFGG(J,K,1)
  502 CONTINUE
      LBG = NBG + 1
      CALL MULREG(BMFMGZ,GOBS,NSG,LBG,GCOMPG,BDENS,SEG2,CORRG2,FTG2,TTG2
     1 )
C          SEE MULREG FOR EXPLANATION OF ARGUMENTS
      WRITE(6,901)
      DO 601 J=1,NSG
      RESG2(J) = GOBS(J) - GCOMPG(J)
      GOBS(J) = GOBS(J) + REGG
      GCOMPG(J) = GCOMPG(J) + REGG
C          GCOMPG = GRAVITY VALUE GENERATED BY EQUIVALENT LAYER
      WRITE(6,201)GOBS(J),GCOMPG(J),RESG2(J),XG(J),YG(J),ZG(J),INDEX1(J)
```

```
      WRITE(7,208)GOBS(J),GCOMPG(J),RESG2(J),XG(J),YG(J),ZG(J),INDEX1(J)
C     LOGICAL UNIT 7 PROVIDES PUNCH CARD OUTPUT
      GOBS(J) = GOBS(J) - REGG
      GCOMPG(J) = GCOMPG(J) - REGG
  501 CONTINUE
      WRITE(6,299)
      WRITE(6,920)
      ABC = BDENS(LBG) + REGG
C     ABC IS BACKGROUND GRAVITY CALCULATED BY MULREG
      WRITE(6,200)ABC
      WRITE(6,299)
      WRITE(6,299)
      WRITE(6,905)
      DO 602 K=1,NBG
      WRITE(6,202)BDENS(K),TTG2(K),CBGX(K),CBGY(K),DBGZ(K),INDEX3(K)
C     BDENS = DENSITY OF PRISM
C     TTG2 = T-VALUE OF QUANTITY BDENS
C     T-VALUE.GT.2 INDICATES BDENS IS SIGNIFICANT
  602 CONTINUE
      WRITE(6,299)
      WRITE(6,299)
      WRITE(6,299)
      WRITE(6,903)
      WRITE(6,200)CORRG2,FTG2,SEG2
C     CORRG2 = MULTIPLE CORRELATION COEFFICIENT SQUARED
C     (I.E. CORRELATION BETWEEN OBS AND COMP FIELDS)
C     FTG2 = F-VALUE OF FIT BETWEEN OBS AND COMP GRAVITY VALUES
C     SEG2 = STANDARD ERROR OF FIT
      WRITE(6,299)
      WRITE(6,299)
C     COMPUTE MAGNETIC ANOMALIES FOR MAGNETIZATION VECTOR LYING IN
C     X  Y  AND  Z  DIRECTIONS
      DO 603 K=1,NBG
      DENS(K,1) = BDENS(K)
      DENS(K,2) = BDENS(K)
      DENS(K,3) = BDENS(K)
      AMAG(K,1) = DENS(K,1)
      AMAG(K,2) = DENS(K,2)
```

```
        AMAG(K,3) = DENS(K,3)
603 CONTINUE
        CALL COEFF(NSM,NBG,3,CBGX,CBGY,DBGZ,DELX,DELY,DELZ,XM,YM,ZM,GINC,
     1 GAZI,BMIN,BMAZ)
C       TO SAVE SPACE WE USE BMFMM AND BMFMG INSTEAD OF BGFMM , BGFMG
        NNNN = 3*NSM
        DO 607 JJJ=1,NNNN
        CFGMM(JJJ) = 0.0
607 CONTINUE
        DO 608 L=1,3
        DO 608 J=1,NSM
        DO 608 K=1,NBG
        JJJ = (L-1)*NSM + J
        CFGMM(JJJ) = CFGMM(JJJ) + BMFMM(J,K,L)
608 CONTINUE
C       USE MULREG TO APPROXIMATE OBS MAG FIELD BY A LINEAR COMBINATION
C       OF THE MAGNETIC FIELDS PRODUCED BY EQUIVALENT LAYERS WHOSE
C       MAGNETIZATIONS LIE IN X Y AND Z DIRECTIONS RESPECTIVELY
        CALL MULREG(CFGMM,MOBS,NSM,4,MCOMPG,CONSM,SEM,CORRM,FTM,TTM)
C       OPTIONAL DO-LOOP TO OUTPUT OBS MAG FIELD AND (UNSCALED) MAG
C       FIELDS PRODUCED BY 3 EQUIV LAYERS (MAGNS IN X Y AND Z DRNS)
C       WRITE(6,922)
C       DO 4005 J=1,NSM
C       JA = NSM + J
C       JAA = 2*NSM + J
C       RESZ(J) = MOBS(J) - CFGMM(J)
C       RESX(J) = MOBS(J) - CFGMM(JA)
C       RESY(J) = MOBS(J) - CFGMM(JAA)
C       MOBS(J) = MOBS(J) + REGM
C       CFGMM(J) = CFGMM(J) + REGM
C       CFGMM(JA) = CFGMM(JA) + REGM
C       CFGMM(JAA) = CFGMM(JAA) + REGM
C       WRITE(6,207)MOBS(J),CFGMM(J),CFGMM(JA),CFGMM(JAA),XM(J),YM(J),
C     1 ZM(J),INDEX2(J)
C       MOBS(J) = MOBS(J) - REGM
C       CFGMM(J) = CFGMM(J) - REGM
C       CFGMM(JA) = CFGMM(JA) - REGM
C       CFGMM(JAA) = CFGMM(JAA) - REGM
```

```
C4005 CONTINUE
      WRITE(6,299)
      WRITE(6,299)
      WRITE(6,906)
      WRITE(6,915)
      DO 650 J=1,NSM
      RESM(J)= MOBS(J) - MCOMPG(J)
      MOBS(J) = MOBS(J) + REGM
      MCOMPG(J) = MCOMPG(J) + REGM
      WRITE(6,201)MOBS(J),MCOMPG(J),RESM(J),XM(J),YM(J),ZM(J),INDEX2(J)
      WRITE(7,208)MOBS(J),MCOMPG(J),RESM(J),XM(J),YM(J),ZM(J),INDEX2(J)
      MOBS(J) = MOBS(J) - REGM
      MCOMPG(J) = MCOMPG(J) - REGM
  550 CONTINUE
      WRITE(6,299)
      WRITE(6,299)
      WRITE(6,299)
      WRITE(6,902)
      DO 651 L=1,4
      WRITE(6,206)CONSM(L),TTM(L),L
C     CONSM(1),CONSM(2),CONSM(3) = X,Y,Z DIRECTION COSINES OF MAGN
C     VECTOR MULTD BY RATIO OF MAGN CONTRAST TO DENSITY CONTRAST
C     CONSM(4) = BACKGROUND LEVEL - REGM
C     TTM = T-VALUES OF CONSM(1) TO CONSM(3)
C     TTM(4) IS AN ARBITRARY NUMBER
  651 CONTINUE
      WRITE(6,299)
      WRITE(6,299)
      WRITE(5,903)
      WRITE(6,200)CORRM,FTM,SEM
C     CORRM = MULTIPLE CORRELATION COEFF SQUARED
C     (I.E. CORRELATION BETWEEN OBS AND COMP FIELDS)
C     FTM = F-VALUE OF FIT BETWEEN OBS AND CALC MAG FIELDS
C     SEM = STANDARD ERROR OF FIT
      WRITE(6,299)
      WRITE(6,299)
C     COMPUTE RATIO OF MAGN TO DENSITY , INCLINATION AND  AZIMUTH
C       OF MAGNETIZATION VECTOR
```

```
      CDCLGM = ATAN2(CONSM(2),CONSM(3))
      CDCLGM = CDCLGM*57.296
      RATIO2 = SQRT(CONSM(1)*CONSM(1)+CONSM(2)*CONSM(2)+CONSM(3)*CONSM(
     1 3))
      CINCGM = ASIN(CONSM(1)/RATIO2)
      CINCGM = CINCGM*57.296
      WRITE(6,907)
      WRITE(6,201)CDCLGM,CINCGM,RATIO2
      WRITE(6,299)
C     CALCULATE ANGLE BTWN EARTHS FIELD AND TOTAL MAGN. VECTOR
      CCC2 = SIN(CINCGM/57.296)*SIN(EINC/57.296) +
     1 COS(CINCGM/57.296)*COS(EINC/57.296)*COS((EAZI-CDCLGM)/57.296)
      BETA2 = ACOS(CCC2)
      BETA2 = BETA2*57.296
      WRITE(6,917)
      WRITE(6,203)BETA2
      WRITE(6,299)
      IF(CCC2)1015,1016,1016
 1015 AAO2 = 1.0
      GO TO 1017
 1016 AAO2 = SORT(1.0 - CCC2*CCC2)
 1017 CONTINUE
      WRITE(5,918)
      WRITE(6,203)AAQ2
      WRITE(6,299)
      DELIN2 = CONSM(1) /(TTM(1)*SQRT(RATIO2*RATIO2-CONSM(1)*CONSM(1)))
      DELIN2 = DELIN2*57.296
      DELAZ2 = (CONSM(3)*CONSM(2)/(CONSM(3)*CONSM(3)+CONSM(2)*CONSM(2)))
     1 *SQRT(1.0/(TTM(3)*TTM(3)) + 1.0/(TTM(2)*TTM(2)))
      DELAZ2 = DELAZ2*57.296
      ZZ1 = CONSM(1)*CONSM(1)/TTM(1)
      ZZ2 = CONSM(2)*CONSM(2)/TTM(2)
      ZZ3 = CONSM(3)*CONSM(3)/TTM(3)
      DRAT2 = (SORT (ZZ1*ZZ1+ZZ2*ZZ2+ZZ3*ZZ3)) /RATIO2
      WRITE(6,916)
      WRITE(6,201)DELAZ2,DELIN2,DRAT2
C     STANDARD DEVIATIONS (67 PER CENT ERROR LIMITS) OF AZIMUTH
C     AND INCLINATION OF MAGNETIZATION VECTOR AND RATIO OF MAGN CONTRAST
```

```
C          TO DENSITY CONTRAST
           WRITE(6,299)
           WRITE(6,298)
C     **************************************************
C     ************* THIS PORTION CALCULATES A """BEST - FITTING"""
C                   GRAVITY ANOMALY FROM THE MAGNETIC ANOMALY
C                   MANY OF THE VARIABLE NAMES CORRESPOND CLOSELY
C                   OR EXACTLY WITH THOSE IN PREVIOUS SECTION

           BMIN(1) = 90.
           BMAZ(1) = 0.
           BMIN(2) = 0.
           BMAZ(2) = 90.
           BMIN(3) = 0.
           BMAZ(3) = 0.
C          BMIN , BMAZ  ARE INCLS AND AZIMS OF BODY MAGNETIZATION VECTORS
C                   WHICH POINT ALONG X , Y , Z  AXES
           DO 801 K=1,NBM
           DO 801 L=1,3
           AMAG(K,L) = 1.0
           RHO(K,L) = 1.0
801 CONTINUE
C          THE PRECEEDING LOOP PROVIDES STANDARD MAGNETIZATION  AND
C                   DENSITY CONTRAST VALUES
           CALL COEFF(NSM,NBM,3,CBMX,CBMY,CBMZ,DBMX,DBMY,DBMZ,DELX,DELY,DELZ,XM,YM,ZM,GINC,
          1 GAZI,BMIN,BMAZ)
           DO 802 K=1,NBM
           DO 802 J=1,NSM
           JJJ = (K-1)*NSM + J
           BMFMMZ(JJJ) = BMFMM(J,K,1)
           BMFMMX(JJJ) = BMFMM(J,K,2)
           BMFMMY(JJJ) = BMFMM(J,K,3)
           BMFMGZ(JJJ) = BMFMG(J,K,1)
           BMFMGX(JJJ) = BMFMG(J,K,2)
           BMFMGY(JJJ) = BMFMG(J,K,3)
802 CONTINUE
C          BMFMMZ MEANS  Z COMPONENT OF MAGNETIC FIELD AT
C                   MAGNETIC FIELD POINTS XM,YM,ZM  DUE TO BODIES AT COORDS
C                   CBMX + DELX, CBMX - DELX  ETC.
```

```
C     BMFMGZ MEANS   Z COMPONENT OF GRAVITY FIELD AT
C        MAGNETIC FIELD POINTS XM,YM,ZM  DUE TO BODIES AT COORDS
C        CBMX + DELX, CBMX -DELX ETC.
C     ABOVE QUANTITIES ARE FOR BODIES OF UNIT DENSITY AND MAGNETIZATION
C     FIND  3 SETS OF MAGNETIZATIONS THAT PRODUCE OBSERVED MAGNETIC
C        ANOMALY
      LBM = NBM + 1
C     X - COMPONENT
      CALL MULREG(BMFMMX,MOBS,NSM,LBM,MCOMPX,BMAGSX,SEX,CORRMX,FTMX,
     1 TTMX)
C     Y - COMPONENT
      CALL MULREG(BMFMMY,MOBS,NSM,LBM,MCOMPY,BMAGSY,SEY,CORRMY,FTMY,
     1 TTMY)
C     Z - COMPONENT
      CALL MULREG(BMFMMZ,MOBS,NSM,LBM,MCOMPZ,BMAGSZ,SEZ,CORRMZ,FTMZ,
     1 TTMZ)
      WRITE(6,911)
      DO 805 K=1,N3M
      WRITE(5,204)BMAGSZ(K),TTMZ(K),BMAGSX(K),TTMX(K),BMAGSY(K),TTMY(K),
     1CBMX(K),CBMY(K),DBMZ(K),INDEX4(K)
  805 CONTINUE
      WRITE(6,299)
      WRITE(6,299)
      WRITE(6,299)
      WRITE(6,912)
      DO 806 J=1,NSM
      RESZ(J) = MOBS(J)  - MCOMPZ(J)
      RESX(J) = MOBS(J)  - MCOMPX(J)
      RESY(J) = MOBS(J)  - MCOMPY(J)
      MOBS(J) = MOBS(J)  + REGM
      MCOMPZ(J) = MCOMPZ(J) + REGM
      MCOMPX(J) = MCOMPX(J) + REGM
      MCOMPY(J) = MCOMPY(J) + REGM
      WRITE(6,205)MOBS(J),MCOMPZ(J),RESZ(J),MCOMPX(J),RESX(J),MCOMPY(J),
     1RESY(J),XM(J),YM(J),ZM(J),INDEX2(J)
      MOBS(J) = MOBS(J)  - REGM
      MCOMPZ(J) = MCOMPZ(J) - REGM
      MCOMPX(J) = MCOMPX(J) - REGM
```

```
          MCOMPY(J) = MCOMPY(J) - REGM
805   CONTINUE
          WRITE(6,299)
          WRITE(6,299)
          WRITE(6,299)
          WRITE(6,903)
          WRITE(6,914)
          WRITE(6,200)CORRMZ,FTMZ,SEZ
          WRITE(6,200)CORRMX,FTMX,SEX
          WRITE(6,200)CORRMY,FTMY,SEY
          WRITE(6,299)
          WRITE(6,299)
          WRITE(6,299)
          DO 804 K=1,NBM
          BMAGS(K,1) = BMAGSZ(K)
          BMAGS(K,2) = BMAGSX(K)
          BMAGS(K,3) = BMAGSY(K)
          RHO(K,1) = BMAGS(K,1)
          RHO(K,2) = BMAGS(K,2)
          RHO(K,3) = BMAGS(K,3)
804   CONTINUE
          IF (IP) 340,341,340
341   CONTINUE
C         COMPUTE Z-COMPONENT OF GRAVITY DUE TO 3 SETS OF MAGNETIZATIONS
C         GRAVITY AT GRAVITY FIELD PTS.,BODIES AT MAG. BODY PTS.
          CALL COEFF(NSG,NBM,3,CBMX,CBMY,DBMZ,DELX,DELY,DELZ,XG,YG,ZG,GINC,
     1 GAZI,BMIN,BMAZ)
C         NOTE GRAVITY VALUES ARE TOO SMALL BY FACTOR AMAG/RHO
C         CMGG ARRAY CONTAINS GRAVITY VALUES
C         CMGM ARRAY CONTAINS MAGNETIC VALUES
          GO TO 350
340   DO 342 K=1,NBM
          DO 342 J=1,NSM
          JJJ = (K-1)*NSM + J
          BMFMG(J,K,1) = BMFMGZ(JJJ)*BMAGSZ(K)
          BMFMG(J,K,2) = BMFMGX(JJJ)*BMAGSX(K)
          BMFMG(J,K,3) = BMFMGY(JJJ)*BMAGSY(K)
342   CONTINUE
```

```
350 CONTINUE
    NNNN = 3*NSG
    DO 401 JJJ=1, NNNN
    CFMGG(JJJ) = 0.0
401 CONTINUE
    DO 402 L=1,3
C       L = 1    Z-COMPONENT
C       L = 2    X-COMPONENT
C       L = 3    Y-COMPONENT
    DO 402 J=1,NSG
    DO 402 K=1,N3M
    JJJ = (L-1)*NSG + J
    CFMGG(JJJ) = CFMGG(JJJ) + BMFMG(J,K,L)
402 CONTINUE
C
C       COMPUTE QUANTITIES INVOLVING DIRECTION COSINES OF MAGNETIZATION
C       VECTOR AND RATIO OF  RHO/MAGN
C   CALL MULREG(CFMGG,GOBS,NSG,4,GCOMPM,CONSG,SEG,CORRG,FTG,TTG)
C       TO SAVE SPACE WE REUSE BMFMG
    WRITE(6,900)
    WRITE(6,901)
    DO 410 J=1,NSG
    RESG(J) = GOBS(J) - GCOMPM(J)
    GOBS(J) = GOBS(J) + REGG
    GCOMPM(J) = GCOMPM(J) + REGG
    WRITE(6,201)GOBS(J),GCOMPM(J),RESG(J),XG(J),YG(J),ZG(J),INDEX1(J)
    WRITE(7,208)GOBS(J),GCOMPM(J),RESG(J),XG(J),YG(J),ZG(J),INDEX1(J)
    GOBS(J) = GOBS(J) - REGG
    GCOMPM(J) = GCOMPM(J) - REGG
410 CONTINUE
    WRITE(6,299)
    WRITE(6,299)
    WRITE(6,299)
    WRITE(6,902)
    DO 411 L=1,4
    WRITE(6,206)CONSG(L),TTG(L),L
411 CONTINUE
    WRITE(6,299)
    WRITE(6,299)
```

```fortran
      WRITE(6,299)
      WRITE(6,903)
      WRITE(5,200)CORRG,FTG,SEG
      WRITE(6,299)
      WRITE(6,299)
C     COMPUTE    RATIO  OF DENSITY TO MAGNETIZATION ,INCLINATION AND
C               AZIMUTH OF MAGNETIZATION   VECTOR
      CDCLMG = ATAN2(CONSG(2),CONSG(3))
      CDCLMG = CDCLMG*57.296
      RATIO1= SQRT(CONSG(1)*CONSG(1)+CONSG(2)*CONSG(2)+CONSG(3)*CONSG(3)
     1 )
      CINCMG =  ASIN(CONSG(1)/RATIO1)
      CINCMG = CINCMG*57.296
      WRITE(6,904)
      WRITE(6,201)CDCLMG,CINCMG,RATIO1
      WRITE(6,299)
C     CALCULATE ANGLE BTWN EARTHS FIELD AND TOTAL MAGN. VECTOR
      CCC1 = SIN(CINCMG/57.296)*SIN(EINC/57.296) +
     1 COS(CINCMG/57.296)*COS(EINC/57.296)*COS((EAZI-CDCLMG)/57.296)
      BETA1 =  ACOS(CCC1)
      BETA1 = BETA1*57.296
      WRITE(6,917)
      WRITE(6,203)BETA1
      WRITE(6,299)
      IF(CCC1)1005,1006,1006
1005  AAQ1 = 1.0
      GO TO 1007
1006  AAQ1 = SQRT(1.0 - CCC1*CCC1)
1007  CONTINUE
      WRITE(6,918)
      WRITE(6,203)AAQ1
      WRITE(6,299)
      DELIN1 = CONSG(1) /(TTG(1)*SQRT(RATIO1*RATIO1-CONSG(1)*CONSG(1)))
      DELIN1 = DELIN1*57.296
      DELAZ1 = (CONSG(3)*CONSG(2)/(CONSG(3)*CONSG(3)+CONSG(2)*CONSG(2)))
     1 *SQRT(1.0/(TTG(3)*TTG(3)) + 1.0/(TTG(2)*TTG(2)))
      DELAZ1 = DELAZ1*57.296
      ZZ1 = CONSG(1)*CONSG(1)/TTG(1)
```

```
      ZZ2 = CONSG(2)*CONSG(2)/TTG(2)
      ZZ3 = CONSG(3)*CONSG(3)/TTG(3)
      DRAT1 = (SQRT(ZZ1*ZZ1+ZZ2*ZZ2+ZZ3*ZZ3)) /RATIO1
      WRITE(6,916)
      WRITE(6,201)DELAZ1,DELIN1,DRAT1
      WRITE(6,299)
      WRITE(6,298)
C********** THIS PORTION CHECKS TRANSFORMATIONS AND
C           CALCULATES VIRTUAL POLE POSITIONS
C     CHECK GRAVITY TO MAGNETIC TRANSFORMATION
      DO 722 J=1,NSM
      JJJ = J
      KKK = NSM + J
      LLL = 2*NSM + J
      MCOMPM(J)= CONSM(1)*CFGMM(JJJ) + CONSM(2)*CFGMM(KKK)
     1          + CONSM(3)*CFGMM(LLL) + CONSM(4)
  722 CONTINUE
      WRITE(6,908)
      DO 723 J=1,NSM
      RESM1(J) = MOBS(J)  - MCOMPM(J)
  723 CONTINUE
      RR= 0.0
      DO 724 J=1,NSM
      RR = RR + RESM1(J)*RESM1(J)
  724 CONTINUE
      ANSM = NSM
      RR = SQRT(RR/ANSM)
      WRITE(6,909)
      WRITE(6,203)RR
C     RR = RMS MAGNETIC RESIDUAL
      WRITE(6,299)
      WRITE(6,299)
      WRITE(6,913)
C     CHECK MAGNETIC TO GRAVITY TRANSFORMATION
      DO 701 J=1,NSG
      JJJ = J
      KKK = NSG + J
      LLL = 2*NSG + J
```

```
      GCOMPG(J) = CONSG(1)*CFMGG(JJJ) + CONSG(2)*CFMGG(KKK)
     1             + CONSG(3)*CFMGG(LLL) + CONSG(4)
701   CONTINUE
      DO 702  J=1,NSG
      RESG1(J) = GORS(J) - GCOMPG(J)
702   CONTINUE
      TT = 0.0
      DO 703  J=1,NSG
      TT = TT + RESG1(J)*RESG1(J)
703   CONTINUE
      ANSG = NSG
      TT = SQRT(TT/ANSG)
      WRITE(6,910)
      WRITE(6,203)TT
C                 TT = RMS GRAVITY RESIDUAL
      WRITE(6,299)
      WRITE(6,299)
      WRITE(6,299)
C        CALC. VIRTUAL MAG. POLES FOR MAG TO GRAV AND GRAV TO MAG TRANSF
C
      NNN = 2
      ALAT(2) = ALAT(1)
      ALONG(2) = ALONG(1)
      AMIN(1) = CINCGM
      AMAZ(1) = CDCLGM
      AMIN(2) = CINCMG
      AMAZ(2) = CDCLMG
      CALL POLE(NNN,ALAT,ALONG,AMIN,AMAZ,VLAT,VLONG)
      CALL EXIT
      END
```

342

```
      SUBROUTINE COEFF(NO,NP,NA,XC,YC,ZD,DX,DY,DZ,XX,YY,ZZ,DFIN,DFAZ,
     1 DMIN,DMAZ)
C     NO = NO. OF FIELD PTS
C     NP = NO. OF PRISMS
C     NA = NO. OF ANGLES OF MAGNETIZATION.
C     XC,YC = VECTORS OF VALUES OF X,Y COORDS OF THE VERTICAL CENTRAL
C     AXES OF PRISMS
C     ZD = VECTOR OF VALUES OF DEPTHS OF TOPS OF PRISMS
C     DX,DY,DZ = SCALARS OF LENGTH,WIDTH AND HEIGHTS OF PRISMS
C     XX,YY,ZZ = VECTORS OF VALUES OF FIELD POINT COORDS
C     DFIN,DFAZ = INCLINATION AND AZIMUTH OF MEASURED FIELD COMPONENT
C     (E.G. TOTAL FIELD,VERTICAL COMP., ETC.)
C     DMIN,DMAZ = INCLINATION AND AZIMUTH OF TOTAL MAGNETIZATION VECTOR
      DIMENSION XC(NP),YC(NP),ZD(NP),XX(NO),YY(NO)
      DIMENSION ZZ(NO),DFIN(NA),DFAZ(NA),DMIN(NA),DMAZ(NA)
C     DIMENSIONS OF AMAG,RHO,AM,AG MUST BE AS IN MAIN PRGRM
      DIMENSION AMAG(22,3),RHO(22,3),AM(30,22,3),AG(30,22,3)
      DIMENSION TFIN(3),TFAZ(3),TMIN(3),TMAZ(3)
      DIMENSION A1(3),A2(3),A3(3),B1(3),B2(3),B3(3)
      COMMON  AMAG,RHO,AM,AG
      RO=1.0
      DO 925 K=1,NA
      TFIN(K) = DFIN(K)/57.2958
      TFAZ(K) = DFAZ(K)/57.2958
      TMIN(K) = DMIN(K)/57.2958
      TMAZ(K) = DMAZ(K)/57.2958
      A1(K) = (COS(TFIN(K)))*(SIN(TFAZ(K)))
      A2(K) = (COS(TFIN(K)))*(COS(TFAZ(K)))
      A3(K) = (SIN(TFIN(K)))*(-1.0)
      B1(K) = (COS(TMIN(K)))*(SIN(TMAZ(K)))
      B2(K) = (COS(TMIN(K)))*(COS(TMAZ(K)))
      B3(K) = (SIN(TMIN(K)))*(-1.0)
  925 CONTINUE
      DO 901 J=1,NO
      DO 901 K=1,NP
      DO 901 L=1,NA
      U1 = XC(K) - DX - XX(J)
      U2 = XC(K) + DX - XX(J)
      V1 = YC(K) - DY - YY(J)
```

```fortran
      V2 = YC(K) + DY - YY(J)
      W1 = ZD(K) - DZ -ZZ(J)
      W2 = ZD(K)     -ZZ(J)
      CALL CG3D(U1,U2,V1,V2,W1,W2,RO,0.0,0.0,0.0,GZDU1,GZDU2,
     1 GZDV1,GZDV2,GZDW1,GZDW2)
      CALL CG3D(V1,V2,W1,W2,U1,U2,RO,0.0,0.0,0.0,GXDU1,GXDU2,
     1 GXDV1,GXDV2,GXDW1,GXDW2)
      CALL CG3D(W1,W2,U1,U2,V1,V2,RO,0.0,0.0,0.0,GYDU1,GYDU2,
     1 GYDV1,GYDV2,GYDW1,GYDW2)
C
C
      GYDU1 = GZDV1
      GYDU2 = GZDV2
      GYDV1 = GXDU1
      GYDV2 = GXDU2
      GYDW1 = -GXDW1 - GZDW1
      GYDW2 = -GXDW2 - GZDW2
      AM(J,K,L) = (AMAG(K,L)/6.664E-05)*
     1((B3(L))*(A1(L)*(GZDU1+GZDU2)+A2(L)*(GZDV1+GZDV2))
     2+      A3(L)*(GZDW1+GZDW2))
     3+(B1(L))*(A2(L)*(GXDU1+GXDU2)+A3(L)*(GXDV1+GXDV2))
     4+      A1(L)*(GXDW1+GXDW2))
     5+(B2(L))*(A3(L)*(GYDU1+GYDU2)+A1(L)*(GYDV1+GYDV2))
     6+      A2(L)*(GYDW1+GYDW2)))
      AG(J,K,L) = RHO(K,L)*(U1*GZDU1+U2*GZDU2+V1*GZDV1+V2*GZDV2
     1 +W1*GZDW1+W2*GZDW2)
  901 CONTINUE
      RETURN
      END
```

```
      SUBROUTINE CG3D(U1,U2,V1,V2,W1,W2,RO,X,Y,Z,DGZDU1,DGZDU2,DGZDV1,
     1 DGZDV2,DGZDW1,DGZDW2 )
C     THIS SUBROUTINE COMPUTES AT A POINT (X,Y,Z) THE VERTICAL COMPONENT
C        OF ATTRACTION  GZ OF A PRISM WHOSE DENSITY(CONTRAST) IS RO AND
C        WHOSE CORNERS ARE AT (U1,V1,W1),(U2,V1,W1),(U1,V2,W1),.....,
C        (U2,V2,W2)
C     THE TERMS DGZDU1,DGZDU2,.....,DGZDW2,DGZDRO ARE DERIVATIVES OF GZ
C        WITH RESPECT TO U1,U2,....,W2 AND RO
C     UNITS OF LENGTH - KILOMETERS  UNITS OF DENSITY(CONTRAST) - GM/CC
C        GZ IS CALCULATED BUT NOT GIVEN IN ARGUMENT LIST
  211 FORMAT(T8,"XXU1",T18,"XXU2",T28,"YYV1",T38,"YYV2",T48,"ZZW1",T58,
     1 "ZZW2"/1X,6F10.4/)
  212 FORMAT(1X,4E20.7/)
  213 FORMAT(1X,2E20.7/)
  214 FORMAT(1X,2F10.4)
      XXU1 = U1 - X
      XXU2 = U2 - X
      YYV1 = V1 - Y
      YYV2 = V2 - Y
      ZZW1 = W1 - Z
      ZZW2 = W2 - Z
      IF(XXU2-XXU1) 431,432,432
  431 SXXU2 = XXU2
      XXU2 = XXU1
      XXU1 = SXXU2
  432 IF(YYV2-YYV1) 433,434,434
  433 SYYV2 = YYV2
      YYV2 = YYV1
      YYV1 = SYYV2
  434 IF(ZZW2-ZZW1) 435,436,436
  435 SZZW2 = ZZW2
      ZZW2 = ZZW1
      ZZW1 = SZZW2
  436 CONTINUE
      EEPS = 1.0E-10
      RAD222 =  SQRT(XXU2*XXU2 + YYV2*YYV2 + ZZW2*ZZW2 )
      RAD122 =  SQRT(XXU1*XXU1 + YYV2*YYV2 + ZZW2*ZZW2 )
      RAD212 =  SQRT(XXU2*XXU2 + YYV1*YYV1 + ZZW2*ZZW2 )
      RAD112 =  SQRT(XXU1*XXU1 + YYV1*YYV1 + ZZW2*ZZW2 )
```

```
      RAD221  =     SQRT(XXU2*XXU2  +  YYV2*YYV2  +  ZZW1*ZZW1 )
      RAD121  =     SQRT(XXU1*XXU1  +  YYV2*YYV2  +  ZZW1*ZZW1 )
      RAD211  =     SQRT(XXU2*XXU2  +  YYV1*YYV1  +  ZZW1*ZZW1 )
      RAD111  =     SQRT(XXU1*XXU1  +  YYV1*YYV1  +  ZZW1*ZZW1 )
      WRITE(6,211)XXU1,XXU2,YYV1,YYV2,ZZW1,ZZW2
      AKONS = 6.664
      AKONST = AKONS*RO
      ALNX1N = (YYV1+RAD112)*(YYV2+RAD121)
      ALNX1D = (YYV2+RAD122)*(YYV1+RAD111)
      ALNX2N = (YYV2+RAD222)*(YYV1+RAD211)
      ALNX2D = (YYV1+RAD212)*(YYV2+RAD221)
      ALNY1N = (XXU1+RAD112)*(XXU2+RAD211)
      ALNY1D = (XXU2+RAD212)*(XXU1+RAD111)
      ALNY2N = (XXU2+RAD222)*(XXU1+RAD121)
      ALNY2D = (XXU1+RAD122)*(XXU2+RAD221)
      IF(ALNX1N)501,501,502
501   ALNX1N = EEPS
502   IF(ALNX1D)503,503,504
503   ALNX1D = EEPS
504   IF(ALNX2N)505,505,506
505   ALNX2N = EEPS
506   IF(ALNX2D)507,507,508
507   ALNX2D = EEPS
508   IF(ALNY1N)509,509,510
509   ALNY1N = EEPS
510   IF(ALNY1D)511,511,512
511   ALNY1D = EEPS
512   IF(ALNY2N)513,513,514
513   ALNY2N = EEPS
514   IF(ALNY2D)515,515,516
515   ALNY2D = EEPS
516   CONTINUE
      ALNX1 = ALNX1N/ALNX1D
      ALNX2 = ALNX2N/ALNX2D
      ALNY1 = ALNY1N/ALNY1D
      ALNY2 = ALNY2N/ALNY2D
      WRITE(6,212)ALNX1,ALNX2,ALNY1,ALNY2
      DGZOU1 = ALOG(ALNX1)*AKONST
```

```
      DGZDU2 = ALOG(ALNX2)*AKONST
      DGZDV1 = ALOG(ALNY1)*AKONST
      DGZDV2 = ALOG(ALNY2)*AKONST
      T1121D = ZZW1*RAD121
      T1221D = ZZW1*RAD221
      T1211D = ZZW1*RAD211
      T1111D = ZZW1*RAD111
      T2122D = ZZW2*RAD122
      T2222D = ZZW2*RAD222
      T2212D = ZZW2*RAD212
      T2112D = ZZW2*RAD112
      IF(T1121D)522,521,522
  521 T1121D = EEPS
  522 IF(T1221D)524,523,524
  523 T1221D = EEPS
  524 IF(T1211D)526,525,526
  525 T1211D = EEPS
  526 IF(T1111D)528,527,528
  527 T1111D = EEPS
  528 IF(T2122D)530,529,530
  529 T2122D = EEPS
  530 IF(T2222D)532,531,532
  531 T2222D = EEPS
  532 IF(T2212D)534,533,534
  533 T2212D = EEPS
  534 IF(T2112D)536,535,536
  535 T2112D = EEPS
  536 CONTINUE
      TARG11 = (XXU1*YVV2)/T1121D
      TARG12 = (XXU2*YVV2)/T1221D
      TARG13 = (XXU2*YVV1)/T1211D
      TARG14 = (XXU1*YVV1)/T1111D
      WRITE(6,212)TARG11,TARG12,TARG13,TARG14
      IF(1-TARG11*TARG13)454,461,454
  454 IF(1-TARG12*TARG14)455,461,455
  455 CONTINUE
C
      TARG1 = (TARG11+TARG13)/(1-TARG11*TARG13)
      TARG2 = (TARG12+TARG14)/(1-TARG12*TARG14)
```

```
C
        WRITE(5,213)TAR11,TAR12
        IF(TAR11)461,462,462
462     IF(TAR12)461,464,464
461     DGZDW1=(- ATAN(TARG11)+ ATAN(TARG12)- ATAN(TARG13)+ ATAN(TARG14))*
       1 AKONST
        GO TO 470
464     CONTINUE
        DGZDW1 = ATAN((TAR12 - TAR11)/(1 + TAR12*TAR11))*AKONST
470     CONTINUE
        TARG21 =(XXU1*YYV2)/T2122D
        TARG22 =(XXU2*YYV2)/T2222D
        TARG23 =(XXU2*YYV1)/T2212D
        TARG24 =(XXU1*YYV1)/T2112D
        WRITE(6,212)TARG21,TARG22,TARG23,TARG24
C
        IF(1-TARG21*TARG23)456,471,456
456     IF(1-TARG22*TARG24)457,471,457
457     CONTINUE
        TAR21 = (TARG21+TARG23)/(1-TARG21*TARG23)
        TAR22 = (TARG22+TARG24)/(1-TARG22*TARG24)
        WRITE(6,213)TAR21,TAR22
C
        IF(TAR21)471,472,472
472     IF(TAR22)471,474,474
471     DGZDW2=(+ ATAN(TARG21)- ATAN(TARG22)+ ATAN(TARG23)- ATAN(TARG24))*
       1 AKONST
        GO TO 480
474     CONTINUE
        DGZDW2 = ATAN((TAR21 - TAR22)/(1 + TAR21*TAR22))*AKONST
480     CONTINUE
        GZ =      (XXU2*DGZDU2 +XXU1*DGZDU1 +YYV2*DGZDV2 +YYV1*DGZDV1
       1 +ZZW2*DGZDW2  + ZZW1*DGZDW1 )
        DGZDRO =  GZ/RO
        RETURN
        END
```

```
      SUBROUTINE MULREG(AA,YOBS,NO,NP,YCOMP,UNS,SE,CORR,FT,TT)
C     MULTIPLE REGRESSION
C     ********* PROGRAM USES MODIFIED DOOLITTLE METHOD METHOD
C               TO TAKE ADVANTAGE OF SOLVING A SET OF EQNS WHOSE
C               MATRIX OF COEFFS IS SYMMETRICAL

      INTEGER V,R,P,Q
      REAL MEAN
C     PROGRAM CURRENTLY DIMENSIONED FOR 55 OBS 54 UNS
      DIMENSION X(55,54),Y(55,55),                U(1,55),      MEAN(55),
     1 A(55,55),B(55,55),C(1,55),SSR(1,2),D(1,1),RSQ(1,1),E(55,55),
     2 EA(55,55),EB(55,55),EC(55,55),SSRES(1,1),EBC(2,55),YEST(72,1),
     3 FTEST(1,1),
     4                  TTEST(1,55),
     5SD(55),SF(1,55),ZF(55,55)
      DIMENSION AA(2970)
      DIMENSION YOBS(72),YCOMP(72),UNS(72),TT(72)
      EQUIVALENCE (EA,EC),(X,E),(A,Y),(ZF,EB)
201   FORMAT(3I5)
202   FORMAT(1X,"DIAGONAL ELEMENTS"//)
203   FORMAT(8(1X,E10.3,1X,I2))
299   FORMAT(1H0)
      EEPS = 1.0E-10
      N = NO
      V = NP
      R = NP-1
      IF(R)651,651,652
651   R = 1
652   CONTINUE
      DO 500 K=1,R
      DO 500 J=1,N
      JJJ = (K-1)*N + J
      X(J,K) = AA(JJJ)
500   CONTINUE
      DO 501 J=1,N
      X(J,V) = YOBS(J)
501   CONTINUE
3     DO 4 I=1,V
      DO 4 J=1,V
      Y(I,J)=0
```

```
4     CONTINUE
      DO 5 L=1,V
      DO 6 M=1,V
      DO 6 K=1,N
      Y(L,M)=Y(L,M)+(X(K,L)*X(K,M))
6     CONTINUE
5     CONTINUE
      DO 9 L=1,V
      SF(1,L)=0
9     CONTINUE
      DO 7 L=1,V
      DO 7 K=1,N
      SF(1,L)=SF(1,L)+X(K,L)
7     CONTINUE
      DO 12 L=1,V
      DO 12 M=1,V
      ZF(L,M)=0
12    CONTINUE
      DO 8 L=1,V
      DO 8 M=1,V
      ZF(L,M)=Y(L,M)-(SF(1,L)*SF(1,M)/N)
8     CONTINUE
      DO 50 L=1,V
      MEAN(L)=SF(1,L)/N
      SD(L)=0.0
      DO 51 K=1,N
      SD(L)=SD(L)+(X(K,L)-MEAN(L))*(X(K,L)-MEAN(L))
51    CONTINUE
      IF(SD(L))151,151,152
151   SD(L) = EEPS
      III = 99
      WRITE(6,201)III,L,L
152   CONTINUE
      AAAN = N
      SD(L) = SQRT(SD(L)/AAAN)
50    CONTINUE
      DO 700 J=1,V
      DO 701 K=1,V
```

350

```
      DEN = ZF(J,J)*ZF(K,K)
      IF(DEN)101,102,101
102   DEN = EEPS
      III = 1
      WRITE(6,201)III,J,K
101   CONTINUE
      B(J,K) = ZF(J,K)*ZF(J,K)/DEN
701   CONTINUE
700   CONTINUE
      DO 970 M=1,V
      TTEST(1,M) = ZF(1,M)
970   CONTINUE
      DO 971 J=1,V
      DO 971 K=1,V
      A(J,K) = 0.0
      EA(J,K) = 0.0
971   CONTINUE
      DO 17 M=1,V
      A(1,M)=TTEST(1,M)
      IF(A(1,1))103,104,103
104   A(1,1) = EEPS
      III = 2
      MM = 1
      WRITE(6,201)III,MM,M
103   CONTINUE
17    B(1,M)=A(1,M)/A(1,1)
      IF(V.LT.3)GOTO 902
      DO 20 J=2,R
      P=J
      DO 18 M=P,V
      Q=P-1
      U(1,1)=0
      DO 19 K=1,Q
      U(1,1)=U(1,1)+A(K,P)*B(K,M)
19    CONTINUE
      A(P,M) = ZF(P,M) - U(1,1)
      IF(A(P,P))105,106,105
106   A(P,P) = EEPS
```

351

```fortran
        III = 3
        WRITE(6,201)III,M,P
105     CONTINUE
        B(P,M)=A(P,M)/A(P,P)
18      CONTINUE
20      CONTINUE
        WRITE(6,299)
        WRITE(5,299)
        WRITE(6,202)
        WRITE(6,203)((A(J,J),J),J=1,R)
        WRITE(6,299)
        WRITE(6,299)
902     C(1,R)=B(R,V)
        IF(V.LT.3)GOTO 903
        DO 21 J=2,R
        U(1,1)=0
        L=J-1
        DO 22 K=1,L
        U(1,1)=U(1,1)+B((V-J),(V-K))*C(1,(V-K))
22      CONTINUE
        C(1,(V-J))=B((V-J),V)-U(1,1)
21      CONTINUE
903     D(1,1) = SF(1,V)
        DO 26 J=1,R
        D(1,1) = D(1,1) - SF(1,J)*C(1,J)
26      CONTINUE
        D(1,1)=D(1,1)/N
        DO 44 K=1,N
        YEST(K,1)=D(1,1)
        DO 41 J=1,R
        YEST(K,1)=YEST(K,1)+C(1,J)*X(K,J)
41      CONTINUE
44      CONTINUE
        DO 991 J=1,V
        DO 991 K=1,V
        E(J,K) = 0.0
991     CONTINUE
        SSR(1,1)=0
```

352

```
      SSR(1,2)=0
      DO 24 J=1,R
      SSR(1,1) = SSR(1,1) + C(1,J)*ZF(J,V)
      SSR(1,2)=SSR(1,2)+A(J,V)*B(J,V)
   24 CONTINUE
      IF(ZF(V,V))107,108,107
  108 ZF(V,V) = EEPS
      III = 4
      WRITE(6,201)III,V,V
  107 CONTINUE
      RSQ(1,1) = SSR(1,1)/ZF(V,V)
      RCORP=1.0-((1.0-RSQ(1,1))*((N-1.0)/(N-V)))
      SEE = SQRT((ZF(V,V)-SSR(1,1))/(N-V))
      SSRES(1,1) = ZF(V,V)-SSR(1,1)
      IF(SSRES(1,1))109,110,109
  110 SSRES(1,1) = EEPS
      III = 5
      MM = 1
      WRITE(6,201)III,MM,MM
  109 CONTINUE
      DO 992 J=1,V
      DO 992 K=1,V
      EB(J,K) = 0.0
  992 CONTINUE
      DO 30 L=1,R
      DO 30 M=1,R
      IF(L.NE.M)GOTO 31
      E(L,M)=1.0
      GOTO 30
   31 E(L,M)=0.0
   30 CONTINUE
      DO 32 M=1,R
      EA(1,M)=E(1,M)
      EB(1,M)=EA(1,M)/A(1,1)
   32 CONTINUE
      IF(V.LT.3)GOTO 912
      DO 34 J=2,R
      P=J
```

```
      DO 35 M=1,R
      Q=P-1
      U(1,1)=0.0
      DO 36 K=1,Q
      U(1,1)=U(1,1)+A(K,P)*EB(K,M)
   36 CONTINUE
      EA(P,M)=E(P,M)-U(1,1)
      EB(P,M)=EA(P,M)/A(P,P)
   35 CONTINUE
   34 CONTINUE
  912 CONTINUE
      DO 981 J=1,R
      DO 981 K=1,R
      EC(J,K) = 0.0
  981 CONTINUE
      DO 301 J=1,R
      EC(R,J)=EB(R,J)
  301 CONTINUE
      IF(V.LT.3)GOTO 913
      L=R-1
      DO 304 M=1,L
      DO 302 J=1,R
      U(1,J)=0.0
      DO 303 K=1,M
      U(1,J)=U(1,J)+B((R-M),(V-K))*EC((V-K),J)
  303 CONTINUE
      EC((R-M),J)=EB((R-M),J)-U(1,J)
  302 CONTINUE
  304 CONTINUE
  913 CONTINUE
      DO 80 J=1,R
      AAARG = EC(J,J)*(SSRES(1,1)/(N-V))
      IF(AAARG)111,112,111
  112 AAARG = EEPS
      III = 6
      MM = 1
      WRITE(6,201)III,MM,J
  111 CONTINUE
```

```
      EBC(1,J) = SQRT(ABS(AAARG))
      FTEST(1,J)=(C(1,J)/EBC(1,J))
   80 CONTINUE
      FTEST(1,1)=(SSP(1,1)/R)/(SSRES(1,1)/(N-V))
      FT = FTEST(1,1)
      CORR = RCORR
      SE = SEE
      DO 600 K=1,R
      UNS(K) = C(1,K)
      TT(K) = TTEST(1,K)
  600 CONTINUE
      UNS(V) = D(1,1)
      DO 609 J=1,N
      YCOMP(J) = YEST(J,1)
  609 CONTINUE
      RETURN
      END
```

```
      SUBROUTINE POLE(NN,ALAT,ALONG,AMIN,AMAZ,VLAT,VLONG)
C     ********* PROGRAM CALCULATES POLE POSN (VLAT,VLONG) OF
C               DIPOLAR FIELD WHICH WOULD INDUCE MAGNETIZATION
C               DIRECTION (AMIN,AMAZ) AT AGIVEN LOCN (ALAT,ALONG)
      DIMENSION ALAT(NN),ALONG(NN),AMIN(NN),AMAZ(NN),VLAT(NN),VLONG(NN)
      COMMON /ANGLE/ P, XBETA
201   FORMAT(1X,6(F10.4))
202   FORMAT(1X,"ALAT,ALONG,AMIN,AMAZ,VLAT,VLONG"//)
203   FORMAT(1X,"VLAT,VLONG --- LAT AND LONG OF VIRTUAL POLE"//)
204   FORMAT(1X," ANGLE P  ",F10.3//)
      DO 301 L=1,NN
      ALAT(L) = ALAT(L)/57.296
      ALONG(L) = ALONG(L)/57.296
      AMIN(L) = AMIN(L)/57.296
      AMAZ(L) = AMAZ(L)/57.296
301   CONTINUE
      WRITE(6,203)
      DO 302 L=1,NN
      P = ATAN(2.0/TAN(AMIN(L)))
      P = P + XBETA
      IF(P)405,405,406
405   P = 3.14159 + P
406   CONTINUE
      PP = P* 57.296
      WRITE(6,204) PP
      WRITE(6,202)
      VLAT(L) = ASIN(COS(P)*SIN(ALAT(L))+ SIN(P)*COS(ALAT(L))*
     1 COS(AMAZ(L)))
      VLONG(L) = ALONG(L) + ASIN((SIN(P)*SIN(AMAZ(L)))/COS(VLAT(L)))
      IF(COS(P)-SIN(ALAT(L))*SIN(VLAT(L)))401,402,402
401   VLONG(L) = 3.14159 -VLONG(L) + 2.0*ALONG(L)
402   CONTINUE
      VLAT(L) = VLAT(L)*57.296
      VLONG(L) = VLONG(L)*57.296
      ALAT(L) = ALAT(L)*57.296
      ALONG(L) = ALONG(L)*57.296
      AMIN(L) = AMIN(L)*57.296
      AMAZ(L) = AMAZ(L)*57.296
      WRITE(6,201)ALAT(L),ALONG(L),AMIN(L),AMAZ(L),VLAT(L),VLONG(L)
```

```
302 CONTINUE
    RETURN
    END
```

INPUT DATA FOR MIDDLE BANK ANOMALY - SCOTIAN SHELF

IP
0

NSG	NBG	NSM	NBM
25	20	25	20

GOBS	XG	YG	ZG	INDEX1
-3.5	4.0	12.0	0.0	101
-13.0	7.0	24.0	0.0	102
-29.8	11.0	37.0	0.0	103
-37.6	4.0	53.0	0.0	104
-32.8	9.0	66.0	0.0	105
-21.9	14.0	79.0	0.0	106
-14.2	8.0	95.0	0.0	107
-8.3	38.0	100.0	0.0	108
-26.3	26.0	72.0	0.0	109
-36.1	21.0	60.0	0.0	110
-41.5	16.0	49.0	0.0	111
-23.2	39.0	39.0	0.0	112
-7.1	33.0	27.0	0.0	113
11.2	41.0	9.0	0.0	114
21.1	54.0	7.0	0.0	115
3.8	64.0	28.0	0.0	116
-32.3	44.0	51.0	0.0	117
-23.4	55.0	73.0	0.0	118
-17.5	60.0	85.0	0.0	119
-10.7	65.0	98.0	0.0	120
-13.2	76.0	92.0	0.0	121
-28.2	72.0	79.0	0.0	122
-16.0	79.0	63.0	0.0	123

16.7 73.0 24.0 0.0 125

MOBS	XM	YM	ZM	INDEX2
200.0	10.0	30.0	0.0	201
100.0	10.0	21.0	0.0	202
100.0	10.0	45.0	0.0	203
-100.0	5.0	70.0	0.0	204
0.0	10.0	90.0	0.0	205
-100.0	15.0	100.0	0.0	206
-200.0	17.0	104.0	0.0	207
-100.0	33.0	108.0	0.0	208
0.0	30.0	92.0	0.0	209
-100.0	30.0	86.0	0.0	210
-100.0	43.0	70.0	0.0	211
0.0	40.0	45.0	0.0	212
100.0	40.0	33.0	0.0	213
100.0	30.0	22.0	0.0	214
100.0	20.0	11.0	0.0	215
100.0	55.0	5.0	0.0	216
150.0	60.0	29.0	0.0	217
100.0	75.0	40.0	0.0	218
-100.0	80.0	54.0	0.0	219
-100.0	70.0	64.0	0.0	220
0.0	70.0	79.0	0.0	221
-100.0	77.0	100.0	0.0	222
0.0	50.0	104.0	0.0	223
0.0	60.0	106.0	0.0	224
-120.0	70.0	70.0	0.0	225

EINC	EAZI
71.	-25.

359

CBMX	CBMY	DBMZ	INDEX4
10.0	20.0	1.0	301
30.0	20.0	1.0	302
50.0	20.0	1.0	303
70.0	20.0	1.0	304
10.0	40.0	1.0	305
30.0	40.0	1.0	306
50.0	40.0	1.0	307
70.0	40.0	1.0	308
10.0	60.0	1.0	309
30.0	60.0	1.0	310
50.0	60.0	1.0	311
70.0	60.0	1.0	312
10.0	80.0	1.0	313
30.0	80.0	1.0	314
50.0	80.0	1.0	315
70.0	80.0	1.0	316
10.0	100.0	1.0	317
30.0	100.0	1.0	318
50.0	100.0	1.0	319
70.0	100.0	1.0	320

CBMX	CBMY	DBMZ	INDEX4
10.0	20.0	1.0	401
30.0	20.0	1.0	402
50.0	20.0	1.0	403
70.0	20.0	1.0	404
10.0	40.0	1.0	405
30.0	40.0	1.0	406
50.0	40.0	1.0	407
70.0	40.0	1.0	408
10.0	60.0	1.0	409
30.0	60.0	1.0	410
50.0	60.0	1.0	411
70.0	60.0	1.0	412

10.0	80.0	1.0	413
30.0	80.0	1.0	414
50.0	80.0	1.0	415
70.0	80.0	1.0	416
10.0	100.0	1.0	417
30.0	100.0	1.0	418
50.0	100.0	1.0	419
70.0	100.0	1.0	420

DEL X	DELY	DELZ
20.	20.	10.

ALAT	ALONG
45.5	-60.5

G87456E //// END OF LIST ////
G87456E //// END OF LIST ////

OUTPUT DATA FOR MIDDLE BANK ANOMALY - SCOTIAN SHELF

DELX   DFLY   DELZ

.23.0000000   20.0000000   10.0000000

MEAN VALUE OF CONS   MCPS

-15.5500000   1.2000000

DIAGONAL ELEMENTS

.557E+05	1	.356E+05	2	.847E+04	3	.577E+05	4	.023E+05	5	.225E+05	6	.557E+04	7	.423E+05	8
.425E+05	9	.236E+05	10	.358E+04	11	.199E+05	12	.405E+05	13	.186E+05	14	.156E+05	15	.381E+05	16
.314E+05	17	.195E+05	18	.734E+03	19	.721E+04	20								

OBS.G	COMP.G	RES.	XG	YG	ZG	STN.NO.

BACKGROUND GRAVITY

23.1002423

DENSITY VALUES   T-VALUES   CDGX   CDGY   DDGZ**-1   BODY NO.

363

CORR COEFF F-VALUE STD ERROR

.8946447   11.1900301   5.4151376

DIAGONAL ELEMENTS

.137E+11 1 .185E+11 2 .106E+11 3

RESULTS OF GRAVITY TO MAGNETIC TRANSFORMATION

OBS.M	COMP.M	RES.	XM	YM	ZM	STN. NO.
200.0000000	124.1954344	75.8045656			10.0000000	36.0000000
100.0000000	42.4196433	57.5803517			10.0000000	21.0000000
100.0000000	39.7666860	60.2331143			10.0000000	45.0000000
-100.0000000	-146.7035504	46.9035504			5.0000000	70.0000000
0.0000000	-3.4949074	3.4949074			10.0000000	90.0000000
-100.0000000	-42.6012903	-57.3127097			15.0000000	100.0000000
-200.0000000	-81.5605310	-118.4394690			17.0000000	104.0000000
-100.0000000	-187.0335035	87.0335035			33.0000000	108.0000000
0.0000000	33.9255882	-33.9255882			30.0000000	92.0000000
-100.0000000	14.9042243	-114.9642243			30.0000000	86.0000000
-100.0000000	-98.6353395	-1.3646605			43.0000000	70.0000000
0.0000000	8.3076671	-8.3076671			40.0000000	45.0000000
100.0000000	71.2524772	28.7475228			40.0000000	33.0000000
100.0000000	21.6618226	78.3381774			30.0000000	22.0000000
100.0000000	144.2945368	-44.2945368			20.0000000	11.0000000
100.0000000	17.8541055	82.1458945			55.0000000	5.0000000
100.0000000	153.7433912	-63.7433912			60.0000000	29.0000000
50.0000000	29.8569438	20.1430562			75.0000000	40.0000000
100.0000000	29.5548461	71.4451539			80.0000000	54.0000000
-100.0000000	-1.4698574	-98.5301426			79.0000000	64.0000000
-100.0000000	-15.4491701	-94.1508299			70.0000000	79.0000000
0.0000000	-73.5381951	23.5381951			77.0000000	100.0000000
-100.0000000	-78.5251154	-61.4748846			50.0000000	104.0000000
0.0000000	-70.1857318	30.1857318			50.0000000	106.0000000
-120.0000000	-40.9132694	-79.0867306			70.0000000	70.0000000

364

COEFFS   T-VALUES

-.0028770   -1.2347720   1
-.0001997   -.3238900   2
-.0037484   -5.0545636   3
-16.1251602   0.0000000   4

CORR COEFF F-VALUE STD ERROR
.4972621   8.9128006   76.1551551

AZIMUTH INCLINATION RATIO MAGN/RHO
-177.0829056 -12.5973508 .0038376

ANGLE BETWN. EARTHS FIELD AND TOTAL MAGN. VECTOR

119.1419?464

Q-MINIMUM

1.00000000

DELAZ,DELIN,DELRATIO
8.8753189   10.3695470   .0007368

DIAGONAL ELEMENTS

.197E+12	1	.659E+10	2	.562E+11	3	.139E+10	4	.894E+09	5	.178E+12	6	.196E+10	7	.558E+10	8
.324E+10	9	.637E+10	10	.302E+10	11	.139E+12	12	.110E+10	13	.377E+09	14	.290E+10	15	.263E+08	16
.156E+11	17	.272E+10	18	.808E+11	19	.235E+11	20								

DIAGONAL ELEMENTS

.201E+12	1	.314E+11	2	.764E+11	3	.745E+10	4	.446E+11	5	.160E+11	6	.376E+10	7	.891E+10	8
.153E+12	9	.117E+11	10	.128E+11	11	.173E+12	12	.135E+12	13	.661E+11	14	.334E+09	15	.754E+09	16
.155E+11	17	.665E+11	18	.905E+10	19	.650E+10	20								

DIAGONAL ELEMENTS

.175E+12	1	.150E+12	2	.213E+11	3	.208E+10	4	.175E+12	5	.481E+11	6	.195E+10	7	.505E+11	8
.149E+10	9	.192E+10	10	.154E+10	11	.110E+12	12	.139E+11	13	.818E+11	14	.850E+10	15	.360E+11	16
.219E+12	17	.733E+11	18	.423E+11	19	.901E+10	20								

MAGN-Z,T-VALUE MAGN-X,T-VALUE MAGN-Y,T-VALUE   CBMX,CBMY,DBMZ*-1, BODY NO.

MAGN-Z	T-VALUE	MAGN-X	T-VALUE	MAGN-Y	T-VALUE	CBMX	CBMY	DBMZ*-1	BODY NO.
.000254	.314959	2.757378	.003222	.210843	10.000000	20.000000	-1.000000
.000429	.425650	3.261459	.003227	.139188	30.000000	20.000000	-1.000000
.001561	.454676	3.215088	.003928	1.309119	50.000000	20.000000	-1.000000
.005782	.466046	3.668756	.003184	-.821903	70.000000	20.000000	-1.000000
.003233	.278033	3.132334	.003728	.771984	10.000000	40.000000	-1.000000
.000191	.049067	-2.652732	.001229	.617256	30.000000	40.000000	-1.000000
.002127	.446653	-2.701307	.000671	-.576043	50.000000	40.000000	-1.000000
.000442	.021636	1.765940	.001940	-.752087	70.000000	40.000000	-1.000000
.002673	-1.579119	-.433356	.001631	2.575306	10.000000	60.000000	-1.000000
.000712	.001683	-2.857310	.004570	-.496844	30.000000	60.000000	-1.000000
.005461	1.101254	2.747510	.007544	.701240	50.000000	60.000000	-1.000000
.006462	.532593	1.031163	.001384	-.284604	70.000000	60.000000	-1.000000
.004633	-.429461	-.703534	.001344	2.660606	10.000000	80.000000	-1.000000
.003484	-.322461	2.309140	.000053	.101371	30.000000	80.000000	-1.000000
.001913	-.647163	-2.182666	.005420	-.706397	50.000000	80.000000	-1.000000
.000107	-.112053	-2.132845	.001048	-.354543	70.000000	80.000000	-1.000000
.000549	-.454852	-.049373	.001448	3.147759	10.000000	100.000000	-1.000000

OBS.M COMPM-Z,RES COMPM-X,RES COMPM-Y,RES   XM YM ZM   STN. NO.

230.000000	134.712354	-5.419606	205.419606	208.420252	-8.420252	76.000000	83.000000	33.000000	-1.000000
100.000000	96.156183	3.443917	98.740044	53.438018	46.561982	10.000000	100.000000	21.000000	-1.000000
100.000000	154.518958	-54.518958	87.907569	98.260298	1.739762	10.000000	100.000000	45.000000	-1.000000
-100.000000	-105.640126	5.640126	-98.912840	-101.467069	1.467069	5.000000	100.000000	70.000000	-1.000000
0.000000	-4.103580	-4.103580	6.882426	-1.063731	1.063731	10.000000	100.000000	90.000000	0.000000
-100.000000	-154.171947	54.171947	-126.532172	-114.172370	14.172370	15.000000	100.000000	104.000000	0.000000
-200.000000	-146.081011	-53.918989	-179.927547	-194.627798	-5.372202	17.000000	100.000000	108.000000	0.000000
-100.000000	-39.437367	-60.562653	-60.142621	-98.304256	-1.696744	33.000000	100.000000	92.000000	0.000000
0.000000	36.927637	36.927637	-42.434583	-45.782030	45.782030	30.000000	30.000000	86.000000	0.000000
-100.000000	-109.045515	9.045515	-75.582933	-52.463020	-47.536980	30.000000	70.000000	70.000000	0.000000
-100.000000	-100.800693	.800693	-99.479922	-101.251056	1.251056	43.000000	45.000000	45.000000	0.000000
100.000000	99.039773	-.914179	-5.056181	1.449044	-1.449044	46.000000	46.000000	33.000000	0.000000
100.000000	87.203459	.967267	104.316952	102.664450	-2.664450	35.000000	22.000000	22.000000	0.000000
100.000000	119.878405	12.795541	89.817487	103.135719	-3.135719	20.000000	11.000000	11.000000	0.000000
100.000000	112.493795	-19.873495	101.504512	102.673094	-.670094	55.000000	5.000000	5.000000	0.000000
100.000000	95.332556	-12.493795	107.955512	102.252846	-2.252846	60.000000	60.000000	29.000000	0.000000
150.000000	146.225536	4.667444	98.594421	100.758843	-.758843	75.000000	40.000000	40.000000	0.000000
100.000000	62.982170	3.774464	146.562199	147.947475	2.052525	80.000000	54.000000	54.000000	0.000000
100.000000	-67.946570	37.017930	99.834430	98.734163	1.265837	70.000000	64.000000	64.000000	0.000000
100.000000	-76.202515	-32.019430	-125.865601	-47.748423	-52.251177	70.000000	79.000000	79.000000	0.000000
-100.000000	-12.969183	-23.707495	-117.477339	-107.863009	7.863009	77.000000	100.000000	100.000000	0.000000
-100.000000	-70.275245	-12.969183	-.432177	13.414360	-13.414360	50.000000	50.000000	104.000000	0.000000
-100.000000	-41.237763	-29.724755	-108.222689	-89.219151	-10.780849	60.000000	60.000000	106.000000	0.000000
-120.000000	-150.091642	41.237763	-.955360	-9.655177	-9.655177	70.000000	70.000000	70.000000	0.000000
	30.091642	30.091642	-79.241668	-137.515072	17.515072				

CORR COEFF F-VALUE STD ERROR

VALUES ARE FOR Z,X,ANDY-COMPONENTS

.4445956	1.9605830	83.0446617
.8212562	6.5136933	45.4078593
.7755737	5.1476825	50.8786335

DIAGONAL ELEMENTS

.9648E+01   1   .4515E+03   2   .411E+01   3

.945E+01 1 .451E+03 2 .411E+01 3

RESULTS OF MAGNETIC TO GRAVITY TRANSFORMATION

OBS.G	COMP.G	RES.	XG	YG	ZG	STN. NO.		
-3.6000000	-12.9602401			9.3602401	4.0000000	12.0000000	0.0000000	-1.0
-13.0000000	-10.9281102			-2.0718898	7.0000000	24.0000000	0.0000000	-1.0
-1.5000000	-1.1565147			-29.6031813	11.0000000	37.0000000	0.0000000	-1.0
-37.0000000	-26.5138849			-11.5461111	4.0000000	53.0000000	0.0000000	-1.0
-32.0000000	-33.3021195			-.3021195	9.0000000	66.0000000	0.0000000	-1.0
-21.0000000	-19.6628150			-2.2371850	14.0000000	79.0000000	0.0000000	-1.0
-14.2000000	-20.2965435			6.0965435	8.0000000	95.0000000	0.0000000	-1.0
-8.3000000	-17.6018200			9.3018200	8.0000000	100.0000000	0.0000000	-1.0
-26.3000000	-14.6867473			-11.6132527	38.0000000	72.0000000	0.0000000	-1.0
-36.1000000	-20.7073733			-15.3926267	26.0000000	60.0000000	0.0000000	-1.0
-41.5000000	-13.7239093			-27.7710107	21.0000000	49.0000000	0.0000000	-1.0
-5.2000000	-10.4914925			-3.3085075	16.0000000	39.0000000	0.0000000	-1.0
-7.0000000	-12.5976666			5.5976666	33.0000000	27.0000000	0.0000000	-1.0
-11.2000000	-6.3100618			18.1000618	41.0000000	9.0000000	0.0000000	-1.0
-21.0000000	-7.1618166			28.2688166	54.0000000	7.0000000	0.0000000	-1.0
3.8000000	-1.9271776			5.7271776	64.0000000	28.0000000	0.0000000	-1.0
-32.3000000	-17.2367718			-15.0032282	44.0000000	51.0000000	0.0000000	-1.0
-23.4000000	-36.0848817			12.6848817	55.0000000	73.0000000	0.0000000	-1.0
-17.5000000	-30.1997175			12.6997175	53.0000000	85.0000000	0.0000000	-1.0
-10.7000000	-14.2344425			3.5344425	65.0000000	98.0000000	0.0000000	-1.0
-13.2000000	-14.7712587			1.3712587	76.0000000	92.0000000	0.0000000	-1.0
-24.2000000	-18.7009329			-9.4990671	72.0000000	79.0000000	0.0000000	-1.0
-16.0000000	-11.6012327			-4.3907173	79.0000000	63.0000000	0.0000000	-1.0
-5.7000000	-5.4593570			-.2400430	68.0000000	42.0000000	0.0000000	-1.0
16.7000000	-3.2700745			19.9700745	73.0000000	24.0000000	0.0000000	-1.0

COEFFS	T-VALUES		
9.0042983	1.6709319	1	
-1.3482427	1.9045140	2	
-13.8455914	-1.4975128	3	
1.2892645	0.0000000	4	

CORR COEFF	F-VALUE	STD ERROR	
.2652211	3.0656929	14.8722016	

AZIMUTH	INCLINATION	RATIO RHO/MAGN	
174.3773191	72.9114912	16.5720951	

ANGLE BETWN. EARTHS FIELD AND TOTAL MAGN. VECTOR

75.17352691

Q-MINIMUM

.96670397

DELAZ,DELIN,DELRATIO

-4.1678467   \ 22.1927459   6.7922287

CHECK GRAVITY TO MAGNETIC TRANSFORMATION

R.M.S. RESIDUAL GAMMA

   69.79735257

CHECK MAGNETIC TO GRAVITY TRANSFORMATION

R.M.S. RESIDUAL MILLIGAL

   13.63151447

VLAT,VLONG --- LAT AND LONG OF VIRTUAL POLE

ANGLE P   96.376

ALAT,ALONG,AMIN,AMA2,VLAT,VLONG

   45.5000   -60.5000   -12.5971   -177.0828   -50.7938   -65.0904
   ANGLE P   72.068

ALAT,ALONG,AMIN,AMAZ,VLAT,VLONG

   45.5000   -60.5000   32.9115   174.3773   -26.3630   -54.5276

**************   G11111ET   //// END OF LIST ////
**************   G11111ET   //// END OF LIST ////

APPENDIX 2.

RELATION BETWEEN T-VALUES OF REGRESSION COEFFICIENTS AND EIGENVALUES

OF THE MATRIX OF COEFFICIENTS OF THE NORMAL EQUATIONS.

Given a system of n equations in m unknowns where n > m we can find

a solution such that a predicted parameter represents an observed para-

meter in a least squares sense by solving:

$$A^T A \underline{x} = A^T \underline{y}$$

A 1.1

where $\underline{x}$ is a vector of length m of unknown quantities,

i.e. the regression coefficients.

$\underline{y}$ is a vector of lenght n of observed quantities

A is a (non-singular) n by m matrix of coefficients

that connects the known and unknown quantities.

Equation A 1.1 may be rewritten as:

$$B \underline{x} = \underline{v}$$

A 1.2

where $B = A^T A$ is an m by m matrix of the coefficients

on the left hand side of the normal equations

$\underline{v}$ is a vector of length m

Equation A 1.2 may be solved for the unknown quantities $\underline{x}$ by computing B^{-1}

and multiplying through on the left, i.e.

$$B^{-1} B \underline{x} = \underline{x} = B^{-1} \underline{v}$$

A 1.3

According to Douglas (1966), the standard deviation, sdx_r, of the

r^{th} regression coefficient, x_r is related to the rth diagonal element, c_{rr}

of the inverse matrix B^{-1} as follows:

$$sdx_r = S \quad c_{rr}$$

where S is the square root of the sum of the residuals

squared divided by the number of degrees of freedom

The t-value, t_r, of the rth regression coefficient, x_r, is:

$$t_r = \frac{xr}{S \quad crr} \qquad\qquad A\ 1.4$$

Equation A 1.2 may be rewritten as follows:

$$B\ \underline{x} = I\ \underline{v} \qquad\qquad A\ 1.5$$

where I is the identity matrix

By a suitable set of additions of a constant multiple (positive or

negative) of one row of B to other rows of B, the matrix B can be

reduced to diagonal form (Westlake, 1968):

$$L\ \underline{x} = J\ \underline{v} \qquad\qquad A\ 1.6$$

where L is a diagonal matrix whose diagonal values l_r

are the eigenvalues of B

J is a matrix whose off-diagonal elements are

generally non-zero.

Equation A 1.6 may be solved by computing L^{-1} (L^{-1} is a diagonal matrix

whose elements are $1/l_r$) and multiplying through on the left.

$$L^{-1}L\ \underline{x} = \underline{x} = L^{-1}\ J\ \underline{V} \qquad\qquad A\ 1.7$$

A comparison of A 1.7 and A 1.3 shows that:

$$B^{-1} = L^{-1}\ J$$

hence the diagonal elements, c_{rr} of B^{-1} are equal to j_{rr}/l_r (j_{rr} is the

r^{th} diagonal element of J) and the t-values are given by:

$$t_r = \frac{xr \quad l_r}{S \quad j_{rr}} \qquad\qquad A\ 1.8$$

The relation between t_r and 1_r is complicated but it is seen that a very small value of 1_r, ($|x_r|>0$), produces a small value of t_r.

It is interesting to note that Westlake (1968) gives the following relation between an inverse matrix and its eigenvalues. To quote but using a convenient change in notation:

"Let E be the matrix whose columns are the eigenvectors of B. Let L be the diagonal matrix of eigenvalues of B in the corresponding order then . . . $B^{-1} = E \, L^{-1} \, E^{-1} = E \, L^{-1} E^{T}$".

Al-Chalabi, M. 1970. Interpretation of two-dimensional magnetic profiles by
        non-linear optimization.
        Boll. Geof. Teor. Appl., 12, pp. 3-20.

Anderssen, R.G. 1969. On the solution of certain overdetermined systems
        of linear equations that arise in geophysics.
        J. Geophys. Res., 74, pp. 1045-1051.

Ansorge, J., Emter, D., Fuchs, K., Lauer, J.P., Mueller, S., and
        Peterschmitt, E. 1970. Structure of the crust and upper mantle
        in the rift system around the Rhinegraben, in Graben Problems,
        edit. by J.H. Illies and S. Mueller, E. Schweizerbart'sche
        Verlagsbuchhandlung, Stuttgart, pp. 190-197.

Badham, J.P.N. and Halls, C. 1975. Microplate tectonics, oblique collisions,
        and evolution of the Hercynian orogenic systems.
        Geology, 3, pp. 373-376.

Baranov, V. 1953. Calcul du gradient vertical du champ de gravite ou du
        champ magnetique mesure a la surface du sol.
        Geophys. Prosp., 1, 171-191.

Baranov, V. 1957. A new method for interpretation of aeromagnetic maps:
        pseudo-gravimetric anomalies.
        Geophysics, 22, pp. 359-383.

Barrett, B.C., Berry, M.J., Blanchard, J.E., Keen, M.J. and McAllister,
        R.E. 1964. Seismic studies on the eastern seaboard of Canada:
        the Atlantic coast of Nova Scotia.
        Can. J. Earth Sci., 1, pp. 10-22.

Beales, F.W., Carracedo, J.C. and Strangway, D.W. 1974. Palaeomagnetism
        and the origin of Mississippi Valley-type ore deposits.
        Can. J. Earth Sci., 11, pp. 211-223.

Bennison, G.M. and Wright, A.E. 1969. The geological history of the British
        Isles, Edward Arnold, London.

Benson, D.G. 1967. Geology of Hopewell map-area, Nova Scotia.
        Geol. Surv. Can. Memoir 343.

Benson, D.G. 1970. Notes to accompany geological maps of Antigonish and
        Cape George map-areas.
        Geol. Surv. Can. Paper 70-8

Benson, D.G. 1974. The geology of the Antigonish Highlands.
        Geol. Surv. Can. Memoir 376.

Berger, J., Blanchard, J.E., Keen, M.J., McAllister, R.E., and Tsong, C.F. 1965. Geophysical observations on sediments and basement structure underlying Sable Island, Nova Scotia.
Bull. Am. Soc. Petrol. Geol. 49, pp. 959-965.

Bhattacharyya, B.K. 1966. A method for computing the total magnetization vector and the dimensions of a rectangular block-shaped body from magnetic anomalies.
Geophysics, 31, pp. 74-96.

Bhattacharyya, B.K. and Raychaudhuri, B. 1967. Aeromagnetic and geological interpretation of a section of the Appalachian belt in Canada.
Can. J. Earth Sci., 4, pp. 1015-1037.

Bird, J.M. and Dewey, J.F. 1970. Lithosphere plate-continental margin tectonics and the evolution of the Appalachian orogen.
Bull. Geol. Soc. Am., 81, pp. 1031-1060.

Black, R.F. 1964. Palaeomagnetic support of the theory of rotation of the western part of the Island of Newfoundland.
Nature, 202, pp. 945-948.

Bosum, W. and Hahn, A. 1970. Interpretation de Flugmagnetometervermessung des Oberrheingrabens, in Graben Problems, edit. by J.H. Illies and S. Mueller, E. Schweizerbart'sche Verlagsbuchhandlung, Stuttgart, pp. 219-223.

Bott, M.H.P. 1961. A gravity survey off the coast of North-east England.
Proc. Yorkshire Geol. Soc., 33, pp. 1-20.

Bott, M.H.P. 1962. A simple criterion for interpreting negative gravity anomalies.
Geophysics, 27, pp. 376-381.

Bott, M.H.P., Smith, R.A. and Stacey, R.A. 1966. Estimation of the direction of magnetization of a body causing a magnetic anomaly using a pseudo-gravity transformation.
Geophysics, 31, pp. 803-811.

Bott, M.H.P., and Smithson, S.B. 1967. Gravity investigations of subsurface shape and mass distributions of granite batholiths.
Bull. Geol. Soc. Am., 73, pp. 859-878.

Bott, M.H.P. 1971. Evolution of young continental margins and formation of shelf basins.
Tectonophysics, 11, pp. 319-327.

Bott, M.H.P. and Hutton, M.A. 1971. Limitations on the resolution possible in the direct interpretation of marine magnetic anomalies.
Earth Planet. Sci. Lett., 8, pp. 317-319.

Bott, M.H.P. and Dean, D.S. 1972. Stress systems at young continental margins.
Nature Phys. Sci., 235, pp. 23-25.

Bott, M.H.P. and Ingles, A.D., 1973. Matrix methods for joint interpretation of two-dimensional gravity and magnetic anomalies with application to the Iceland-Faeroe ridge.
Geophys. J. Roy. Ast. Soc. 30, pp. 55-67.

Bott, M.H.P. and Browitt, C.W.A. 1975. Interpretation of geophysical observations between the Orkney and Shetland Islands.
J. Geol. Soc., 131, pp. 353-371.

Boyle, R.W. 1963. Geology of the Barite, Gypsum, Manganese, and Lead-Zinc-Copper-Silver deposits of the Walton-Cheverie area, Nova Scotia.
Geol. Surv. Can. Paper 62-25.

Briden, J.C., Morris, W.A., and Piper, J.D.A. 1973. Palaeomagnetic studies in the British Caledonides - IV regional and global implications.
Geophys. J. Roy. Ast. Soc., 34, pp. 107-134.

Bullard, E.C., Everett, J.E. and Smith, A.G. 1965. The fit of the continents around the Atlantic.
Phil. Trans. Roy. Soc., Ser. A, 258, 41-51.

Bullerwell, W. 1965. Aeromagnetic map of Great Britain, Sheet 2.
Geol. Surv. of Gt. Britain, published by Ordinance Survey, Chessington, Surrey.

Burrett, C.F. 1972. Plate tectonics and the Hercynian orogeny.
Nature, 239, pp. 155-156.

Cameron, H. 1956. Tectonics of the Maritime area.
Trans. Roy. Soc. Can., 50, pp. 45-51.

Canadian Hydrographic Service. 1974. Natural Resource Maps 15056-C and 15058-C. Dept. of Environment, Ottawa.

Carmichael, C.M. and Palmer, H.C. 1968. Paleomagnetism of the late Triassic, North Mountain Basalt of Nova Scotia.
J. Geophys. Res., 73, pp. 2811-2822.

Cherkis, N.Z., Fleming, H.S., and Massingill, J.V. 1973. Is the Gibbs Fracture Zone a westward projection of the Hercynian Front into North America?
Nature Phys. Sci., 245, pp. 113-115.

Cordell, L. and Taylor, P.T. 1971. Investigation of magnetization and density
of a North Atlantic seamount using Poisson's theorem.
Geophysics, 36, pp. 919-937.

Cormier, R.F. 1974. Radiometric age of the Keppoch Formation, Brown's
Mountain Group, northern mainland of Nova Scotia.
Can. J. Earth Sci., 11, pp. 1325-1329.

Cox, A. and Doell, R.R. 1960. Review of Paleomagnetism.
Bull. Geol. Soc. Am., 71, pp. 645-768.

Deutsch, E.R. 1969. Palaeomagnetism and North Atlantic Palaeography.
Am. Ass. Petr. Geol. Memoir 12, pp. 931-954.

Deutsch, E.R. and Rao, K.V. 1970. Paleomagnetism of Ordovician sedimentary
rocks from Bell Island, Newfoundland.
Trans. Am. Geophs. Un., 51, pp. 272.

Douglas, A. 1966. A special purpose least squares program.
AWRE Report No. 0-54/66, Atomic Weapons Research Establishment,
Aldermaston, Berkshire.

Drake, C.L., Ewing, M. and Sutton, G.H. 1959. Continental margins and
geosynclines: The East Coast of North America north of Cape Hatteras,
in Physics and Chemistry of the Earth, vol. 3, eds. L.H. Ahrens
et. al., Pergamon Press, New York, pp. 110-198.

Draper, N.R. and Smith, H. 1966. Applied regression analysis.
John Wiley and Sons, New York.

Du Bois, P.M. 1959. Palaeomagnetism and the rotation of Newfoundland.
Nature, 184, pp. 63-64.

Eisbacher, G.H. 1969. Displacement and stress field along part of the Cobequid
Fault, Nova Scotia.
Can. J. Earth Sci., 6, pp. 1095-1104.

Eisbacher, G.H. 1970. Deformation mechanics of mylonitic rocks and fractured
granites in Cobequid Mountains, Nova Scotia, Canada.
Bull. Geol. Soc. Am., 81, pp. 2009-2020.

Eotvos, R. von. 1906. Bestimmung der Gradienten der Schwerkraft und ihrer
Niveauflachen mit Hilfe der Drehwage, in Roland Eotvos Gesammelte
Arbeiten, ed. P. Selenyi, Akademiai Kiado, Budapest, 1953, pp. 91-160.

Ewing, G.N., Dainty, A.M. Blanchard, J.E., and Keen, J.J. 1966. Seismic
studies on the eastern seaboard of Canada: the Appalachian system.
Can. J. Earth Sci., 3, pp. 89-109.

Ewing, G.N. and Hobson, G.D. 1966. Marine seismic refraction investigation over the Orpheus gravity anomaly off the east coast of Nova Scotia. Geol. Surv. Can. Paper 66-38.

Fahrig, W.F., Christie, K.W., and Schwarz, E.J. 1974. Paleomagnetism of the Mealy Mountain anorthosite suite and of the Shabogamo Gabbro, Labrador, Canada. Can. J. Earth Sci., 11, pp. 18-29.

Fairbridge, R.W. 1970. Geomagnetic south pole in the Ordovician of Africa. Trans. Am. Geophys. Un., 51, pp. 272.

Francheteau, J. 1970. Palaeomagnetism and Plate Tectonics. Scripps Institution of Oceanography, Reference 70-30, pp. 345.

Garland, G.D. 1951. Combined analysis of gravitational and magnetic anomalies. Geophysics, 16, pp. 51-62.

Garland, G.D. 1953. Gravity measurements in the Maritime Provinces. Publ. Dom. Obs., 16, Dominion Observatories, Ottawa, pp. 184-275.

Geological Survey of Canada. 1970. Magnetic anomaly map of Canada - 1255A. Department of Energy, Mines and Resources, Ottawa.

Golub, G. 1965. Numerical methods for solving linear least squares problems. Num. Math., 7, pp. 206-216.

Goodacre, A.K. 1964. A shipborne gravimeter testing range near Halifax, Nova Scotia. J. Geophys. Res., 69, pp. 5373-5381.

Goodacre, A.K. and Nyland, E. 1966. Underwater gravity measurements in the Gulf of St. Lawrence. Roy. Soc. Can. Spec. Pub. No. 9, pp. 114-128.

Goodacre, A.K., Brule, B.G. and Cooper, R.V. 1969. Results of regional underwater gravity surveys in the Gulf of St. Lawrence. Grav. Map. Ser. Dom. Obs. No. 86, Dominion Observatories, Ottawa.

Goodacre, A.K. 1972. Generalized structure and composition of the deep crust and upper mantle in Canada. J. Geophys. Res., 77, pp. 3146-3161.

Goodacre, A.K. 1973. Some comments on the calculation of the gravitational and magnetic attraction of a homogeneous rectangular prism. Geophys. Prosp. 21, pp. 66-69.

Goodacre, A.K., Stephens, L.E. and Cooper, R.V. 1973. A gravity survey
    of the Scotian Shelf.
    Geol. Surv. Can. Paper 71-23, pp. 241-252.

Goulden, C.H. 1952. Methods of Statistical Analysis.
    John Wiley and Sons, New York.

Haworth, R.T., Barrett, L.F. and MacIntyre, J.B. 1972. Bathymetry, Gravity
    and Magnetic Data Cruise Bl 72-009 Dawson.
    Bedford Institute of Oceanography Data Series Bl-D-72-14.

Haworth, R.T. 1975. Paleozoic continental collision in the northern Appalachians
    in light of gravity and magnetic data in the Gulf of St. Lawrence.
    Geol. Surv. Can. Paper 74-30, pp. 1-10.

Hicken, A., Irving, E., Law, L.K. and Hastie, J. 1972. Catalogue of palaeo-
    magnetic directions and poles.
    Pub. Earth Phys. Br., 45, pp. 1-35.

Hjelt, S.E. 1973. Experiences with automatic magnetic interpretation using
    the thick plate model.
    Geophys. Prosp., 21, pp. 243-265.

Hobson, G.D. and Overton, A. 1973. Sedimentary refraction seismic surveys,
    Gulf of St. Lawrence.
    Geol. Surv. Can. Paper 71-23, pp. 325-336.

Hood, P.J. 1966. Magnetic survey of the continental shelves of eastern Canada.
    Geol. Surv. Can. Paper 66-15, pp. 19-32.

Howie, R.D. and Cumming, L.M. 1963. Basement features of the Canadian
    Appalachians.
    Geol. Surv. Can. Bulletin 89.

Irving, E. and Park, J.K. 1972. Hairpins and superintervals.
    Can. J. Earth Sci., 9, pp. 1318-1324.

Jansa, L.F. and Wade, J.A. 1975. Geology of the continental margin off Nova
    Scotia and Newfoundland, in Offshore geology of eastern Canada.
    Geol. Surv. Can. Paper 74-30, pp. 51-105.

Kay, M. 1951. The tectonics of middle North America.
    Princeton Univ. Press, Princeton, N.J.

King, L.H. and McLean, B. 1970. Continuous seismic-reflection study, Orpheus gravity anomaly.
Bull. Am. Ass. Petr. Geol., 54, pp. 2007-2031.

King, P.B. 1951. The Tectonics of Middle North America.
Princeton Univ. Press, Princeton, N.J.

Larochelle, A. and Wanless, R.K. 1966. The paleomagnetism of a Triassic diabase dike in Nova Scotia.
J. Geophys. Res., 71, pp. 4949-4953.

Laving, G. 1971. Automatic methods for the interpretation of gravity and magnetic field anomalies and their application to marine geophysical surveys.
Ph.D. thesis, University of Durham, England.

Lecolazet, R. 1970. La carte gravimétrique d'Alsace, in Graben Problems, edit. by J.H. Illies and S. Mueller, E. Schweizerbart'sche Verlagsbuchhandlung, Stuttgart, pp. 233-234.

Loncarevic, B.C. and Ewing, G.N. 1967. Geophysical study of the Orpheus gravity anomaly.
Proc. 7th World Petrol. Cong. pp. 827-835.

Lundbak, A. 1956. Combined analysis of gravimetric and magnetic anomalies and some palaeomagnetic results.
Geophys. Prosp., 4, pp. 226-235.

Malcolm, W. 1912. Gold fields of Nova Scotia.
Geol. Surv. Can. Memoir 20-E.

McGrath, P.H. 1970. Magnetic investigations of the Charlotte and Pokiok intrusions, southern New Brunswick.
Proc. Geol. Ass. Can., 21, pp. 25-32.

McGrath, P.H., Hood, P.J. and Cameron, G.W. 1973. Magnetic surveys of the Gulf of St. Lawrence and the Scotian Shelf.
Geol. Surv. Can. Paper 71-23, pp. 339-358.

McIver, N.L. 1972. Cenozoic and Mesozoic stratigraphy of the Nova Scotia shelf.
Can. J. Earth Sci., 9, pp. 54-70.

McKenzie D. and Parker, R.L. 1967. The north Pacific: an example of tectonics on a sphere.
Nature, 216, pp. 1276-1280.

McKerrow, W.S. and Ziegler, A.M. 1972. Paleozoic oceans.
Nature, Phys. Sci., 240, pp. 92-94.

McLearn, F.H. 1924. Palaeontology of the Silurian rocks of Arisaig, Nova Scotia.
Geol. Surv. Can. Memoir 137.

Mueller, S. 1970. Geophysical aspects of graben formation in continental rift systems, in Graben Problems, edit. by J.H. Illies and S. Mueller, E. Schweizerbart'sche Verlagsbuchhandlung, Stuttgart, pp. 27-37.

Morgan, W.J. 1968. Rises, Trenches, Great Faults and Crustal Blocks.
J. Geophys. Res., 73, pp. 1959-1982.

Nairn, A.E.M., Frost, D.V. and Light, B.G. 1959. Palaeomagnetism of certain rocks from Newfoundland.
Nature, 183, pp. 596-597.

Nova Scotia Department of Mines. 1965. Geological Map of the Province of Nova Scotia.

Officer, C.B. and Ewing, M. 1954. Geophysical investigations in the emerged and submerged Atlantic coastal plain. Part VII. Continental shelf, continental slope and continental rise south of Nova Scotia.
Bull. Geol. Soc. Am., 65, pp. 653-670.

Papezik, V.S., Hodych, J.P., and Goodacre, A.K. 1975. The Avalon magnetic lineament - a possible continuation of the Triassic dike system of New Brunswick and Nova Scotia.
Can. J. Earth Sci., 12, pp. 332-335.

Petersen, J.J., Fox, P.J. and Schreiber, E. 1974. Newfoundland Ophiolites and the geology of the oceanic layer.
Nature, 247, pp. 194-196.

Pitman, W.C. and Talwani, W. 1972. Sea-floor spreading in the North Atlantic.
Bull. Geol. Soc. Am., 83, pp. 619-646.

Poisson, M. 1826. Memoire sur la theorie du magnetisme.
Memoires de l'Academie royale des Sciences de l'Institut de France, 5, pp. 247-338.

Poole, W.H. 1967. Tectonic evolution of Appalachian region of Canada, in Geology of the Atlantic region.
Geol. Ass. Can. Special Paper No. 4, pp. 9-51.

Poole, W.H. 1970. Geology of southeastern Canada, in Geology and economic minerals of Canada.
Geol. Surv. Can. Economic Geol. Rept. No. 1, pp. 228-304.

Press, F. and Beckmann, W.C. 1954. Geophysical investigations in the emerged and submerged Atlantic coastal plain. Part VIII: Grand Banks and adjacent shelfs.
Bull. Geol. Soc. Am., 65, pp. 299-313.

Ramberg, I.B. 1972. Crustal structure across the Permian Oslo Graben from gravity measurements.
Nature Phys. Sci., 240, pp. 149-152.

Ramberg, I.B. and Smithson, S.B. 1975. Geophysical interpretation of crustal structure along the southeastern coast of Norway and Skagerrak.
Bull. Geol. Soc. Am., 86, pp. 769-774.

Rast, N. and Grant, R. 1973. Transatlantic correlation of the Variscan – Appalachian Orogeny.
Am. J. Sci., 273, pp. 572-579.

Rodgers, J. and Neale, E.R.W. 1963. Possible "Taconic" Klippen in western Newfoundland.
Bull. Geol. Soc. Am., 48, pp. 1573-1588.

Rodgers, J. 1970. The tectonics of the Appalachians.
Wiley-Interscience, New York.

Rosenbrock, H.H. 1960. An automatic method for finding the greatest or least value of a function.
The Computer J. 3, pp. 175-184.

Roy, J.L. 1972. A pattern of rupture of the eastern North American-western European palaeoblock.
Earth and Planet. Sci. Lett., 14, pp. 103-114.

Saad, A.H. 1969. Magnetic properties of ultramafic rocks from Red Mountain, California.
Geophysics, 34, pp. 974-987.

Schenk, P.E. 1971. Southeastern Atlantic Canada, northwestern Africa, and continental drift.
Can. J. Earth Sci., 8, pp. 1218-1251.

Schenk, P.E. 1972. Possible late Ordovician glaciation of Nova Scotia.
Can. J. Earth Sci., 9, pp. 95-107.

Schiller, E. 1961. Guysborough, Nova Scotia.
Geol. Surv. Can. Map 27-1961.

Schuchert, C. 1925. Significance of the Taconic orogeny.
Bull. Geol. Soc. Am., 36, pp. 343-350.

Sheridan, R.E. and Drake, C.L. 1968. Seaward extension of the Canadian Appalachians.
Can. J. Earth Sci., 5, pp. 337-373.

Sherwin, D.F. 1972. Oil and gas - offshore.
Can. Inst. Min. Bulletin, 65, pp. 73-82.

St. Julien, P. and Hubert, C. 1975. Evolution of the Taconian Orogen in The Quebec Appalachians.
Am. J. Sci., 275-A, pp. 337-362.

Stephens, L.E., Goodacre, A.K. and Cooper, R.V. 1971. Results of underwater gravity surveys over the Nova Scotia continental shelf.
Grav. Map Ser. Earth Phys. Br. No. 123,
Earth Physics Branch, Ottawa.

Stephens, L.E. and Cooper, R.V. 1973. Results of underwater gravity surveys over the southern Nova Scotian continental shelf.
Grav. Map Ser. Earth Phys. Br. No. 149,
Earth Physics Branch, Ottawa.

Stevenson, I.M. 1959. Chedabucto Bay map-area, Nova Scotia.
Geol. Surv. Can. Map 3-1959.

Tanner, J.G. 1969. A geophysical investigation of structural boundaries in the eastern Canadian Shield.
Ph.D. Thesis, University of Durham, Durham, England.

Tarling, D.H. and Sutton, D.H. 1967. Palaeomagnetic stability results of a reconnaissance survey of red sandstones in Morocco.
Phys. Earth Planet. Interiors, 1, pp. 35-43.

Taylor, F.C. and Schiller, E.A. 1966. Metamorphism of the Meguma Group of Nova Scotia.
Can. J. Earth Sci., 3, 959-974.

Taylor, F.C. 1967.   Reconnaissance geology of Shelburne map-area, Queens, Shelburne and Yarmouth Counties, Nova Scotia.
Geol. Surv. Can. Memoir 349.

Taylor, F.C. 1969. Geology of the Annapolis-St. Mary's Bay map-area, Nova Scotia.
Geol. Surv. Can. Memoir 358.

Turner, F.J. 1968.   Metamorphic Petrology.
McGraw-Hill, New York.

Weaver, D.F. 1967.   A geological interpretation of the Bouguer anomaly field of Newfoundland.
Pub. Dom. Obs., 35, Dominion Observatories, Ottawa, pp. 223-251.

Weber, J.R. and Goodacre, A.K. 1966. A reconnaissance underwater gravity survey of Lake Superior, in The Earth beneath the Continents, edit. by J.S. Steinhart and T.J. Smith.
Am. Geophys. Un. Monograph, 10, pp. 56-65.

Weeks, L.J. 1948.   Londonderry and Bass River map-areas, Colchester and Hants Counties, Nova Scotia.
Geol. Surv. Can. Memoir 245.

Weeks, L.J. 1954.   Southeast Cape Breton Island, Nova Scotia.
Geol. Surv. Can. Memoir 277.

Westlake, J.R. 1968.   A handbook of numerical matrix inversion and solution of linear equations.
John Wiley and Sons, New York.

Williams, H. 1964.   The Appalachians in northeastern Newfoundland: a two-sided symmetrical system.
Am. J. Sci., 262, pp. 1137-1158.

Williams, H. 1967.   Geology, Island of Newfoundland.
Geol. Surv. Can. Map 1231A.

Williams, H., Kennedy, M.J. and Neale, E.R.W. 1970. The Hermitage Flexure, the Cabot Fault, and the disappearance of the Newfoundland central mobile belt.
Bull. Geol. Soc. Am., 81, pp. 1563-1568.

Williams, H., Kennedy, M.J. and Neale, E.R.W. 1972. The Appalachian structural province, in Variations in tectonic styles in Canada. R.A. Price and R.J.W. Douglas, eds. Geol. Ass. Can. Special Paper No. 11. pp. 181-261.

Williams, M.Y. 1912. Geology of the Arisaig-Antigonish district, Nova Scotia. Am. J. Sci., 34, pp. 242-250.

Willmore, P.L. and Scheidegger, A.E. 1956. Seismic observations in the Gulf of St. Lawrence. Trans. Roy. Soc. Can., 50, pp. 21-46.

Wilson, J.T. 1954. The development and structure of the crust, in The Earth as a planet. G.P. Kuiper, ed. Univ. of Chicago Press, Chicago, pp. 138-214.

Wilson, J.T. 1966. Did the Atlantic close and then reopen? Nature, 211, pp. 676-677.

Worzel, J.L. 1968. Survey of continental margins, in Geology of Shelf Seas. D.T. Donovan, ed. Oliver and Boyd, Edinburgh, pp. 117-154.

Zen, E. 1968. Nature of the Ordovician Orogeny in the Taconic Area, in Studies of Appalachian Geology: Northern and Maritime. edit. by E. Zen et al., John Wiley and Sons, New York, pp. 129-139.